Investigating the role of Rab GTPases in medulloblastoma pathogenesis

Susannah J. Entwistle, MSci

Thesis submitted to the University of Nottingham for degree of Doctor of Philosophy

March 2024

Abstract

Introduction: Medulloblastoma is the most common malignant paediatric brain cancer, accounting for 20% of paediatric brain tumours and 10% of all cancer deaths. It is located within the cerebellum and is defined by four molecular subgroups: Wingless (WNT), Sonic Hedgehog (SHH), group 3 and group 4. Whilst WNT and SHH are named after the pathways which drive these tumours, the mechanisms underlying groups 3 and 4 are less well understood. Group 3 tumours are the group most likely to be metastatic at diagnosis and are therefore associated with the poorest prognosis. There is therefore a particular need to investigate the mechanisms that drive these tumours, to enhance diagnostic methods and treatment strategies and eventually improve patient outcomes. Exosomes are small membrane-bound extracellular vesicles (EV) of endosomal origin. They contain a variety of cargo, including RNA and proteins. Increased exosome release has been associated with disease progression and metastasis in multiple cancers. Rab GTPases (Rabs) are a family of small GTPases (66 in humans) which regulate vesicle trafficking. Several Rabs have been shown to regulate exosome biogenesis and secretion and may consequently contribute to cancer progression. Rabs also have non-exosomal associations with tumourigenesis through roles in intracellular vesicular trafficking. The role of Rabs in medulloblastoma pathogenesis has not yet been investigated. This study aims to therefore explore the pathways in which Rabs may contribute to medulloblastoma pathogenesis.

Methods and results: Analysis of medulloblastoma patient datasets such as the Cavalli dataset on the R2 genomics analysis and visualisation platform, showed an association between high expression of specific Rabs and poor prognosis. This included *Rab11A* and *Rab40B* in group 3 medulloblastoma (p values ranging from 0.00075 to 0.03). RT-qPCR analysis showed no subgroup-specific enrichment of *Rab11A* expression, but *Rab40B* had significantly higher expression in the group 3 cell line HD-MB03 (p<0.01). CRISPR-Cas9 technology was then used disrupt the *Rab11A* and *Rab40B* genes to generate stable protein knockout in the group 3 HD-MB03 cell line. Nine Rab11A knockout lines were fully validated, validation of Rab40B knockout lines was however inconclusive. From then on exploring the function of Rab11A in group 3 medulloblastoma became the focus of the study.

Analysis of EV secretion showed no statistical difference in median diameter and concentration of EVs secreted between Rab11A knockout and non-targeting CRISPR control cell lines. The effect of Rab11A knockout on the endocytic pathways through analysis of transferrin uptake was inconclusive. Proteomic analysis using SWATH-MS was then conducted on Rab11A knockout cell lysates and EVs. Differential protein expression analysis of cell lysates identified statistically significant downregulation of the mitochondrial metabolism pathways, oxidative phosphorylation and the TCA cycle, which occur in the inner mitochondrial membrane and mitochondrial matrix respectively. This finding is particularly interesting since recent studies showed that the HD-MB03 cell line has high TCA cycle and oxidative phosphorylation activity, a finding that was also present in other group 3 cell lines with a *MYC* amplification. Thereby suggesting that Rab11A is a regulator of mitochondrial metabolism in MYC amplified group 3 medulloblastoma. In EVs from Rab11A knockout versus control cells, proteomic analysis identified protein sidekick 2 (SDK2) as being significantly downregulated. SDK2 is associated with several functional pathways, including maintenance of neural circuits in the retina, that have recently been associated with genetic signatures of the cell of origin for group 3 medulloblastoma, thus linking Rab11A-regulated EV cargo and fundamental mechanisms driving the formation of the disease.

Conclusions: This study has identified, for the first time, a prognostic association between Rab GTPases and medulloblastoma. It has also identified subgroup-specific Rab targets for further exploration. Including a potential novel role for one Rab, Rab11A, in regulation of mitochondrial metabolism pathways. In addition to this, an association has been made between Rab11A-regulated EV cargo and mechanisms that are thought to drive group 3 medulloblastoma. Further exploration of the role of Rab11A may therefore give valuable insight into mechanisms driving pathogenesis and tumour initiation in group 3 medulloblastoma.

__Acknowledgements__

After a rollercoaster of a four and a half years, it feels surreal to be finally submitting this work. Despite the many personal and professional challenges that I have faced whilst completing my PhD, I continue to feel very fortunate to have gotten this opportunity. This has been one of the biggest challenges I have faced in life so far and I would not have been able to come close to submission without the guidance and support of the people mentioned in this section.

I would firstly like to thank my supervisors Alistair, Beth, and Ian. To Alistair, your curiosity and dedication has been inspirational. I am also so grateful that you took the chance on me and helped facilitate me working on a Rab that wasn't Rab27. To Beth, your support has made me a better scientist and a stronger person. The way you fight for your students is something else and I am so grateful for the kindness you have shown me during this process. To Ian, I am so appreciative of your sense of humour, honesty and emotional intelligence.

To Deb, there are not enough words, I hope you know how much you mean to me.

To the people that have supported me through the most turbulent period of my life so far. To Liv, Becky, James J, Alice, Kate, Courtney, Em and my Charnock girls Han, Lou, Rhia and Bry. There are not enough words to describe how grateful I am to have you in my life, this PhD would not have been possible without you.

I would also like to thank some of the people I have been so lucky to have worked alongside, both in the QMC and BDI. To Hannah J, Anya, Sophie F, Paula, Elliot, Hannah B, Izzie, Harry E, James MW, Louisa, and the rest of the Coyle lab and QMC D61.

To the best friends I never asked for but could not live without, Josh, Leah, Jacob, Amber and Alfie. I am so lucky to have you guys in my life.

Lastly to my grandparents Bob and Jenny, to whom I dedicate this thesis. Your love and support means more to me than you'll ever know.

<u>Table of contents</u>

List of figures

List of tables

Abbreviations

2D – Two-dimensional

3D – Three-dimensional

ACLY – Adenosine triphosphate citrate lyase

AFC – Automatic fraction collector

ALIX - Programmed cell death 6 interacting protein

ANOVA – Analysis of variance

ANXA2 – Annexin 2

ANXA6 – Annexin 6

ARF1 – Adenosine diphosphate ribosylation factor 1

ARFGAP1 - Adenosine diphosphate-ribosylation factor GTPase activating protein 1

AU – Arbitrary units

BRCA2 – Breast cancer gene 2

BSA – Bovine serum albumin

CA14 – Carbolic anhydrase 14

CART - Cytoskeleton-associated recycling or transport

Cas9 – CRISPR-associated protein 9

CASP3 – Caspase 3

CBS – Cystathionine beta synthase

CHMP3 – Charged multivesicular body protein 3

CNS – Central nervous system

CRISPR – Clustered Regularly Interspaced Short Palindromic Repeats

CSF – Cerebrospinal fluid

CT – Computed tomography

CTH – Cystathionine gamma-lyase

CTNNA1 – α-catenin

CTNNB1 – β-catenin

CV – Coefficient of variation

DAPI - 4'6-diamidino-2-phenylindole

DAVID – the Database for annotation, visualisation and integration discovery

DENN – Differentially expressed in normal and neoplastic cells

DIA – Data-independent acquisition

DIA-NN – Data-independent acquisition by neural networks

DMEM – Dulbecco's modified Eagle's medium

DMSO – Dimethyl sulfoxide

D/N – Desmoplastic/ nodular

DNM1 – Dynamin 1

ECL – Enhanced chemiluminescence

ECM – Extracellular matrix

EDTA – Ethylenediaminetetraacetic acid

EGF – Epidermal growth factor

EGFP – Enhanced green fluorescent protein

EGFRs – Epidermal growth factor receptors

EHD4 – EH domain-containing 4

ELP1 – Elongator acetyltransferase complex subunit 1

EMBOSS – European molecular biology open software suite

EMMPRIN – Extracellular matrix MMPs inducer

EMT – Epithelial-to-mesenchymal transition

ENO2 – Enolase 2

ER – Endoplasmic reticulum

ERK – Extracellular signal-regulated kinase

ESCRT – Endosomal sorting complexes required for transport

EV – Extracellular vesicle

EXOC6 – Exocyst complex component 6

ExPASy – Expert protein analysis system

FACS – Fluorescence activated cell sorting

FAP – Familial Adenomatous Polyposis

FASTA – Fast all

FBS – Foetal bovine serum

FGF – Fibroblast growth factor

FSC – Forward scatter

GAP – GTPase hydrolase-activating proteins

GAPDH - Glyceraldehyde-3 phosphate dehydrogenase

GCSH - Glycine cleavage system protein H

GDF – GDP displacement factor

GDI – Guanine dissociation inhibitor

gDNA – Genomic DNA

GDP – Guanine diphosphate

GEF – Guanine exchange factor

GFP – Green fluorescent protein

GLUL – Glutamine synthetase

GLUT4 – Glucose transporter 4

HGG – High grade glioma

HK2 – Hexokinase 2

HLA-G - Human leukocyte antigen G

HNRNPH1 – Heterogeneous ribonuclear protein H

HRP – Horseradish peroxidase

i17q – Isochromosome 17q

IDH – Isocitrate dehydrogenase

InDel – Insertion or deletion mutation

ISEV – International society of extracellular vesicles

KCNA1 – Potassium voltage-gated channel subfamily A member 1

kDa – Kilodaltons

KDM6A – Lysine demethylase 6A

KEGG – Kyoto encyclopaedia of genes and genomes

LAMP-1 – Lysosomal-associated membrane protein-1

LAMP-2 – Lysosomal-associated membrane protein-2

LC/A – Large cell/ anaplastic

LIMMA – Linear models for microarray analysis

LOF – Loss of function

mA – Milliamps

MBEN – Medulloblastoma with extensive nodularity

MICALL2 - Molecule interacting with CasL-like 2

MISEV – Minimal information for studies of extracellular vesicles

MMP – Matrix metalloproteinase

mRNA – Messenger RNA

MRI – Magnetic resonance imaging

MRPS - Mitochondrial ribosomal protein

mTORC1 – Mechanistic target of rapamycin complex 1

MT1-MMP – Matrix type 1 metalloproteinase

MUSCLE – Multiple sequence comparison by log-expectation

MVB – Multivesicular body

MYO5 – Myosin-5

NADH – Nicotinamide adenine dinucleotide

NCBI – National centre for biotechnology information

NDUFS - NADH-ubiquinone oxidoreductase

NEDD4L - Neuronal precursor cell-expressed developmentally downregulated 4-like E3 ubiquitin protein ligase

NHEJ – Non-homologous end joining

NRT – No reverse transcriptase

NTA – Nanoparticle tracking analysis

NTC – No transcript control

OCRL1 – Inositol polyphosphate-5-phosphatase

OTX2 – Orthodenticle homeobox 2

PAM – Protospacer-adjacent motif

PBS – Phosphate buffered saline

PBT – PBS-Tween 20

PBX – PBS-Triton X100

PCA – Principal component analysis

PCK2 – Phosphoenol pyruvate carboxykinase 2

PCR – Polymerase chain reaction

PCV – Purified collection volume

PE - Phosphatidylethanolamine

PI3K – Phosphoinositide 3-kinase

PKA – Protein kinase A

PS - Phosphatidylserine

RAC1 - Ras-related C3 botulinum toxin substrate 1

Rab – Rab GTPase

RBD – Rab binding domain

REP – Rab escort protein

RHOA - Ras Homolog Family Member A

rRNA – Ribosomal ribonucleic acid

RUFY1 - RUN and FYVE domain containing 1

SC – Single cell

SDK2 – Protein sidekick-2

SDS – Sodium dodecyl sulfate

sgRNA – Single guide RNA

SHH – Sonic hedgehog

SMAD4 - Mothers against decapentaplegic homolog 4

SMARCA4 – Transcription activator BRG1

SMN1 – Survival of motor neuron 1

SNARE – Snap receptors

SNV – Single nucleotide variation/variant

SNX2 – Sorting nexin 2

SOCS – Suppressor of cytokines signalling

SSC – Side scatter

STRING – Search tool for the retrieval of interacting genes/proteins

SWATH-MS – Sequential window acquisition of all theoretical mass spectra

TBC – Tre-2/Bub2/Cdc16

TBE – Tris/Borate/EDTA

TCA – Tricarboxylic acid

TGF-β – Transforming growth factor beta

TIMP-1 – Tissue inhibitor of metalloproteinase 1

TIP47 – Perilipin-3

TP53 – Tumour protein 53

TSG101 – Tumour susceptibility gene 101

TWIST1 – Twist family basic helix loop helix (BHLH) transcription factor 1

UMI – Unique molecular identifier

UPX – Ultraplex

UTP - U3 small nucleolar RNA-associated protein

VCAN - Versican

VCL – Vinculin

VEGR – Vascular endothelial growth factor

WHO – World Health Organisation

WNT – Wingless-related integration site

ZEB1 – Zinc finger E-box binding homeobox 1

Chapter 1:

Introduction

1. Introduction to cancer

Cancer is a large group of diseases characterised by the uncontrollable growth of abnormal cells. It can occur in almost any organ or tissue in the body and is capable of invading into surrounding tissues and spreading to other organs either locally or distantly. Cancer is the second leading cause of death globally, with approximately 20 million new cases and 10 million deaths each year, accounting for 1 in 6 total deaths ("World Cancer Day 2023: Close the care gap - PAHO/WHO | Pan American Health Organization,").Lung, prostate, colorectal, stomach, liver, breast, cervical and thyroid cancers are` the most common types across men and women (Louis et al., 2016).

Childhood cancers are much rarer with 280,000 children and adolescents (aged 0-19 years) being diagnosed and 110,000 dying in 2020 ("Childhood cancer – IARC,"). The most common types of cancer in children are also very different to adult with leukaemia, tumours of the brain and central nervous system (CNS), lymphomas, soft tissue sarcomas, germ cell tumours and bone tumours being diagnosed most frequently (Siegel et al., 2018). Tumours of the brain and CNS are the most common solid tumours in children. In most cases they arise from normal cells of the brain and spinal cord (neurones and glia) and are often named according to their tissue of origin, genetic alterations within the tumour and whether it most commonly arises in children or adults. Mortality and morbidity rates for brain and CNS remain the highest of all childhood tumours with current treatment options resulting in developmental, neurological and health complications (Pollack et al., 2019). Survival rates are affected by high rates of chemoresistance, the highly metastatic nature of certain tumours and the lack of clinical trials which focus on developing new treatment options for children with these tumours. Therefore, there is a need for research and insight into the mechanisms of disease progression to inform the development of new targeted therapies with reduced side effects.

The most common forms of childhood brain tumours are astrocytomas, ependymomas and medulloblastomas ("Medulloblastoma | Children's brain tumours,"). This study focuses on medulloblastoma, the most common malignant paediatric brain tumour.

1.1. Medulloblastoma

Medulloblastoma accounts for 20% of paediatric brain tumour cases and 10% of all paediatric cancer deaths ("Medulloblastoma Statistics | medulloblastoma.org,") (Northcott et al., 2019a). It is classified by the World Health Organisation (WHO) as a grade IV tumour type due to its malignant and fast-growing nature. It is the main embryonal tumour located in the infratentorial region of the brain (cerebellum; Figure 1.1.) (Louis et al., 2021a) (Formentin et al., 2023) and most often affects children aged 3-8 years although it also occurs in infants, adolescents and less commonly, adults.

Approximately 50 children are diagnosed in the UK each year and it is more common in boys than girls ("Medulloblastoma, Children's brain tumours, Cancer Research UK,"). It is a biologically heterogeneous disease, consisting of four distinct molecular subgroups; Wingless (WNT), Sonic hedgehog (SHH), Group 3 and Group 4 and is found in the cerebellum and fourth ventricle of the posterior fossa (Figure 1.1.) (Schwalbe et al., 2017) (Pizer and Clifford, 2009).

1.1.1. Diagnosis

Medulloblastoma is diagnosed using CT (computed tomography) and MRI (magnetic resonance imaging) where patients present with a solid mass in their cerebellum with variable enhancement, abnormal restricted diffusion and absence of intratumoural haemorrhage or calcifications (Figure 1.2.) (Rapalino et al., 2016). A positive MRI is generally considered a compulsory requirement before treatment options can be explored (Massimino et al., 2016).

Diagnosis typically occurs after symptoms occur. These symptoms are typically slow to develop, over weeks or months prior to diagnosis. Many of these symptoms are non-specific to the disease resulting in a diagnostic delay (Millard and De Braganca, 2016). Symptoms include headaches, nausea, double vision, ataxia, behavioural changes, loss of appetite and irritability. Symptoms are most often associated with the effects of tumoural growth within the cerebellum which leads to cerebellar

dysfunction and an increase in intracranial pressure (Millard and de Braganca, 2016).
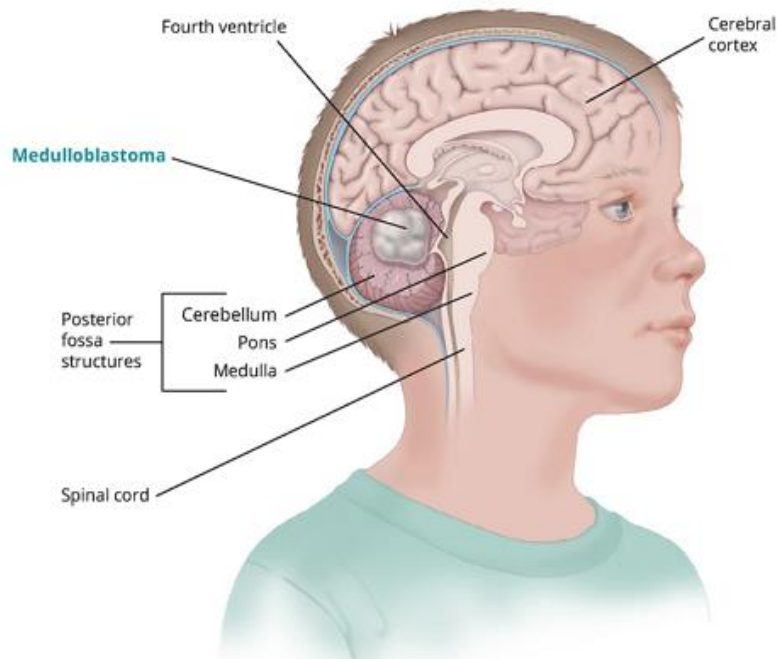
Figure 1.1. Medulloblastoma location within the brain
Medulloblastoma is found in the infratentorial region of the brain in the cerebellum of the posterior fossa adjacent to the fourth ventricle. Image adapted from stjude.org.
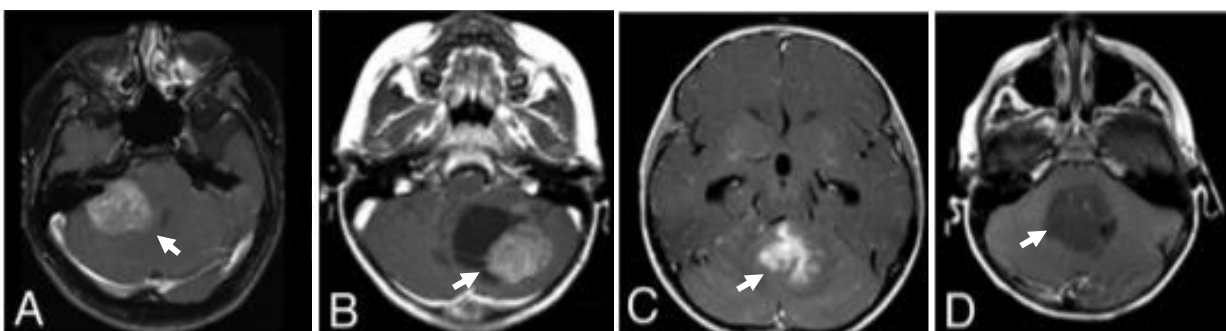
Figure 1.2. – MRI characteristics of the medulloblastoma subgroups *Position of tumour is highlighted by a white arrow. A) WNT. Characteristic location in cerebellopontine angle, or the lower rhombic lip of the dorsal midbrain, is shown. B) SHH. Tumours are shown in the cerebellar hemispheres. C) Group 3. Tumours are seen along the midline of the fourth ventricle. D) Group 4. They are also seen along the midline of the fourth ventricle but are non-enhancing and harder to observe compared to Group 3 tumours. Figure adapted from Perreault et al., 2014.*

<u>1.1.2. Treatment and prognosis</u>

When deciding treatment options, overall post-treatment quality of life is the biggest consideration. Tumour invasiveness and age at diagnosis are also important factors. Treatment options differ between patients aged over three years and patients under three years of age. In patients over three years old, a combination of surgery, radiotherapy to the entire brain and spinal cord, and high-dose chemotherapy is used (Millard and de Braganca, 2016) (Wu et al., 2012). In those under the age of three, surgery followed by chemotherapy only is used, as long-term side effects of radiotherapy are deemed too detrimental (Grill et al., 2005). The outcome of this treatment is strongly associated with the age of the patient and the pathological features of the disease, as well as the extent of tumour resection, which is thought to affect prognosis in certain children (Albright et al., 1996) (Northcott et al., 2019).

Common side effects of current treatment include long-term neurological and sensory impairments, endocrine deficits such as growth impairments and secondary tumours. Core cognitive deficits result from cerebellar damage from the tumour and the effect of radiation on white matter development and are most often associated with working memory difficulties, low processing speed and attention difficulties which lead to lifelong psychosocial limitations (Chevignard et al., 2017). There is therefore a requirement for the better understanding of disease mechanisms such that therapies can be developed which reduce the requirement for or the impact of radiation.

Medulloblastoma prognosis is most strongly associated with age at diagnosis, extent of the disease and molecular subgroup (Cavalli et al., 2017) (Northcott et al., 2019). At diagnosis, patients are put into either a standard risk or high-risk group. These groups indicate likely five-year survival dependent on factors at diagnosis such as age, metastatic status and whether the tumour is fully surgically resectable (Millard and De Braganca, 2016) (Chang et al., 1969) (Cavalli et al., 2017) (Northcott et al., 2019).

Standard risk patients have a 70-85% five-year survival rate. This risk group includes patients that are over the age of three, non-metastatic and receive a total surgical resection (Gajjar et al., 2006) (Gandola et al., 2009). High risk patients have the

poorest prognosis and highest morbidity rate with five-year survival of less than 70%. They include patients which are either younger than three years old or are metastatic at diagnosis or have >1.5cm^2 of postoperative residual tumour (Millard and De Braganca, 2016) (Albright et al., 1996).

'Chang's Staging System' was developed in 1969. It is a system used to help classify medulloblastoma patients as it gives an indication of the stage of the disease and thus potential prognosis (Table 1.1.). It considers factors including size and location of the tumour and the presence and extent of metastasis. An adapted version of it is still used to classify medulloblastoma patients today (Chang et al., 1969).

Table 1.1. – Chang's Staging System for medulloblastoma *Adapted from Chang et al., 1969 and Dufour et al., 2012.*

Tumour stage		Metastasis	
T1	Tumour is <3 cm in diameter. Present in the vermis, roof of the fourth ventricle or cerebellar hemisphere	M0	No metastases
T2	Tumour is >3 cm in diameter. Invading an adjacent structure or partially filling the fourth ventricle.	M1	Migrating cells present in the cerebrospinal fluid.
T3a	Tumour is invading two adjacent structures or completely fills the fourth ventricle.	M2	Presence of intracranial dissemination.
T3b	Tumour arises from the floor of the fourth ventricle or the brain stem. Tumour fills the fourth ventricle	M3	Presence of intraspinal dissemination.
T4	Tumour invades the third ventricle or midbrain or the cervical cord.	M4	Systematic dissemination outside of the cerebrospinal axis (i.e. to bone marrow).

There are currently no known environmental causes of medulloblastoma, with heritable factors being the only proven risk factors for the disease (Northcott et al., 2019). Germline mutations are thought to account for 5-6% of medulloblastoma diagnoses (Waszak et al., 2018). Most mutations result in the deregulation of specific cellular pathways which then go on to cause tumour development. Individuals with syndromes deriving from mutations in the WNT or SHH signalling pathways, for example, present with an increased likelihood of developing brain tumours. People with Gorlin syndrome and Familial Adenomatous Polyposis (FAP) syndrome, which are associated with mutations in the SHH (such as *PTCH1* and *SUFU*) and WNT (such as *APC*) pathways respectively are more likely to develop medulloblastoma, Rubinstein-Taybi syndrome is also a risk factor (Smith et al., 2014) (Cohen, 1982) (Evans et al., 1993). These genetic predispositions are also thought to have a detrimental effect on the five-year overall survival rate, with survival estimates being closer to 65% (Waszak et al., 2018). Specific germline mutations which are associated with an increased risk of developing medulloblastoma include *BRCA2* (breast cancer gene 2), biallelic mutations of which are responsible for Fanconi Anaemia for which there is also an association with medulloblastoma (Waszak et al., 2018) (Tischkowitz et al., 2004). Loss of function variants of *ELP1* (elongator acetyl transferase complex subunit) have also been associated with particularly younger patients with SHH medulloblastoma (Waszak et al., 2020).

Certain demographic factors have been shown to increase likelihood and development of medulloblastoma. These include age, with children being ten times more likely to develop medulloblastoma than adults, and sex, with 1.7 males for every 1 female between the ages of 0 and 14 (Giordana et al., 1999) (Smoll and Drummond, 2012) (Johnston et al., 2014) (Ostrom et al., 2017).

1.1.4. Medulloblastoma molecular subgroups

Medulloblastoma is a biologically heterogeneous disease with four principal molecular subgroups; WNT, SHH, Group 3 and Group 4 (Taylor et al., 2012) (Figure 1.3.). These groups are regarded as discrete biological and transcription variants of the disease based on differences in their demographics, clinical, genetic and cytogenetic features (Louis et al., 2016). WNT and SHH are named after the signalling pathways that are believed to play prominent pathogenic roles. Less is known about the biology and specific mechanisms which drive Groups 3 and 4 which are consequently named generically. A summary of each subgroup is shown in Table 1.2.

Subsequent research has also identified distinct intra-subgroup heterogeneity allowing for the characterisation of twelve subtypes within the medulloblastoma subgroups (Figure 1.4.). These are WNT α and β, SHH α, β, γ and δ, Group 3 α, β and γ, and Group 4 α, β and γ (Cavalli et al., 2017).
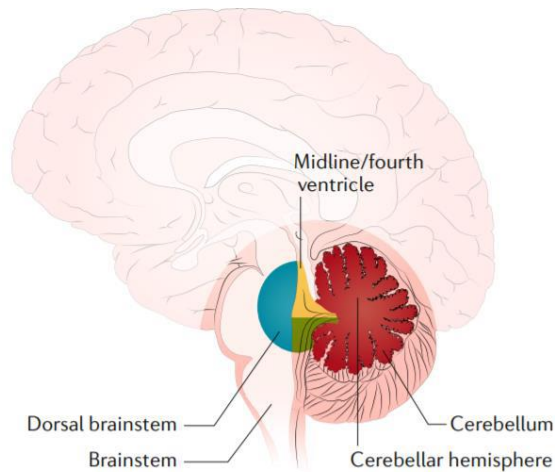
Figure 1.3. - Medulloblastoma subgroup location within the brain. *Medulloblastoma can be found within the posterior fossa of the fourth ventricle of the cerebellum. Localisation of the subgroups are colour coded; WNT (blue – lower rhombic lip and embryonic dorsal brainstem), SHH (red – cerebellar hemispheres), Group 3 (yellow – fourth ventricle touching the brainstem), Group 4 (green – centrally in the fourth ventricle). Figure reproduced from Northcott et al., 2019.*
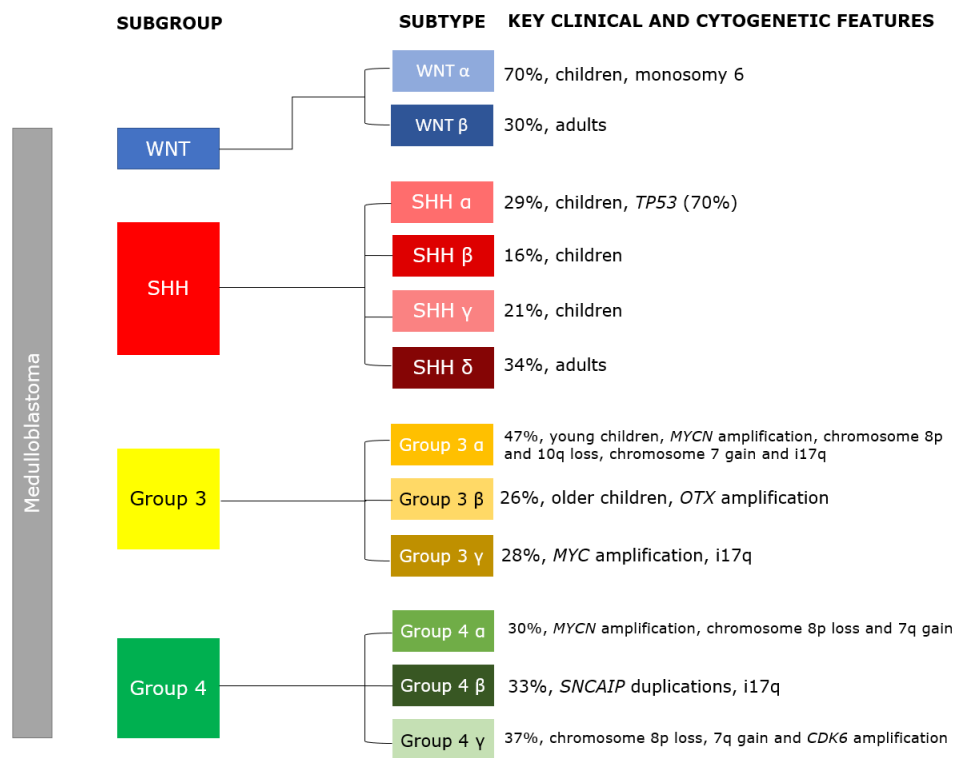
Figure 1.4. Medulloblastoma subgroups and their subtypes. *WNT (blue), SHH (red), group 3 (yellow), group 4 (green). Adapted from Cavalli et al., 2017.*

Table 1.2. – Medulloblastoma Molecular subgroups *References: Smith et al., 2022, Taylor et al., 2012, Northcott et al., 2012, Northcott et al., 2019*

		WNT	SHH	Group 3	Group 4
DEMOGRAPHICS	Age group				
	Gender ratio	♂♂:♀♀	♂♂:♀♀	♂♂ : ♀	♂♂ : ♀
CLINICAL FEATURES	Proportion of diagnoses	10%	30%	25%	35%
	Prognosis (5-year survival rate)	>90%	75%	<60%	75%
	Proportion which are metastatic upon diagnosis	<5%	20%	40-50%	35-40%
	Relapse pattern	Local and metastatic	Mostly local	Metastatic	Metastatic
	Location	Lower rhombic lip and embryonic dorsal brainstem	Cerebellar hemisphere	Fourth ventricle touching the brainstem	Centrally in the fourth ventricle
	Cell type of origin	Progenitor cells of the lower rhombic lip of the dorsal midbrain	Granule cell progenitors	Rhombic lip (photoreceptor)	Rhombic lip (unipolar brush cell)
	Histology	Classic	Classic, large cell/anaplastic, desmoplastic/nodular, MBEN	Classic, large cell/anaplastic	Classic, large cell/anaplastic
GENETICS	Distinctive genetic and cytogenetic aberrations	*CTNNB1*, *TP53* and *APC* mutations WNT pathway amplification Monosomy 6 (65% tumours) MYC +	*PTCH1*, *SMO* and *SUFU* somatic mutations *MYCN*, *GLI1* and *GLI2* amplifications HOX gene family amplification Chromosome 9q deletion MYCN +	*MYC* and OTX2 amplification *SMARCA4* mutation *GFI1/1B* activation I17q present (26% tumours) Chromosome 1q, 7, 17q gain Chromosome 5q, 9q, 10q, 11, 16q and 17p loss MYC +++	*MYCN*, *CDK6* and *SNCAIP* amplification *KDM6A* deletion *BRCA2*, *KCNA1* and *KDM* family member mutations GRM1, GRM8, KCNA1 and KCNA5 expression I17q present (66% tumours) Chromosome 7 gain Chromosome 8p, 10q and 17p loss X chromosome loss (80% females) Chromosome 11p and 18q aberrations Minimal MYC/MYCN

WNT medulloblastoma is the best characterised subgroup. It arises in older children and accounts for approximately 10% of medulloblastoma diagnoses (Gibson et al., 2010) (Kool et al., 2012a). Metastatic disease is rare in this subtype as metastases are seen in less than 10% of diagnoses (Ellison et al., 2011) (Gajjar and Robinson, 2014). It has the best prognosis of the subgroups with five-year survival exceeding 90% (Cavalli et al., 2017). Overall, WNT tumours occur almost equally in males and females. Peak incidence is in children over the age of three years old with WNT tumours being uncommon in infants (Kool et al., 2012) (Doussouki et al., 2019). It often has classic histology and is found in the lower rhombic lip of the dorsal midbrain (Figure 1.3.) and as such originates from progenitor cells of this area (Northcott et al., 2012) (Pietsch et al., 2014) (Cavalli et al., 2017) (Gajjar and Robinson, 2014).

The molecular mechanism of this subgroup is defined by the activation of the WNT/Wingless signalling pathway (Figure 1.5.) (Thomas and Noël, 2019). WNT is a family of growth factor receptors which act as a regulator of the nuclear transcription factor β-catenin (Crawford et al., 2007) (Thomas and Noël, 2019). WNT/β-catenin signalling has roles in the regulation of cellular process such as proliferation, differentiation, migration, and apoptosis through the nuclear accumulation of β-catenin (Doussouki et al., 2019) (Clifford et al., 2006). Sporadic mutations at residues 32 to 34 of *CTNNB1* (which encodes β-catenin) are present in 85-90% of WNT medulloblastoma patients (Thomas and Noël, 2019) (Eberhart et al., 2000) (Thompson et al., 2006).

Other mutations in WNT patients include loss of function mutations in APC regulator of WNT signalling pathway (*APC*) and a heterozygous mutation of Tumour Protein 53 (*TP53*, which encodes p53) (Coluccia et al., 2016) (Northcott et al., 2012b). The most common chromosomal aberration is the loss of chromosome 6 (monosomy 6) which occurs in approximately 80% of WNT patient tumours (Thompson et al., 2006) (Cavalli et al., 2017).
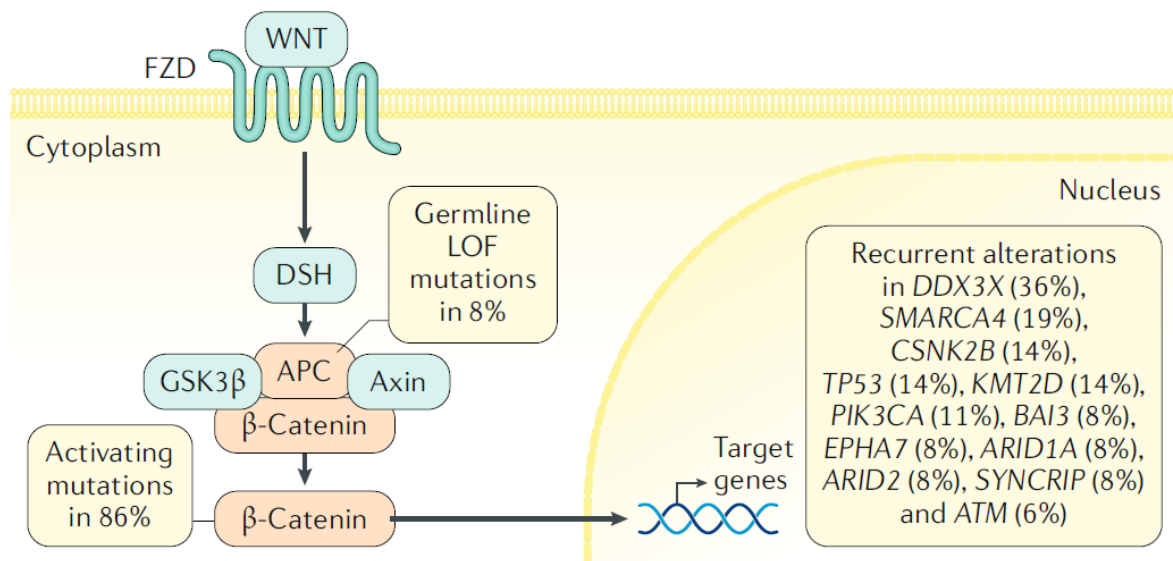
Figure 1.5. Mutations within the molecular mechanism of the wingless (WNT) subgroup *The WNT medulloblastoma subgroup is characterised by mutations within various stages of the WNT signalling pathway. Percentage values indicate the proportion of patients with WNT medulloblastoma which have the genetic mutation. LOF – loss of function. Figure obtained from Northcott et al., 2019.*

This subgroup can be separated into two further subgroups: WNT-α (70%) and WNT-β (30%) both of which are associated with good survival outcomes (Figure 1.4.) (Cavalli et al., 2017).

1.1.4.2. Sonic hedgehog medulloblastoma

Sonic hedgehog (SHH) medulloblastoma accounts for approximately 30% of medulloblastomas (Kool et al., 2012). It has a bimodal age distribution, affecting those aged less than three years or those over sixteen years of age and has an equal male: female gender incidence ratio (Kool et al., 2014) (Kool et al., 2012). Tumours are found in the cerebellar hemispheres (Figure 1.3.) and are thought to originate from granule cell progenitors which migrate from the upper rhombic lip to the external granule layer (Gibson et al., 2010). Cells commonly have a nodular/desmoplastic histology with most medulloblastoma tumours of this histology belonging to this subtype (89%) (Northcott et al., 2012) (Kool et al., 2012).

SHH has an intermediate overall five-year survival prognosis of 75%. Survival appears to depend on age at diagnosis with prognosis being better in young children and poorer in adults (Kerleroux et al., 2020). SHH metastases are found in 20% of patients at diagnosis (Kool et al., 2014). Metastasis occurs more commonly in infants (17%) and children (22%) than adults (Kool et al., 2012).

SHH medulloblastoma is named after the Sonic Hedgehog signalling pathway, which is thought to drive tumour initiation in most, if not all, patients. Germline mutations in *SMO*, *PTCH* and *SUFU* of the Sonic Hedgehog pathway are common in patients with tumours of this subgroup (Kool et al., 2014) (Thompson et al., 2006). Patients with a *PTCH* mutation have Gorlin syndrome which gives a predisposition to developing medulloblastoma (Bale et al., 1998). Deletion of chromosome 9q is limited to SHH medulloblastomas which fits with other genetic aberrations as the *PTCH* gene is located on chromosome 9q22 (Northcott et al., 2011). Amplifications of *GLI1* and *GLI2* have also been associated with this subgroup (Northcott et al., 2011).

This subgroup can be further subdivided into four subtypes: SHH-α (29%), SHH-β (16%), SHH-γ (21%) and SHH-δ (34%). SHH-β has the worst prognosis of the
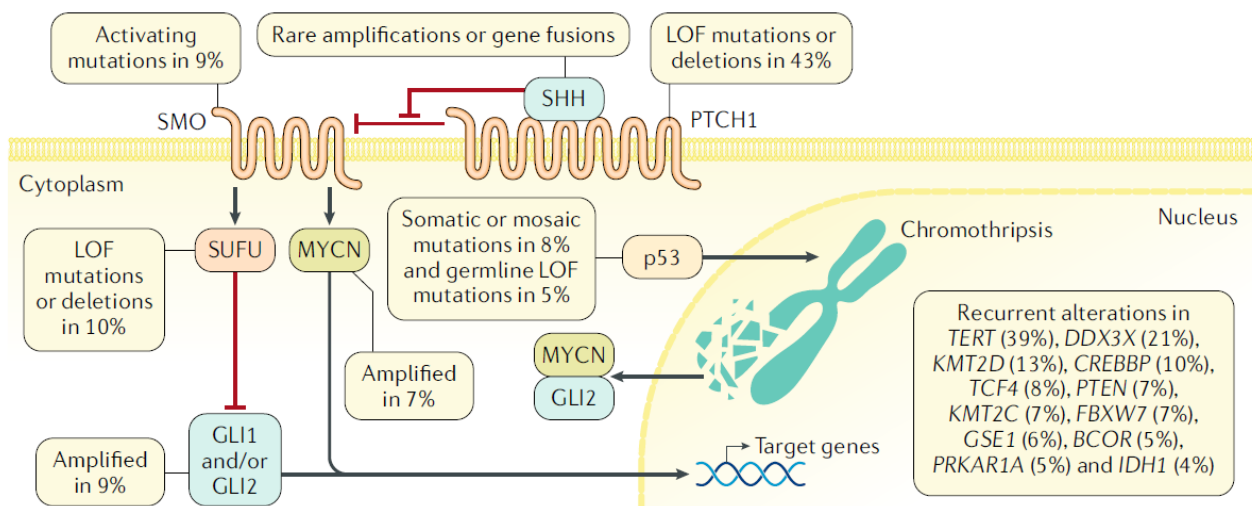
Figure 1.6. Mutations within the molecular mechanism of the sonic hedgehog (SHH) subgroup *The SHH medulloblastoma subgroup is characterised by mutations within the SHH signalling pathway. Percentage values denote the proportion of patients with SHH medulloblastoma which have the genetic mutation. LOF – loss of function. Figure obtained from Northcott et al., 2019.*

subtypes (67% five-year survival) followed by SHH-α (70%), SHH-γ (88%) and SHH-δ (88.5%) (Figure 1.4.) (Cavalli et al., 2017) (Doussouki et al., 2019).

<u>1.1.4.3. Group 3 medulloblastoma</u>

Group 3 medulloblastoma accounts for 25-30% of medulloblastomas (Kool et al., 2012) (Doussouki et al., 2019). It most often affects patients under the age of three years and there is a slight male predominance with a 2:1 male: female ratio of incidence (Taylor et al., 2012). Group 3 has the worst prognosis of the medulloblastoma subgroups with a five-year survival of 50-60% (Kool et al., 2012) (Northcott et al., 2019). Metastases are present at diagnosis in 45% cases which is believed to contribute to the poor overall prognosis (Taylor et al., 2012) (Kool et al., 2008) (Ramaswamy et al., 2014). Tumours are usually located on the midline of the fourth ventricle, touching the brainstem (Figure 1.3.). Cells of the early rhombic lip that have enrichment of photoreceptor gene sets are the proposed cell of origin of this subgroup (Perreault et al., 2014) (Smith et al., 2022a). Cells of this subgroup have either classic or large cell/anaplastic (LC/A) histology with the majority of medulloblastomas with LC/A histology being in this subgroup (Kool et al., 2012) (Coluccia et al., 2016).

Only a few somatic mutations and no germline mutations have been associated with the development of group 3 tumours (Gajjar and Robinson, 2014). Mutations of the oncogene *MYC* are the most common mutations in Group 3 tumours (Hatten and Roussel, 2011) (Northcott et al., 2012). Mutations in *OTX2* (orthodenticle homeobox 2) and *SMARCA4* (transcription activator BRG1) are also common (Jones et al., 2012) (Adamson et al., 2010). Group 3 tumours also over express several genes with roles in retinal development, however the role of these in group 3 pathogenesis is currently unclear (Smith et al., 2022). Chromosomal rearrangements are also common in this subgroup including the chromosomal aberration isochromosome 17q (i17q).

Isochromosome 17q is the most common chromosomal aberration across the medulloblastoma subgroups with 20-30% of patients presenting with it (Koczkodaj et al., 2021). It is a cytogenetic feature of both group 3 and group 4 patients but is only

associated with poor prognosis in group 3 patients, suggesting that it could be a prognostic biomarker of this subgroup (Cavalli et al., 2017) (Shih et al., 2014). It is characterised by the duplication of the q long arm of the chromosome and the loss or almost total loss of the p short arm, with multiple variants of this aberration being observed within the patient population (Pan et al., 2005) (Mendrzyk et al., 2006). The majority of breakpoints (or location within the chromosome where DNA may be deleted, inverted or swapped around) are close to the centromere, leading to the generation of an isodicentric chromosome, or chromosome with two centromeres, and a short, mirrored replication of part of the p short arm (Figure 1.7.). A common breakpoint occurs at 17p11.2 (Mendrzyk et al., 2006). Therefore, these patients possess three q long arms of the chromosome and one full p short arm. As such, there is a gain of copies of genes present on the q long arm of the chromosome and a loss of copies of genes present on the p short arm.

Other chromosomal aberrations identified in tumours of this subgroup include the gain of chromosomes 1q and 7, and the deletion of chromosomes 5q, 9q, 10q, 11 and 16q (Kool et al., 2012).
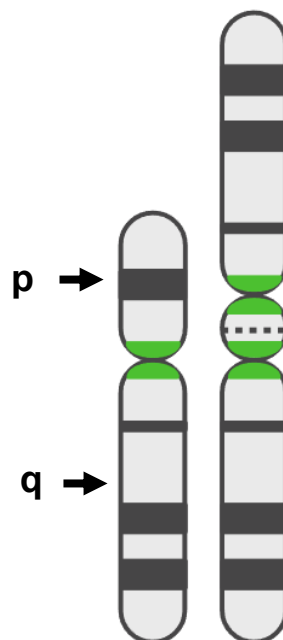
*Figure 1.7. – **Isochromosome 17q** Isochromosome 17q is characterised by the presence of one chromosome with a long and a short arm (left) and a second chromosome with a duplication of the long arm and a small portion of the short arm leading to two centromeres (right). Sequence either side of the centromere is shown in green. The point of duplication of the short arm sequence is shown by a dotted line.*

Group 3 medulloblastoma can be subdivided into three subtypes; Group 3-α (47%), Group 3-β (25%) and Group 3-γ (28%) with Group 3-γ having the worst prognosis (42% 5-year survival) of the subtypes (group 3 α and β, 66% and 56% respectively) (Figure 1.4.) (Cavalli et al., 2017).

1.1.4.4. Group 4 medulloblastoma

Group 4 medulloblastoma is the most common subgroup, accounting for approximately 35% of diagnoses (Kool et al., 2012). Patients with tumours of this subgroup have an intermediate prognosis (75% 5-year survival) and 30-40% are metastatic at diagnosis (Northcott et al., 2012) (Ramaswamy et al., 2016). Tumours are non-enhancing on MRI scans, making them less visible and thus harder to diagnose than tumours of other subgroups (Figure 1.2.) (Perreault et al., 2014).

Group 4 occurs most frequently in children aged 3-16 years and is much more common in males than females across all age groups (Northcott et al., 2012) (Kool et al., 2012). Tumours are found in the midline of the fourth ventricle (Figure 1.3.) and frequently present with classic histology with large cell/anaplastic histology also being observed in some patient tumours (Kerleroux et al., 2020) (Archer et al., 2017). Unipolar brush cells arising from cells of the early rhombic lip are the proposed cell type of origin of this subgroup (Smith et al., 2022).

Groups 3 and 4 are the most similar of the subgroups (Sharma et al., 2019). Whilst they are demographically, clinically and genetically distinct, they still share some genetic and cytogenetic features (Taylor et al., 2012). The most prominent commonality and the most common cytogenetic change in group 4 tumours is isochromosome 17q (Figure 1.5.) (see section 1.1.4.3.) which is present in 60-70% of group 4 patients, it is not prognostically significant in this subgroup, however (Kool et al., 2012). Another notable cytogenetic change is the loss of an X chromosome in 80% of females with group 4 medulloblastoma (Taylor et al., 2012). Other genetic features of this subgroup include mutations in *KCNA1* (potassium voltage-gated channel subfamily A member 1) and a *KDM6A* (lysine demethylase 6A) deletion (Menyhárt et al., 2019) (Northcott et al., 2012).

As with group 3, group 4 can be subdivided into three subtypes: Group 4-α (30%), Group 4-β (33%) and Group 4-γ (37%) (Figure 1.4.) (Cavalli et al., 2017).

1.1.4.5. Modelling the medulloblastoma molecular subgroups

With understanding of the molecular landscape of the subgroups and the cells from which they originate growing, it is important to consider how the subgroups may be studied. This is so that accurate preclinical models can be established, which allow for further insight into medulloblastoma pathogenic mechanisms.

Murine models of all four subgroups have been invaluable for furthering the understanding of the molecular mechanisms which drive the medulloblastoma subgroups. Generally, these models involve genetic engineering or in utero electroporation.

These models have been predominantly established for the SHH subgroup for which there are multiple definable mutations which can be genetically exploited including *PTCH1*, *SMO* and *SUFU* (Wu et al., 2011). Gibson et al. (2010) were able to establish the first bona fide mouse model of non-SHH medulloblastoma through the development of a WNT mouse model which manipulated the *CTNNB1* gene. Other models which are independent of the SHH hedgehog pathway often have a *Tp53* null background or involve the modifications of the *MYC/MYCN* genes (Kawauchi et al., 2012).

Models which involve genetic engineering have been successfully developed which are able to recapitulate the molecular landscape of groups 3 and groups 4 (Kawauchi et al., 2012) (Forget et al., 2018). Whilst these models are able to provide insight into molecular properties of the subgroups, developmental differences between human and murine cerebellums mean that there is an absence of rhombic lip cells with either photoreceptor or unipolar brush cell signatures which delineate the group 3 and group 4 cell types of origin respectively (Smith et al., 2022a). Therefore, murine models may not be the most suitable for the development of effective models for group 3 and 4 medulloblastomas.
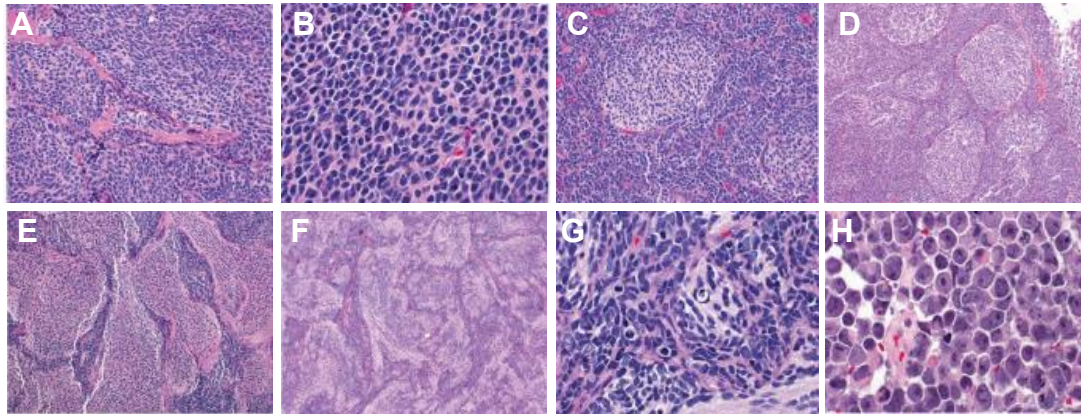
Figure 1.8. Histological images of the four medulloblastoma histology variants. *Classic medulloblastoma (A and B) shown by small cells with round nuclei and the presence of Homer Wright rosettes (A). Desmoplasmic/nodular (C and D) shown by nodules of neurocytic cells surrounded by in internodular areas. Medulloblastoma with extensive nodularity (E and F) larger extended nodules which sometimes group together and are surrounded by small internodular areas. Large cell/anaplastic medulloblastoma (G and H). Anaplastic cells (G) which are large and show cell moulding. Large cells (H) which are large with prominent nuclei. Image adapted from* Orr, 2020 *with figure legend details based off information provided by Orr.*

1.1.5. Histology

Medulloblastoma is classified as an embryonal grade IV tumour with multiple distinct histological variants (Louis et al., 2016). These histological variants are themselves distinct from the four molecular subgroups (WNT, SHH, Group 3 and Group 4). There are four histological variants associated with medulloblastoma: classic, desmoplastic/nodular (D/N), medulloblastoma with extensive nodularity (MBEN) and large cell/anaplastic (LC/A) (Gilbertson and Ellison, 2008). The classic and large cell/ anaplastic histologies are associated with a poor prognosis whilst desmoplasmic/ nodular and MBEN correlate with better patient outcomes (Liu et al., 2022). Physical features of each histological variant are shown in Figure 1.8.

Classic medulloblastoma is the most common histological subtype with approximately 70% of medulloblastoma tumours presenting with this variant. It characteristically presents with cells which have a high nuclear-to-cytoplasmic ratio and round-to-oval or triangular hyperchromatic nuclei (Massimino et al., 2016)

(Figure 1.8. A and B). These cells are typically densely packed and are small with a round or ellipsoid morphology with Homer Wright rosettes (differentiated tumour cells grouped around a central region) being frequently observed (Orr, 2020).

Desmoplastic/nodular medulloblastoma accounts for approximately 10% of tumours. Cells have a uniform neurocytic phenotype with dense intercellular reticulin-positive (fiber in connective tissues which form a fine meshwork of crosslinks) and nodular reticulin-free zones (Figure 1.8. C and D) (Orr, 2020) (Massimino et al., 2016). These reticulin-free zones are thought to represent areas of neuronal maturation whilst reticulin-positive cells are mitotically active and produce a dense network of reticulin fibres. Additionally, cells have a reduced nuclear-to-cytoplasmic ratio (Massimino et al., 2016).

Medulloblastoma with extensive nodularity is the rarest histological form, accounting for 3% tumours. It is thought to be a variant of the desmoplastic/nodular histology but differs due to the presence of elongated reticulin-free zones giving it an expanded lobular appearance. Cells themselves are generally small with round nuclei with nodules tending to be irregular with a 'streaming' pattern wherein neurocytic cells connect adjacent cellular nodules (Figure 1.8. E and F) (Massimino et al., 2016) (Orr, 2020).

Large cell/anaplastic medulloblastoma is the second most common histology, representing approximately 17% of tumours. It is comprised of two main histologies, large cell and anaplastic cells (Giangaspero et al., 1992) (Eberhart et al., 2002). Large cells have increased size with round, vesicular nuclei and prominent nucleoli and an abundant eosinophilic cytoplasm. They are surrounded by anaplastic cells which have also have an increased side, but have marked nuclear pleomorphism and nuclear moulding, are mitotically active and have visible apoptotic bodies (Figure 1.8. G and H) (Massimino et al., 2016) (Orr, 2020) (Gilbertson and Ellison, 2008).

1.1.6. Metastatic medulloblastoma

Metastases around found in approximately 40% of patients at the time of diagnoses (Wu et al., 2012b). This incidence varies from subgroup to subgroup with WNT medulloblastomas rarely metastatic (<10%) and metastases present in SHH, groups

3 and 4 in 20%, 45% and 30-40% of patients respectively (Ellison et al., 2011)(Gajjar and Robinson, 2014) (Kool et al., 2014) (Taylor et al., 2012) (Northcott et al., 2012).

Medulloblastoma metastases are confined to the cerebral spinal fluid (CSF) pathways and are almost always identified in the leptomeninges (Figure 1.9.) (Bailey et al., 1995). The leptomeninges are the two innermost layers of tissue which cover the brain and spinal cord and contain CSF which is believed to facilitate the dissemination of medulloblastoma cells. Systemic metastasis has been identified in medulloblastoma patients, but this is rare and often associated with patients who present with advanced disease (Garzia et al., 2018).

There are two principal patterns of metastatic dissemination in medulloblastoma metastases: nodular and laminar. Nodular metastases are rounded in appearance and are easily measured in three dimensions whilst laminar metastases are not detectable in three dimensions and are less easily identifiable as they resemble a 'sugar-coating' on MRI scans (Figure 1.10.) (Dufour et al., 2012). Subgroup-specific associations with these patterns of metastatic dissemination have been observed, with SHH presenting with exclusively nodular, Group 3 predominantly laminar (87.5%) and Group 4 mostly nodular with some presenting with laminar metastases (Zapotocky et al., 2018).

Patterns of medulloblastoma metastasis also appear to be subgroup specific. SHH rarely show metastatic dissemination and more commonly have local recurrences if the disease recurs (Ramaswamy et al., 2013). If seen, however, dissemination is most often observed in the cerebellar hemispheres (Zapotocky et al., 2018). Group 3 metastases are often found in the fourth ventricle and suprasellar metastases delineate Group 4 metastases which are commonly found in the fourth ventricle and in the infundibulum (Ramaswamy et al., 2013) (Zapotocky et al., 2018).
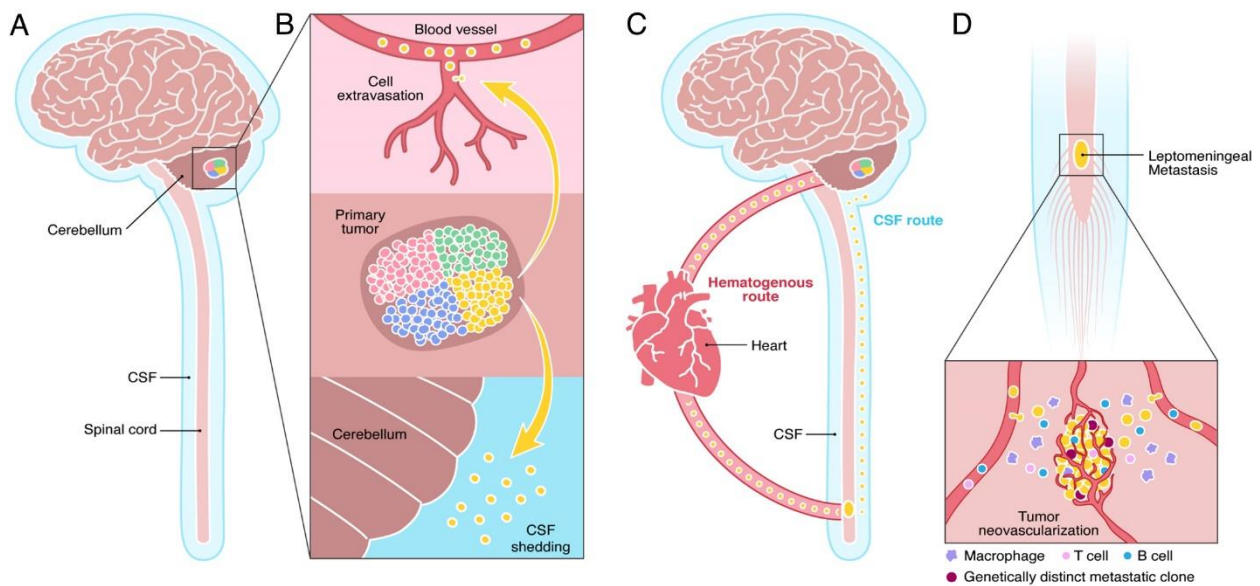
Figure 1.9. Mechanisms and patterns of medulloblastoma metastasis *A) Primary tumours are located within the cerebellum. Cells display intratumoural heterogeneity in which subpopulations may have metastatic potential. B) Metastatic cells shed into the CSF or extravasate into blood circulation. C) Metastatic tumour cells colonise distant sites by travelling via a CSF or haematogenous route. D) Once at a metastatic niche, metastatic cells genetically diversify from primary tumour cells and begin interactions with the local microenvironment. Image obtained from Juraschka and Taylor, 2019.*
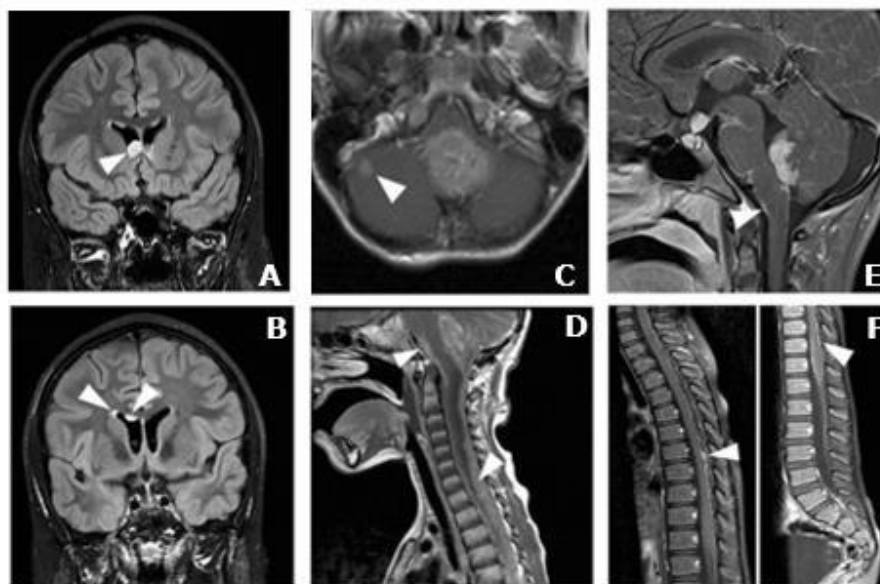
Figure 1.10. – Medulloblastoma nodular and laminar metastasis patterns *MRI images of medulloblastoma metastases. Metastases are highlighted using white arrows – A and B) Nodular supratentorial metastases. C) Solitary nodular metastasis. D) Laminar metastasis of the spinal column. E and F) Laminar metastases with nodules of the brainstem (E) and spinal column (F). Figure adapted from* Svalina et al., 2016.

Presence of metastases at diagnosis is an indicator of poor prognosis in all subgroups except WNT (Kuzan-Fischer et al., 2018). In fact, mortality among medulloblastoma is rarely due to the effects of the primary tumour and more commonly associated with the presence of metastasis both initially and at the time of recurrence (Garzia et al., 2018) (Morrissy et al., 2016). Patients with metastasis see a vastly reduced five-year survival prognosis with those with nodular metastases having a 59% chance of five-year survival and those with laminar having a 35% chance (Dufour et al., 2012). Consequently, the presence of metastatic dissemination and/or recurrence is the most important clinical feature when predicting patient prognosis (Van Ommeren et al., 2020).

There is currently no cure for medulloblastoma metastasis, with little known about the specific molecular mechanisms that allow for cellular dissemination into and survival within the leptomeninges. It is known that metastatic tumours are heterogeneous compared to the primary tumour and that certain pathways may play a role in driving metastasis, including the PI3K (phosphoinositide 3-kinase) pathway (Veneroni et al., 2017) (Wu et al., 2012). However, there is currently no metastasis-specific treatment options available. There is, therefore, a requirement for the investigation into the mechanisms of medulloblastoma metastasis and the development of novel therapeutics to improve prognosis of metastatic patients.

1.2. Extracellular vesicles

1.2.1. Cell-to-cell communication

Cell-to-cell communication is the evolutionarily conserved way in which a cell is able to interact with its microenvironment. It is essential for the maintenance of homeostasis, allowing cells to respond to alterations within its surrounding environment. It is also involved in the pathogenesis of many diseases such as immune deficiency disorders and cancer metastasis (Armingol et al., 2020).

Communication can be either direct; involving the exchange of molecules through gap junctions or nanotubes or indirect; involving the secretion of signalling molecules into the extracellular space where they interact with recipient cell membrane receptors (Grimmelikhuijzen and Hauser, 2012) (Abounit and Zurzolo, 2012) (Orellana et al., 2012) (Simons and Raposo, 2009). Signalling molecules include cytokines, inflammatory mediators, metabolites, hormones, nucleic acids and active enzymes. It is now widely recognised that extracellular vesicles (EVs) play a role in indirect cell-to-cell communication pathways wherein they transport a wide variety of cargo, including proteins, DNA and RNA, to cells both locally and at further distances within an organism (Simons and Raposo, 2009).

'Extracellular vesicle' is a general term referring to any particle released from a cell which have a lipid bilayer and are unable to replicate (Théry et al., 2018). The term encompasses an expanding category of heterogeneous vesicles with diverse contents, properties and functions (Van Niel et al., 2018). These contents are specific to the cell of origin and are able to influence recipient cell function (Yáñez-Mó et al., 2015).

1.2.2. Types of extracellular vesicle

Extracellular vesicles are a heterogeneous population of vesicles, subtypes of which are differentiated through their size and biogenesis pathway (Théry et al., 2018) (Yáñez-Mó et al., 2015). Consensus has not yet been met on specific markers of EV

subtypes but it is generally accepted that there are three primary classifications; those of endosome-origin 'exosomes', those which are plasma-membrane derived 'ectosomes' (microparticles/microvesicles) and apoptotic bodies (Figure 1.11.) (El Andaloussi et al., 2013) (Théry et al., 2018). Other forms of EVs include autophagic EVs, stressed EVs (stressome), matrix vesicles, exomeres and non-vesicular particles (Sheta et al., 2023).
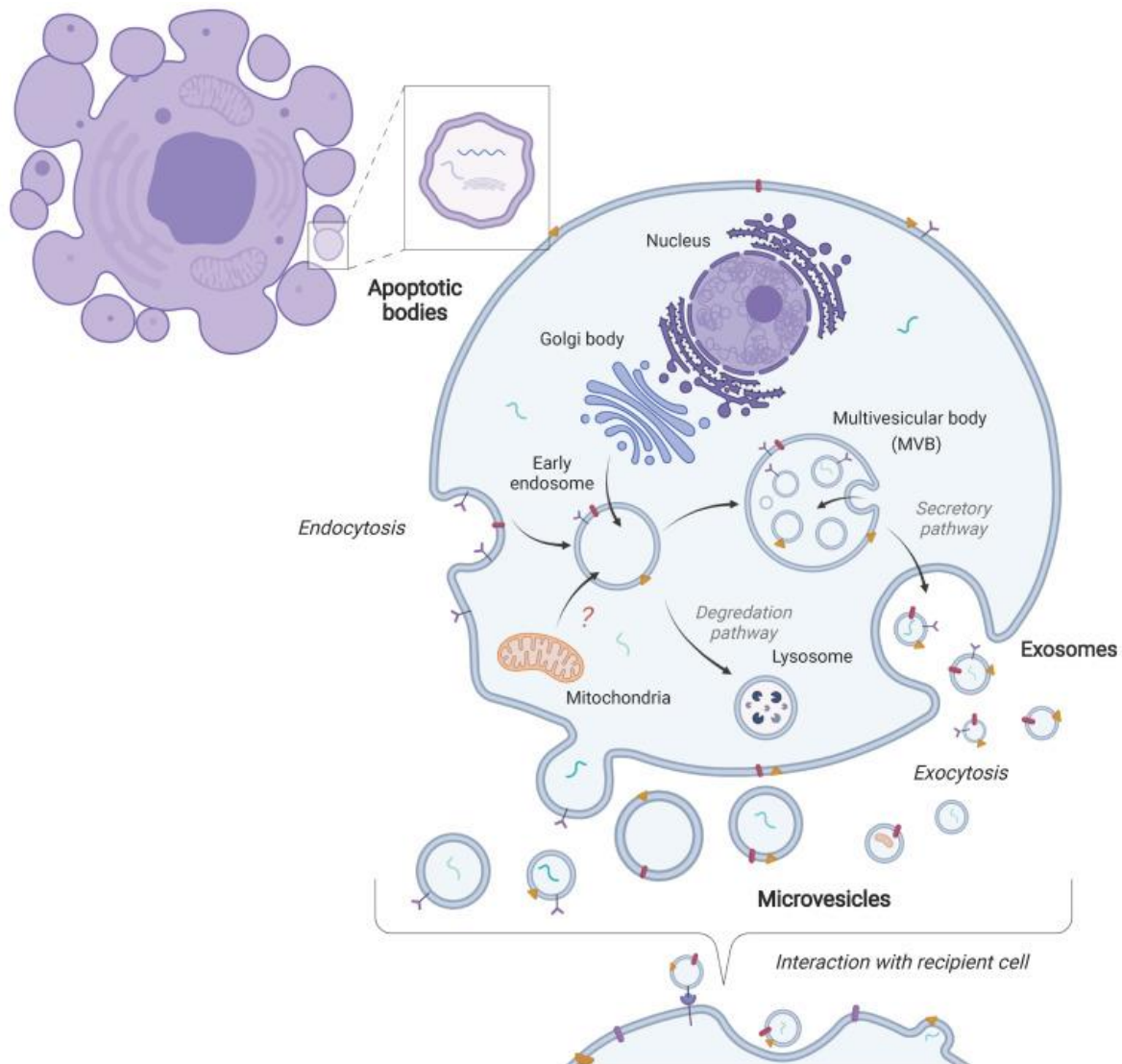
Figure 1.11. Overview of mechanisms of microvesicle, exosome and apoptotic body biogenesis and release (Bottom) Microvesicles are released through budding and shedding mechanisms from the cell membrane and contain a diverse range of cargo including cell surface proteins. (Centre) Exosomes are generated through the endosomal pathways and exocytosed. (Top left) Apoptotic bodies bleb from the plasma membrane during apoptosis. As microvesicles and exosomes are both derived from healthy donor cells and apoptotic bodies originate from apoptotic cells, there is believed to be greater cargo similarities between microvesicles and exosomes than with apoptotic bodies. Image obtained from Noren Hooten et al., 2022.

1.2.2.1. Apoptotic bodies

Apoptotic bodies are a form of extracellular vesicle which are released by cells that are in the last stage of apoptosis. They appear after the disassembly of an apoptotic cell into subcellular fragments and their formation is considered a hallmark of apoptosis (Nederveen et al., 2021) (Ihara et al., 1998). Apoptotic bodies are the largest form of extracellular vesicle with a diameter of 50-5000 nm and are morphologically and compositionally distinct from other forms of EV. They are also distinct in their method of secretion (Liu et al., 2018) (Théry et al., 2001). They contain a wide variety of cellular components including degraded proteins, DNA fragments, large amounts of RNA, lipids, chromatin remnants and intact organelles (Crescitelli et al., 2013) (Bayraktar et al., 2017). The only markers of apoptotic bodies is the presence of phosphatidylserine (PS) on the outer membrane. During apoptosis, lipids are rearranged such that PS which is usually present on the cytoplasmic face of the cell membrane is externalised this can then be detected to identify apoptotic bodies (Durcin et al., 2017) (Rani et al., 2023).

Little is currently known about the specific function of apoptotic bodies with most scientific progress particularly in terms of EV contribution to disease pathology has been conducted through the investigation of exosomes or microvesicles (Colombo et al., 2014).

1.2.2.2. Microvesicles

Microvesicles or ectosomes are plasma membrane-derived vesicles derived from the outward budding of the plasma membrane (Cocucci et al., 2009) (Raposo and Stoorvogel, 2013). They are approximately 100-1000 nm and are secreted from both healthy and damaged cells (Muralidharan-Chari et al., 2010). Microvesicles are highly heterogeneous in both size and composition with cargo being representative of their cell of origin. Cargo includes proteins, mRNAs and miRNAs. Secretion varies depending on cellular states and secretion stimulation. Therefore, there can also be a large variation between different cell types (Cocucci and Meldolesi, 2011).

Microvesicle biogenesis is mediated by the regulated outward budding of plasma membrane domains and the local disassembly of the cytoskeleton as well as the segregation of lipids that contribute to vesicle budding. Prior to budding, cargo proteins accumulate within the vesicle lumen. Budding then occurs after stimulation with ATP, this budding is then sustained by an increase in the concentration of free Ca^{2+} (Cocucci and Meldolesi, 2011) (Cocucci and Meldolesi, 2015). Precise mechanisms of microvesicle biogenesis are not fully characterised with work required to better understand specific mechanisms (Colombo et al., 2013).

1.2.2.3. Exosomes

The term exosome was first used by (Trams et al., 1981) to define secreted vesicles. Six years later, the term was further refined to specifically describe vesicles of endosomal origin (Johnstone et al., 1987). They are secreted from almost all cell types, including those of the CNS (central nervous system), and are found in a variety of bodily fluids including, blood, saliva and cerebrospinal fluid (CSF) (Keller et al., 2011) (Trams et al., 1981).

Exosomes are the smallest type of EV at 40-150 nm in diameter (Stoorvogel et al., 1991). As with microvesicles, they are secreted from both healthy and damaged cells and have roles in normal pathology including the immune system, brain and heart (Raposo et al., 1996) (Fröhlich et al., 2014) (Frühbeis et al., 2013) (Gupta and Knowlton, 2007) (Waldenström et al., 2012) (Vrijsen et al., 2010).

Exosomal cargo includes cell of origin-dependent composition of proteins, lipids, DNA, mRNAs and microRNAs (Figure 1.12). The specificity of this composition has been debated. Early studies on exosome composition regarded contents as cellular waste. It is now accepted that exosomes may contain specific contents which elicit changes in recipient cells and form the basis of a cell-to-cell communication network in addition to containing unwanted material (Sancho-Albero et al., 2019) (Harding et al., 2013).

Common protein constituents include the Ras family of monomeric G proteins (such as Rab GTPases, section 1.2.5.) which are thought to aid exosome docking and
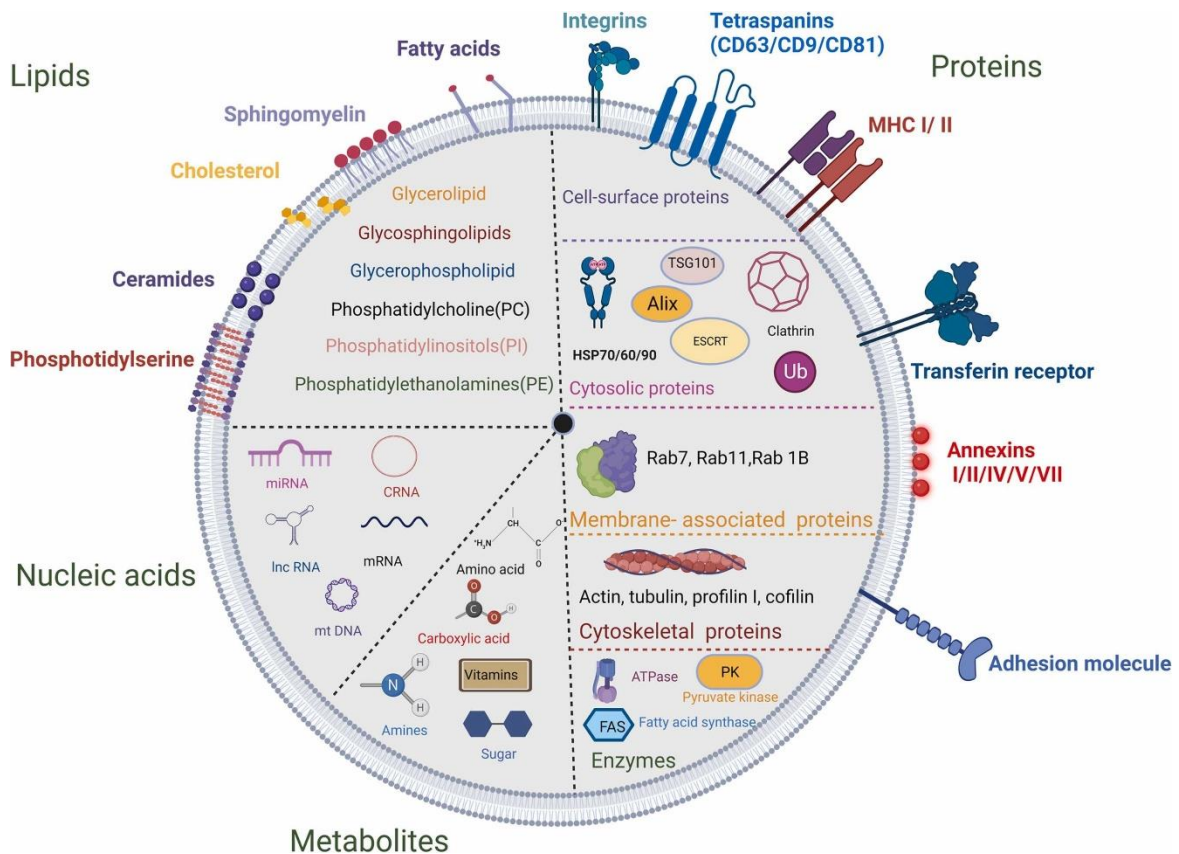
Figure 1.12. Exosomal cargo *Exosomes contain a wide variety of cargo which are present within the vesicles themselves as well as on their membranes. These include lipids such as sphingomyelin, fatty acids and glycerolipids, nucleic acids, metabolites, enzymes, cytoskeletal proteins such as actin, membrane-associated proteins including Rab GTPases, various forms of cytosolic proteins and cell-surface proteins including tetraspanins, integrins, adhesion molecules and receptors. Image obtained from Rani et al., 2023.*

fusion with other cell membranes (Schorey and Bhatnagar, 2008) (Taylor and Gerçel-Taylor, 2005). In the field of diagnostics, certain protein constituents can also be used to identify exosomes. Common exosomal marker proteins include tetraspanins such as CD9, CD63 and CD81, heat shock proteins including HSP70, HSPA8 and HSP90AA1, ALIX (Programmed cell death 6 interacting protein), GAPDH (glyceraldehyde-3 phosphate dehydrogenase) and beta actin (Figure 1.12.) (Baietti et al., 2012) (Yakimchuk, 2015) (Mathivanan and Simpson, 2009).

1.2.3. Extracellular vesicles and disease

The secretion of EVs is an evolutionarily conserved process. Similar pathways of secretion can be observed across multiple kingdoms including eukaryotes, bacteria, archaea and plants (Raposo and Stoorvogel, 2013) (Deatherage and Cookson, 2012) (Robinson et al., 2016). Initially secretion was described as a means of eliminating unrequired cellular components (Johnstone et al., 1987). Over the past few decades, however, there has been an increasing emergence of evidence suggesting a further role of EVs in the pathogenesis of many diseases (György et al., 2011).

The involvement of EVs in disease is thought to include abnormalities in EV-mediated cell-to-cell communication. Whether this is at the level of protein cargo, EV membrane protein alterations, mis-delivery to target cells or EV processing at the target, may vary between disease type or pathology. EVs have been implicated in diseases including obesity, cardiac disease, neurological diseases and cancer metastasis and spread (Shah et al., 2018) (Thomou et al., 2017) (Lyu et al., 2015) (Oggero et al., 2019) (Takahashi et al., 2002) (Verbeek et al., 2002) (Saman et al., 2012) (Hoshino et al., 2015). There is also evidence that a difference in the contents of cancer-derived EVs between early and late-stage disease phenotypes (Graves et al., 2004), suggesting that EV involvement in disease progression may be fluid depending on stage of the disease. For example, in cancers such as medulloblastoma, EVs deriving from the primary tumour may contain factors which are useful in developing the initial metastatic niche. Conversely, EVs deriving from metastases may contain factors which aid in the continued metastatic spread of the disease.

Independently of each other, both microvesicles and exosomes have been linked with disease pathogenesis and cancer progression specifically.

Microvesicles have been shown to contain bioactive molecules, nucleic acids and proteins (Cocucci et al., 2009). They can travel away from primary sites, allowing for horizontal transfer of these molecules to distant target sites and promotion of cancer metastatic niche development (Ratajczak et al., 2006) (Dolo et al., 1999) (Dolo et al., 1998) (Proia et al., 2008).

Exosomes have been implicated in a variety of diseases including stroke, neurodegenerative disease including Parkinson's disease, Alzheimer's disease and prion diseases, liver disease including inflammation and viral hepatitis, cardiomyopathy and cancer, including medulloblastoma (Li et al., 2023) (Otero-Ortega et al., 2019) (Wu et al., 2017) (Zagrean et al., 2018) (Takahashi et al., 2002) (Verbeek et al., 2002) (Hartmann et al., 2017) (Cervenakova et al., 2016) (Tamai et al., 2012) (Deng et al., 2009) (Halkein et al., 2013) (Jackson et al., 2023).

The contribution of apoptotic bodies to disease pathology is less well defined. It is hypothesised that contribution could be due to defective clearance of them or the presence of apoptotic bodies which are infected entering the extracellular space, that are then uptaken by other cells which then become infected (Yu et al., 2023). It is also suggested that they may have anti-tumour capabilities by containing tumour-associated antigens. Therefore, suggesting a that apoptotic bodies may have a therapeutic role in certain diseases instead of a pathogenic role (Palma et al., 2012) (Ruben et al., 2014) (Yu et al., 2023).

1.2.3.1. Exosomes and cancer progression

Successful metastasis is dependent on the site selected for secondary tumour formation (Fidler, 2003). Therefore, the microenvironment of a given site plays a critical role in the development of a suitable pre-metastatic niche to which the tumour cells metastasise (Guise, 2010). Tumour microenvironment evolution is driven by multiple factors including the genetic instability of malignant cells, environmental selection forces such as hypoxia and oxidative stress and the immune response (Hanahan and Weinberg, 2011). This leads to the secretion of factors including matrix metalloproteinases and VEGR (vascular endothelial growth factor) and the upregulation of processes including angiogenesis (Grange et al., 2011)(Hanahan and Weinberg, 2011). Recruitment of immune cells also enhances angiogenesis, dissemination and tumour invasion (Joyce and Pollard, 2009).

Exosomes are regularly released by tumour cells (Iero et al., 2008). As forms of cell-to-cell communication, they are thought to contain specifically packaged oncogenically active proteins and aid in the manipulation of the local primary tumour

environment to facilitate cancer progression and the early stages of metastasis (Hood et al., 2011) (Isola and Chen, 2016). Increased exosome release has been implicated in multiple cancer types including glioblastoma, melanoma, breast cancer and medulloblastoma (Skog et al., 2008) (Guo et al., 2019) (Luga et al., 2012) (Epple et al., 2012) (Bisaro et al., 2015).

There are multiple levels of the metastatic cascade that exosomes are thought to contribute to, including manipulating the local tumour environment to facilitate primary tumour progression (Seo et al., 2018), enhancing tumour cell migration and invasion (Huang et al., 2020), aiding the development of a pre-metastatic niche at a potential secondary tumour site, developing drug resistance (Lv et al., 2014) (Musi and Bongiovanni, 2023) and roles in immunosuppression (J. Liu et al., 2020). The roles of exosomes in cancer are thought to be wide-ranging and varied from cancer-to-cancer.

Studies have shown that exosomes upregulate processes including angiogenesis and contain proteins such as TGF-β, IL6, TNF-1α, matrix metalloproteinases (MMPs) and extracellular matrix MMPs inducer (EMMPRIN). These modify the tumour microenvironment are involved in the promotion of metastasis as well as the induction of stem cell-like properties (Vong and Kalluri, 2011) (Ramteke et al., 2015) (Sidhu et al., 2004) (Webber et al., 2010). In medulloblastoma, exosomal surface expression of EMMPRIN and MMP-2 (matrix metalloproteinase-2) have been associated with creating a favourable extracellular environment through signalling which drives metastasis (Jackson et al., 2023). Therefore, connecting exosome release with modification of the tumour microenvironment to aid cancer progression.

Exosomes have also been implicated in the transfer of epidermal growth factor receptors (EGFRs) from cells expressing them to non-expressing cells. This causes downstream effects which include anchorage-independent cell growth and upregulation of anti-apoptotic gene expression, all of which drive cancer progression (Al-Nedawi et al., 2008).

Exosomes have been connected to the management of the tumour cell-initiated immune response. Immune cells play a critical role in the recognition and elimination

of tumour cells during tumour development. Tumour cells can modulate this response however, by releasing exosomes which play a role in the intercommunication between immune cells and cancer cells, creating a balance which will dictate whether the tumour-inflammatory or anti-tumoural immunity predominates (Wang and Shi, 2022) (Dvorak, 2015) (Grivennikov et al., 2010). Exosomes are believed to inhibit the anti-tumour abilities of the immune system through the activation of myeloid-derived suppressor cells which suppress the T-cell response (Chalmin et al., 2010). They are also thought to help trigger the inflammatory response by containing microRNA which act as ligands and bind to Toll-like receptors (Fabbri et al., 2012). Exosomes released from immune cells as well as from the tumour can also have complementary roles. Dendritic cell-derived exosomes are believed to activate helper and cytolytic T-cells which then kill tumour cells (Théry et al., 2002). They are also thought to enhance the activity of natural killer cells which the induce apoptosis of tumour cells (Viaud et al., 2009).

Research has shown that exosomes are involved in epithelial-mesenchymal transition (EMT). During EMT, cells lose their epithelial cell characteristics and begin to transition into mesenchymal cell phenotypes, including increased motility, which drives metastasis (Hanahan and Weinberg, 2011). Proteins involved in pathways of epithelial adherens junction and cytoskeleton remodelling, EMT (e.g. vimentin and annexin A2) and those involved in cellular movement and cell-cell signalling have all been reported within cancerous exosomes (Ramteke et al., 2015) (Jeppesen et al., 2023). In addition to this, transcription factors such as ZEB1 (zinc finger E-box homeobox 1), TGF-β (transforming growth factor beta) and TWIST1 (Twist family BHLH transcription factor 1) which induce EMT to promote tumour invasion have also been identified in exosomes, meaning that exosomal cargo could affect this process at many stages of the transition (Dai et al., 2016). Conversely, microRNAs have been identified in exosomes deriving from certain cancers, such as lung cancer which suppress EMT meaning that exosomes could have a broader role in the general regulation of metastasis through EMT (X. N. Liu et al., 2021).

Finally, exosomes are thought to facilitate the transfer of proteins such as drug transporters to one another, providing drug-sensitive tumour cells the means to pump chemotherapeutics out of the cell before cellular damage can occur and

therefore increasing the ability of cells to become chemo-resistant (Corcoran et al., 2012). This can cause downstream effects including lack of responsiveness to treatment which in turn can lead to a reduced prognosis. In addition to this, transfer of anti-apoptotic factors and DNA damage repair machinery, and influence of the tumour microenvironment are thought to affect drug resistance (Haider et al., 2020).

1.2.4. Exosome biogenesis

The contents of exosomes are determined by their biogenesis pathway. Biogenesis and release are dependent on the fusion of late endosomes and multivesicular bodies (MVBs) with the plasma membrane. This process was first visualised in rat reticulocytes in 1983 (Harding et al., 1983).
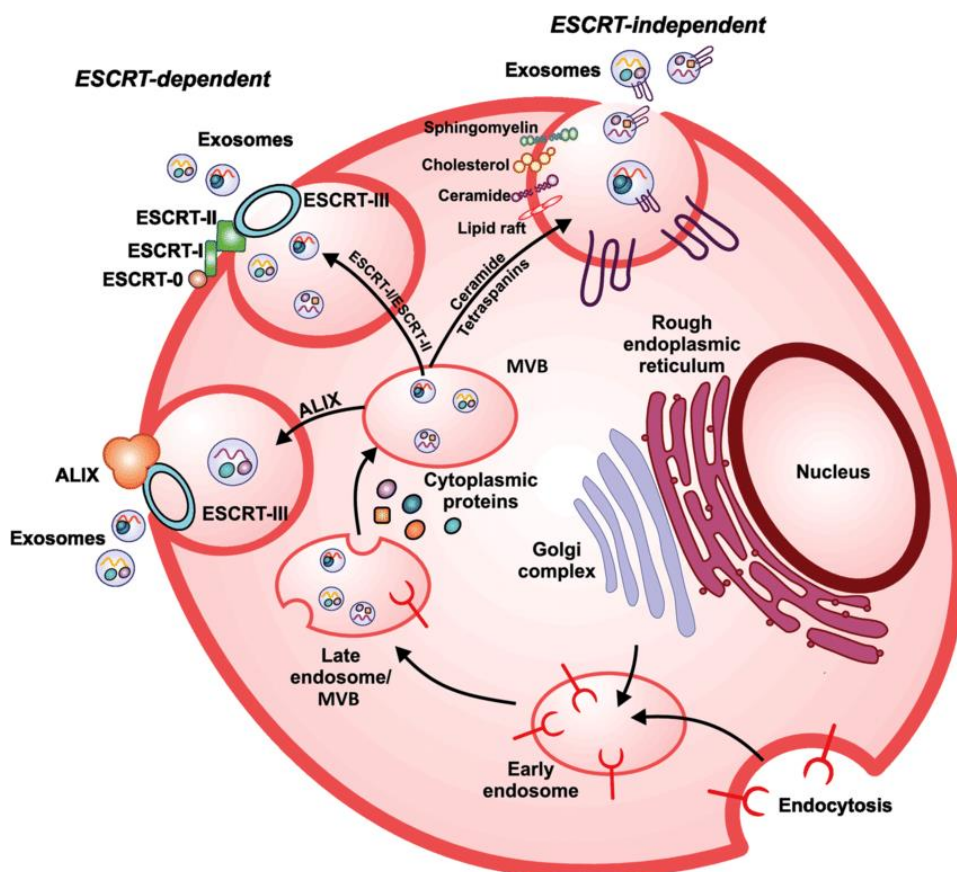
Figure 1.13. Mechanisms of exosome biogenesis *Inward budding of the cell membrane during endocytosis leads to endosome formation. Early endosomes are then formed and mature into late endosomes or MVB (multivesicular bodies). Vesiculation of the MVB occurs and cargo is loaded into the newly formed vesicles. Vesicles are then secreted through endosomal sorting complex required for transport (ESCRT)-dependent or independent mechanisms. Figure reproduced from Jadli et al., (2020).*

33

The general process of exosome formation involves firstly, activation of a growth factor receptor on the plasma membrane surface. This then leads to target protein activation and endocytosis of ligand-receptor complexes which in turn causes inward budding of small vesicles from the plasma and/or endosome membranes. This causes early endosome formation which then matures into a late endosome or MVB. This maturation involves the action of ESCRT (endosomal sorting complexes required for transport) machinery, tetraspanins and lipids. This is followed by vesiculation within the MVB wherein there is an exchange of cargo with endocytosed cargo internalised and cargo from the cytosol loaded into vesicles within the MVB or late endosome which allows for formation of exosomes. The exosome-containing MVBs or late endosomes are then transported to the plasma membrane through the cytoskeletal and microtubule network. The MVB then docks and fuses to the plasma membrane with the aid of proteins including, the SNARE (snap receptors), syntaxin and Ral and Rab GTPases such as Rab11. Exosomes are then secreted via exocytosis into the extracellular space (Figure 1.13.) (Isola and Chen, 2016) (Roma-Rodrigues et al., 2014) (Pegtel and Gould, 2019) (Mashouri et al., 2019) (Gurung et al., 2021).

Exosome biogenesis is usually an ESCRT-dependent process. Their involvement was initially described by Théry et al. (2001) who identified the roles of TSG101 (tumour susceptibility gene 101) and ALIX (programmed cell death 6 interacting protein). ALIX has since been shown to have a key role in exosome biogenesis alongside syndecan and syntenin (Baietti et al., 2012). In this process, syntenin connects syndecans to ALIX. ALIX then mediates the recruitment of the ESCRT machinery, including ESCRT-III, to late endosomes which causes endosomal membrane budding and abscission from the cell membrane (Baietti et al., 2012) (Larios et al., 2020).

Lipids also play a critical role in exosomal formation with exosomes having outer leaflets rich in PE (phosphatidylethanolamine) and PS which aid in shape formation (Booth et al., 2006) (Fang et al., 2007). Clathrin, and similar proteins, aid in the initial inward budding of the membrane (Isola and Chen, 2016).

1.2.5. Rab GTPases

Rab GTPases (Rabs) are a family of evolutionarily conserved small GTPase proteins that are part of the Ras superfamily (Seabra et al., 2002). There are 66 Rab encoding genes in the human genome and Rab proteins are responsible for regulating intracellular membrane trafficking through roles in vesicle budding, motility and fusion (Figure 1.14.) (Li and Marlin, 2015) (Agola et al., 2011) (Stenmark, 2009). Five Rabs (Rab1, Rab5, Rab6, Rab7 and Rab11) are conserved across all eukaryotic genomes suggesting they are critical for eukaryotic cell survival (Klöpper et al., 2012). In fact, Rab GTPase encoding genes are present within all eukaryotic genomes. Homologs to all Rabs present within the human genome are not present in every species, however. For example, RabX1 is present in the *Saccharomyces cerevisiae* genome but not present in humans and Rab28 is present in humans but not in *Saccharomyces cerevisiae* (Li and Marlin, 2015).

Each Rab targets to a specific membrane compartment such as endoplasmic reticulum (ER), Golgi apparatus or endosomal compartments and regulates a specific vesicular trafficking step (Chavrier et al., 1990). Membrane specificity can be regulated by GDP displacement factors (GDFs) which recognise Rabs bound to GDIs (guanine dissociation inhibitors) that aid in the shuttling of Rabs between membranes (Sivars et al., 2003) (Müller and Goody, 2018). The targeting of Rabs to specific membranes requires post-translational isoprenylation (geranylgeranylation) of usually two conserved C-terminal cysteine residues. This post translational modification involves the Rab binding to a Rab escort protein (REP) which enables a geranylgeranyl transferase to prenylate the Rab (Leung et al., 2006). These prenyl groups can act as anchors, enabling the Rab to bind to membranes. Other key structural features of Rabs include the Switch 1 and Switch 2 domains which are separated by the interswitch region. The switch domains interact with effector proteins when the Rab is GTP-bound (Zhen and Stenmark, 2015). Rabs also have hyper-variable C-terminal domain which is the most heterogeneous region of Rab structure across the Rab protein family (Pylypenko et al., 2018).

Rab action also involves them functioning as molecular switches, switching between GTP-bound active and GDP-bound inactive forms (Figure 1.15.). These active and
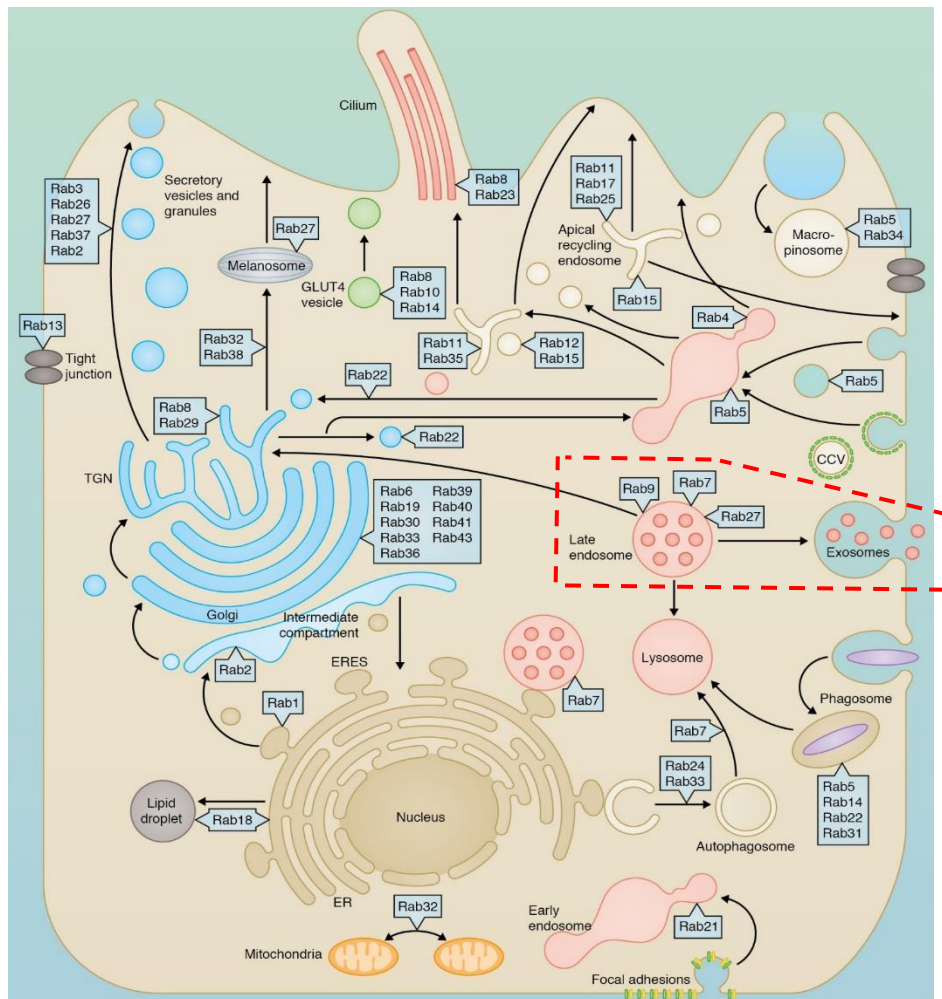
Figure 1.14. Cellular roles of Rab GTPases *Rab GTPases primarily function through the intracellular vesicular pathways transporting proteins from the endoplasmic reticulum to the Golgi apparatus and then the cell membrane. Specialised cells contain organelles such as melanosomes and cell surface features including cilia which Rabs also contribute to the transport pathways of. Each Rab GTPase has its own cell compartment-specific role. Exosome biogenesis is highlighted in red. Adapted from Zhen and Stenmark et al., 2015.*

inactive forms are regulated by GEFs (guanine exchange factors) and GAPs (GTPase hydrolase-activating proteins) which activate and inactivate them respectively (Yoshimura et al., 2010) (Haas et al., 2007).

Upon activation by GEFs, which catalyse the nucleotide exchange of GDP with GTP on the Rab, Rabs are able to interact with effector proteins. Effector proteins are recruited or activated by activated Rab GTPases and mediate cytoskeletal movements and membrane tethering, allowing Rabs to carry out their functions (Gillingham et al., 2014). Therefore, the ability for Rabs to switch between GTP
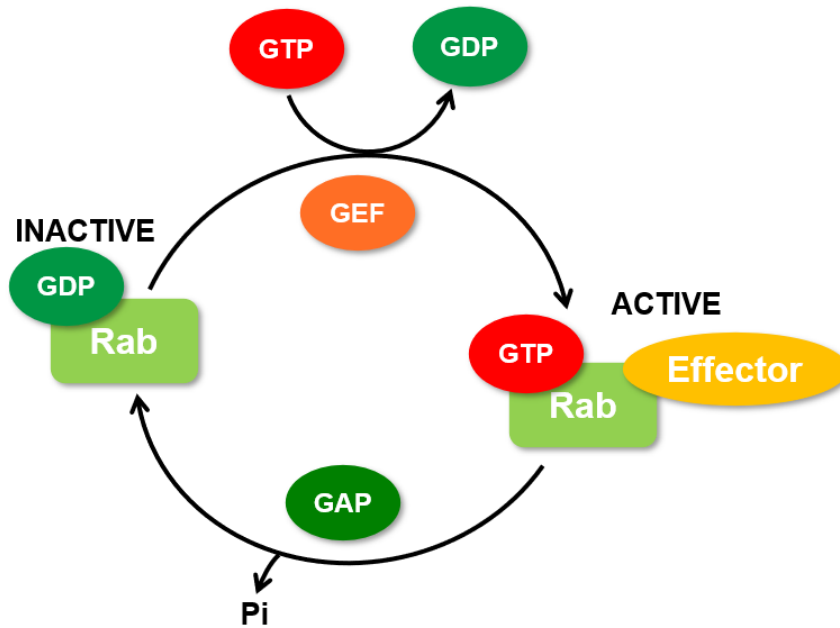
Figure 1.15. Rab GTPase cycle of activation and inactivation *Rabs cycle between GTP-bound active forms and GDP-bound inactive forms. These are regulated by guanine exchange factors (GEFs) and GTPase hydrolase activating proteins (GAPs) which activate and inactive them respectively. When GTP bound and activated, Rabs are able to bind to effector proteins which mediate cytoskeletal movement and membrane tethering.*

bound active and GDP bound inactive states can help determine the subcellular localisation of the Rab through effector binding.

1.2.5.1. Rab GTPase cycle of activation and deactivation

As mentioned, Rab GTPase function as molecular switches. In order to allow for binding of GDP and GTP, all Rabs share a conserved fold or G-domain (Vetter, 2014). This G-domain contains approximately 180 residues (Wittinghofer and Vetter, 2011) and comprises of a six-stranded β sheet surrounded by five α helices. Five loops connect the α helices and β strands. They are responsible for guanine nucleotide, and magnesium ion binding. Residues within the loops become closely associated with phosphates of the guanine nucleotide or the magnesium ion and are highly conserved amongst all Rab GTPases (Figure 1.16) (Stenmark and Olkkonen,

2001). They are surrounded by conserved fingerprint sequence motifs which surround the nucleotide-binding site. This comprises of three phosphate/magnesium binding motifs and three guanine-binding motifs. Upon GTP binding these regions mediate constraining interactions which stabilise two Switch protein domains and allows for the protein to maintain its activation state (Vetter and Wittinghofer, 2001) (Pylypenko et al., 2018).

The cycle of action of Rabs is firstly initiated by the conversion of GDP to GTP by GEFs. This induces a conformational change, allow the Rab to bind effector proteins, which include vesicular surface proteins. This allows for the Rab to be transported to vesicular membranes where it can insert the isoprenoid group which it has been post-translationally modified to have. This isoprenoid group acts as an anchor, allowing the Rab to attach to the membrane (Hutagalung and Novick, 2011).
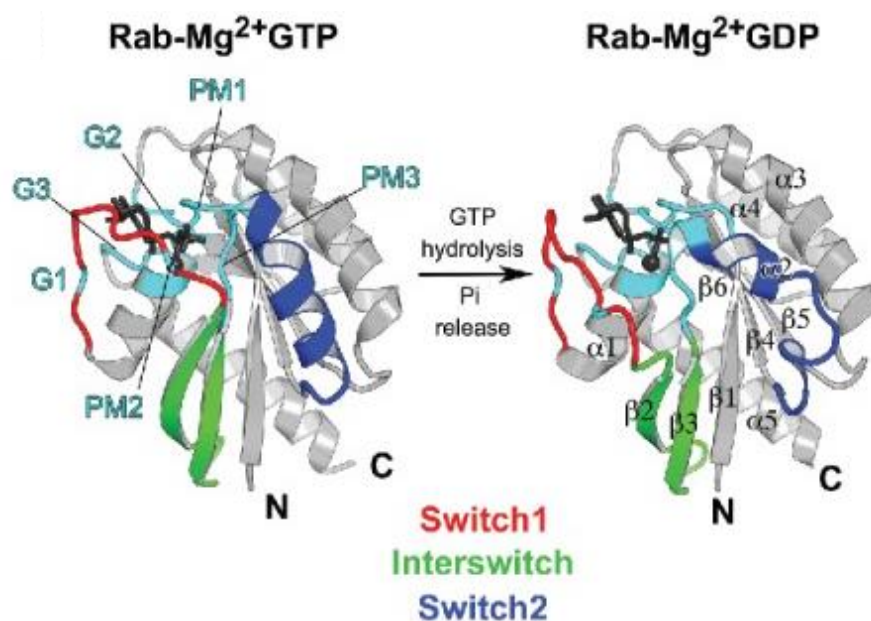
Figure 1.16. – Structures of Rab GTPase active and inactive forms Crystal structure of yeast Rab Sec4p in its GTP (left) and GDP-bound (right) forms. Both states are magnesium ion-bound (black). Switch 1 region – red, interswitch – green, switch 2 – blue. Figure adapted from Pylypenko et al., 2018.

GEFs are able to exchange GTP for GDP and GDP for GTP. The exchange of GDP for GTP bound to the Rab occurs because GTP is approximately 10-fold more abundant in the cytosol than GDP. This saturates the GEF with GTP meaning that GDP is unable to bind (Barr and Lambright, 2010). GEFs are commonly specific to a particular Rab but have been known to also act as effectors of other Rabs, generating 'Rab cascades'. In these cascades, a Rab recruits a GEF, the GEF then acts as an effector and then mediates the function of a second Rab (Homma et al., 2021). The largest group of mammalian GEFs is differentially expressed in normal and neoplastic cells (DENN) domain-containing proteins (Marat et al., 2011).

The activated Rab then interacts with effectors which are recruited from the cytosol to a membrane by interacting with an active Rab-GTP. The Rab then docks the vesicle onto the appropriate target membrane and GTP is hydrolysed to GDP by Rab GAPs, releasing the Rab from the docked vesicle. Rabs are GTPases so are able to hydrolyse GTP to GDP themselves, however Rab GAPs are able to complete this conversion much more rapidly and efficiently (Homma et al., 2021). Most GAPs are part of the TBC (Tre-2/Bub2/Cdc16) domain-containing protein family. These proteins are specific to a specific Rab and thus are associated with specific cellular functions (Fukuda, 2011) (Itoh et al., 2006)

The Rab is then recycled through the action of GDIs (guanine dissociation inhibitors) which extract the inactivated Rab from the membrane and mask the isoprenyl group allowing for retention of the Rab in the cytosol meaning that the cycle of activation, action and deactivation can start again (Müller and Goody, 2018).

1.2.5.2. Rab GTPase effectors

Rab effectors are a diverse range of proteins which are able to transduce different functions and effects (Zerial and McBride, 2001). These downstream effects include helping to select cargo, form and bud vesicles from donor membranes, transport vesicles along cytoskeletal tracks and attach and fuse vesicles with target membranes.

Effectors may have multiple different cellular functions and are often multidomain proteins, including having a Rab binding domain (RBD) which mediates the binding of the effector to the Rab and therefore Rab-specific recruitment (Wandinger-Ness and Zerial, 2014). The binding of most Rab effectors occurs at the Switch1-interswitch-Switch2 region when the Rab is in its GTP-bound active state (Pereira-Leal and Seabra, 2000) (Pylypenko et al., 2018). A secondary site has also been identified for certain Rab11 effectors which comprises of the guanine group of the nucleotide and β5-α4 (Vetter, 2014).

Certain effectors are specific to a particular Rab whilst some interact with multiple Rabs. OCRL1 (inositol polyphosphate 5-phosphatase) is able to bind to Rab1, Rab5, Rab6, Rab8, Rab14 and Rab25 through interaction with conserved residues in the Switch1-interswitch-Switch2 region (Hyvola et al., 2006). Examples of Rab-specific effectors include the Rab9 effector TIP47 (perilipin-3) which has a role in mannose 6-phosphate receptor recycling from late endosomes to the trans-Golgi network (Carroll et al., 2001). Additionally, Sec15 is a Rab11A effector. Sec15 is a subunit of the exocyst complex which is an octameric complex required for the tethering of secretory vesicles to the plasma membrane (Zhang et al., 2004) (Mei and Guo, 2018).

1.2.5.3. Rab GTPases and exosome biogenesis

Due to their roles in intracellular vesicle transport, Rab GTPases are considered to be closely associated with exosome biogenesis (Pegtel and Gould, 2019). Evidence suggests that several Rabs have fundamental roles in the process. This includes Rab27B which aids in the transfer of multivesicular bodies (MVBs) from the perinuclear area to the plasma membrane and Rab27A which facilitates docking to the membrane itself (Ostrowski et al., 2010). Rab35 is also thought to be involved in MVB docking to the plasma membrane whilst also functioning alongside Rab11 in the endosomal recycling pathway (Arya et al., 2024) (Sato et al., 2008). Rabs 11A and 11B are thought to mediate the calcium-induced homotypic fusion/maturation of MVBs and their docking and fusion with the plasma membrane (Savina et al., 2002). Rab11A interacts with members of the exocyst complex, a multi subunit complex which mediates the tethering of MVBs to the plasma membrane (Niedziółka et al.,

2024) (as shown in Figure 3.6.). The exocyst complex is believed to connect Rab11A, MVBs and the plasma membrane so that exosomes can be secreted (Bai et al., 2022a).

The role of Rab GTPases in exosome biogenesis is considered heterogeneous, however, with specific Rabs having roles depending on cell type and cargoes. Fundamentally, Rabs play a crucial role in the intracellular trafficking of vesicles, including those involved in endocytic recycling.

Other Rabs that have been associated with exosome secretion include Rab7 which is associated with late endosomes/MVBs and the cellular fate determination of whether they become lysosomes or secreted vesicles in a cell type-dependent role (Han et al., 2022) (Ostrowski et al., 2010). Rabs 2B, 5A and 9A are also thought to contribute through the enhancement of exosome secretion (Ostrowski et al., 2010).

Certain Rab GTPases have also been found within exosomes, including Rab11A and Rab11B. Those found most commonly have roles in the endocytic pathway and those with roles in other trafficking pathways are less commonly found. This highlights the endosomal origin of MVBs and the involvement of Rabs in endosomal pathways (Blanc and Vidal, 2018). This therefore poses questions about the reason for Rab presence within exosomes as it is possible for Rabs to be identified as cargo because of their involvement in exosome biogenesis (i.e. as contaminants) or packaged deliberately to be released from the cell of origin.

1.2.5.4. Rab GTPases and disease

Rab GTPases have roles in many cellular trafficking pathways and are important in maintaining cellular homeostasis. Certain Rabs, including Rab27, have been involved in the secretion of specific components that derive from different cellular compartments and are cell of origin dependent (Bobrie et al., 2012). This selective secretion as well as aberrant Rab GTPase production in general has been connected with onset of disease phenotypes. These diseases include: Alzheimer's and other neurodegenerative disorders, immune disorders, genetic disorders e.g. Griscelli syndrome (Rab27), and cancer (Veleri et al., 2018) (Kiral et al., 2018) (Prashar et al., 2017) (Ménasché et al., 2000) (Krishnan et al., 2020).

1.2.5.4.1. Rab GTPases and cancer

Over the past few decades, the role of Rab GTPases in many adult cancer types has emerged. The contribution of Rab GTPases to cancer progression may be broad due to their wide range of associations with vesicle trafficking, which may affect multiple cellular compartments. This contribution may be indirect through the alteration of pathways such as exosome biogenesis which then go on to play a role in cancer or more direct through effector binding associations. Abnormal Rab expression has been connected to both oncogenic and tumour suppressive roles within cancer (Figure 1.17.) (Krishnan et al., 2020).

Tumour suppression is less common and can be tissue or cancer-type specific. These Rabs inhibit tumour initiation and progression through functions including inducing cancer cell apoptosis and inhibition of angiogenesis (Gopal Krishnan et al., 2020). Rab17 has been shown to supress cell proliferation and migration of hepatocellular carcinoma cells *in vitro* and *in vivo*. *In vivo* Rab17 reduces the growth of tumour xenografts in an ERK (extracellular signal-regulated kinase) signalling-dependent manner (K. Wang et al., 2015). Rab37 inhibits MMP9 through interaction with Tissue Inhibitor of Metalloprotease-1 (TIMP1). TIMP-1 is a glycoprotein which prevents extracellular matrix turnover through actions including inactivation of specific matrix metalloproteinases (C. Y. Wu et al., 2009) (Tsai et al., 2014). Rab23 has been related to the inhibition of cell growth and proliferation and the induction of apoptosis in breast cancer cells through Gli1 and Gli2 expression (Liu et al., 2015) (Xu et al., 2024). Finally, low Rab25 expression is linked to lower overall survival of oesophageal squamous cell carcinoma patients. Tong et al. (2012) also showed that it exerts anti-angiogenesis and anti-invasion functions by deregulating the FAK-Raf-MEK1/2-ERK signalling pathway.

Cancer progression involves migration, invasion, metabolism, drug resistance, autophagy and exosome secretion. Rab GTPase interaction with effector proteins is critical for maintaining intracellular trafficking pathways. As such, interactions Rab-effector interactions within pathways also have influence on Rab contribution to tumour progression

Oncogenic functions of Rab GTPases themselves are most often associated with Rab gene amplification instead of mutation within Rab genes. This is believed to be due to modulation of growth and survival signalling pathways with broad effects including: modulation of the cytoskeleton to increase cell motility, regulation of cytokinesis and regulation of the immune response, such as transport of immune receptors, secretion of cytokines and chemokines, and endocytosis and phagocytosis (Kjos et al., 2018) (Husebye et al., 2010) (G. M. Wilson et al., 2005) (Prashar et al., 2017) (Flannagan et al., 2012). Aberrations of post-translational modifications of Rab proteins are also thought to affect these pathways, contributing to oncogenesis within cells (Xu et al., 2024).

Multiple Rabs including Rab1, Rab5, Rab8, Rab11, Rab13, Rab23, Rab25, Rab27 and Rab40B among others have been associated with cancer progression through actions within intracellular signalling pathways (Tzeng and Wang, 2016).

Rab8 mediates exocytosis of MT1-MMP (membrane type 1 matrix metalloproteinase), an MMP involved in cell invasion (Bravo-Cordero et al., 2007). Rab21 is associated with aneuploidy (Pellinen et al., 2006). Rab23 has been connected to gastric cancer through its control of sonic hedgehog signalling (Hou et al., 2008) (Eggenschwiler et al., 2001). Rab25 is connected to tumour progression in solid tumour types including breast, ovarian, prostate and intestinal cancer (Agarwal et al., 2009).

Rab11 has been associated with gastric, cervical and breast cancer oncogenesis. This is predominantly through the promotion of invasion and migration in hypoxic conditions, which drives metastasis. This involves the Rab11-mediated trafficking of integrins including integrin α6β4 in pathways such as the αvβ3/FAK/PI3K pathway (Dong et al., 2016) (Yoon et al., 2005). In non-small cell lung cancer, over expression of Rab11A is connected with decreased signalling within the Hippo pathway leading to tumour cell invasion (Dong et al., 2017). Additionally, in colorectal cancer, Rab11 promotes cell migration though elevated E-cadherin distribution which increases cell connections. Increases MMP2 expression has also been observed in colorectal cancer cells which overexpress Rab11 which is thought to contribute to cell invasion and migration (Chung et al., 2016).

Rab25 has also been shown to promote tumourigenesis through association with integrins. Rab25 interacts with α5β1 integrin to promote migration of ovarian cancer cells in 3D matrices (Caswell et al., 2007). As Rab25 has shown to be tumour suppressive in non-small cell lung cancer, this supports the idea that Rab influence on cancer progression is likely to be tissue-specific and may be influenced by interaction with different effector proteins.

Like Rab8, Rab40B is also associated with MMP-related cell invasion. Rab40B has been shown to regulate the transport of MMP2/9 during invadopodia formation and metastasis of breast cancer cells (Jacob et al., 2013a)

Rab27 is one of the best characterised Rabs in disease progression. It has two isoforms: a and b, both of which have been associated with enhanced cell proliferation, tumour development, cell invasion and metastasis, and chemoresistance (Ostenfeld et al., 2014) (Akavia et al., 2010) (Hendrix et al., 2013). It has also been linked to increased exosome secretion *in vitro* from bladder, cervical, breast, melanoma and lung adenocarcinoma cells (Ostenfeld et al., 2014) (Ostrowski et al., 2010) (Zheng et al., 2013)(Bobrie et al., 2012) (Peinado et al., 2012) (Li et al., 2014). Additionally, exosomes associated with Rab27 have been associated with changes in naïve cells (Bobrie et al., 2012) (Peinado et al., 2012).

Additional roles of Rabs in tumourigenesis include regulation of apoptosis through either direct or indirect modulation of PI3K/AKT and other pathways, aiding the tumour in one of the hallmarks of cancer – evading apoptosis (Krishnan et al., 2020) (Hanahan and Weinberg, 2011). Rabs implicated here include Rab2B, Rab25, Rab31 and Rab35 (Jin et al., 2018) (Casanova et al., 1999) (Sui et al., 2015) (Wheeler et al., 2015). Rabs have also been implicated in enhancing tumourigenesis through regulation of cell cycle progression including Rab2B, Rab13, Rab18 and Rab21 (Krishnan et al., 2020) (Diao et al., 2016) (Ge et al., 2017) and Rab8, Rab13 in drug resistance (Shen and Gottesman, 2012) (Yousaf and Ali, 2020).
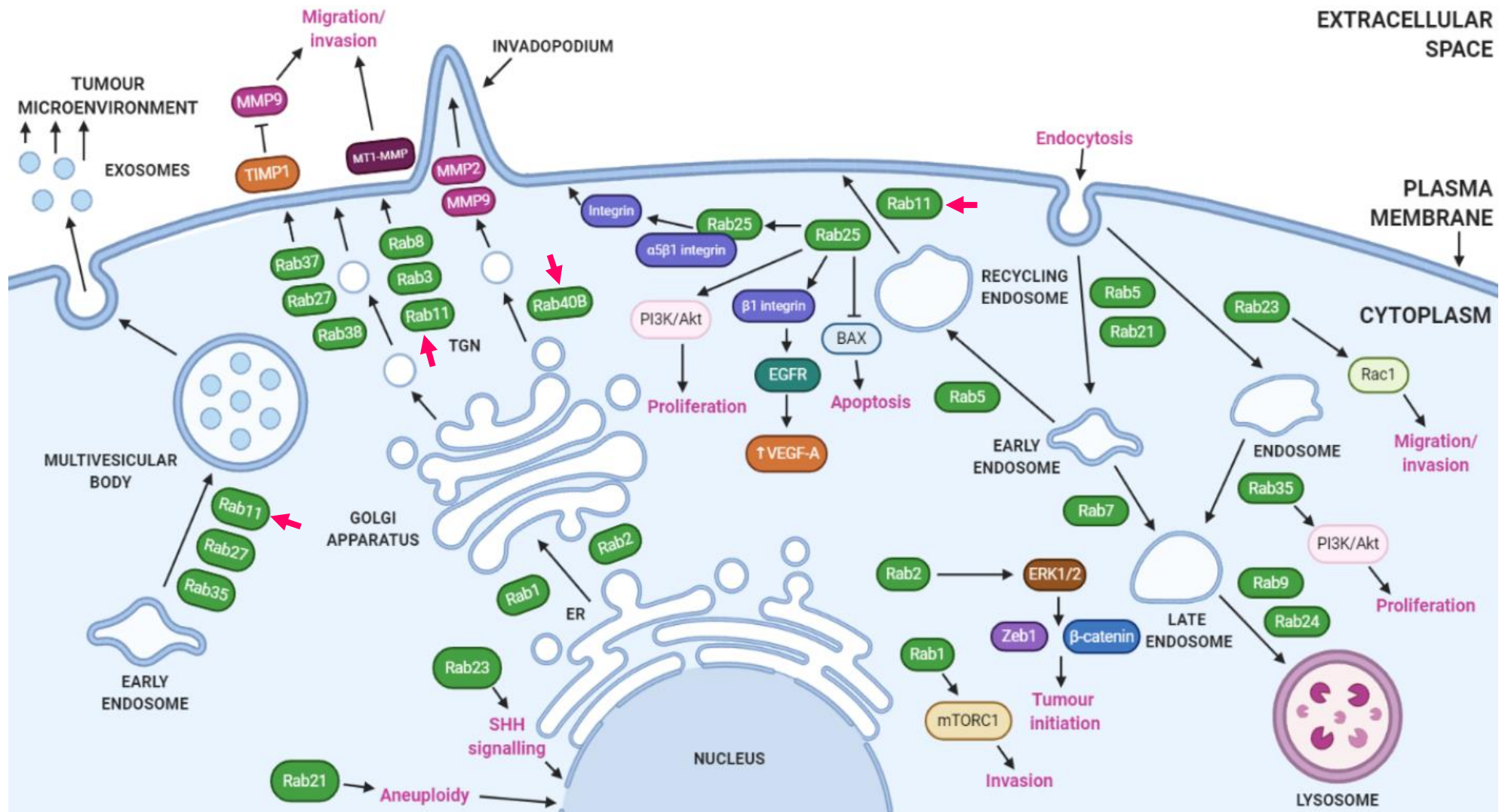
Figure 1.17. Rab GTPase involvement in tumourigenic pathways *Adapted from Tzeng and Wang, 2016. Created using BioRender.com. Rabs known to be involved in tumourigenic pathways include Rab11 and Rab40B (highlighted with pink arrows).*

Finally, Rabs are thought to influence metabolic signalling pathways through their regulation of vesicular transport. For example, the regulation of the GLUT1 glucose transporter by Rab25 and the formation of lipid droplets in the glucose and lipid metabolism of cancer cells by Rab8A. Rab25 increases the glycogen reserve in ovarian cancer cells, which leads to increased transport of GLUT1 to the cell surface, increasing glucose uptake (Yang et al., 2021) (Cheng et al., 2012). Tumour cells are able to utilise lipids as well as glucose through metabolic reprogramming. Lipid droplets function as intracellular lipid storage, allowing the cell to maintain the cellular level of free lipids for use as metabolites. An example of Rab action in this process is Rab8B in hepatocellular carcinoma (Wu et al., 2014).

1.3. Hypothesis and aims

Medulloblastoma is the most common malignant form of paediatric brain cancer with a five-year survival of over 70%. When metastatic, patient survival decreases to 35-60%, creating a requirement for the better understanding of specific mechanisms which drive metastasis. Previous work has connected EV secretion with metastatic medulloblastoma pathogenesis as Jackson et al., (2023) showed that more EVs were secreted from metastatic medulloblastoma cell lines than non-metastatic cell lines. However, there is a complete absence of published literature on the role of Rab GTPases in trafficking and EV secretion in metastatic medulloblastoma, and brain tumours or paediatric cancers in general. This includes no literature implicating specific Rabs or the Rab GTPase family of proteins in medulloblastoma pathogenesis.

This study aims to address this knowledge gap and hypothesises that members of the Rab GTPase protein family contribute to medulloblastoma pathogenesis through roles in vesicular trafficking pathways.

This study aims to establish firstly whether Rab GTPases contribute to medulloblastoma pathogenesis through roles as exosomal cargo. Secondly, whether Rabs contribute to medulloblastoma pathogenesis through roles in exosome biogenesis, whether this be by aiding in the enhanced secretion or selective packaging of pro-tumourigenic factors. Finally, whether Rabs contribute to

medulloblastoma pathogenesis through a pathway which is unrelated to exosome biogenesis, such as trafficking of matrix metalloproteinases during invadopodium formation during migration and invasion.

In order to achieve this, this study will firstly identify Rab GTPase targets which could have a role in medulloblastoma pathogenesis. It will then validate the expression of these targets in patient-derived cell lines before designing and creating a model to study the function of that Rab in medulloblastoma cells.

Chapter 2: Materials and methods

2.1. Cell culture methodology

2.1.1. Standard Cell culture

Nine cell lines were cultured during this study. All cell lines were cultured in an incubator at 37°C with 5% CO_2 in cell culture medium. Cells were either cultured in treated T-25 or T-75 (ThermoFisher Scientific; 130189, 130190) or untreated T-25 (Eppendorf; 0030710029) cell culture flasks. Details of the cell culture medium used for each cell line can be seen in Table 2.1. Characteristics of cell lines used can be found in Table 2.2.

Table 2.1. Cell culture medium constituents

Cell line	Media	Flask
HEK293A	Dulbecco's modified Eagle's medium (DMEM) (Sigma-Aldrich; D6429) supplemented with 10% (v/v) foetal calf serum (Sigma-Aldrich; F7524) and 1% (v/v) penicillin/streptomycin (Sigma-Aldrich; P4333)	Cell culture treated
ONS-76	Roswell Park Memorial institute-1640 (RPMI-1640; Sigma-Aldrich; R8758) + 10% foetal bovine serum (FBS; HyClone; SH30541.03)	Cell culture treated
DAOY	DMEM (Gibco; 31885) + 10% FBS	Cell culture treated
HD-MB03	RPMI-1640 + 10% FBS	Cell culture treated
D425	DMEM (Gibco) + 10% FBS	Cell culture treated
D458	DMEM (Gibco) + 10% FBS	Cell culture treated
D283	DMEM (Gibco) + 10% FBS	Cell culture treated
CHLA-01	DMEM F12 (Gibco; 17504044) + 2% (v/v) B27 (Gibco; 17504044) + 20 ng/ml recombinant basic fibroblast growth factor (bFGF; Gibco; PHG0266) + 20 ng/ml recombinant epidermal growth factor (EGF; Gibco; PHG0315)	Untreated
CHLA-01-R	DMEM F12 + 2% (v/v) B27 + bFGF + EGF	Untreated

Table 2.2. – Medulloblastoma cell line details

Cell line	Medulloblastoma subgroup	Culture growth type	Metastatic stage	Origin	Genetic features	Reference
DAOY	SHH	Adherent	Non-metastatic (M0)	Primary tumour	*TP53* mutant *CDKN2A* deletion	Jacobsen et al., 1985
ONS-76			Metastatic (M2)	Primary tumour	*TP53* wildtype	Yamada et al., 1989
D283	Group 3	Semi-adherent	Metastatic (M2)	Metastasis removed from ascites	Trisomy of chromosome 11 8q+, 17p+, 20q+	Friedman et al., 1985
D425			Non-metastatic (M0)	Primary tumour	*MYC* amplification *TP53* mutant	Bigner et al., 1990
D458			Metastatic (M+)	Metastasis taken from CSF		He et al., 1991
HD-MB03			Metastatic (M3)	Primary tumour	*MYC* amplification Isochromosome 17q	Milde et al., 2012
CHLA-01	Group 4	Suspension	Non-metastatic (M0)	Primary tumour	*BRCA2* 6174T mutation *MYC* amplification Isochromosome 17q	Erdreich-Epstein et al., 2014
CHLA-01-R			Metastatic (M3)	Metastasis taken from pleural effusion		

2.1.2. Sub culturing cell lines

2.1.2.1. Adherent cell lines

Adherent cell lines DAOY, ONS-76 and HEK293A were sub-cultured by disposing of culture medium. Flasks were then washed using HBSS (DAOY and ONS-76) or 1x PBS (HEK293A) before being incubated for five minutes with 1X trypsin-EDTA (ethylenediaminetetraacetic acid) (Sigma; T4174). Cell culture medium (see Table 2.1 for the correct medium for each cell line) was then added to the flask to neutralise the trypsin and the whole flask contents centrifuged at 800 *xg* for 5 minutes. The cell pellet was then resuspended in fresh cell culture medium and cells were transferred to a new cell culture flask, pre-warmed medium added, and cells incubated at 37°C (as above). All adherent cell lines were split 1:10 at each split or in accordance with cell culture requirements at the time.

2.1.2.2. Semi-adherent cell lines

The semi-adherent group 3 cell lines HD-MB03, D425, D458 and D283 consist of two subpopulations of cells when in culture; adherent cells which adhere to the flask and semi-adherent cells which float in the cell culture medium just above the adherent cell population.

These cell lines are cultured as described for the adherent cell lines with the exception that cell culture medium and washes are retained and centrifuged alongside the trypsinised cell fraction to avoid loss of suspension cells present within the cell culture medium. HD-MB03 cells were split 1:10, D425 and D458 1:6-1:8 and D283 1:3-1:6.

2.1.2.3. Suspension cell lines

The suspension cell lines CHLA-01 and CHLA-01-R consist of clusters of cells which float freely in the cell culture medium (Table 2.1.) without any form of adherent cell population. To culture these cells, volumes of media were periodically removed and

replaced with fresh medium. Removed medium was centrifuged at 800 *xg* for 5 minutes. The cell pellet was then resuspended in fresh medium and a 1:5 – 1:10 split performed depending on cell pellet or freezer stock requirements.

2.1.3. Preparation of cell pellets for molecular analysis

Cells were cultured as described above. After pellet resuspension in fresh medium and a split occurring, the remaining cell suspension was centrifuged again at 800 *xg* to generate another cell pellet. Medium was removed from the cell pellet and the pellet was resuspended in 1 ml of medium before being transferred to an Eppendorf tube. The Eppendorf was then centrifuged at 800 *xg* for 5 minutes, supernatant discarded, and cell pellet washed using 1X PBS (Lonza; BE17-517Q) and centrifuged again at 800 *xg* for 5 minutes. Supernatant was then discarded, and cell pellets placed in the -80°C freezer.

2.1.4. Preparation of cells for cryo-storage

Cells were cultured as described above. After cell splitting, the remaining cell suspension was centrifuged again at 800 *xg* to generate another cell pellet. Medium was removed from the cell pellet and the pellet resuspended in freezing medium (see Table 2.3 for details) and placed in a cryogenic vial (Starlab; E3090-6212) and then into a Mr Frosty in the -80°C freezer. Samples were left overnight in the -80°C freezer before being transferred to liquid nitrogen for long-term storage.

Table 2.3. Cell freezing medium constituents

Cell line	Freezing medium constituents
HEK293A	90% FCS (Sigma-Aldrich; F7524) 10% dimethyl sulfoxide (DMSO; Sigma; D8418)
DAOY, ONS-76, HD-MB03, D425, D458, D283, CHLA-01, CHLA-01-R	90% (v/v) FBS (HyClone; SH30541.03) 10% (v/v) DMSO

2.1.5. Recovering cells from liquid nitrogen cryo-storage

Cryogenic vials of cells were thawed at 37°C. Cells were then placed into a T-25 flask with fresh medium and left overnight. Thawed cells were then left for 24-48 hours. For adherent cell lines, the medium was then removed, discarded and replaced with fresh medium. For semi-adherent and suspension cell lines, medium was removed, centrifuged at 800 *xg* for 5 minutes, supernatant discarded, and any cell pellet resuspended in fresh medium before being returned to the original flask.

2.1.6. Cell counting

Cells were cultured as described above. Cell pellets were resuspended in 1 ml of medium and 10 µl of the suspension were pipetted onto a CellDrop cell counter (DeNovix CellDrop BF; S-05215). A haemocytometer (Hawksley, depth 0.1mm, BS.748) was also used to verify results from the CellDrop. 10 µl of cell suspension was pipetted into the glass chamber of the haemocytometer. A brightfield microscope was then used to count cells by eye per square of the chamber and cells per ml calculated using the following formula:

$$Cells\ per\ ml = \frac{(Number\ of\ cells\ counted)}{(Number\ of\ large\ squares\ counted)} x\ 10{,}000$$

2.2. Molecular biology

2.2.1. RNA extraction

RNA samples from cell pellets frozen at –80°C were extracted using the RNeasy mini kit from Qiagen (74104) following manufacturer's instructions. Samples were eluted into 30μl of RNA-free water (provided with the RNA extraction kit). RNA was then quantified using a NanoDrop 2000 machine (Thermo Scientific) and kept at –80°C until use.

2.2.2. cDNA synthesis

cDNA was prepared using RNA extracted as described above. 2 μg of RNA was added to Milli-Q water to give a final volume of 11 μl. Two of these tubes were set up per RNA sample. A master mix of random primers dNTPs and Milli-Q water was then made as shown in Table 2.4. and 2 μl of master mix added to each tube containing RNA. Samples were incubated at 65°C for 5 minutes and left on ice for a further minute. Two master mixes were then made, one for cDNA synthesis and one to act as a no-reverse transcriptase (NRT) control (see Table 2.5.). 7 μl of each master mix was added to one RNA tube per RNA sample. The cDNA synthesis was then run using a SensoQuest Labcycler as described in Table 2.6. and resulting cDNA stored at –20°C.

Table 2.4. Master mix of random primers, dNTPs and Milli-Q water constituents

Reagent	Volume per reaction (μl)
Random primers (Promega; C1181)	0.5
dNTPs (20mM) (Promega; U120A, U121A, U122A, U123A)	0.5
Milli-Q water	1
Total	2

Table 2.5. Master mix constituents for cDNA synthesis and no reverse transcriptase (NRT) control reactions

cDNA synthesis reaction		NRT	
Reagent	Volume per reaction (µl)	Reagent	Volume per reaction (µl)
DTT 0.1M (Invitrogen; provided with Superscript III reverse transcriptase)	1	DTT 0.1M	1
5X First strand buffer (Invitrogen; provided with Superscript III reverse transcriptase)	4	5X First strand buffer	4
RNaseOUT (Invitrogen; 2358618)	1	RNaseOUT	1
Superscript III reverse transcriptase (200units/µl; Invitrogen; 18080-044)	1	Milli-Q water	1
Total volume	7	**Total volume**	7

Table 2.6. cDNA synthesis PCR machine programme

Temperature (ºC)	Time (minutes)
25	5
50	60
70	15

2.2.3. qPCR primer optimisation

2.2.3.1. Gradient PCR

The following tubes were set up for each cDNA per primer pair; one tube per temperature with cDNA, one tube per temperature with NRT control and one tube per temperature with Milli-Q water (no transcript control; NTC). A master mix was then prepared (see table 2.7). and 14 µl added to each PCR tube. Details of primers used in this reaction throughout the study can be found in Table 2.12.

Table 2.7. Gradient PCR master mix constituents

Reagent	Volume per reaction (µl)
iQ SYBR green Supermix (Bio-Rad; 1708884)	7.5
Forward primer (150nM)	2.25
Reverse primer (150nM)	2.25
Milli-Q water	2
Total	14

cDNA and non-RT control samples were then diluted to a concentration of 10 ng/µl and 1 µl added to give a final reaction volume of 15 µl. 1 µl was added to NTC tubes to also give a final reaction volume of 15 µl. PCR tubes were then placed in a SensoQuest Labcycler PCR machine in the correct positions according to the temperature gradient programmed into the PCR machine. Tubes were then run on the PCR programme detailed in Table 2.8. NRT and NTC tubes were run at 60°C.

Table 2.8. Gradient PCR machine programme

Temperature (°C)	Time (minutes)	Cycles
94	3	1
94	0.5	30
58, 60 or 62	0.5	30
72	5	1
4	Hold	-

5 µl of PCR product was then added to 1 µl of 6X loading dye (New England Biolabs (NEB); B7024S) with 100bp ladder (New England Biolabs; N3231S) and run on a 2% agarose gel at 100V for 45-60 minutes until the dye front had reached the end of the gel. Gels were imaged using a Syngene Genius gel documentation system. Full details on agarose gel electrophoresis can be found in section 2.2.6.

2.2.3.2. Calculating primer efficiencies

A master mix for each primer pair was made as detailed in Table 2.9. Eppendorf tubes were then labelled for serial dilutions of cDNA samples were set up using the following dilution ratios; 1, 0.5, 0.25, 0.125, and 0.0625. 20 µl of Milli-Q water was

added to each dilution tube. Tube 1 was then prepared with 40 ng/µl (16 µl cDNA (100 ng/µl) and 4 µl Milli-Q water in addition to the 20 µl Milli-Q water added in a final volume of 40 µl. 20 µl of tube 1 was added to tube 0.5. 20 µl of tube 0.5 was then added to tube 0.25 and so on.

8 µl of master mix was then added to one well of a 384-well qPCR plate (BioRad; HSP3805) per serial dilution. 2 µl of each serially diluted cDNA was then added to these wells. 2 µl of Milli-Q water and 2 µl of 5 ng/µl non-RT control sample were also added to one additional well per primer pair to act as NTC and NRT controls respectively. The PCR plate was then covered with an adhesive seal and centrifuged using an Eppendorf 5810 centrifuge at maximum speed for 10 seconds. The plate was then run on a BioRad C1000 CFX96 RT-PCR machine using a programme detailed in Table 2.10.

Table 2.9. Calculating primer efficiencies qPCR master mix constituents

Reagent	Volume per reaction (µl)
SYBR Green	5
Forward primer (150nM)	1.5
Reverse primer (150nM)	1.5
Total	8

Table 2.10. Calculating primer efficiencies qPCR machine programme

Temperature (ºC)	Time (minutes)	Cycles
94	3	1
94	0.5	40
30	1	40
72	5	40
65-95	Sections of 0.5ºC increasing every five seconds	Melt curve

2.2.4. RT-qPCR

A master mix was prepared per primer pair as detailed in Table 2.11. and 8 µl added to wells of a 384-well qPCR plate. qPCR primer pairs used in this study can be found in Table 2.12. All primers used in this study were purchased from Eurofins Genomics.

Table 2.11. RT-qPCR master mix constituents

Reagent	Volume per reaction (µl)
SYBR green	5
Forward primer (150nM)	1.5
Reverse primer (150nM)	1.5
Total	8

The appropriate amount of each cDNA to be used was then diluted to a concentration of 10 ng/µl and made up to a final volume of 2 µl. The same was done for non-RT control samples. 2 µl of cDNA and non-RT samples were then added to corresponding wells of the 384-well qPCR plate. 2 µl of Milli-Q water was added to one well per primer pair to act as an NTC control. The PCR plate was then covered with an adhesive seal and centrifuged using at maximum speed for 10 seconds. The plate was then run on a BioRad C1000 CFX96 RT-qPCR machine using a programme detailed in Table 2.13.

Table 2.12. Primer sequences used for RT-qPCR

Target Gene	Primer	Sequence	Optimised annealing temperature (°C)
Rab1B	Forward	5' TCATGGCATCATCGTGGTGT 3'	60
	Reverse	5' TGACGTTCTCGCTGGCATAG 3'	60
Rab8B	Forward	5' AGCATGCCTCTTCCGATGTC 3'	60
	Reverse	5' GCACTGATTTTGCGCTTGT 3'	60
Rab11A	Forward	5' CTTCGGCCCTAGACTCTACA 3'	60
	Reverse	5' GGAACCACATTGTTGCTTGGA 3'	60
Rab13	Forward	5' GTTGGCTCGAGAGCATGGAA 3'	60
	Reverse	5' GTACTGGGAGGCTTGTTGCC 3'	60
Rab40B	Forward	5' CTGCAGCTCTCGGGATACT 3'	60
	Reverse	5' CATCGATCAATGCCGTCA 3'	60
GAPDH	Forward	5' ATGTTCGTCATGGGTGTGAA 3'	60
	Reverse	5' GTCTTCTGGGTGGCAGTGAT 3'	60
Calnexin	Forward	5' AGCCAAGAAAGACGATACCG 3'	60
	Reverse	5' CAGAGATGGCATGATGCTTG 3'	60

Table 2.13. RT-qPCR machine programme

Temperature (°C)	Time (minutes)	Cycles
94	3	1
94	0.5	40
Optimised annealing temperature	1	40
72	5	1
4	Hold	-

2.2.5. Immunoblotting

Samples were prepared for loading by adding 6x sample buffer (0.125M Tris-HCl pH6.8, 10% (w/v) SDS (Sodium Dodecyl Sulfate), 10% (w/v) glycerol, 0.5M EDTA, 0.2% (v/v) Bromophenol blue in ethanol, 0.5% (v/v) 2-Mercaptoethanol) and denatured at 96°C for 15 minutes. Samples were resolved into a 12% polyacrylamide gel by running at 40 mA/gel for 90 minutes in 1X Running Buffer (190 mM Glycine, 25 mM Tris-Base, 0.1% (w/v) SDS, dH$_2$O). BLUeye pre-stained protein

59

ladder (Sigma-Aldrich, 94964) was run alongside samples as a molecular weight marker. Proteins were then transferred onto a PVDF membrane (Immobilon, IPVH00005) for 2 hours at 200 mA (milliamps) in 1X Transfer Buffer (190 mM Glycine, 25 mM Tris-Base, 10% (v/v) methanol, dH_2O). The membrane was then blocked in 5% (w/v) milk in 1X PBS-Tween 20 (10% (v/v) PBS, 0.1% (v/v) Tween-20) (Marvel; Lonza; BE17-S17Q) for 1 hour at room temperature. Membranes were cut based on molecular weight markers from the BLUeye pre-stained protein ladder so that individual sections could be probed using a different antibody. These sections were then probed using primary antibodies as detailed in Table 2.14. and incubated at $4^{o}C$ overnight. All antibodies were diluted in 5% milk blocking buffer. Membranes were then washed in 1X PBS-Tween 20 and incubated with secondary antibodies at room temperature for 1 hour, washed in 1X PBS-Tween 20 and imaged. The details of secondary antibodies and the detection systems used are detailed in Table 2.15.

Table 2.14. – Summary of primary antibodies used for immunoblotting in this study

Target Protein	Concentration	Manufacturer	Species reactivity	Clonality
Calnexin	1:1000	Sicgen AB0041-200	Goat	Polyclonal
GFP	1:1000	Sicgen AB0020-200	Goat	Polyclonal
	1:1000	Roche 11814460001	Mouse	Monoclonal
Rab1B	Various	Sicgen AB0017-100	Goat	Polyclonal
	Various	Gift from Nori Fukuda, Tohoku University, Sendai, Miyagi, Japan	Rabbit	
Rab8B	Various	ProteinTech 55295-1-AP	Rabbit	Polyclonal
Rab11A	Various	Sicgen AB0034-100	Goat	Polyclonal
	1:1000	ProteinTech 20229-1-AP	Rabbit	Polyclonal
Rab13	Various	Abcam 180936	Rabbit	Monoclonal
Rab40B	1:1000	Invitrogen PA5-106719	Rabbit	Polyclonal

Table 2.15. – Summary of secondary antibodies used for immunoblotting in this study and its corresponding detection system

Detection system	Species reactivity	Manufacturer	Concentration
LI-COR	Rabbit	LI-COR, IRDye 800CW Donkey anti-Rabbit, 926-32213	1:10000
	Goat	LI-COR, IRDye 800CW Donkey anti-Goat, 926-32214	
	Mouse	LI-COR, IRDye 800CW Donkey anti-Mouse, 926-32212	
ECL (HRP)	Rabbit	Dako P0217	1:2000
	Goat	Dako P0160	

2.2.6. Agarose gel electrophoresis

6X purple loading dye (NEB, B7024S) was added to samples to be loaded. Agarose gels were prepared by placing 1X TBE (Tris/Borate/EDTA) buffer (1.08% (w/v) Tris base, 0.55% (w/v) boric acid, 0.0585% (w/v) EDTA in dH_20, adjusted to pH8.0) and agarose in a conical flask and heating in a microwave until the agarose had dissolved. The mixture was then cooled, and 0.001% (v/v) ethidium bromide added. After mixing well, the gel was poured into a gel casting tray to create a gel that was approximately 5mm thick. A comb was then inserted to create lanes in the gel and the gel was left to solidify at room temperature. The set gel was then placed in a gel tank and filled with 1x TBE. The comb was then removed, and sample loaded into each well alongside one well of 1kb ladder (NEB, N3232S). The gel was then run at 100V until the dye front had reached the end of the gel. The gel was then imaged using a Syngene Genius gel documentation system (NuGenius; Syngene).

2.2.7. Cell lysis

Cells were lysed using 200 µl RIPA buffer (50 mM Tris-HCl pH 7.4, 1% (v/v) NP-40, 0.5% (w/v) Na-deoxycholate, 0.1% (w/v) sodium dodecyl sulfate, 150 mM NaCl, 2 mM EDTA, dH_2O to 100 ml) and 1% (v/v) protease inhibitors (Protease inhibitor

cocktail set III; Merck; 539134-1SET) and homogenised. Samples were then left for 45 minutes before further processing.

<u>2.2.8. Protein quantification</u>

Protein content of cell lysates was measured using a BioRad DC protein assay. A BSA (bovine serum albumin) standard curve was plated alongside cell lysates to allow for quantification. The following amounts of BSA (Sigma Aldrich; A7030) were plated for the standard curve; 0 µg, 1 µg, 2 µg, 3 µg, 4 µg, 5 µg, 6 µg, 7 µg, 8 µg, 9 µg, 10 µg. 0.5, 2.5 and 5 µl of each cell lysate were then plated. All volumes were made up using distilled water. 20 µl of assay buffer A and 200 µl of assay buffer B were then added and the assay was left for 15 minutes at room temperature before absorbances were read at 750nm on a SpectraMax iD3 plate reader.

Absorbances of samples were corrected by subtracting the absorbance of the 0 µg BSA standard curve value. Values were then divided by the gradient of the standard curve and this value divided by the volume of cell lysate added to the reaction to give the protein concentration of the sample in µg/µl.

2.3. RNA sequencing

<u>2.3.1. mRNA sequencing</u>

3' UPX next generation sequencing was conducted on the mRNA cargo of medulloblastoma cell line-derived exosomes; D425 and D458 (group 3 medulloblastoma) and CHLA-01 and CHLA-01-R (group 4 medulloblastoma). This work was carried out by Hannah K. Jackson from the Coyle laboratory (Jackson, 2021). Mapping of the sequence data by Jackson was also performed which identified Unique Molecular Index (UMI) values. The Unique Molecular Index (UMI) values of all Rab GTPases expressed within all samples were subsequently obtained.

2.3.2. Single cell RNA sequencing

Franziska Linke from the Coyle lab conducted single cell RNA sequencing on 5,000 HD-MB03 or ONS-76 cells. Samples were prepared according to the 10x Genomics Chromium Single Cell 3' Reagent Kit v2 User Guide, Rev D, prior to RNA sequencing. Linke then analysed the data using K-means cluster analysis. Any upregulated Rab GTPases were identified using 'CTRL F' search for 'Rab GTPases' and filtered using a log2 fold change >0 and p value of ≤0.05.

2.4. Bioinformatics

2.4.1. Patient dataset analysis

To identify target gene expression profiles and association with patient survival across the medulloblastoma subgroups, genomics analysis of the Cavalli dataset of 763 medulloblastoma patient samples (DNA methylation data) was obtained using the hugene11t platform on the R2: Genomics Analysis and Visualisation Platform (Cavalli et al., 2017) (http://r2.amc.nl).

2.4.2. Review of the literature

The terms 'Rab GTPase' AND 'cancer' were inputted into NCBI PubMed (https://pubmed.ncbi.nlm.nih.gov/). Subsequent searches, also into NCBI PubMed included 'Rab1A', 'Rab1B', 'Rab3A', 'Rab7A', 'Rab8B', 'Rab10', 'Rab11A', 'Rab13' and, 'Rab40B'. This analysis was conducted between October 2019 and October 2020.

2.4.3. ExoCarta

ExoCarta.org exosome database (http://exocarta.org) was used to identify Rab GTPases which have been identified in exosomes isolated from either cancer-derived cell lines or tissues. A series of 'CTRL F' searches using the term 'Rab' were conducted on the 'browse results for organism: Homo sapiens' page of the website during February 2020.

2.4.4. Protein feature analysis

2.4.4.1. SWISS-MODEL

SWISS-MODEL (https://swissmodel.expasy.org) was used to generate ribbon structural models of Rab11A and a modified Rab11A amino acid sequence containing amino acid alterations caused by CRISPR-Cas9 gene editing. Target sequences were uploaded and 'build model' selected. AlphaFold models generated were then exported.

2.4.4.2. Protter

The Protter open-source tool for visualisation of proteoforms and interactive integration of annotated and predicted sequence features (https://wlab.ethz.ch/protter) was used to generate a model of the amino acid sequence of Rab11A. The UniProt protein accession number was imported and 'submit' selected. The 'styles' tab was then selected and used to annotate sequence features, including the position of protein fragments obtained from SWATH-MS. The 'export' button was then used to generate and export the image.

2.5. Generation and validation of CRISPR Rab GTPase knockout cell lines

2.5.1. Transfection of HD-MB03 medulloblastoma cells with GFP plasmid

$5x10^5$ HD-MB03 group 3 medulloblastoma cells were transfected with a GFP plasmid (pmaxGFP^{TM} Vector) using a Cell Line Nucleofector® kit V (Lonza; VCA-1003) according to manufacturer's instructions. Samples were electroporated using a Nucleofector II Device (Lonza; AAB-1001) using programme A0-33.

After electroporation, 500 ml of cell culture medium was added to the electroporation cuvette and whole contents of the cuvette seeded into a T-25 flask containing pre-warmed medium and incubated at 37°C.

2.5.2. Co-transfection of HD-MB03 medulloblastoma cells with EGFP Cas9 nuclease mRNA and synthetic sgRNAs

$1x10^6$ HD-MB03 group 3 medulloblastoma cells were co-transfected with EGFP Cas9 nuclease mRNA (Horizon; CAS12217) as well as either *Rab11A* (Horizon; SG-004726-01-0005), *Rab40B* (Horizon; SG-008353-01-0005) or non-targeting Edit-R synthetic sgRNA (Horizon; U-009501-01-05). The sequence for each sgRNA can be found in Table 2.16.

Prior to co-transfection, synthetic sgRNAs were resuspended in 50 µl of 10mM Tris-HCl buffer (pH 7.4; Horizon; B-006000-100). EGFP Cas9 nuclease mRNA was thawed on ice. These were both then added to cells suspended in electroporation buffer from a Cell Line Nucleofector® kit V (Lonza; VCA-1003) to give a final concentration of 0.05 µg/µl (EGFP Cas9 nuclease mRNA) and 5 µM (synthetic sgRNAs). Cells were then co-transfected using a Nucleofector II Device (Lonza; AAB-1001; programme A0-33) and 500 µl pre-warmed media added. Cells were then seeded into a T-25 flask containing pre-warmed media and incubated at 37°C overnight.

Table 2.16. – Sequence of synthetic single guide RNAs used in this study

Synthetic single guide RNA	Product Code	Sequence
Rab11A	SG-004726-01-0005	5' GAGTGATCTACGTCATCTCAGGG 3'
Rab40B	SG-008353-01-0005	5' AATGCCAGGATGATGCACGGCGG 3'
Non-targeting control	U-009501-01-05	5' GATACGTCGGTACCGGACCG 3'

2.5.3. Fluorescence activated cell sorting (FACS)

The whole contents of T-25 flasks containing cells co-transfected with EGFP Cas9 nuclease mRNA and synthetic sgRNA were spun at 800 *xg* for 5 minutes to pellet. The cell pellet was then resuspended in 1 ml of phenol red-free RPMI medium (Sigma; R-7509-500ML) and transferred to an Eppendorf tube. 2.5µl of 200 µg/ml 4', 6-diamidino-2-phenylindole (DAPI) was then added to the cells as a viability stain.

A MoFlo Astrios cell sorter (Beckman Coulter) was then used to sort single cells which were both positive for GFP staining and negative for DAPI staining into a 96-well plate containing pre-warmed medium.

All FACS and related analysis was conducted by Dr David Onion, Nicola Croxall or Maria Haig from the University of Nottingham's Flow Cytometry facility.

2.5.4. Imaging of CRISPR-Cas9 potential knockout clonal cell lines

After FACS and whilst clonal cell lines were being grown from a 96-well plate into a T-25 flask, cells were periodically imaged to monitor growth. This was conducted using a ZOE Fluorescent Cell Imager (BioRad; 1450031; 742BR3282). Standard settings were used for brightfield imaging (Gain – 8, Exposure (ms) – 300, LED intensity – 40, Contrast – 0). Fluorescence imaging using the 'green' channel was also conducted for the first 6 days post-FACS, standard settings were also used (Gain – 40, Exposure (ms) – 500, LED intensity – 50, Contrast – 0).

2.5.5. Genomic DNA (gDNA) extraction

Cell pellets were thawed on ice and genomic DNA extracted following the cultured cells methodology in the Machery-Nagel Nucleospin® tissue mini kit for DNA from cells and tissue (Machery-Nagel; 740952.50) following manufacturer's instructions. Samples were eluted into 100 µl Buffer BE (from kit) and stored at -20°C.

2.5.6. T7 endonuclease I DNA mismatch detection assay

To determine whether CRISPR edited cells contained one or multiple *Rab11A* or *Rab40B* alleles a T7 endonuclease assay using a T7 Endonuclease I Assay Kit (GeneCopoeia™; IC006) was performed on PCR products deriving from genomic DNA (gDNA) isolated (see section 2.5.5. for gDNA isolation methodology) from the clonal cell lines. PCR products were generated by adding 1 µl of 50 ng/µl gDNA to the master mix described in Table 2.17. in a 0.2 ml PCR tube. Details for the primers used in this reaction are shown in Table 2.18. Primers were designed such that sgRNA target site was a different distance from each of the primer sequences by between 60 nucleotides and 200 nucleotides. This was to give different cleavage product sizes formed by the T7 endonuclease that could be visualised on an agarose gel. All primers were reconstituted and diluted in dH$_2$O (distilled water). The PCR was then conducted using an SensoQuest Labcycler thermocycler using the programme detailed in Table 2.19. The same PCR products for each gDNA were used for the mismatch detection assay and subsequent sequencing analysis (see section 2.5.7). A positive control that is part of the GeneCopoeia T7 Endonuclease I assay kit and contains two different mismatched sequences was also amplified using the amplification PCR protocol detailed in this methodology. The positive control DNA and primers were provided in the assay kit. PCR products were then quantified using a 2000c UV/IV Spectrophotometer (Nanodrop; ThermoFisher Scientific).

For the mismatch detection assay, 1.5 µg of PCR product was added to 2 µl 10x T7EN buffer and the reaction volume made up to 19 µl using dH$_2$O. Samples were briefly mixed and heated at 95°C for 5 minutes and then cooled at room temperature for 10 minutes. 1 µl of 2 U/µl T7 Endonuclease I was then added at the reaction incubated at 37°C for 1 hour. 5 µl of each product was then analysed by agarose gel

electrophoresis (see section 2.2.6. for agarose gel electrophoresis methodology). The presence of three DNA bands on the gel indicated multiple alleles being present within each sample.

Table 2.17 – Master mix constituents for mismatch detection assay amplification PCR

Reagent	Supplier	Volume per reaction (µl)
10X reaction buffer	New England Biolabs; B9014S	5
20mM dNTPs	Promega; U120A, U121A, U122A, U123A	0.5
Forward primer (1mM)	Eurofins	10
Reverse primer (1mM)	Eurofins	10
Taq polymerase	New England Biolabs; M0273S	0.25
dH$_2$O	N/A	23.25
Total reaction volume		49

Table 2.18 – Primer sequences for mismatch detection assay amplification PCR

Primer	Sequence
Rab11A forward	5' CAGCCTAAGTCTCATGGT 3'
Rab11A reverse	5' GCTATACAGTCATCACAAAC 3'
Rab40B forward	5' CATGTACAAGCCAGGGCCAC 3'
Rab40B reverse	5' CATGCACATCCACGTAGA 3'

Table 2.19 – Reaction summary of mismatch detection assay amplification PCR

Temperature (ºC)	Time (minutes)	Number of cycles
95	1	1
95	1	35
58	1	
72	1	
72	10	1
4	N/A	Infinite hold

Due to the presence of the chromosomal aberration isochromosome 17q within the HD-MB03 cell line, three copies of the *Rab40B* gene were present which meant that Oxford nanopore sequencing had to be used to analyse these samples instead of Sanger sequencing (this is all detailed in section 4.6.2). For this reason, Sanger sequencing methods and analysis apply to Rab11A samples only and Oxford nanopore to Rab40B samples only.

2.5.7.1. Sanger sequencing

Rab11A target sites of potential *Rab11A* knockout and non-targeting cell lines were amplified using PCR as described in section 2.5.6. PCR products were purified using the ExoSAP-IT™ Express PCR Product Clean up kit (Thermofisher; 75002) following manufacturer's instructions. The purified PCR products were then sent to GeneWiz from Azenta Life Sciences for Sanger sequencing analysis. The primers used for sequencing are detailed in Table 2.20. All samples were sequenced in both the forward and reverse direction. The same forward primer was used for sequencing as used in the initial amplification PCR, but an alternative reverse primer was designed specifically for the sequencing.

Table 2.20. – Rab11A primers for Sanger sequencing

Primer	Sequence
Rab11A forward	5' CAGCCTAAGTCTCATGGT 3'
Rab11A reverse	5' CATTGGAAGGTATCAAAACC 3'

2.5.7.1.1. Sanger sequencing analysis

To identify the presence of insertion and deletion mutations (InDels) within the *Rab11A* sgRNA target site of each clonal cell line, the Indigo InDel discovery tool

(https://www.gear-genomics.com/indigo/) was used to analyse Sanger sequencing chromatograms. The chromatograms of non-targeting sgRNA control cell lines were uploaded using the 'chromatogram file' input and aligned to the genome using the 'Homo sapiens – GRCh38' option and clicking 'launch analysis' to verify that the control cell lines did not contain any InDels. The chromatograms of potential *Rab11A* knockout cell lines were then uploaded and comparisons made to the non-targeting control by uploading non-targeting control chromatograms using the 'align to' function. 'Launch analysis' was then clicked and results exported into a PDF before manual analysis for InDels.

2.5.7.2. Oxford Nanopore Sequencing

Rab40B target sites of potential Rab40B knockout and non-targeting cell lines were amplified using PCR as described in section 2.5.6. Samples were then sent to the University of Nottingham Deep Seq facility for Oxford Nanopore sequencing. The workflow of sample processing and analysis conducted by Dr Sonal Henson from the Deep Seq facility is as follows.

Prior to sequencing, samples were quality controlled by measuring their concentration using the Qubit 4 Fluorometer (Thermo Fisher Scientific) and the Qubit 1X dsDNA HS Assay Kit (Thermo Fisher Scientific; Q33231). 50 ng of each sample and the Native Barcoding Kit 24 V14 (Oxford Nanopore Technologies; SQK-NBD114.24) was then used to prepare barcoded sequencing libraries for each amplicon using the Ligation Sequencing Amplicons – Native Barcoding Kit 24 V114 protocol (Oxford Nanopore Technologies; Version: NBA_9168_v114_revG_15Sep2022). Purification steps were performed using AMPure XP beads (Beckman Coulter; A63882). Barcoded libraries were pooled in equal amounts for the final sequencing-adapter ligation before being loaded onto a PromethION R10.4.1 M flow cell (Oxford Nanopore Technologies; FLO-PRO114M) and run on the PromethION. Barcoding options were set to require a barcode to be detected at both ends but apart from that default sequencing parameters were used.

Guppy (version 6.5.7+ca6d6af) was used for adapter trimming and Nanoplot (v1.41.3) was used to generate read summary plots. Reads were then filtered using chopper (v.0.5.0) to remove nucleotides with a quality score of less then 10, reads shorter than 200 bp (base pairs) and longer than 1100 bp. Duplicate reads were removed from the trimmed reads using fastx_uniques command and were clustered using the cluster_otus command in usearch (v11.0.667). Sequences of 97% identity threshold were clustered and chimeras were removed using the cluster_otus command. Clusters were then manually examined and the otutab command used to determine cluster sizes where reads of ≥ 97% identity were assigned to that cluster. Reads assigned to a cluster were then mapped to a reference amplicon sequence using minimap2 (v2.26) and multiple sequence alignments of the clusters with the reference amplicon were performed using MUSCLE (Multiple Sequence Comparison by Log-Expectation; Edgar, 2004).

2.5.7.2.1. Oxford Nanopore Sequencing analysis

FASTA files for each sample were open using SnapGene Viewer (SnapGene software; www.snapgene.com) to confirm the presence of the sgRNA target site within the sequencing clusters. EMBOSS (European Molecular Biology Open Software Suite) Water (www.ebi.ac.uk/Tools/psa/emboss_water/), which used the Smith-Waterman algorithm to calculate the local alignment of two sequences, was used to align firstly non-targeting sequences with wildtype to confirm the lack of InDel present within the control samples, and then the potential knockout cluster sequences with the non-targeting to identify the sequence of any InDels present. Nucleotide sequences of each cluster were copied and pasted into the programme and 'pair' selected as the output format before 'submit' was clicked to generate an alignment. Results were then exported into a PDF for manual analysis.

2.5.8. Translating Sanger Sequencing and Oxford Nanopore Sequencing data into an amino acid sequence

The effect of any amino acid alterations caused by the CRISPR-Cas9 editing process on the sequence of Rab11A and Rab40B was determined by using the ExPASy (Expert protein analysis system) translate tool (https://web.expasy.org/translate/) to translate nucleotide sequences obtained from sequencing (as detailed above). Nucleotides sequences were copied and pasted into the translation tool and the 'TRANSLATE!' button clicked. Results were then exported as a Microsoft word document and Clustal Omega (https://www.ebi.ac.uk/Tools/msa/clustalo/) used to align the amino acid sequence of the non-targeting cell lines with the wildtype and then the non-targeting with the potential knockout amino acid sequences. The amino acid sequence of the samples to be aligned were copied and pasted into the alignment tool, separated by a space and 'submit' clicked. Results were then exported into a Microsoft Word document for manual analysis.

2.6. Cellular function assays

2.6.1. Transferrin uptake assay

25,000 cells were seeded onto glass coverslips in one 4-well dish per assay time point, covered with 1ml RPMI medium (Sigma-Aldrich; R8758) with 10% FBS (HyClone; SH30541.03). Cells were left overnight at 37°C before being placed on ice for 10 minutes. Cell culture medium was removed, and cells were washed with phenol red-free RPMI medium (Sigma-Aldrich; R7509). Transferrin (from human serum, Alexa Fluor™ 568) was added to phenol red-free RPMI to give a concentration of 25µg/ml and cells incubated for 10, 20 or 30 minutes at 37°C. A 0-minute and no-transferrin control for each time point were also carried out. At the end of each time point, transferrin was removed, and cells washed in phenol red-free

RPMI. Cells were then fixed using 4% paraformaldehyde (PFA; Sigma-Aldrich; P6148) and stored in PBS at 4°C.

2.6.1.1. Flow cytometry analysis of transferrin uptake

A transferrin uptake assay was carried out as described in section 2.6.1. with the following alteration, 75,000 cells were seeded into two wells of a 6-well plate per time point. After fixing, cells were scraped into 1 ml phenol red-free RPMI using a cell scraper and pipetted into an Eppendorf tube. Cells were then spun at 800 *xg* for 5 minutes and resuspended in 500 µl phenol red-free RPMI. Flow cytometry analysis was then conducted using a CytoFLEX S flow cytometer (Beckman Coulter) using a Y610 laser.

Gating for flow cytometry analysis was conducted as follows: a forward scatter (FSC) and side scatter (SSC) plot was used to firstly separate cells from debris and a cells gate generated. Data within the cells gate was then further filtered to separate clusters of cells from single cells using a FSC-A (forward scatter area) and FSC-H (forward scatter height) plot. A single cells gate was then generated. Finally, data within the single cells gate was plotted on a Y610 (laser used for the flow cytometry) and count plot to identify the range of fluorescence of single cells from which median fluorescence and transferrin uptake could be inferred. All gating was based on cells which had not been exposed to fluorescent transferrin, therefore for the final gating, all cells which had higher fluorescence that those within the gate were assumed to have uptaken fluorescent transferrin.

2.6.1.2. Immunofluorescence analysis of transferrin uptake

Cells which had been fixed after undergoing a transferrin uptake assay (as detailed in section 2.6.1.) were permeabilised using 0.1% PBX (0.1% (v/v) Triton X-100 and PBS) for 30 minutes at room temperature. Coverslips were then blocked in 10% goat serum in PBS (Fisher Scientific; 11530526) for 1 hour at room temperature. Cells were then incubated in 1:200 anti-LAMP1 (Anti-CD107; Mouse; Invitrogen; 14-1079-90) in 10% goat serum in PBS for 1 hour at room temperature. Coverslips were then

washed in PBT (0.1% Tween-20 in PBS) three times for five minutes each. 1:100 Alexa Fluor™ 488 (Anti-mouse; Invitrogen; A11029) secondary antibody was added to coverslips for 1 hour at room temperature before another three five-minute washes in PBT. 300 nM DAPI (Invitrogen; D1306) was added to slides for 3 minutes at room temperature and coverslips washed in PBS twice for three minutes each. Coverslips were then mounted onto glass microscope slides using x mounting medium, left to dry completely and stored at 4ºC. Confocal microscopy was conducted using a Zeiss LSM 710 microscope by Dr Alistair Hume. Images were analysed using Fiji Image J software.

2.7. Extracellular vesicle techniques

2.7.1. Preparation of media for extracellular vesicle isolation

FBS (HyClone; SH30541.03) was ultracentrifuged in a Beckman Coulter Optima LE-80K centrifuge at 100,000 xg for 18 hours to pellet endogenous extracellular vesicles (EV). 10 ml of EV-depleted FBS was then added to a 500 ml bottle of medium to give a 2% solution.

2.7.2. Cell culture and media preparation for extracellular vesicle isolation

Cells were seeded using media with 10% FBS at a seeding density such that they would achieve confluency 72 hours later. After 24 hours, media was changed to 2% EV-depleted FBS medium and left for 48 hours.

After 48 hours, media was removed and placed into a 50 ml Falcon tube. For semi-adherent cell lines, the media was centrifuged at 110 xg to pellet any suspension cells and then transferred to a new falcon tube and spun again at 1500 xg for 10 minutes. Whilst the media was centrifuged, cell were counted (as described in 2.1.6.) so that EV concentration per 1 million cells could later be calculated. Once the media had centrifuged, it was transferred to a new 50 ml falcon and centrifuged at 10,000

xg for 10 minutes at 4°C and then filtered using a 0.22 µm filter (Millipore Express; SLGP033RS) into a falcon tube.

To concentrate media for EV isolation by size exclusion chromatography, filtered media was added to a 100k MWCO protein concentrator column (Thermo Scientific; 88528) and centrifuged at 3000 *xg* at 4°C until it was concentrated to 0.5 ml.

2.7.3. Extracellular vesicle isolation by size exclusion chromatography

Prior to extracellular vesicle isolation, qEV original 70nm size exclusion chromatography columns (Izon; qEVorigGEN2/70nm; ICO7010031) were removed from the fridge and left until they had reached room temperature. The column was then placed in an Izon Automatic Fraction Collector (AFC) and the AFC calibrated following instructions in the 'Scale' tab on the touch screen and a 10 g weight provided by the machine. Eppendorf tubes were then added to the carousel and settings for collection selected. For this project, a 2.5 ml void and 0.4 ml fractions were selected. The column was then cleaned using 20 ml calcium and magnesium ion-free PBS (Sigma; D8537-500ML). 0.5ml of media concentrate was added to the top of the column and allowed to enter the column before 6 ml of PBS was added to the column. EV fractions were then automatically collected by the machine. The machine was cleaned between samples using 10 ml PBS. All EV fractions were left on ice before being stored at -80°C.

2.7.4. Nanoparticle tracking analysis

A ZetaView® (Analytik Ltd) was used to perform nanoparticle tracking analysis (NTA) on EV samples. Prior to use, the machine was calibrated using polystyrene beads (Merck; 90517) that were diluted 1:250 000 in sterile MilliQ water. The machine was then flushed using 20 ml sterile MilliQ water and primed using calcium and magnesium ion-free PBS. EV samples were then diluted 1:500 in calcium and magnesium ion-free PBS and 1 ml injected into the ZetaView. The dilution factor of the sample was inputted, and the machine was run using the following settings: 488nm laser set to scatter, 11 positions, 3 cycles and 'high' quality. The size

distribution and concentration of particles was measured and data was saved as a PDF. Two technical replicates were completed per sample to improve accuracy of measurements.

2.8. SWATH-MS

2.8.1. Preparation of samples for SWATH-MS

2.8.1.1. Cell lysates

Cell pellets were lysed using RIPA buffer (50 mM Tris-HCl pH 7.4, 1% (v/v) NP-40, 0.5% (w/v) Na-deoxycholate, 0.1% (w/v) sodium dodecyl sulfate, 150 mM NaCl, 2 mM EDTA, dH$_2$O to 100 ml) with 1% (v/v) protease inhibitors (Protease inhibitor cocktail set III; Merck; 539134-1SET) and left for 45 minutes at room temperature before protein was quantified using a protein assay (as described in section 2.2.8.). 50 µg of each cell lysate was then added to an Eppendorf tube and stored at 4°C before being sent for analysis.

2.8.1.2. Extracellular vesicles

Extracellular vesicle (EV) fractions were combined by concentrating using Vivaspin® 500 centrifugal concentrator columns (Sartorius; VS0101) and spun at 8000 *xg* until a volume of 50µl was reached. Samples were then transferred to fresh Eppendorf tubes before being stored at 4°C and sent for analysis. As whole EV fractions were used, number of particles differed between samples (quantified as described in section 2.7.4.). Approximate particle numbers were provided, however, to aid analysis after data acquisition had occurred.

2.8.2. SWATH-MS data acquisition

All samples were prepared and digested using Protifi S-Trap standard protocol (reducing the trypsin added for the EVs). Data was acquired on a Sciex 7600 tripleTOF using zSWATH a data independent acquisition (DIA), then searched against a September 2023 Swissprot download of the human proteome alongside common contaminants using the DIA-NN (Data-independent acquisition by neural networks) software. DIA-NN normalises the output to allow differential expression comparison, for this reason final output of EVs and cell lysates are separate though a library of all samples was generated as a midpoint to optimise protein matching.

All SWATH-MS (Sequential window acquisition of all theoretical mass spectra) data acquisition, sample preparation detailed in this section and initial analysis was conducted by Dr David Boocock and Dr Clare Coveney from the Mass Spectrometry and Proteomics group at Nottingham Trent University.

2.8.3. SWATH-MS analysis

2.8.3.2. Principle component analysis

Principle component analysis (PCA) was conducted using GraphPad Prism (version 10.1.2). The raw expression values of the top 25 most expressed peptides in cell lysates samples and the top 25 most expressed peptides in extracellular vesicle samples were inputted for three biological replicates of each Rab11A knockout cell line (A12, B11, B12), non-targeting control (F3, F11, H4) and the wildtype, unedited, HD-MB03 cell line. A principle component (PC) plot was then generated using the principle components 1 and 2.

2.8.3.1. Identification of differentially expressed proteins

SWATH-MS output data was analysed using the StatsPro software (www.omicssolution.com/wukong/StatsPro/). This software allows for the

identification of differentially expressed proteins. Data was imported and pre-processed using an NA ratio of 0.33 and CV (coefficient of variation) threshold of 1. A LIMMA (linear models for microarray data) parametric test was then conducted and a p value threshold of 0.05 and $\log_2$(fold change) threshold of 0.3 was applied to the results. Data was then plotted on a volcano plot using GraphPad Prism (version 10.1.2).

2.8.3.2. STRING analysis of differentially expressed proteins

The STRING (Search tool for the retrieval of interacting proteins) open access online software (https://string-db.org/) was used to identify protein-protein interaction networks of differentially expressed proteins. Proteins were uploaded to the 'Multiple Proteins' function and a confidence score of 0.7 was applied to generate protein lists using all interaction sources.

2.8.3.3. KEGG pathway analysis of differentially expressed proteins

Kyoto Encyclopaedia of Genes and Genomes (KEGG) pathway (Kanehisa and Goto, 2000) analysis was conducted using the online bioinformatics tool DAVID (the database for annotation, visualisation and integration discovery) (https://david.ncifcrf.gov/tools.jsp) to identify molecular pathways that differentially expressed proteins were associated with. Lists of differentially expressed proteins were uploaded to the site and analysis was conducted using the 'Functional annotation tool'. 'KEGG_PATHWAY' was selected and pathways were generated using a p-value cut off for associated pathways of $p \leq 0.05$ with p-value being calculated using a modified version of Fisher's Exact test. Diagrams for each associated network pathway could then be examined to identify any sequential interactions of differentially expressed proteins within the pathway.

Chapter 3: Identification of Rab GTPase targets in medulloblastoma

3.1. Introduction

Rab GTPases are a family of Ras-related small GTPase proteins which regulate intracellular trafficking and control vesicle budding, motility and fusion (Pereira-Leal and Seabra, 2000) (Pfeffer, 2005) (Stenmark, 2009). In humans, there are 66 Rab GTPases (Rabs) (Gillingham et al., 2014) that function as molecular switches, alternating between GTP-bound active and GDP-bound inactive conformations. Rabs are activated by GEFs (guanine nucleotide exchange factors) which catalyse exchange of GDP for GTP and inactivated by GAPs (GTPase activating proteins) which catalyse the hydrolysis of GTP to GDP and inorganic phosphate (Pi). Regulation of action by GEFs and GAPs allows Rabs to then carry out their cellular functions through interaction with a diverse range of effector proteins which include GEFs and GAPs but also other proteins (Yoshimura et al., 2010) (Haas et al., 2007) (Gillingham et al., 2014).

Previous work conducted by Dr Hannah K. Jackson from the Coyle lab showed that metastatic medulloblastoma cell lines secrete more exosomes than their matched primary tumour cell lines, suggesting that exosome biogenesis may have a role in medulloblastoma metastasis (Jackson et al., 2023). Exosomes are small extracellular vesicles which are secreted by the majority of cell types and are believed to participate in cancer progression and metastasis through the transfer of bioactive molecules (Tai et al., 2018). Multiple Rabs including Rab11A, Rab35 and Rab27A, have been directly linked with the exosome biogenesis pathway wherein they have been implicated in the fusion of late endosomes and multivesicular bodies with the plasma membrane (Pegtel and Gould, 2019) (Savina et al., 2002) (Ostrowski et al., 2010). As Rab GTPases have a direct involvement in exosome biogenesis and secretion, it was hypothesised that they may have a role in the observed increased biogenesis by metastatic cell lines, and therefore could be drivers of medulloblastoma metastasis. As the potential role of Rab GTPases in medulloblastoma metastasis was as yet unexplored, it was important to establish what was already known about Rab contribution to tumourigenic pathways in general, and then build on this by focusing specifically on available medulloblastoma datasets. This was then used to inform the selection of Rab targets in medulloblastoma for further experimental study. The first step of which was to

experimentally verify the expression of these targets in medulloblastoma patient-derived cell lines.

Aims of the chapter:

- To identify Rab GTPases associated with cancer progression.
- To identify whether Rab GTPases have been identified as exosomal cargo in exosomes secreted by cancer cells and tumours.
- To analyse online databases and data collected by previous students in the Coyle lab to identify novel Rab GTPase targets which could contribute to the progression of medulloblastoma.
- To test the expression of these novel targets in medulloblastoma patient-derived cell lines.

3.2. Pathway to identification of potential Rab GTPase targets

The initial stage of this project was to identify whether there was evidence that any of the 66 Rab GTPases (Rabs) found in humans may have a contribution to medulloblastoma pathogenesis. It was important that a systematic approach, that considered all of the available evidence, was used to prevent overlooking any Rabs which may have a significant contribution. This approach is outlined in Figure 3.1.

3.3. Analysis of the literature to identify Rab GTPases known to be associated with cancer

3.3.1. Review of the literature

To begin to identify Rabs for further investigation and determine what is already known about Rab GTPase contribution to pathways of tumourigenesis, an NCBI (National Centre for Biotechnology Information) PubMed literature search using the terms 'Rab GTPase' AND 'cancer' was conducted between October 2019 and October 2020. This identified numerous review papers including Tzeng and Wang (2016) and Krishnan et al. (2020) which described the potential contribution of 31 Rabs to the pathogenesis of a broad range of cancers including breast, colon, liver and glioma (Table 3.1).

The search highlighted that, generally higher expression of Rabs was associated with aiding oncogenic processes (see 'role' column of Table 3.1.), such as metastasis, and poorer prognosis for patients. Notably, none of the papers reviewed presented these findings in paediatric cancers meaning that no conclusion could be made about the potential effect of aberrant Rab expression in a childhood cancer model.
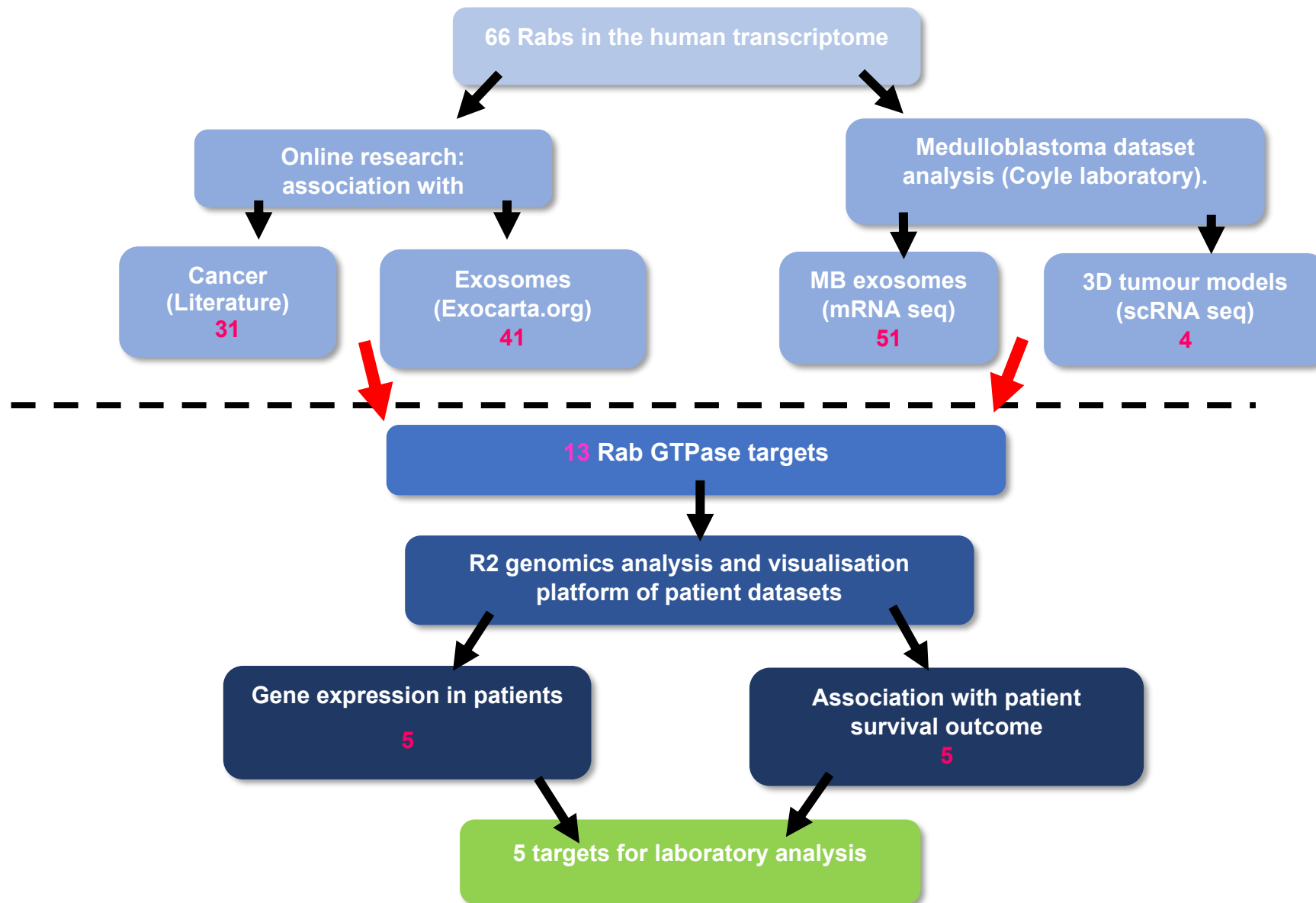
Figure 3.1. – Pathway to Rab GTPase targets Number of Rabs identified or which meet selection criteria (e.g. statistical significance p<0.05) are highlighted in pink font. 13 Rabs were narrowed down from 66 if they were associated with cancer or identified in cancerous cells and if they had been identified within exosomes. All 13 underwent analysis using the R2 genomics analysis and visualisation platform. MB – medulloblastoma. Seq – sequencing.

84

Table 3.1. Literature summary of Rab GTPases involved in cancer

Rab GTPase	Cancer type	Role	Expression compared to normal tissue	Clinical implication / cancer-related function	PubMed ID / DOI	Rab GTPase	Cancer type	Role	Expression compared to normal tissue	Clinical implication / cancer-related function	PubMed ID / DOI
Rab1A	Colon	Oncogenic	Increased	Increased cell invasion, poor prognosis	27716280	Rab5	Lung	Oncogenic	N/A	Increased cell motility	27121131
	Liver	Oncogenic	Increased	Increased cell invasion, Poor prognosis	27716280		Melanoma	Oncogenic	Increased	Induces hypoxia-driven metastasis	31973201
	Glioma	Oncogenic	Increased	Poor prognosis	24279471	Rab5A	Breast	Oncogenic	Increased	Increased cell motility	25049275
Rab1B	Colorectal	Oncogenic	Increased	Poor prognosis	28316326	Rab8B	Testicular	Oncogenic	Increased	Accelerated tumourigenesis	10.4172/ jcsb.1000231
	Triple-negative breast cancer	Tumour suppressive	Decreased	Promotion of metastasis	25970785	Rab9	Breast	Oncogenic	Increased	Anti-apoptotic	31973201
Rab2A	Breast	Oncogenic	Increased	Poor prognosis	27716280	Rab10	Hepatocellular carcinoma	Oncogenic	Increased	Anti-apoptotic	31973201
Rab2B	Pancreatic	Oncogenic	Increased	Anti-apoptotic	31973201	Rab11	Breast	Oncogenic	N/A	Increased cell motility	27716280
Rab3A	Glioma	Oncogenic	Increased	Tumour progression	27716280	Rab11A	Ductal carcinoma in situ	Oncogenic	Increased	Increased proliferation and cell motility	16791477
Rab3D	Breast	Oncogenic	Increased	Increased cell motility, induction of epithelial to mesenchymal transition	27716280 31973201		Non-small cell lung cancer	Oncogenic	Increased	Promotion of proliferation and invasion	28468127
	Lung	Oncogenic	Increased	Increased metastatic behaviour	31973201	Rab12	Gastric	Oncogenic	Increased	Anti-apoptotic	31973201
Rab4	Breast	Oncogenic	Increased	Increased cell motility	25049275	Rab13	Glioma	Oncogenic	Increased	Anti-apoptotic	31973201

Table 3.1. continued

Rab GTPase	Cancer type	Role	Expression compared to normal tissue	Clinical implication / cancer-related function	PubMed ID / DOI	Rab GTPase	Cancer type	Role	Expression compared to normal tissue	Clinical implication / cancer-related function	PubMed ID / DOI
Rab14	Gastric	Oncogenic	Increased	Anti-apoptotic	31973201	Rab27B	Breast	Oncogenic	Increased	Poor prognosis	20484105
Rab17	Hepatocellular carcinoma	Tumour suppressive	Decreased	Inhibition of tumourigenic properties	27716280	Rab27A/B	Colorectal	Oncogenic	Deletion/missense mutation	Anti-apoptotic	31973201
Rab17	Non-small cell lung cancer	Tumour suppressive	Decreased	Promotion of cell proliferation and invasion	31841274		Pancreatic	Oncogenic	Deletion/missense mutation	Anti-apoptotic	31973201
Rab18	Gastric	Oncogenic	Increased	Anti-apoptotic	31973201	Rab31	Cervical	Oncogenic	Increased	Anti-apoptotic	31973201
Rab21	Cervical cancer	Oncogenic	Increased	Increased cell motility	27716280	Rab31	Gastric	Oncogenic	Increased	Anti-apoptotic	31973201
Rab21	Glioma	Oncogenic	Increased	Anti-apoptotic	31973201	Rab31	Liver	Oncogenic	Decreased	Pro-apoptotic	31973201
Rab21	Breast	Oncogenic	N/A	Multi-drug resistance	31928387	Rab31	Brain	Oncogenic	Increased	Anti-apoptotic	31973201
Rab23	Stomach	Oncogenic	Increased	Poor prognosis	27716280	Rab35	Kidney	Oncogenic	Increased/ missense mutation	Anti-apoptotic	31973201
Rab23	Breast	Tumour suppressive	Increased	Pro-apoptotic	31973201	Rab35	N/A	Oncogenic	Gain of function mutations	Anti-apoptotic	26338797
Rab25	Ovarian	Oncogenic	Increased	Poor prognosis, increased cell motility	27716280 31973201	Rab37	Lung	Tumour suppressive	Decreased	Poor prognosis, inhibits MMP9 activity	27716280 31973201
						Rab38	Glioma	Oncogenic	Increased	Poor prognosis	27716280
Rab25	Breast	Oncogenic	Increased	Poor prognosis, anti-apoptotic	27716280 31973201	Rab40B	Gastric	Oncogenic	Increased	Promotion of migration, invasion and metastasis	25790780
Rab25	Claudin-low breast cancer	Tumour suppressive	Decreased	Poor prognosis	31973201	Rab40B	Hepatocellular carcinoma	Oncogenic	Increased	Promotion of cell proliferation and metastasis via PI3K/AkT signalling pathway	33116869
Rab25	Oesophagus	Tumour suppressive	Decreased	Poor prognosis	27716280	Rab45	Leukaemia	Tumour suppressive	Increased	Pro-apoptotic	31973201
Rab27A	Melanoma	Oncogenic	Increased	Increased proliferation	21129771						

3.3.2. Use of Exocarta.org to identify Rab GTPases found in exosomes

Given the potentially pivotal role of exosomes in metastasis and cancer, the Rab GTPase content of exosomes was investigated in February 2020 using ExoCarta database (http://exocarta.org) which collates exosomal cargo from approximately 300 published studies. These cargoes include protein, mRNA, microRNA and lipids and were identified in various sample types such as cancer cells, breast milk, neurones, epithelial cells, plasma, saliva and urine. It also provides information on the contents of exosomes from multiple organisms such as humans, mice and *Drosophila*. This search was conducted to identify Rab GTPases that have been reported in human cancer-derived exosomes. This identified the presence of 41 Rabs in the exosomes secreted by various cancer cell lines and cancer tissue samples (Table 3.2).

3.3.3. Literature search of Rab GTPases in medulloblastoma exosomes

As no medulloblastoma exosome data was identified on Exocarta.org, a literature search was conducted to identify medulloblastoma exosome datasets which could be analysed for Rabs. An NCBI PubMed literature search using the terms 'medulloblastoma' AND 'exosomes' in February 2020 revealed that two medulloblastoma exosome studies had been published at the time of this part of the study, both of which focused on SHH (sonic hedgehog) medulloblastoma cell lines (Epple et al., 2012) (Bisario et al., 2015). Supplementary figures published by Epple et al. (2012) did however show the results of mass spectrometry on the exosomes of the group 3 medulloblastoma cell line D283MED and this identified the presence of Rab1B. No other Rabs were reported in medulloblastoma exosomes in either study.

Table 3.2. Rab GTPases in the ExoCarta.org exosome database identified in the exosomes of human cancers

Cancer type	Rab GTPases identified
Bladder	Rab1B, Rab5A, Rab5C, Rab6A, Rab7A, Rab10
Colorectal	Rab1A, Rab1B, Rab2A, Rab4B, Rab5A, Rab5B, Rab5C, Rab6B, Rab8A, Rab8B, Rab10, Rab11A, Rab11B, Rab13, Rab14, Rab15, Rab18, Rab20, Rab21, Rab23, Rab27B, Rab33B, Rab35, Rab43
Hepatocellular carcinoma	Rab5A, Rab5B, Rab5C, Rab9B, Rab13, Rab14
Liver	Rab43
Melanoma	Rab1A, Rab1B, Rab1C, Rab2A, Rab5B, Rab5C, Rab6A, Rab6B, Rab7A, Rab8A
Nasopharyngeal carcinoma	Rab1A
Neuroblastoma	Rab1B, Rab3A, Rab3B, Rab3C, Rab4A, Rab5A, Rab5B, Rab5C, Rab6A, Rab6B, Rab7A, Rab8A, Rab10, Rab11A, Rab11B, Rab13, Rab14, Rab23, Rab32, Rab34
Ovarian	Rab1A, Rab1B, Rab2A, Rab2B, Rab3B, Rab4A, Rab5A, Rab5B, Rab5C, Rab6A, Rab6B, Rab7A, Rab8A, Rab8B, Rab9A, Rab10, Rab11B, Rab12, Rab13, Rab14, Rab18, Rab21, Rab22A, Rab23, Rab32, Rab33B, Rab34, Rab35, Rab43
Prostate	Rab1A, Rab1B, Rab2A, Rab3A, Rab3B, Rab3C, Rab5A, Rab5B, Rab5C, Rab7A, Rab8A, Rab8B, Rab9A, Rab10, Rab11B, Rab13, Rab14, Rab21, Rab27B, Rab35
Squamous cell carcinoma	Rab1A, Rab1B, Rab2A, Rab2B, Rab5A, Rab5B, Rab5C, Rab7A, Rab8A, Rab8B, Rab13, Rab14, Rab18, Rab21, Rab34, Rab35, Rab39A, Rab43

3.4. Analysis of previous data collected by the Coyle laboratory

3.4.1. Rab GTPase mRNA is present in group 3 and group 4 exosomes

To determine whether Rab GTPase mRNA is present in exosomes derived from group 3 and group 4 primary and metastatic cell lines, mRNA sequence data collected by Jackson et al. (2021) was analysed. Jackson et al. conducted 3' UPX (ultraplex) next generation sequencing on the mRNA cargo of medulloblastoma-derived exosomes from the primary and metastatic matched tumour pairs of group 3 (D425, D458) and group 4 (CHLA-01, CHLA-01-R) cell lines. 3'UPX next generation sequencing analysis was conducted by QIAGEN and expression values of mRNAs detected were normalised using DESeq2, an R package which uses size factor normalisation. In this method, the geometric means of raw unique molecular identifier (UMI) values of each mRNA detected is calculated. A ratio of the raw UMIs of all mRNAs respective to their geometric means is then created for a given sample which is used to generate a normalisation factor for that sample. Finally, the raw UMI of each mRNA is divided by the normalisation of its sample to generate the normalised UMI values which can be analysed.

Analysis identified the presence of 51 Rab GTPase gene transcripts (Figure 3.2). Data also shows that more Rab mRNAs were present in group 3 exosomes compared to group 4 exosomes. Certain Rab mRNAs also had higher UMI values in the primary group 3 cell line D425 than the metastatic cell line D458 (Figure 3.2 B) suggesting that overall there is an enrichment of Rab mRNA in exosomes derived from primary group 3 cells than metastatic.
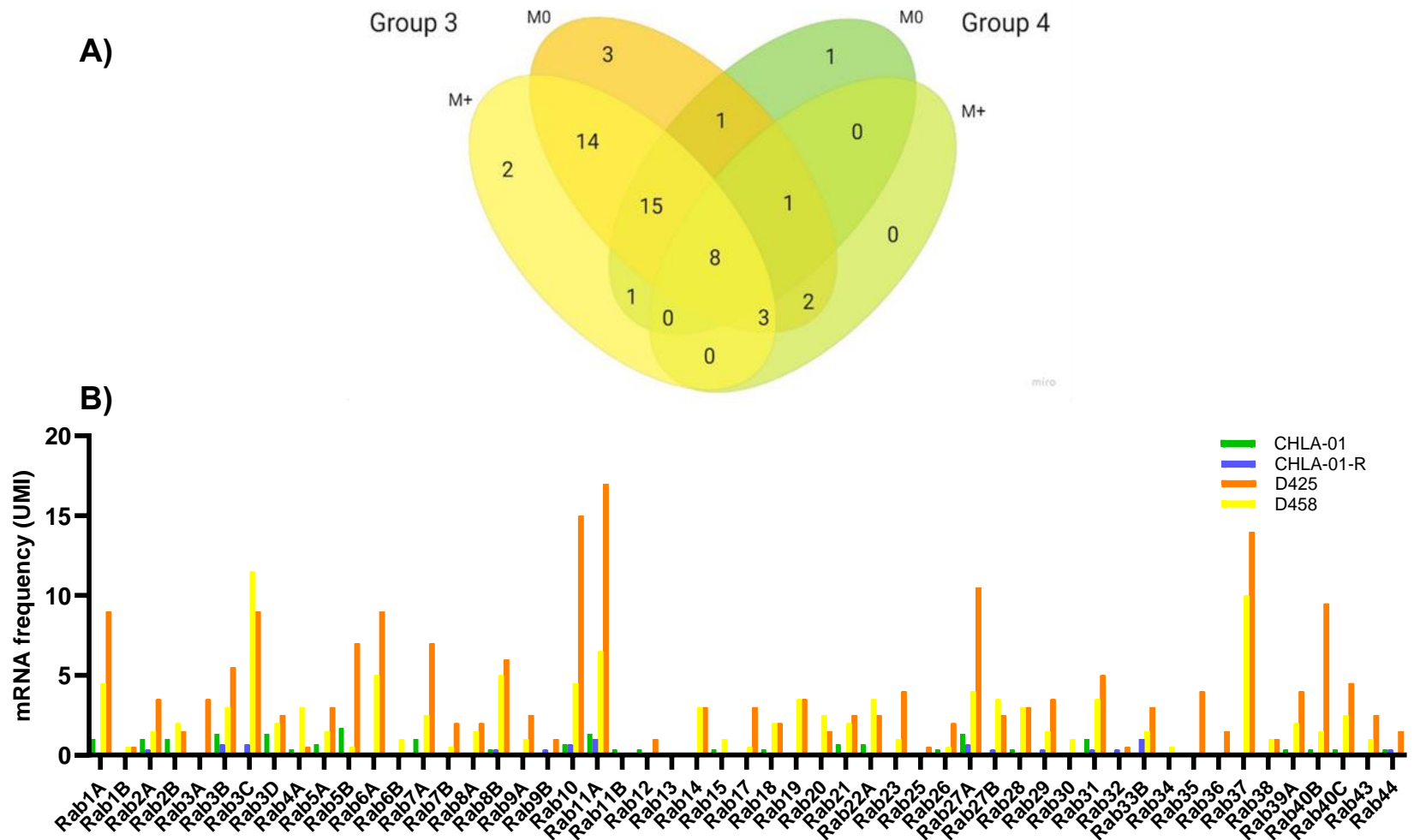
Figure 3.2 Rab GTPase mRNA expression in Group 3 and Group 4 exosomes. *(A) Venn diagram of the number of all Rab GTPase mRNAs expressed in group 3 and group 4 exosomes. Numbers refer to the number of Rab GTPase genes detected. The mRNA of 52 Rab GTPases were identified in the exosomes of group 3 and group 4 primary tumour and metastatic cell lines. Primary tumour-derived cell lines are denoted by 'M0' and metastatic tumour by 'M+'. For group 3, the D425 (M0) and D458 (M+) cell lines are shown and for group 4, the CHLA-01 (M0) and CHLA-01-R (M+) cell lines are shown. (B) Bar chart highlighting expression of specific Rab GTPase mRNAs expressed in group 3 and group 4 exosomes. Gene expression in the group 3 cell lines D425 (M0) and D458 (M+) are highlighted in orange and yellow respectively and in the group 4 cell lines CHLA-01 (M0) and CHLA-01-R (M+) in green and blue respectively. EV = extracellular vesicle. UMI = unique molecular identifier.* 90

3.4.2. *Rab1A*, *Rab5C*, *Rab7A* and *Rab11A* are upregulated genes in HD-MB03 scRNAseq analysis

A further dataset that was available for analysis came from experiments conducted by Linke et al. (2023). In these experiments, the group 3 cell line HD-MB03 and the SHH cell line ONS-76 were grown in a 3D hydrogel model to better mimic the growth and migration of these two subgroups *in vitro*. Single cell (sc) RNA sequencing on tumour nodules from hydrogels allowed for the clustering of cells based on their genetic similarities using K-means cluster analysis conducted by Linke et al. (2023). For the HD-MB03 cell line this yielded nine clusters of genetically similar cells from the 4,148 cells analysed. Up- and downregulated genes were then identified based on comparison of gene expression data between each of the clusters. Results were then filtered using a log2 fold change >0 and p-value ≤0.05.

This identified four Rabs which were upregulated in one or more of the nine clusters identified for HD-MB03 cells; Rab1A, Rab5C, Rab7A and Rab11A (Figure 3.3.). Linke et al. identified cellular pathways which were associated with upregulated genes in each cluster (Appendix 1.1.). All four Rabs were upregulated in clusters 1, 2 and 3 which Linke et al. showed to have an upregulation of genes associated with amino acid biosynthesis, metabolism and exosome biogenesis. Other clusters including 4,5, 7 and 8 did not have these genetic signatures. Therefore, the Rabs shown to be upregulated in HD-MB03 cells were upregulated in the populations of cells which appear to be the most metabolically active. No Rabs were upregulated in any cluster of the ONS-76 cell line.
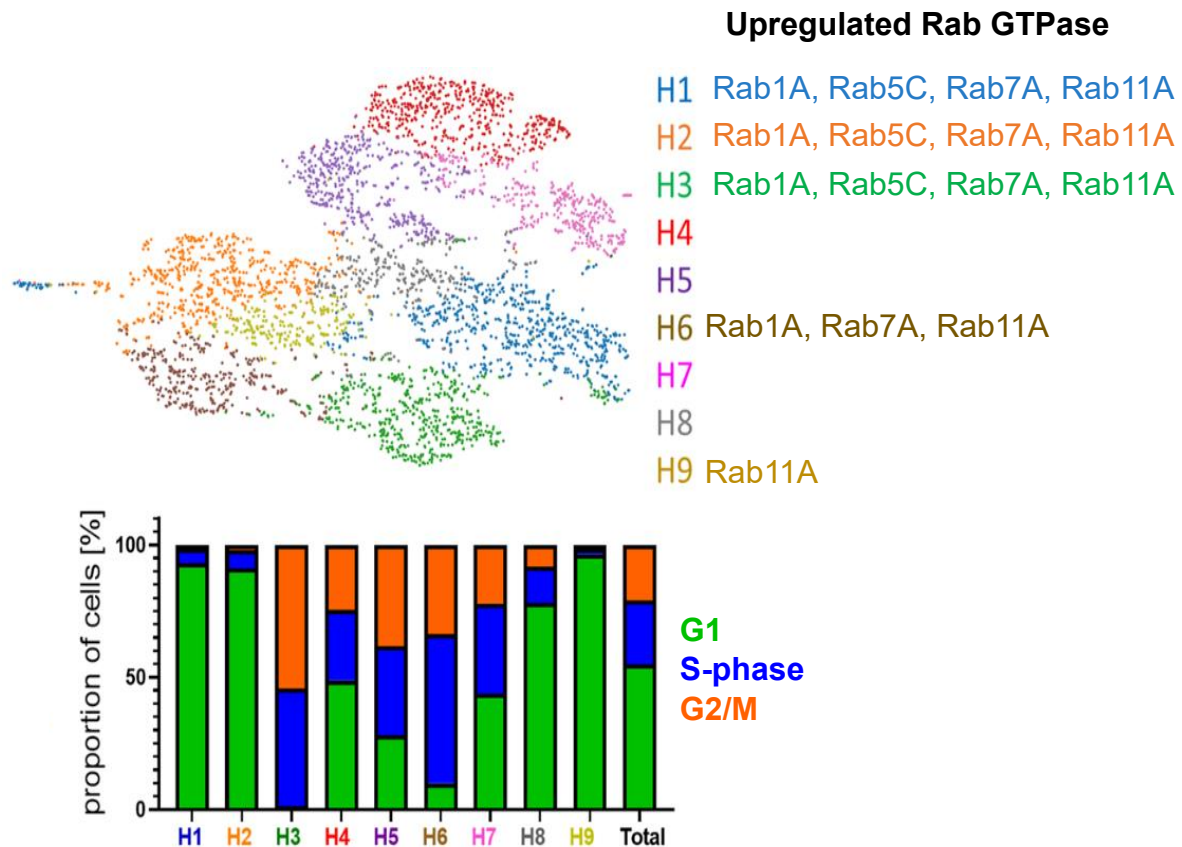
Figure 3.3. Upregulated Rab GTPase genes in HD-MB03 medulloblastoma cells after single cell RNA sequencing analysis *K-means clustering grouped 4148 HD-MB03 group 3 medulloblastoma cells grown in 3D hydrogel models into nine genetically distinct clusters. Cluster map and Rab GTPases with upregulated expression in clusters (top), relative proportion of cells in G1 (green), S (blue) and G2/M (orange) phase of the cell cycle in each cluster (bottom). Figure adapted from Linke et al., 2023.*

3.5. Analysis of Rab GTPase expression across publicly available medulloblastoma datasets

The decision was made to select specific candidates for further analysis using publicly available medulloblastoma patient datasets such as the R2: genomics analysis and visualisation platform. This was to begin the process of focusing the number of Rabs analysed so that eventually only the Rabs believed to have the most association with medulloblastoma pathogenesis were functionally examined.

These candidates were selected based on whether they had been associated with cancer or identified in cancerous cells (literature or work by Linke et al.) and whether

they had been identified in exosomes (Exocarta.org or work by Jackson et al), as the initial focus of this study was to identify Rab GTPases that contributed to medulloblastoma pathogenesis through roles in exosome biogenesis or exosomal cargo loading.

Thus 13 Rabs: Rab1A, Rab1B, Rab3A, Rab3C, Rab7A, Rab8B, Rab10, Rab11A, Rab11B, Rab13, Rab27A, Rab37 and Rab40B, were selected for further analyses.

3.5.1. Gene expression of Rab GTPases in medulloblastoma patient datasets

Patient dataset analysis was used to compare the relative gene expression of the thirteen shortlisted Rabs across each of the medulloblastoma subgroups (WNT, SHH, group 3 and group 4). For this analysis, the Cavalli dataset of 763 medulloblastoma patients (Cavalli et al., 2017) on R2: Genomics analysis and visualisation platform (R2) (http://r2.amc.nl) was used (Figure 3.4.). Statistical significance of gene expression of each Rab in one subgroup compared to each of the other subgroups was assessed using Brown-Forsythe and Welch analyses with Dunnett's T3 multiple comparison test.

Generally, no statistical significance could be attributed to differences in expression of any Rab between the subgroups, with the exception of Rab13 which had statistically significant more expression in WNT ($p \leq 0.01$) and SHH ($p \leq 0.05$) than group 4.
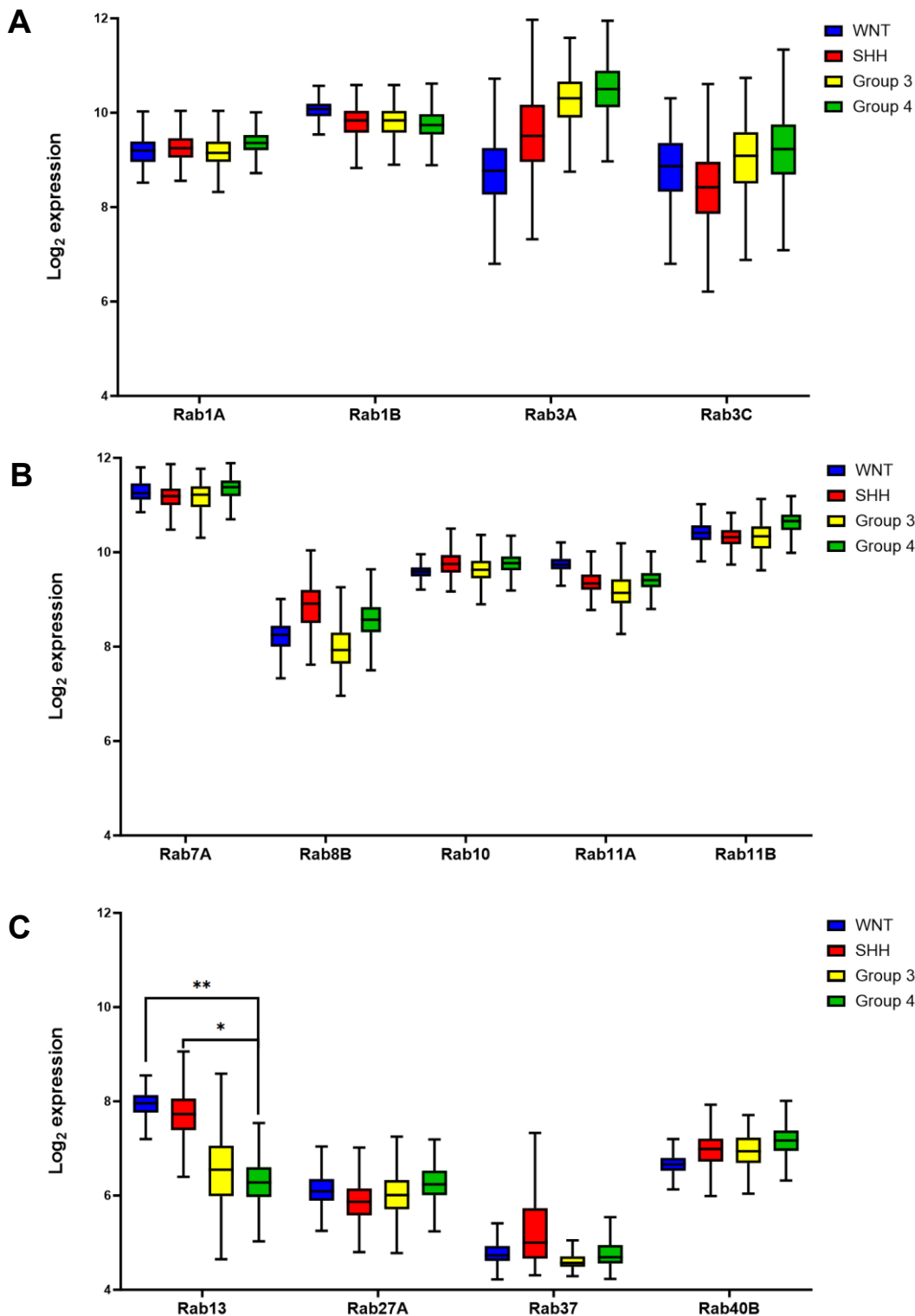
Figure 3.4. Gene expression of selected Rab GTPase targets in medulloblastoma subgroups *Log2 gene expression was determined using the Cavalli medulloblastoma dataset from the R2: Genomics Analysis and Visualisation Platform. WNT: n=70 (blue), SHH: n=223 (red), Group 3: n=33 (yellow), Group 4: n=326 (green). Expression is displayed as box plots with minimum (lower line), lower quartile (bottom line of box), Median (middle line of box), upper quartile (top line of box) and maximum (top line) patient expression shown. Statistical significance of gene expression of each Rab within each subgroup compared to other subgroups was assessed using Brown-Forsythe and Welch analyses with Dunnett's T3 multiple comparison test. * p ≤ 0.05, ** p ≤ 0.01. Those without lines or significance stars had no significance in gene expression upon statistical analysis.*

94

3.5.2. Analysis of medulloblastoma patient survival outcomes with high or low Rab GTPase expression

The Cavalli dataset on R2 has data from 763 patients and for 612 patients this includes data on disease progression and survival. This allows for the exploration of the relationship between the expression of the thirteen shortlisted Rabs and patient prognosis. To generate Kaplan-Meier curves, the R2:KaplanScan tool was used. This divides the expression of a gene in a patient population into 'high' and 'low' expression groups based on statistical testing instead of the mean or median. Samples are listed from highest to lowest expression of a single gene. They are then separated into two groups with a minimum of 8 samples per group, starting with the eight patients with the lowest expression of a particular gene in one group and the rest of the sample size in another. The individual gene expression values of each patient within each group are then added together and a log-rank (Mantel-Cox) test is run to determine the p-value of the difference in the sum of the expression between the groups. The combined gene expression value of the patients with the nine lowest expression is then compared to the remainder of the sample size and a p-value is produced, and so on until the patients with the eight highest expression values are compared to the rest of the dataset. The cutoff between high and low expression is placed between the groups with the most significant p-value with samples with higher expression becoming the 'high' expression group and those lower than becoming the 'low' expression group. A Kaplan-Meier survival curve showing the survival of the two groups is then plotted by R2. As expression cutoffs are based on statistical significances, the number of patients in the 'high' and 'low' expression group therefore varies between genes analysed. If statistical significances are equal for two different analyses for the same gene, the chi squared value is used to set the cutoff with a higher chi squared value taking precedent. When assessing whether KaplanScan produced the most optimal high and low expression groups, the median and mean were also used as cutoff values. For each of the genes tested using the Cavalli dataset, KaplanScan produced the highest statistical significance between expression groups (data not shown). As such, KaplanScan cutoffs were used in this study.

Initial analysis focused on association of expression with survival outcome among medulloblastoma patients overall as well as between those in different molecular subgroups. Analysis was also further refined to identify survival outcomes of only patients which were metastatic at diagnosis. This was conducted on patients with SHH, group 3 and group 4, no metastatic data was available for patients with the WNT subgroup as there was an insufficient sample size (Table 3.3 and Appendix 1.2).

For this part of the study, the focus was on identifying Rabs whose high expression correlated with poorer survival in a subgroup-specific fashion. This was primarily because firstly, as previously described, medulloblastoma is subdivided into molecular subgroups all of which have different metastasis patterns, ages of onset and mechanistic pathways that are believed to contribute to pathogenesis (Table 1.2.). As such, to identify specific prognostic or mechanistic markers, the subgroups should be regarded separately. Secondly, it is pharmacokinetically simpler to design drugs to inhibit an overexpressed druggable target instead of constitutively overexpressing an under expressed protein (Khorkova et al., 2023) (Hopkins and Groom, 2002). If this study identifies a metastatic driver of a subgroup of medulloblastoma, it will therefore be more therapeutically beneficial if this target has high expression.

Across all medulloblastoma subgroups, high expression was significantly ($p \leq 0.05$) associated with poorer survival for Rab3A, Rab7A, Rab10, Rab27A and Rab40B (Table 3.3.). Of the medulloblastoma subgroups, group 3 patients had the most Rabs in which there was a statistically significant link between high expression and poor survival, suggesting a subgroup-specific contribution of Rabs to medulloblastoma pathogenesis. In group 3 patients, high expression of Rab1B, Rab8B, Rab11A, Rab13 and Rab40B was correlated with poor survival, with p-values ranging from 0.044 (Rab11A) to 0.00075 (Rab40B) (Table 3.3.). When stratified for metastatic status, high expression of Rab1B, Rab8B, Rab11A, Rab27A and Rab40B was correlated with poorer survival with p values ranging from 0.037 (Rab27A) to 0.0003 (Rab40B).

High expression of fewer Rabs was significantly associated with poorer survival in SHH and group 4 patients (Appendix 1.2.) (SHH – Rab7A and Rab10, group 4 –

Rab1B, Rab7A and Rab13) and SHH and group 4 metastatic patients (SHH – Rab3C and Rab37, group 4 – Rab1B).

This data showed that of the Rab target shortlist, high expression of Rab40B is associated with poorer survival in group 3 but not other patient groups (Figure 3.5.), suggesting a group 3-specific effect of Rab40B. This was also the case for Rab8B and Rab11A but with lower statistical significances. High Rab1B was associated with poorer group 3 and group 4 patient survival (both overall and in metastatic patients) and high Rab13 is associated with poorer survival overall in groups 3 and 4 (Table 3.3.). Despite the association with both group 3 and group 4, Rabs 1B and 13 may still be of interest as groups 3 and 4 are regarded as 'Medulloblastoma, non WNT/non SHH' by the 2021 WHO classification of tumours of the central nervous system (Louis et al., 2021b) as the specific pathways are not currently understood.

Table 3.3. – Summary Kaplan-Meier survival curves of potential Rab GTPase targets in all medulloblastoma subgroups and group 3 *Overall survival probability of both non-metastatic and metastatic patients was determined using the Cavalli medulloblastoma dataset from the R2: Genomics Analysis and Visualisation Platform. All subgroups: n=612, group 3 (all patients; M0 + M+): n=113, group 3 (M+): n=41. M0 denotes patients that were not metastatic at diagnosis. M+ denotes patients that were metastatic at diagnosis. Shaded green – high expression has a statistically significant (p≤ 0.05) better outcome. Shaded red – high expression has a statistically significant (p≤ 0.05) poorer outcome.*

Rab GTPase	n		All subgroups p-value	n		Group 3 only p-value	n		Group 3 (M+) only p-value
	High	Low		High	Low		High	Low	
Rab1A	255	357	0.019	105	8	0.178	13	26	0.191
Rab1B	357	255	0.072	67	46	0.00094	22	19	0.019
Rab3A	521	91	0.0024	97	16	0.095	9	32	0.075
Rab3C	227	385	0.001	61	52	0.00087	32	9	0.00046
Rab7A	11	601	0.047	101	12	0.215	14	27	0.378
Rab8B	191	421	0.004	94	19	0.030	30	11	0.024
Rab10	63	549	0.01	49	64	0.181	28	13	0.133
Rab11A	109	503	0.032	100	13	0.044	29	12	0.013
Rab11B	596	16	0.0021	104	9	0.050	20	21	0.207
Rab13	119	493	0.000014	17	96	0.0051	8	33	0.257
Rab27A	9	603	0.0035	103	10	0.155	8	33	0.037
Rab37	590	22	0.061	102	11	0.0077	9	32	0.164
Rab40B	444	168	0.026	13	100	0.00075	11	30	0.0003
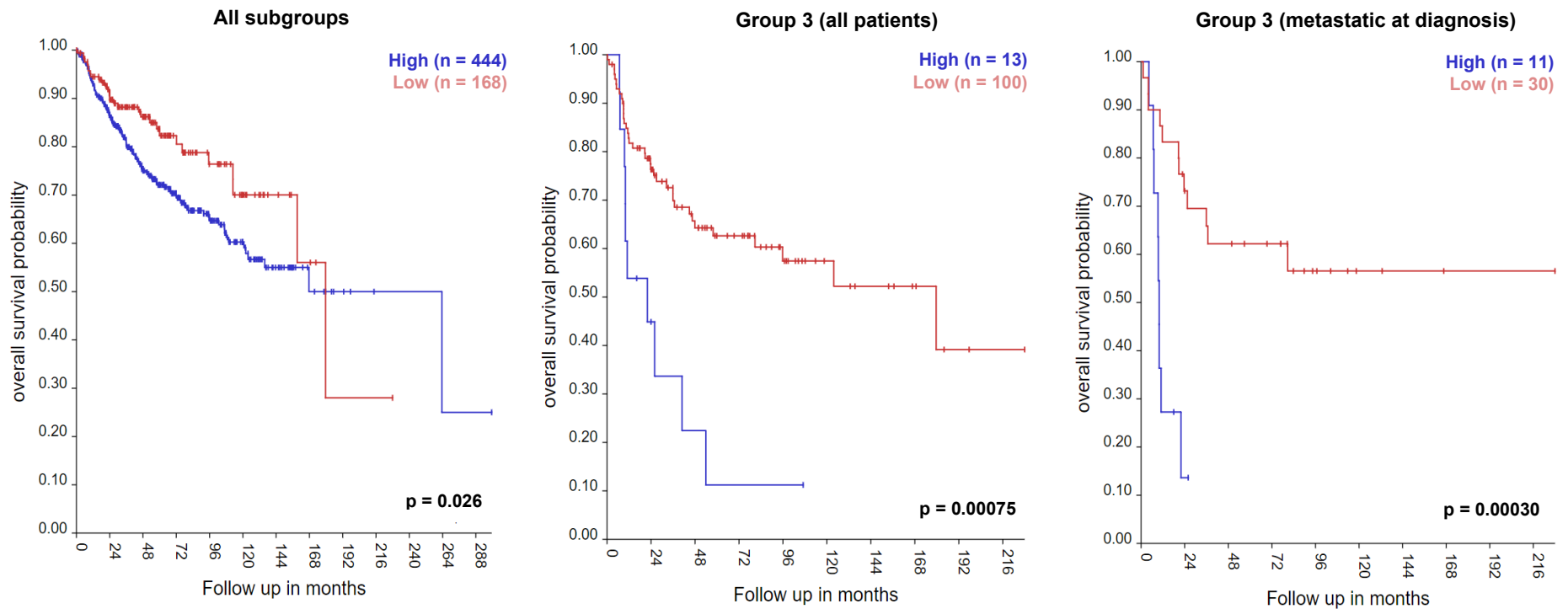
Figure 3.5. – Kaplan-Meier survival curve analysis of Rab40B in all medulloblastoma subgroup patients, group 3 patients and group 3 patients who were metastatic at diagnosis *Gene expression-based survival curve analysis using the Cavalli dataset on the R2: Genomics analysis and visualisation platform. Medulloblastoma patients from all subgroups (left, n = 612), group 3 (centre, n = 113) and group 3 patients who were metastatic at diagnosis (right, n = 41). The R2:Kaplan Scan tool was used to generate survival curves. Statistical significance (p ≤ 0.05) between curves was determined using the log-rank (Mantel-Cox) test.*

3.6. Rab1B, Rab8B, Rab11A, Rab13 and Rab40B are potential targets for further study in group 3 medulloblastoma

Based on evidence showing associations with disease as highlighted in sections 3.3. and 3.4., Rab1B, Rab8B, Rab11A, Rab13 and Rab40B were proceeded with as candidates for further exploration in group 3 medulloblastoma. A summary of analyses and whether an association was made with indicators of potential contribution to pathogenesis is shown in Table 3.4. As the five chosen Rabs were the only Rabs that had an association across all three analyses, they were selected.

Table 3.4. Summary of results of analysis of Rab GTPase target shortlist
Green – association was identified, red – association was not identified.
Asterisks indicate Rab GTPases taken forward for further study.

Rab GTPase	Associated with tumourigenesis?	Identified as EV cargo?	High expression associated with poor survival in group 3 patients?
Rab1A	green	green	red
*Rab1B	green	green	green
Rab3A	green	green	red
Rab3C	red	green	red
Rab7A	red	green	red
*Rab8B	green	green	green
Rab10	green	green	red
*Rab11A	green	green	green
Rab11B	red	green	red
*Rab13	green	green	green
Rab27A	green	green	red
Rab37	red	green	red
*Rab40B	green	green	green

3.6.1. Additional cellular functions of Rab1B, Rab8B, Rab11A, Rab13 and Rab40B

To begin to explore the specific pathways in which each of the selected Rabs may be contributing to medulloblastoma pathogenesis and to inform downstream investigation of these targets, a more focused literature search was conducted prior to the end of the COVID lockdown and return to the laboratory (Table 3.5.). This provided evidence that the selected Rabs have roles in addition to those in vesicle budding, motility and fusion. Rab13 and Rab40B contribute actin cytoskeleton dynamics and Rab8B, Rab13 and Rab11A are regulators of pathways such as Wnt/β-catenin, PKA (protein kinase A) signalling and cell polarisation respectively (Köhler et al., 2004) (Linklater et al., 2021) (Demir et al., 2013) (Roland et al., 2011) These roles are known facilitate cancer progression and metastasis through functions including modulation of growth factor signalling, cancer stem cell renewal and epithelial-to-mesenchymal transition, when altered in cancer cells.

Table 3.5. – Cellular roles of top 5 Rab GTPase target shortlist

Rab GTPase	Cellular roles	Reference
Rab1B	Recruitment of downstream effectors to membranes for vesicle formation, movement, tethering and fusion. Regulates vesicular transport between the ER and successive Golgi compartments.	Overmeyer et al., 1998
Rab8B	Roles in polarised vesicular trafficking and neurotransmitter release. Positive regulator of Wnt/β-catenin signalling. Involved in adherens junction dynamics in Sertoli cells.	Mignogna and D'Adamo, 2018 Demir et al., 2013 Lau and Mruk, 2003 Aboubakr et al., 2016
Rab11A	Regulates endocytic recycling. Major regulator of membrane delivery during cytokinesis. Role in epithelial cell polarisation alongside MY05B and Rab8A.	Wilson et al., 2005 Lock and Stow, 2005 Roland et al., 2011
Rab13	Involved in endocytic recycling. Regulates the transport of transmembrane proteins such as occludin (tight junction protein) to the plasma membrane. Regulates tight junction assembly by reorganising the actin cytoskeleton and activating the PKA signalling pathway.	Marzesco et al., 2002 Morimoto et al., 2005 Kohler et al., 2004
Rab40B	Regulation of actin cytoskeleton dynamics during cell migration and invasion. Role in invadopodia formation and function.	Linklater et al., 2021 Jacob et al., 2016

Pathway analysis using the STRING (**S**earch **T**ool for the **R**etrieval of **In**teracting **G**enes/ proteins): functional protein association network tool was conducted (string-db.org) (Szklarczyk et al., 2019). This was to find known protein interactors and explore specific pathways in which the Rabs selected may be contributing to medulloblastoma pathogenesis, informing laboratory exploration of these targets. This tool pools known interactors from the literature using an average linkage algorithm and generates functional protein networks based on evidence of interaction provided by the literature. Default settings on STRING were used for this analysis. These were a minimum interaction score of 0.4 (on a scale of 0 to 1, where 1 is highest confidence) and a maximum number of interactors shown of 10. As such, the interaction partners given are the top ten most likely interactors. Results can be seen in Figure 3.6. and functional information about interaction partners in Appendix 1.3.

This showed that Rab1B (Figure 3.6. A) interacts with Rab11B and Rab1A, the Rab GDP dissociation inhibitors (GDI) GDI1 and GDI2, which are regulators of Rab function. It also interacts with geranylgeranyl transferase component A (CHM) and other proteins associated with the known Rab1B function of trafficking between the Golgi apparatus and endoplasmic cellular compartments (TRAPPC proteins, GOLGA2).

Rab8B (Figure 3.6. B) is an interactor of Rab1B and Rab8A, guanine nucleotide exchange factor DENND1C, and as with Rab1B it is an interactor of the Rab GDP dissociation inhibitors GDI1 and GDI2. It also interacts with MICALL2 (Molecule interacting with CasL-like 2) which is involved in tight junction complex assembly and with the Rab3A interacting proteins Rab3IP and Rab3IL1.

As with Rab8B, Rab3IP is also an interactor of Rab11A. Rab11A is a known regulator of endocytic recycling (Ullrich et al., 1996). Consequently, the remaining partners predicted by STRING have functions associated with these pathways. For example, it interacts with many Rab11FIP proteins which have roles in endocytic trafficking, EXOC6 (exocyst complex component 6) which is involved in exocytic vesicle docking

and MYO5A and B (myosin-5 A and B) which are thought to be involved in vesicular trafficking through the CART (cytoskeleton-associated recycling or transport) complex.

Rab13 shares many of its interactors with Rab8B, with DENND1C and MICALL2 being common to both Rabs. It also interacts with six EXOC proteins which, as previously mentioned, have roles in exocytic vesicle docking.

Finally, Rab40B interacts with Cullin-5, a core component of the E3 ubiquitin-protein ligase complexes and Rab40AL and Rab40C which are thought to be substrate-recognition components of this complex. It also interacts with homeobox protein cut-like proteins 1 and 2 (CUX1 and CUX2) which are thought to be involved in neuronal specification during development. It also interacts with elongin-C (TCEB1) and SAP domain-containing ribonucleoprotein (SARNP). Lastly, it interacts with the metalloproteinase inhibitor 2 (TIMP2), which inhibits matrix metalloproteinase-2 (MMP-2) has been shown to potentiate medulloblastoma migration (Jackson et al., 2023). Thus, suggesting that Rab40B-TIMP2 interaction could regulate medulloblastoma progression.

For the most part, STRING analysis supported the functionality of each Rab identified in the literature. For example, Rab1B interacts with GOLGA2 which is required for protein transport from the endoplasmic reticulum (ER) to the Golgi apparatus and Rab1B is associated with the regulation of vesicular transport between the ER and successive Golgi apparatus compartments (Figure 3.6.A) (Table 3.5.) (Diao et al., 2008) (Overmeyer et al., 1998). Rab40B was identified through literature analysis as having roles in cell migration and invasion (Linklater et al., 2021). STRING pathway analysis showed that it interacts with Cullin-5, which is a core component of the E3 ubiquitin-protein ligase complexes and has a role in cell migration through the ubiquitylation and degradation of target proteins (Gao et al., 2020). This supports the idea that Rab GTPases may also have roles in medulloblastoma pathogenesis through roles other than the vesicular trafficking pathways.
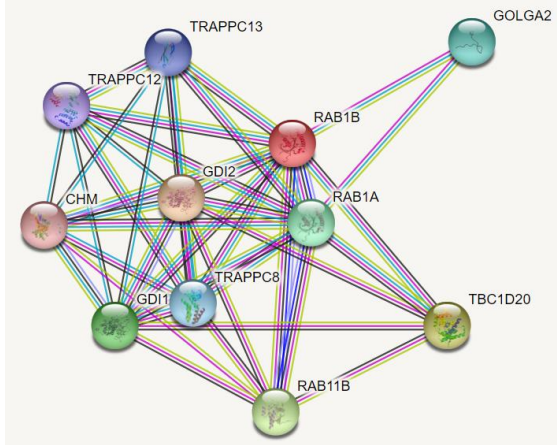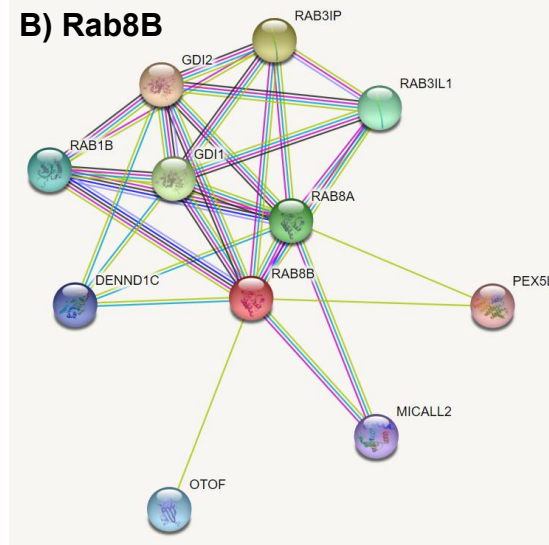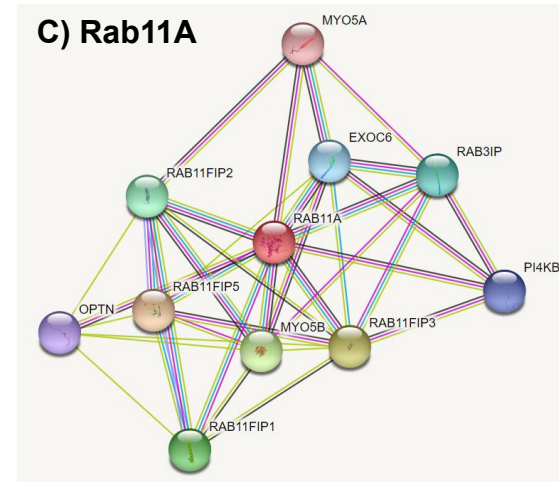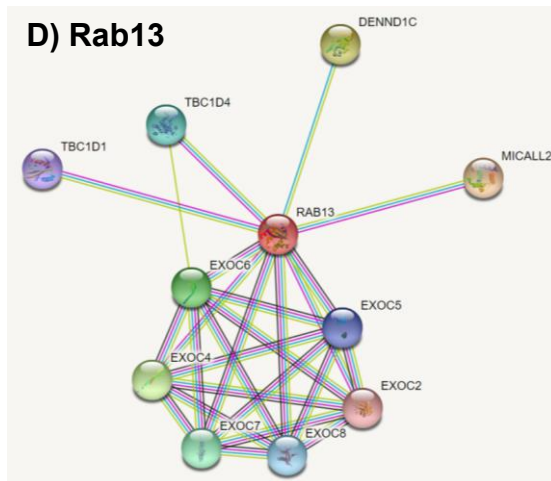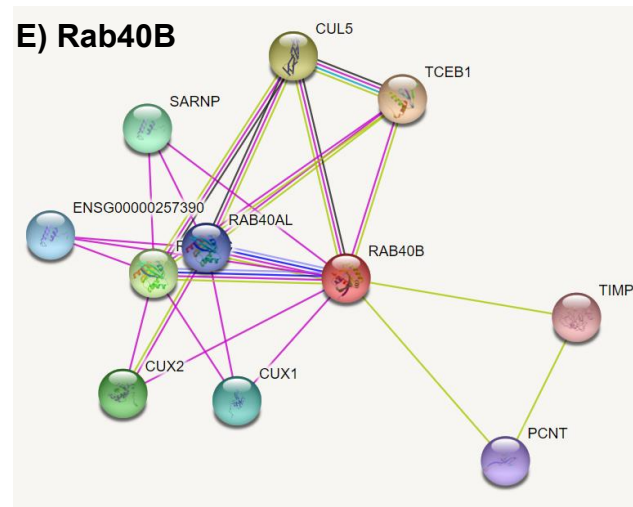
Figure 3.6. – STRING pathway networks of Rab1B (A), Rab8B (B), Rab11A (C), Rab13 (D) and Rab40B (E) *Functional partner networks generated using the STRING: protein network tool (string-db.org). All images were generated by STRING. Lines correspond to the type of resource used to generate interaction information. Pale blue line – known interactions from curated databases. Pink line – experimentally determined interactions. Green line – gene neighbourhood predicted interactions. Red line – gene fusion predicted interactions. Dark blue line – gene co-occurrence predicted interactions. Yellow line – text mining. Black line – co-expression. Lilac line – protein homology.*

3.7. Assessing target Rab GTPase expression in medulloblastoma patient-derived cell lines

After Rab1B, Rab8B, Rab11A, Rab13 and Rab40B were identified as candidate Rabs, the decision was made to begin expression analysis in patient-derived cell lines. Allowing for a baseline of candidate Rab expression to be determined in a laboratory context. This candidate expression can be used to inform future functional analysis and can be compared to patient expression data to provide a link between research conducted in this project and the actual disease context for this research (Figure 3.4.). Cell lines deriving from SHH, group 3 and group 4 medulloblastoma patients were used for expression analysis, allowing for identification of whether protein expression of a candidate Rab was enriched in a particular subgroup.

3.7.1. Investigating endogenous protein expression of target Rabs in medulloblastoma patient-derived cell lines

As Rabs are functional within cells as proteins, the initial approach was to verify endogenous protein expression in patient-derived cell lines using western blotting. HEK-293A cells were transfected with plasmids expressing Rabx-GFP conjugates to act as a positive control for Rab expression when optimising antibodies. The goal for this phase of the project was to identify an antibody which could specifically detect the endogenous expression of each of the five Rabs in the target shortlist. This was then to be used to assess the expression of that Rab in cell lines derived from SHH (DAOY and ONS-76), group 3 (HD-MB03, D425, D458 and D283) and group 4 (CHLA-01 and CHLA-01-R) patients.

Some of the reagents trialled and the outcome of those trials are summarised in Table 3.6. For the most part, it was difficult to obtain antibodies that could detect endogenous Rab protein or were specific to the Rab target. This was likely due to low levels of the endogenous Rab within the cell lysates studied and the

Table 3.6. Summary of antibodies trialled in this study *Red shading – band of expected molecular weight not detected, green shading – band of expected molecular weight detected*

Rab GTPase	Antibody supplier	Reporter	Imaging method tested	Band of expected molecular weight detected?	Conclusion
Rab1B	Sicgen Ab0017-100	Fluorescent secondary antibody HRP	LI-COR LAS-3000 X-ray film	X	Only able to visualise protein once at a 1:100 dilution on LAS (protein was not visible on subsequent attempts).
	Gift from Nori Fukuda. Tohoku University, Sendai, Miyagi, Japan	Fluorescent secondary antibody HRP	LI-COR LAS-3000	X	Unable to visualise protein bands.
Rab8B	ProteinTech 55295-1-AP (Tried two batches)	Fluorescent secondary antibody HRP	LI-COR LAS-3000 X-ray film	X	Unable to visualise protein bands.
Rab11A	Sicgen Ab0034-100	Fluorescent secondary antibody	LI-COR	X	Unable to visualise protein bands.
	ProteinTech 20229-1-AP	Fluorescent secondary antibody HRP	LI-COR LAS-3000	✓	Suitable for endogenous protein detection.
Rab13	Abcam 180936	Fluorescent secondary antibody HRP	LI-COR LAS-3000 X-ray film	X	Unable to visualise protein bands.
Rab40B	Invitrogen PA5-106719	Fluorescent secondary antibody HRP	LI-COR LAS	X	Unable to consistently visualise protein bands. Shown to be non-specific (Chapter 4).

high sequence homology amongst Rab GTPases meaning that it is difficult to identify specific sequences for each Rab which could have antibody epitopes designed against them.

Each of the primary antibodies shown in this study were initially trialled at a 1:1000 dilution in blocking buffer as this was the standard dilution used for multiple other primary antibodies in the laboratory. For each primary antibody, as mentioned previously, HEK293A cells which were transfected with plasmid vectors allowing for the expression of Rabx-GFP fusion proteins were used as a positive control for Rab expression. In addition to this, HeLa cell lysates were used as a model cell line, and for Rab8B, Rab11A and Rab13 foetal mouse cerebellar lysates were used as ProteinTech and Abcam respectively use mouse brain lysate as example cell lines highlighting the efficacy of the antibody. Blots were cut at the 63 kDa molecular weight marker and probed with a 1:1000 dilution of Rabx primary antibody in blocking buffer (< 63 kDa) and with anti-calnexin as a loading control (> 63 kDa). LI-COR scanner images (Figure 3.7.) showed that protein bands could only be clearly observed for the Rab11A primary antibody (shown by pink arrows in Figure 3.7.) and as such it was concluded that use of this antibody at a 1:1000 dilution was suitable. A potential band was observed in HEK293A Rab1B-GFP samples (highlighted by a blue arrow in HEK-Rab1B lane of Figure 3.7.) and no bands were observed for either the Rab8B or Rab13 primary antibodies. Therefore, it was deemed that further antibody optimisation was required to determine the suitability of these antibodies for endogenous Rab expression analysis.

For the further optimisation, multiple Western blot development methods were used to try and establish protein expression including using the LI-COR system with fluorescent secondary antibodies and HRP (horseradish peroxidase) conjugated secondary antibodies with ECL (enhanced chemiluminescence) with X-ray film or LAS-3000 imaging system (Fuji). This was in case one method was more effective at detecting endogenous protein than others. Unfortunately, after trialling with each system and due to time limitations of the project, it was not possible to obtain primary antibodies for detection of endogenous Rab1B, Rab8B and Rab13 in medulloblastoma cell lines. An example Western blot of primary antibody optimisation using a dilution series for each of these three targets is shown in Figure 3.8.
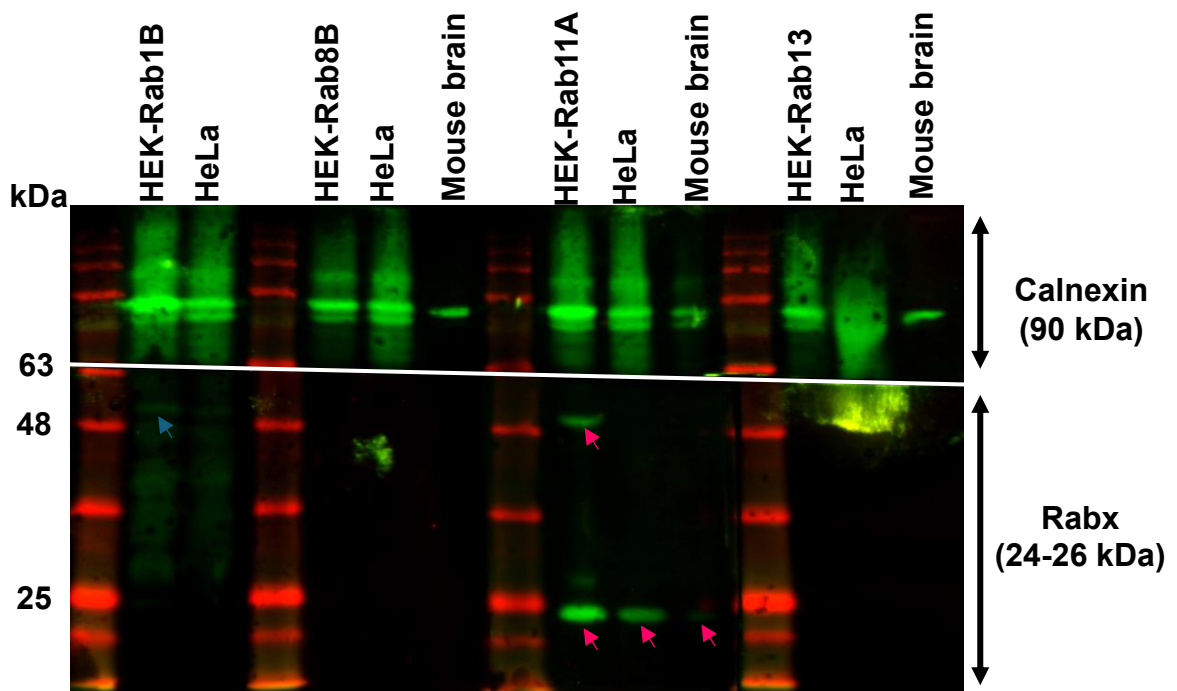
Figure 3.7. – Initial optimisation of Rab1B, Rab8B, Rab11A and Rab13 primary antibodies *LI-COR scanner Western blot images of Rab1B (Sicgen - far left), Rab8B (ProteinTech – centre left), Rab11A (ProteinTech – centre right) and Rab13 (Abcam – far right) primary antibody optimisations. Western blots were cut at the 63kDa molecular weight marker. Top blot section was probed with anti-calnexin (Sicgen) and bottom section further subdivided for probing with different Rab GTPase primary antibodies. Primary antibodies were diluted at 1:1000 in blocking buffer. 'HEK-Rab' samples are HEK293A cells which were transfected with plasmid vectors allowing for the expression of GFP-Rabx fusion proteins. Blue arrow represents potential protein band observed in the HEK293A GFP-Rab1B sample and pink arrows represent protein bands observed with the Rab11A primary antibody.*
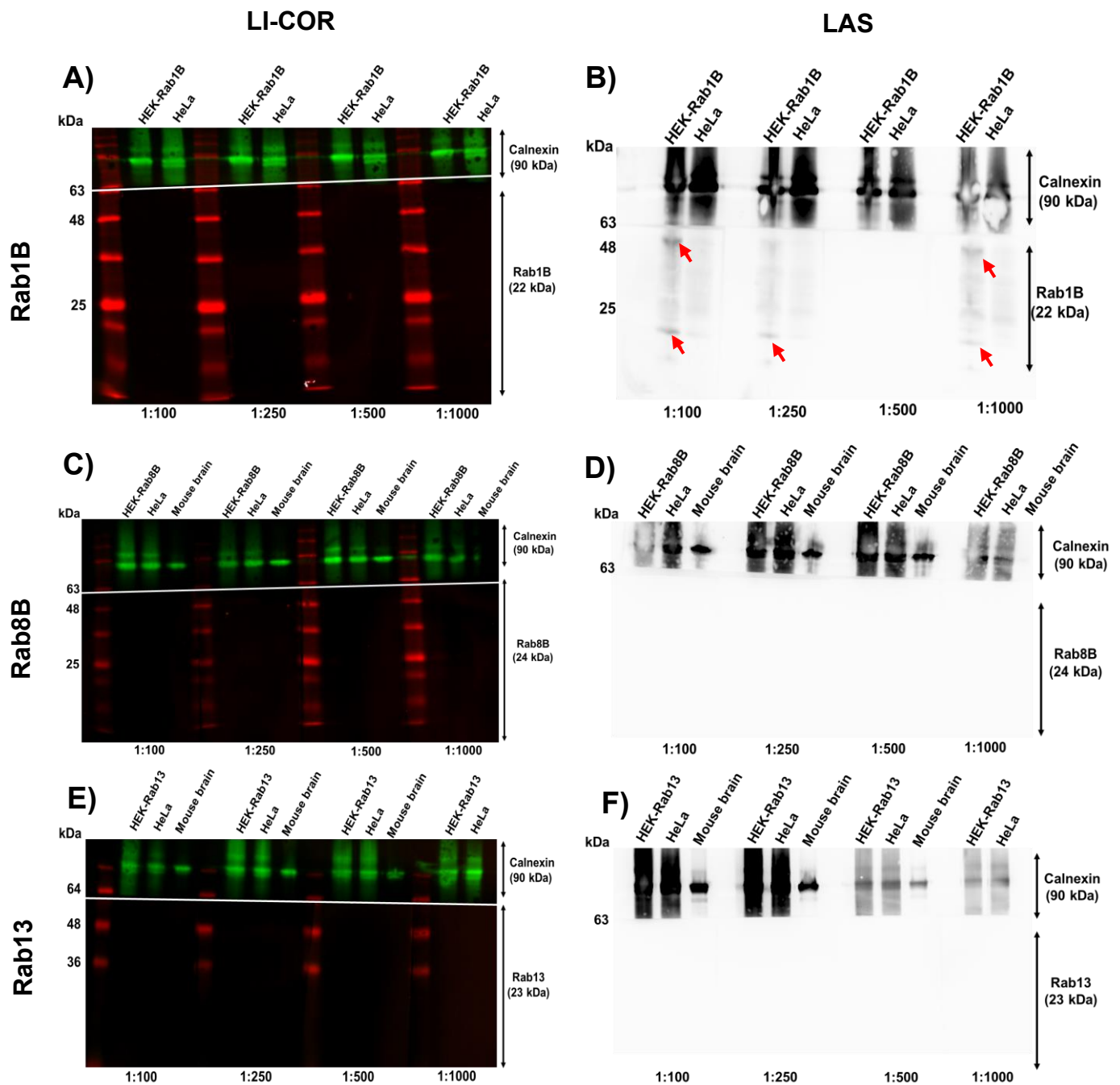
Figure 3.8. – Optimisation dilution series of Rab1B, Rab8B and Rab13 primary antibodies
LI-COR (left) and LAS-3000 (right) Western blot images of Rab1B (Sicgen - A, B), Rab8B
(ProteinTech - C, D) and Rab13 (Abcam - E, F) antibody dilution series optimisations. Western
blots were cut at the 63kDa molecular weight marker. Top blot section was probed with anti-
calnexin (Sicgen) and bottom section further subdivided for probing with different dilutions of
primary antibodies. Primary antibodies were diluted 1:100, 1:250, 1:500 or 1:1000 in blocking
buffer. 'HEK-Rab' samples are HEK293A cells which were transfected with plasmid vectors
allowing for the expression of GFP-Rabx fusion proteins. Arrows on section B represent protein
bands.

In such blots, the membrane section below the 63 kDa marker was cut vertically into four sections which were probed with either a 1:100, 1:250, 1:500 or 1:1000 dilution of Rabx primary antibody in blocking buffer. Results showed that whilst the Rab1B blot showed bands corresponding to the correct molecular weight in the HEK293A Rab1B-GFP wells after using 1:100, 1:250 and 1:1000 primary antibody dilutions and the LAS detection system (red arrows, Figure 3.7-part B) this was not reproducible, so this antibody was discounted as an option for future analysis. The Rab8B and Rab13 blots were completely blank with any antibody dilution and with both the LI-COR and LAS detection systems. Therefore, none of these blots show consistent evidence of protein expression and consequently the protein expression of Rabs 1B, 8B and 13 within medulloblastoma patient-derived cell lines could not be determined.

Initially, it was believed that the Rab40B primary antibody (summarised in Table 3.6.) was suitable for endogenous Rab40B detection (Appendix 1.4). However, it was later discovered through further blotting that this antibody is non-specific for Rab40B as it detects the Rab40 protein Rab40C, which has high sequence homology with Rab40B. Therefore, the results any expression analysis collected using this antibody are not solely indicative of endogenous Rab40B expression. As such, this antibody was deemed unsuitable for the specific detection of Rab40B. This is discussed more in Chapter 4 (section 4.7.) and was unknown at this point of the study.

After primary antibody optimisation was concluded and it was determined that only the Rab11A primary antibody from ProteinTech was able to detect endogenous protein, analysis of expression in medulloblastoma patient-derived cell lines was performed. Cell lysates from medulloblastoma cell lines derived from SHH (DAOY and ONS-76), group 3 (HD-MB03, D425, D458 and D283) and group 4 (CHLA-01 and CHLA-01-R) patient groups were analysed (Figure 3.9.). As previously reported, a LI-COR scanner was used for protein band detection and calnexin was used as a loading control. Positive Rab11A antibody staining was visible for all eight medulloblastoma cell lines analysed. Full length blots are shown in Appendix 1.4. these blots include expression analysis for the Rab40B primary antibody discussed above, however, no conclusions can be drawn from these blots about Rab40B expression.

Relative expression of Rab11A between medulloblastoma cell lines was determined by normalising Rab11A expression to calnexin expression using Fiji Image J software. Values from this normalisation were then plotted (Figure 3.9.B) with error bars representing standard error of the mean. All values are shown as arbitrary units (AU). A Brown-Forsythe and Welch ANOVA with Dunnett's T3 multiple comparisons test was conducted between each of the cell lines to test for statistical significance between expression values. This showed no statistically significant difference in protein expression between any of the cell lines. This shows that there is no subgroup-specific enrichment of Rab11A and is consistent with the patient *Rab11A* expression shown in Figure 3.4.
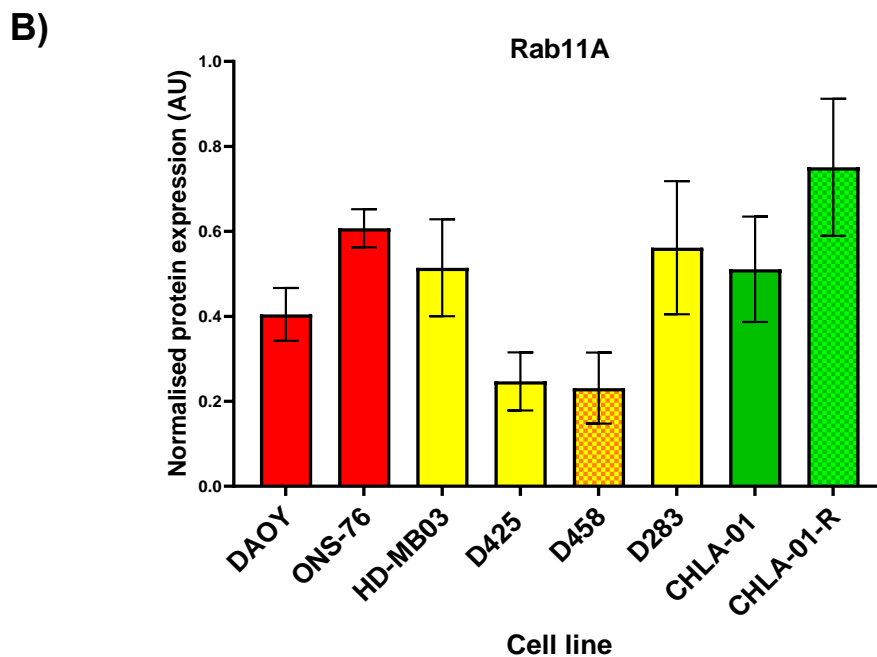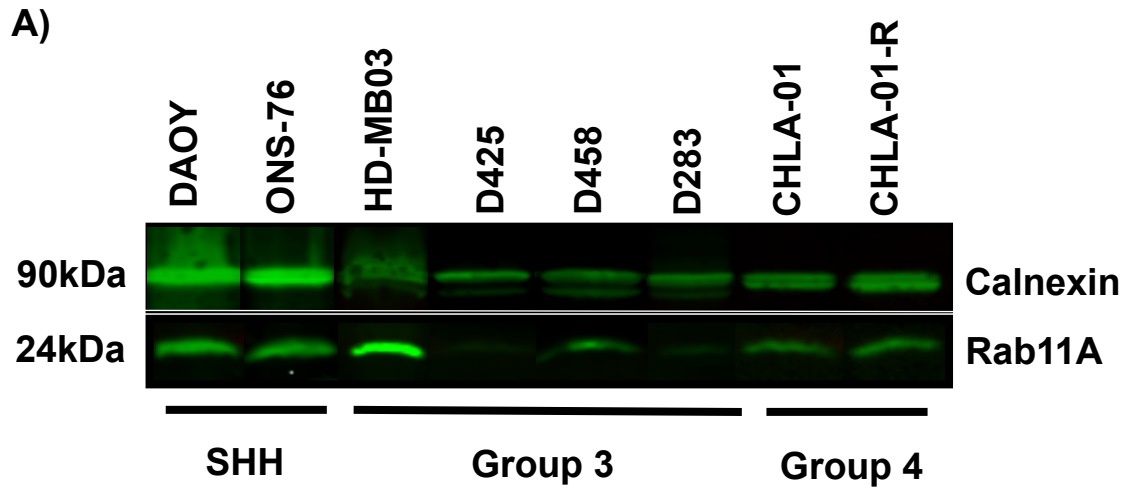
Figure 3.9. – Rab11A endogenous protein expression across medulloblastoma patient-derived cell lines *Expression of Rab11A in the SHH medulloblastoma cell lines DAOY and ONS-76, group 3 cell lines HD-MB03, D425, D458 and D283 and group 4 cell lines CHLA-01 and CHLA-01-R. A) Western blot of protein expression. Image obtained using a LI-COR machine. Anti-calnexin (Sicgen) used as a housekeeping gene. B) Normalisation of Rab11A protein expression from Western blot with calnexin expression shown in arbitrary units (AU). Error bars represent standard error of the mean. SHH cell lines (red), group 3 (yellow) and group 4 (green). N = 3.*

3.7.2. Investigating gene expression of target Rabs in medulloblastoma patient-derived cell lines

As protein expression for all five Rab GTPase targets could not be verified, RT-qPCR was used to measure and compare the gene expression of all targets in cell lines derived from SHH (DAOY and ONS-76), group 3 (HD-MB03, D425, D458, D283) and group 4 (CHLA-01 and CHLA-01-R) medulloblastoma patients.

RT-qPCR primers were designed and optimised for Rab1B, Rab8B, Rab11A, Rab13 and Rab40B (Appendix 1.5. and 1.6.). As was the case for identifying primary antibodies to detect endogenous Rab protein expression, the process for designing and optimising primers for each Rab took a considerable amount of time. The high sequence homology observed between Rab GTPase family members restricted primer design. In addition to this, nucleotide sequences within target cDNA were suboptimal for primer design as they contained runs of repeating single and/or pairs of nucleotides which can lead to the formation of primer dimers and hairpin loops during the PCR reaction. Consequently, multiple pairs of primers for each Rab target were tested before identifying primers which could be optimised for use in RT-qPCR reactions. Primers were designed using Rab cDNA sequences and tested using nucleotide BLAST (https://blast.ncbi.nlm.nih.gov/Blast.cgi) to ensure specificity and therefore, primers were not tested using the Rabx-GFP constructs mentioned in section 3.7.2.

Overall, Rab1B and Rab11A had the highest expression across the subgroups followed by Rab8B, Rab13 and Rab40B (Figure 3.10.). Rab1B and Rab11A had no statistical significance in expression across any of the cell lines or medulloblastoma subgroups assessed. Rab8B was most highly expressed in the SHH cell lines ONS-76 and DAOY with this being statistically significantly higher in ONS-76 in comparison with the group 3 cell lines D458 and D283 (p = 0.0127; 0.0196 respectively). Rab13 was more significantly more highly expressed in both SHH cell lines than group 3 cell lines with significantly higher expression in DAOY and ONS-76 than D458 (p = 0.0294; 0.0479 respectively). Finally, Rab40B was more highly expressed in group 3 and group 4 with statistical significance in the HD-MB03 cell line compared to the SHH cell lines DAOY and ONS-76 (P = 0.0026; 0.0027 respectively).
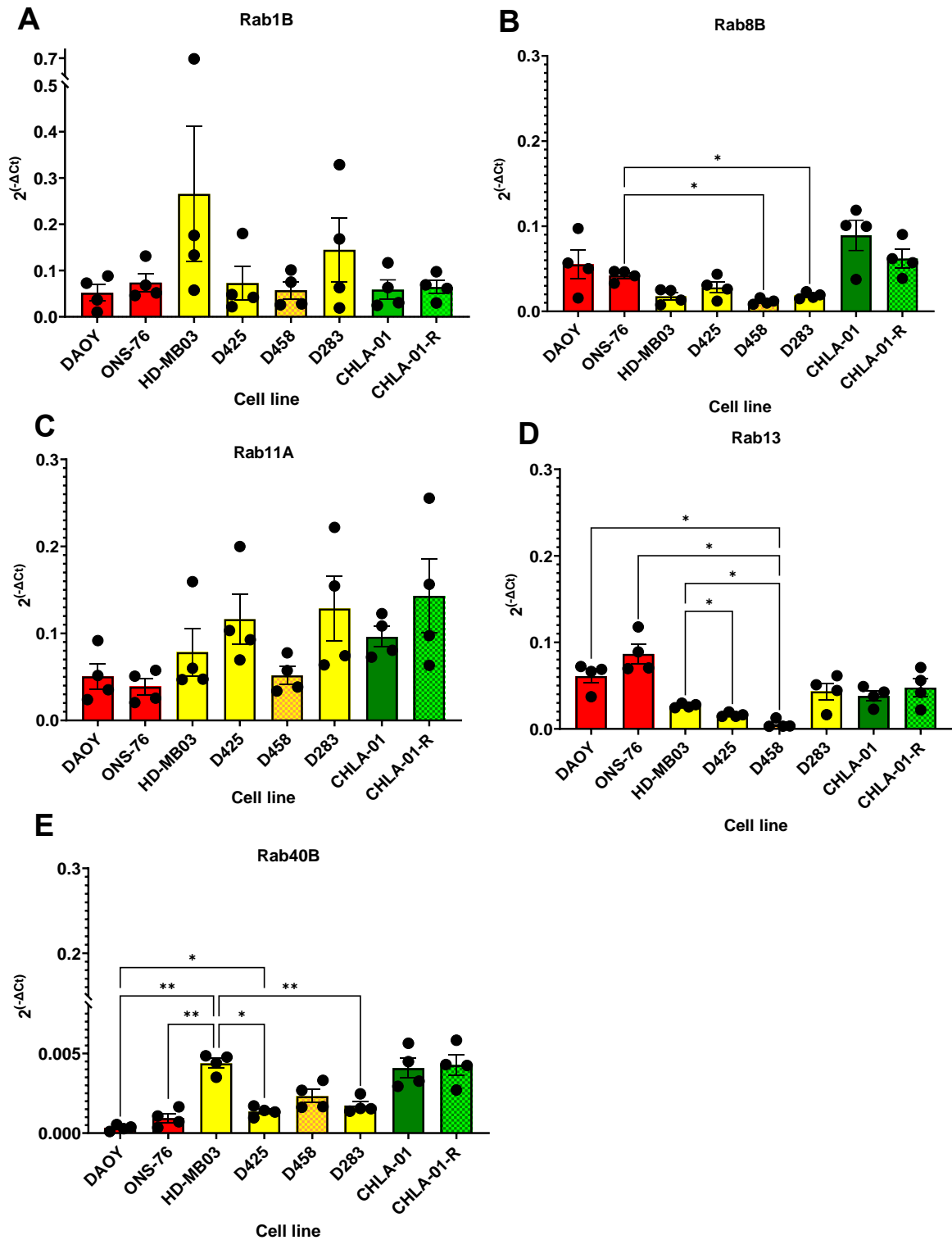
Figure 3.10. – RT-qPCR analysis of Rab GTPase gene expression in medulloblastoma patient-derived cell lines *The expression of Rab1B (A), Rab8B (B), Rab11A (C), Rab13 (D) and Rab40B (E) was analysed in the SHH medulloblastoma cell lines DAOY and ONS-76 (red), group 3 cell lines HD-MB03, D425, D458, and D283 (yellow) and group 4 cell lines CHLA-01 and CHLA-01-R (green). Log (ΔCt) values are shown which were calculated using the geometric mean of the Ct values of the reference genes GAPDH and CANX. Error bars are shown as standard error of the mean. A Brown-Forsythe and Welch ANOVA with Dunnett's T3 multiple comparisons test was conducted between cell lines of different medulloblastoma subgroups with p value ≤ 0.05 shown as '*', ≤ 0.01 shown as '**' and ≤ 0.001 shown as '***'.*

3.8. Summary

In this chapter, the 66 Rabs of the human genome were screened to identify candidates for laboratory study. To do this, the literature, online exosome databases, medulloblastoma datasets and patient gene expression and survival outcomes were analysed for Rab GTPases. This allowed for the identification of candidate Rabs Rab1B, Rab8B, Rab11A, Rab13 and Rab40B.

Review of the literature showed that Rabs are mostly associated with pro-oncogenic roles and reduced prognosis in cancer patients and cancer patient cell line models. It also showed that there is currently very little published research describing potential roles of Rabs in paediatric cancers, creating a literature niche for this study.

Analysis of medulloblastoma group 3 and group 4 exosomal mRNA cargo expression showed that group 3 small EVs contain more Rab mRNA than group 4. It also showed that across both subgroups there was more varied Rab mRNAs in exosomes secreted by primary tumour cells than metastatic tumour cells. Finally, it showed that Rab10, Rab11A, Rab27A, Rab37 and Rab40B were the most enriched Rab mRNAs in exosomes compared to other Rab GTPases.

Analysis of scRNAseq data and subsequent functional pathway analysis conducted on HD-MB03 cells grown in a 3D model showed increased Rab1A, Rab5C, Rab7A and Rab11A expression in metabolically active HD-MB03 cells.

Upon patient dataset survival outcome analysis, high expression of Rabs correlated with reduced medulloblastoma survival outcomes, thereby suggesting a connection between Rab candidate expression and medulloblastoma pathogenesis. Group 3 was the subgroup that had the most Rabs in which high expression was associated with poor prognosis. For Rab8B, Rab11A and Rab40B this was group 3-specific. Rab1B and Rab13 had high expression associated with poorer prognosis in groups 3 and 4.

Survival data combined with other analysis detailed above, led to the selection of Rab1B, Rab8B, Rab11A, Rab13 and Rab40B as Rab targets for further study.

Baseline expression of the five candidate Rabs was then established within immortalised medulloblastoma patient-derived cell lines. Initially, protein expression

was going to be used as an indicator of subgroup specificity of the target Rabs. Examination and optimisation of primary antibodies identified only one antibody which was suitable for endogenous Rab expression analysis and this was for Rab11A.

In contrast, gene expression of all candidates was possible with RT-qPCR. This showed no significant subgroup specificity of Rab1B and Rab11A. It did show that Rab8B and Rab13 were significantly more highly expressed in SHH cell lines and that Rab40B was significantly more highly expressed in group 3 cell lines. This supported gene expression patterns identified through patient dataset analysis.

Future work in this study aimed to begin functional analysis of Rabs in medulloblastoma. For this functional work, the five candidates were assessed using all of the data presented in this study. Rab11A and Rab40B were then selected as targets for future work. Reasons for selecting Rab11A included the statistical significance of high expression being associated with poor prognosis in group 3 patients, and the identification of a primary antibody that was specific to Rab11A. Reasons for selecting Rab40B included high expression being associated with poor prognosis in group 3 patients, and the statistically significant expression of *Rab40B* in group 3 cell lines compared to SHH after RT-qPCR analysis. Rationale for this decision is summarised in Table 3.7.

Table 3.7. Summary of rationale for choosing Rab11A and Rab40B as candidates for functional study *Green – association was identified, red – association was not identified.*

Rab GTPase	High expression associated with poor survival in group 3 patients?	Different gene expression in group 3 samples compared to the other subgroups?	Western blot antibody identified?
Rab1B			
Rab8B			
Rab11A			
Rab13			
Rab40B			

Chapter 4:

Generation of CRISPR-Cas9 Rab GTPase group 3 medulloblastoma knockout cell lines

4.1. Introduction

In Chapter 3, review of the literature, patient dataset analysis and medulloblastoma dataset analysis led to the identification of Rab1B, Rab8B, Rab11A, Rab13 and Rab40B as potential contributors to medulloblastoma pathogenesis. Expression analysis using medulloblastoma patient-derived cell lines then led to the selection of Rab11A and Rab40B as candidates for functional analysis. This was primarily because Rab11A and Rab40B showed higher gene expression in group 3 and group 4 cell lines after RT-qPCR analysis and had statistically significant high expression correlating with poor patient survival upon patient dataset analysis. As the mechanisms that drive pathogenesis of group 3 and group 4 are less well understood than the WNT and SHH subgroups, there is therefore a requirement for the identification of targets which may drive pathogenesis of these subgroups.

The focus of this chapter is the generation of separate *Rab11A* and *Rab40B* knockout (KO) cell lines for functional analysis of these two Rabs in medulloblastoma. CRISPR-Cas9 (Clustered Regularly Interspaced Short Palindromic Repeats/CRISPR associated protein 9) technology was used to generate these cell lines. CRISPR-Cas9 was used because it involves the electroporation of only two reagents (Cas9 mRNA and single guide RNA) into the model cell line. This should allow for a stable knockout cell line to be created quickly, with high specificity and efficiency, and with low cytotoxicity to cells (Xiaoshuai et al., 2022) (Uddin et al., 2020).

HD-MB03 cells which are derived from a patient with group 3 medulloblastoma (Milde *et al*., 2012) were used to generate the knockout cell lines. It has well understood culture conditions in the laboratory which afforded confidence in its use as a model cell line for CRISPR-Cas9 gene editing. This is because changes in growth and morphology caused by the gene editing and optimisation for it will be easily noticed and therefore culture conditions altered accordingly to increase the chance of successfully generating a knockout cell line. The HD-MB03 cell line only was initially explored as it was unknown what the potential effect of a complete Rab knockout would be in medulloblastoma cells. Whilst Rab knockout cells have been

successfully established in human cell lines, knockout out Rab11A, for example, is embryonically lethal in murine models (Zulkefli *et al*., 2019) (Sobajima et al., 2015). Therefore, to give an initial impression about whether group 3 medulloblastoma cells could survive either a Rab11A or Rab40B knockout, one medulloblastoma cell line was used in this study.

Three molecular validation techniques were used to establish whether knockout cell lines had been generated. Firstly, a T7 endonuclease I assay was used to identify the number of alleles present within the genomic DNA extracted from each clonal cell line produced. Secondly, Sanger or Oxford Nanopore sequencing was used to identify specific nucleotide changes within the sgRNA target site. Finally, western blotting was used to detect the presence of full-length protein present within cell lysates, absence of which indicated that a knockout cell line had been generated.

Aims of the chapter:

• To determine whether HD-MB03 cells were a suitable model cell line for the generation of a knockout cell line using CRISPR-Cas9 technology.

• To generate *Rab11A* and *Rab40B* knockout cell lines.

• To validate the success of the gene editing using three molecular techniques.

4.2. Assessing the suitability of the HD-MB03 group 3 medulloblastoma cell line as a model from CRISPR-Cas9 mutagenesis

4.2.1. Optimisation of nucleofection as a method for transfection of HD-MB03 cells

Previous work by the Coyle laboratory had optimised the use of electroporation to transfect SHH medulloblastoma cell lines with CRISPR reagents (Johnson, 2023). Prior to addition of these CRISPR reagents, it was important to ascertain whether the HD-MB03 cell line could survive nucleofection. HD-MB03 cells were nucleofected with a control GFP expression plasmid and plated in wells of a six-well plate as described in section 2.5.1. A population of cells was also plated, that were not nucleofected and acted as a control condition. Cells were then imaged at 24-, 48-, 72- and 96-hours post transfection to determine firstly, how long post-transfection GFP signal could be visualised, which would give an indication of how long fluorescence signal from CRISPR reagents is likely to be detectable for. Secondly this would give an indication of whether there was a noticeable difference in the number of cells visible in wells of each condition, this could indicate that nucleofection was negatively affecting cell viability.

Results confirmed a successful transfection as GFP signal was visible 24-hours post-transfection meaning that cells had survived nucleofection (Figure 4.1.). This was sustained until 72-hours post-transfection but appeared to decline at the 96-hour time point as GFP signal could no longer be visualised. No noticeable difference in the total number of surviving cells between each condition was observed, however this was not quantified, as the same cells were not imaged each day. As such, this experiment gives an indication that firstly, the nucleofection is not causing a noticeable decline in cell viability and secondly that fluorescent signal is visible in the cells for several days post-transfection. Therefore, it was concluded that nucleofection is a suitable method of transfection for CRISPR-Cas9 gene editing reagents in HD-MB03 cells.
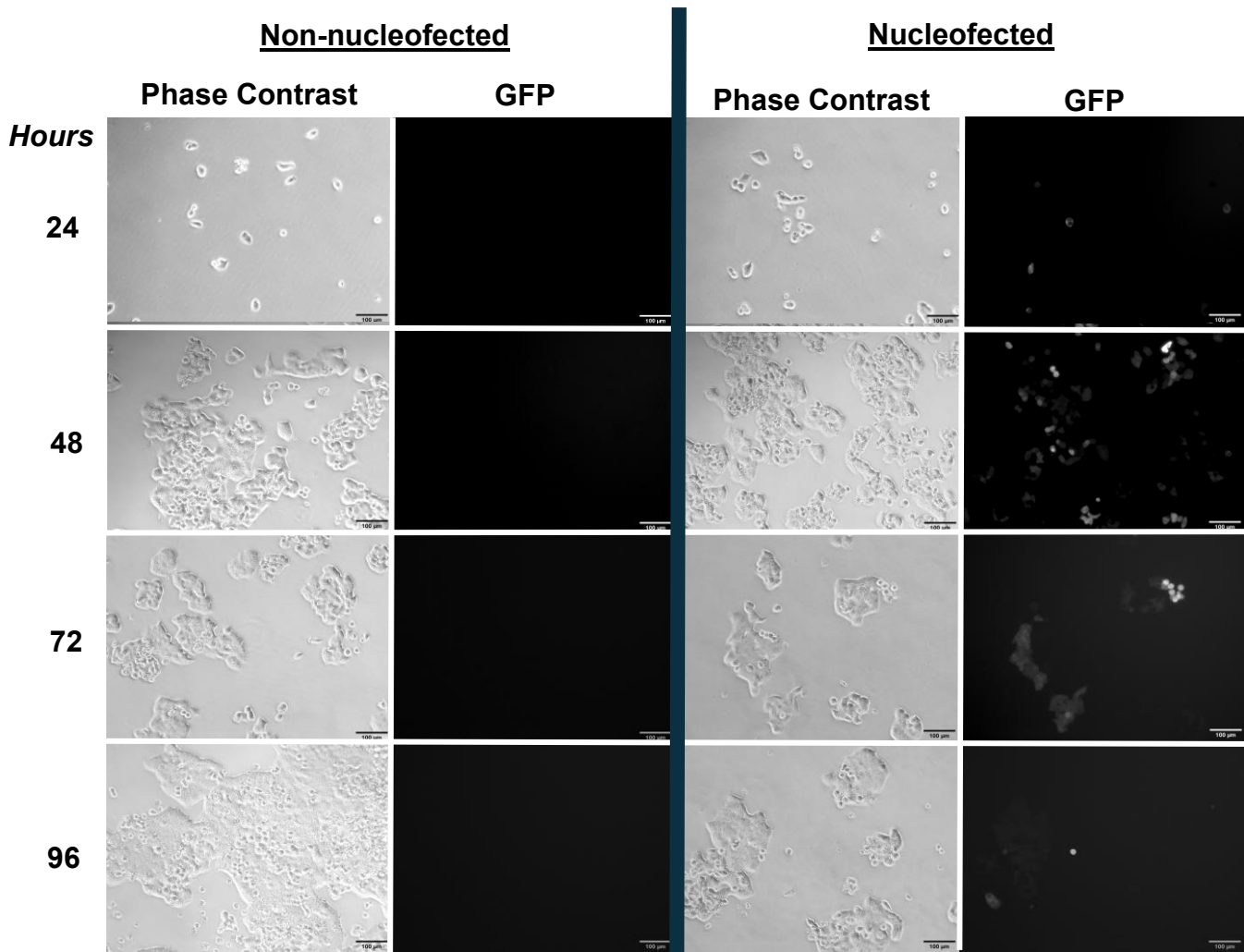
Figure 4.1. – Nucleofection of HD-MB03 cells with GFP plasmid *Phase contrast and fluorescence microscopy images of HD-MB03 cells which were either non-nucleofected (left) or nucleofected (right) with a GFP plasmid. Cells were then cultured for 24-, 48-, 72- or 96 hours before imaging using a 20X lens. 100μm scale bars.*

4.2.2. Determination of whether HD-MB03 cells are viable after single cell seeding

To increase the likelihood of generating a clonal cell line with a stable gene mutation, cultures of gene edited cells are usually derived by expansion from single cells. This aims to result in homogeneity within the population such that every cell in that culture contained the same CRISPR mutation. After nucleofection was determined to be a suitable method of HD-MB03 cell transfection, the suitability of the HD-MB03 cell line was further tested by nucleofecting cells with a GFP plasmid and single cell sorting them. HD-MB03 cells grow semi-adherently in two morphologically distinct populations (adherent and suspension), therefore a single cell culture could arise from a cell from either population. Thus, it was important to establish a baseline for how HD-MB03 cells grow from a single cell so that any morphological changes after CRISPR gene editing can be attributed to the gene editing and not the effect of single cell sorting or nucleofection of the cells.

Fluorescence activated cell sorting (FACS) was used to single cell sort HD-MB03 cells nucleofected with a GFP expression plasmid into wells of a 96-well plate. Control conditions (non-nucleofected and non-nucleofected but exposed to nucleofection reagents) were also single cell sorted into wells of a 96-well plate. Cells were then cultured for 14-days and imaged using a BioRad fluorescent cell imager (Figure 4.2.A).

This showed that after three days, cells from all 3 conditions had survived single cell sorting and were all adherent cultures with the same intracultural morphology. For each condition approximately 8 or more cells were detected which is in line with the expected division rate of HD-MB03 cells of approximately 23.5 hours (Milde et al., 2012). After six days, some suspension cells were evident in the two control populations (red arrows), but none were visible in the nucleofected population. There were also comparatively fewer cells in the nucleofected population suggesting that nucleofection slows proliferation rate. After 14-days, suspension cells were visible for all conditions with cell morphology was similar to the parental HD-MB03 cell line (Figure 4.2. B) but with cells being more densely packed.

This suggests that HD-MB03 cells can be propagated from a single cell, allowing for homogeneity amongst clonal cell lines. Additionally, cells retain the semi-adherent

morphology present in the parental cell line. Combined with results from section 4.2.1., it was thereby concluded that HD-MB03 is a suitable model cell line for CRISPR-Cas9 gene knockout. As no toxicity effects such as membrane blebbing were observed from any of the transfection reagents, it is also concluded that transfection by nucleofection is a suitable method for transfection of CRISPR reagents. Cytotoxicity was not experimentally assessed, however, with all conclusions about toxicity of transfection made from the physical appearance of the cells.
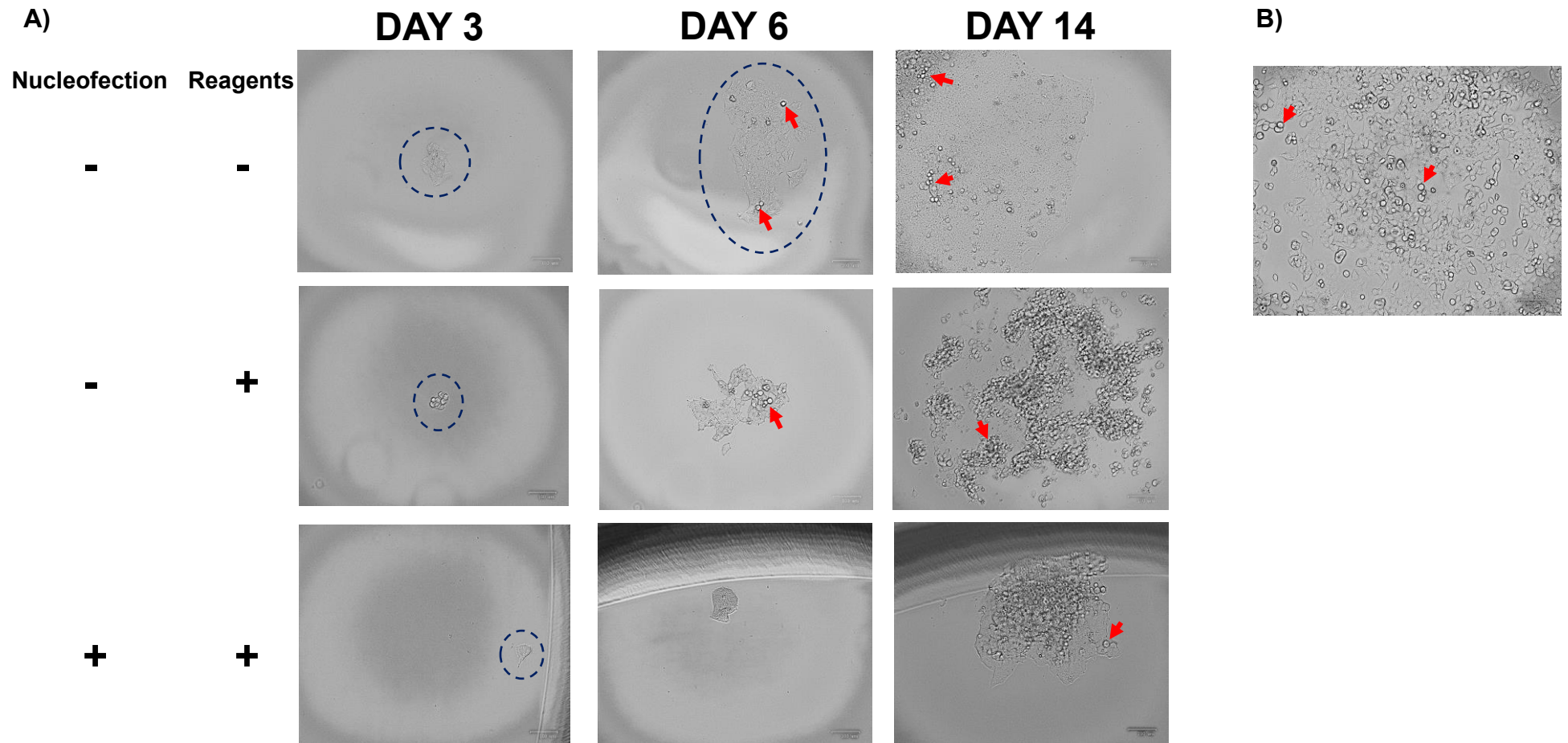
Figure 4.2. HD-MB03 cells can be grown from single cells following nucleofection *A) Single HD-MB03 cells were seeded into 96-well plates using FACS after no reagent exposure (top) or after nucleofection reagent exposure either without electroporation (middle) or with electroporation (bottom). B) Brightfield image of HD-MB03 cells grown in a T-75 cell culture flask. Cells were imaged using 20X magnification and brightfield images shown. Scale bars correspond to 100 μm. Day indicates days in culture. Red arrows shown the position of suspension cells within the culture. Dark blue dashed shapes indicate position of cell clusters.*

4.3. CRISPR-Cas9 gene editing workflow

After it had been demonstrated that recovery of HD-MB03 cells was possible following single cell plating and the tolerance of the cell line to nucleofection the following gene editing workflow was adopted (Figure 4.3).
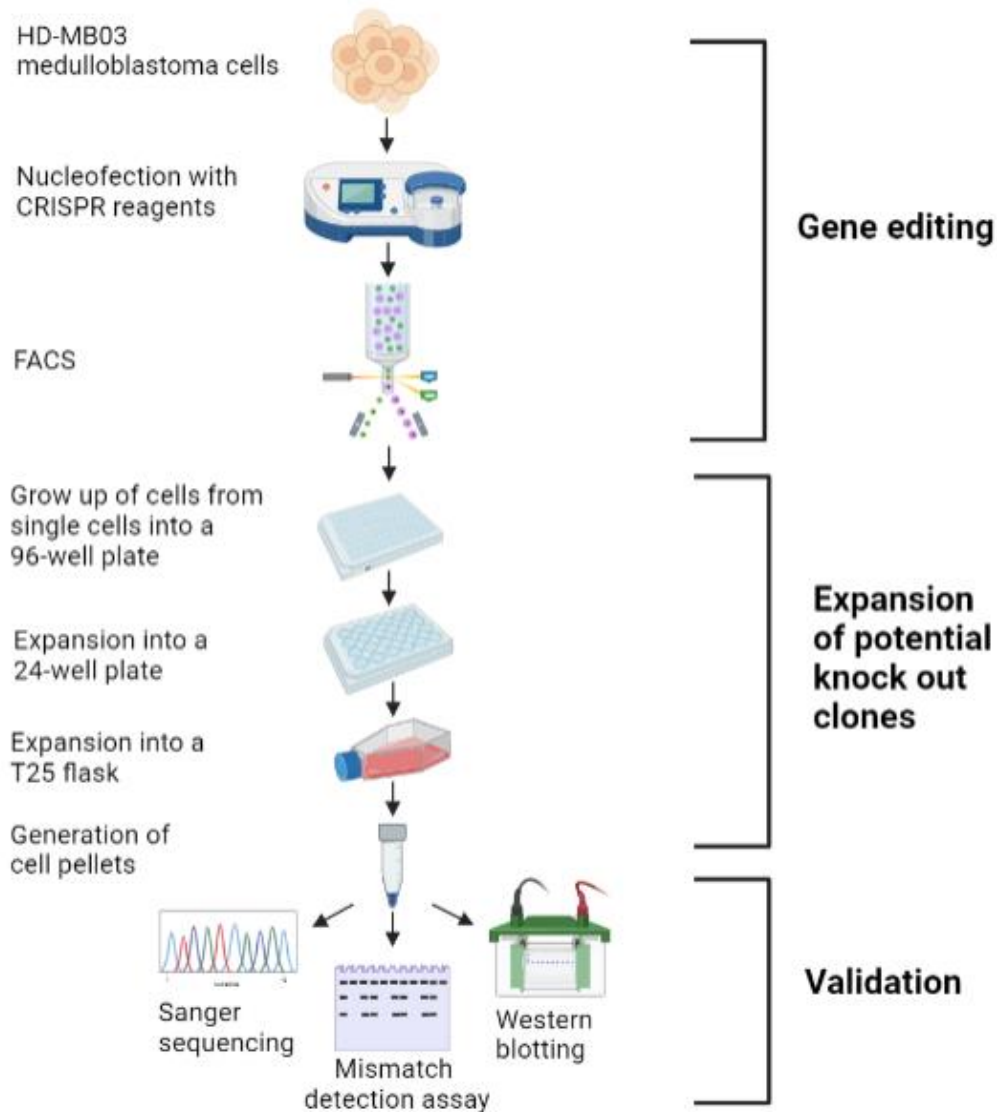
Figure 4.3. – Workflow of generation of CRISPR-Cas9 knockout cell lines

Figure made using BioRender.com.

The first stage was gene editing which involved culturing HD-MB03 cells and nucleofection with CRISPR reagents as described in detail in 2.5.2. and shown diagrammatically in Figure 4.4. These CRISPR reagents included a short RNA sequence (single guide, sgRNA) which is complementary to the gene of interest. This allows for direct targeting of a specific gene. For this project, sgRNAs were designed which were specific to sequences within either *Rab11A* or *Rab40B*. Additionally, non-targeting sgRNA was used. This is a sgRNA that is designed to target no specific genes within the genome and acts as a control for the baseline cellular response to CRISPR-Cas9 genome editing.
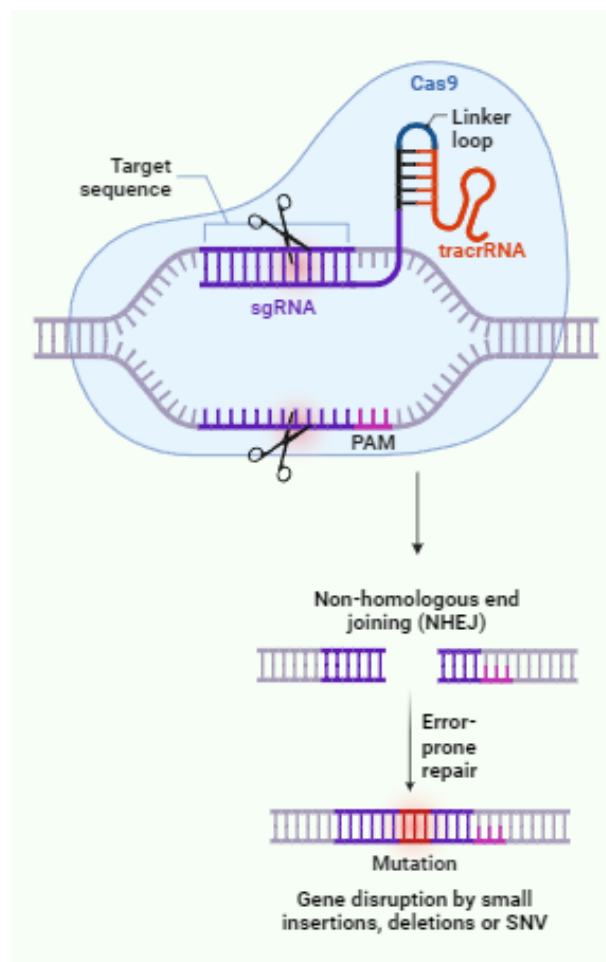
Figure 4.4 – CRISPR-Cas9 gene editing process principles. *A single guide (sg) RNA with a protospacer-adjacent motif (PAM) site specific to the target sequence allows for targeting by the Cas9 enzyme. The Cas9 creates a double strand break which the cell repairs using non-homologous end joining (NHEJ). NHEJ is error prone which can lead to single nucleotide variation (SNV), insertion or deletion mutations which potentially lead to premature termination of the transcript. Figure made using BioRender.com.*

Additionally, mRNA that allowed for the expression of a Cas9-EGFP fusion protein, was added to the HD-MB03 cells. The EGFP (enhanced green fluorescent protein) moiety allows for selection of single cells using FACS (fluorescence-activated cell sorting) as GFP signal within cells is a sign of Cas9 mRNA uptake and is therefore an indication that gene editing has occurred. Cas9 is responsible for generating double strand breaks at sites of the genome determined by the annealing of sgRNA to target sites. The cell then repairs the double strand break by non-homologous end joining (NHEJ) which is an error-prone form of DNA repair (Ran et al., 2013). Therefore, there is the potential for mutations to occur during this repair process through an insertion, deletion, or single nucleotide variation mutation. Insertion or deletion (InDels) mutations can cause frameshifts within the DNA sequence and single nucleotide variations may change nucleotides, all of which may lead to a premature stop codon being introduced into the polypeptide sequence upon translation (Figure 4.4). This premature stop codon causes the loss of a functional protein, due to the position of the *Rab11A* and *Rab40B* target sites within the transcript, and therefore a functional protein knockout.

The second stage was expansion of potential knockout clones. This involves the culturing of single cells in a 96-well plate. These were propagated and visual examination of cell densities was used to determine when clonal cell lines were ready for expansion into a 24-well plate and then into a T-25 cell culture flask. Medium and culture practices were the same as optimised for the parental HD-MB03 cell line.

The third and final phase was validation. There are multiple methods of validation of CRISPR knockout cell lines, for this study three were used. Firstly, a T7 endonuclease I assay which was used to detect mutations at the sgRNA target site. Secondly, DNA sequencing was used to determine the sequence of the sgRNA target site and therefore detect the specific location and sequence of any mutations. Finally, western blotting was used to detect the presence of endogenous target protein within the clonal cell line. All three validation techniques were used to examine every clonal cell line which had been successfully propagated into a T-25 cell culture flask.

4.4. Nucleofection and fluorescence activated cell sorting of Cas9-EGFP positive HD-MB03 cells

HD-MB03 cells were nucleofected with either Rab11A, Rab40B or non-targeting sgRNA along with Cas9 enzyme mRNA conjugated with EGFP mRNA. Following overnight culture at 37°C in a T-25 flask, cells were sorted using FACS. Prior to FACS, cells were stained with 4'6-diamidino-2-phenylindole (DAPI) to act as a viability stain to ensure that only live cells were seeded into the 96-well plate (section 2.5.3.).

There were four stages of flow cytometry gating prior to cell seeding. This aimed to ensure that only live single cells which expressed EGFP were seeded. Untransfected cells were used as a negative control to act as a baseline for cellular autofluorescence. Scatter graphs of cells through the gating stages are shown in Appendix 1.7. Analysis of EGFP expression levels in single cells showed a transfection efficiency of 77.7 % for non-targeting cell lines, 72.2% for *Rab11A* potential knockout and 66.5 % for *Rab40B* potential knockout cell lines (Figure 4.5.).
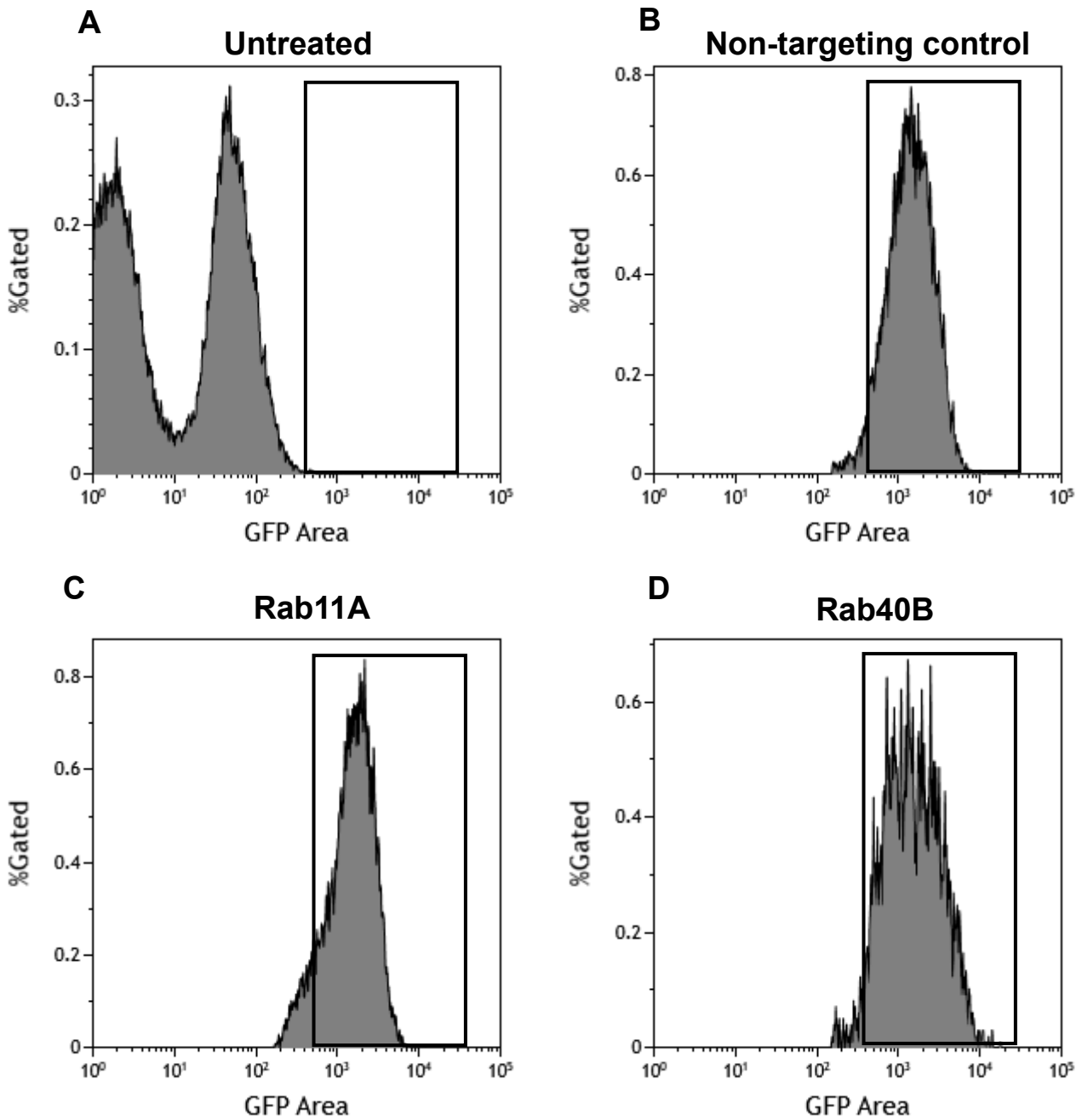
Figure 4.5. – EGFP expression of single cells sorted through fluorescence activated cell sorting *Histograms of EGFP of untreated HD-MB03 cells (A) and HD-MB03 cells nucleofected with either non-targeting (B), Rab11A-specific (C) and Rab40B-specific (D) sgRNAs. Black boxes indicate fluorescence gating of GFP signal measured by the cell sorter. '%Gated' indicates the percentage of cells within the population with a particular level of GFP fluorescence on a 0-1 scale.*

4.5. T7 endonuclease I mismatch detection assays of Rab11A and Rab40B clonal cell lines

Following single cell dilution cloning and expansion, twenty-three Rab11A potential knockout cell lines and ten Rab40B potential knockout cell lines had were successfully obtained and able to be analysed for gene editing events. For each Rab, three non-targeting control cell lines had also been propagated alongside. All clonal cell lines were named after their position in the original 96-well plate that single cells were seeded into.

The first stage of validation was to conduct a T7 endonuclease I or mismatch detection assay. This is a PCR-based assay which uses primers designed to amplify specific sequences either side of the sgRNA target site within genomic DNA (gDNA) extracted from the potential knockout cell lines (Figure 4.6.). During this process, PCR products are denatured by heating and renatured by cooling before being incubated with a T7 endonuclease I enzyme. If there are multiple alleles present within the genomic DNA of the potential knockout cell line, heteroduplexes will form when the PCR product is renatured. The T7 endonuclease will then cleave any heteroduplexes resulting in the formation of multiple different sized DNA fragments (Figure 4.6.). These fragments can then be visualised by agarose gel electrophoresis, allowing for an assessment of the number of alleles present within the PCR product to be made. It should be noted that this technique is not definitive in determining whether a knockout cell line has been produced. This is because the presence of a single DNA band on an agarose gel instead of multiple, indicates that the clonal cell line is a homozygote but cannot distinguish between a wildtype genome or a cell line with the same mutation, in the same position within the target site on each copy of the chromosome which the cell possesses.

The results of the assay are shown in Figure 4.7. All non-targeting control cell lines (NT-) suggest the presence of a single allele which was to be expected as no gene editing should have occurred within the genes of interest. Of the 23 *Rab11A* potential knockout cell line, only one,11A A12, (Figure 4.7. A) had a single product band meaning that it is likely homozygous. Twenty-one cell lines had three bands and one cell line, 11A F2 had an additional fourth band. Of the 10 *Rab40B* potential knockout cell lines, two, 40B E4 and 40B F9 had one band, suggesting that they are

homozygous (Figure 4.7. C and D respectively). The remaining eight had multiple bands. None of these eight had a band pattern which corresponded to the expected digest product band sizes with 40B A9, B10, C12, F5 and G8 all having larger products than expected and B10, G11 and H1 having more than three product bands (Figure 4.7. C and D). This could be due to insertion or deletion mutations (InDels) within these cell lines being much larger than expected (10's of nucleotides) or the presence of a chromosomal aberration known isochromosome 17q (Figure 1.4., section 1.1.4.3.) which is present in HD-MB03 cells. This results in the duplication of one of the q long arms of chromosome 17 of which the gene locus of *Rab40B* is positioned (ensembl.org). Therefore, there is an additional copy of the gene which could mismatch, leading to a larger number of heteroduplex combinations being possible and therefore more T7 endonuclease digest products forming.
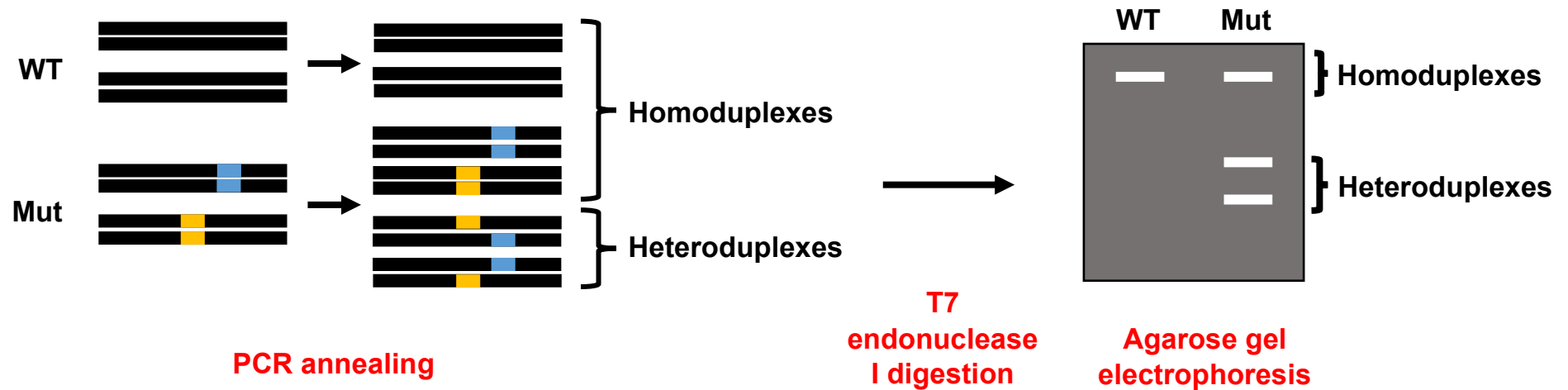
Figure 4.6. – T7 endonuclease I mismatch detection assay *Amplification PCR is used to generate PCR products from genomic DNA. During this PCR, products reanneal. If multiple alleles are present (Mut; caused by CRISPR gene editing events), this generates a mixture of homo- and heteroduplexes within the PCR product pool. T7 endonuclease I recognises heteroduplexes where DNA mismatches occur and cleaves them creating different sized PCR products. This can be visualised using agarose gel electrophoresis as a multiple product band pattern. WT (wildtype) have a single allele and therefore only homoduplexes are formed which are not cleaved by T7 endonuclease I and therefore only one sized PCR product is formed which is shown as a single band after agarose gel electrophoresis. Blue and orange represent different alleles, generated through CRISPR gene editing. Adapted from Zhu et al.. 2014.*
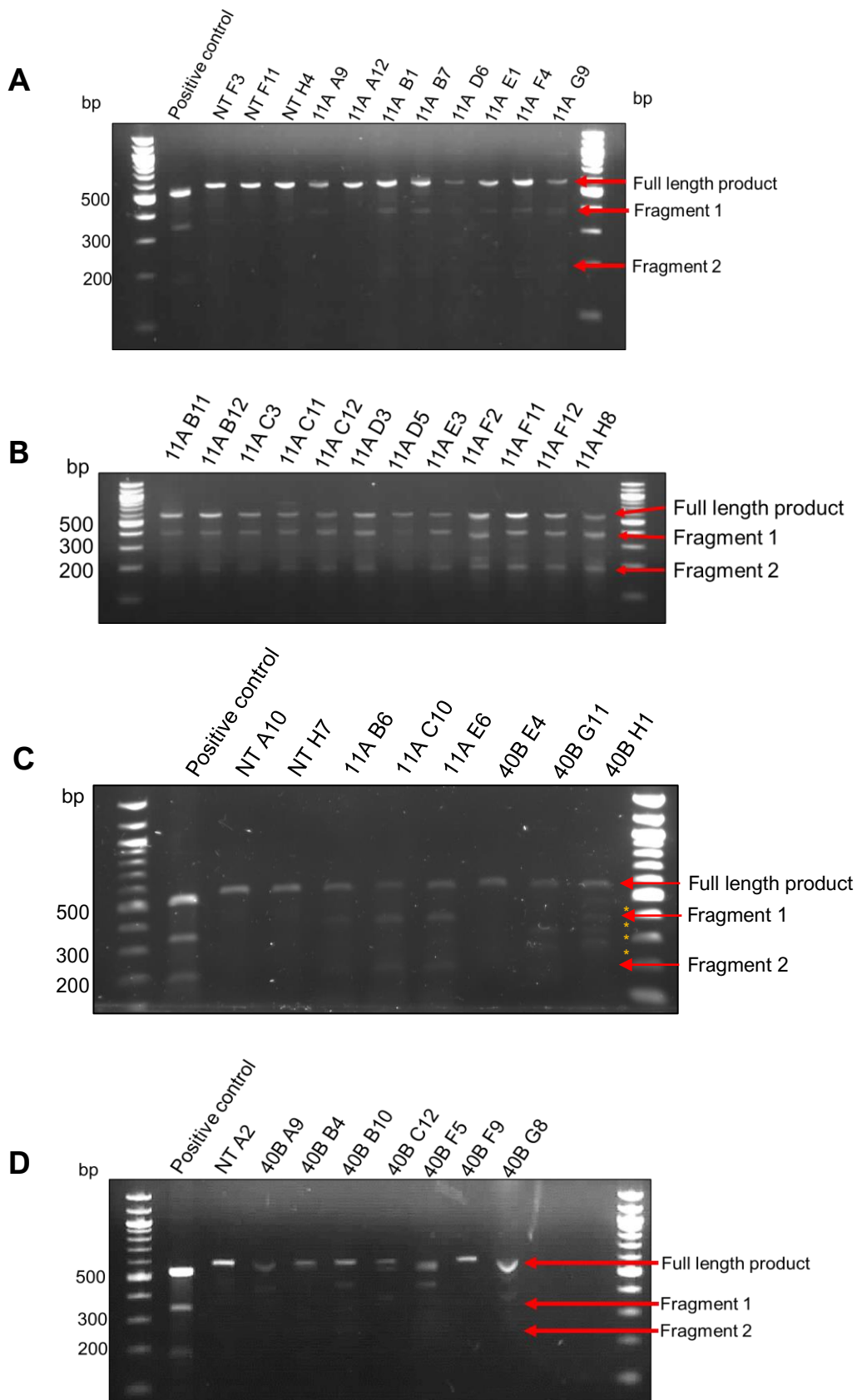
Figure 4.7. – Agarose gel electrophoresis of T7 endonuclease I DNA mismatch detection assay indicates the presence of insertion or deletion mutations in the majority of Rab11A and Rab40B potential knockout cell lines derived from HD-MB03 cells *PCR product digests from genomic DNA extracted from Rab11A (A, B, C) and Rab40B (C, D) potential knockout cell lines. For Rab11A samples, primers are designed such that full length product sits at 562bp, fragment 1 at 376bp and fragment 2 at 186bp. For Rab40B samples, primers are designed such that full length product is at 567bp, fragment 1 at 312bp and fragment 2 at 255bp. The red arrows indicate the expected position of these products on the gel image. Samples were loaded with a positive control sample (from Genecopoeia T7 endonuclease assay kit) and a 100bp ladder. Orange * indicates examples of additional bands caused by the presence of multiple different gene editing events which have resulted in insertion or deletion mutations which are 10s of nucleotides in length.*

134

4.6. Characterisation of insertion and deletion mutations by sequencing

To fully characterise any specific nucleotide alterations within the sgRNA target sites of the potential knockout cell lines, PCR products generated using the same primers used for the T7 endonuclease I assay were sent for sequencing.

4.6.1. Sanger sequencing of Rab11A potential knockout cell lines

Sanger sequencing is a highly accurate form of sequencing which is considered the gold standard for the detection of insertion and deletion mutations (InDels) and single nucleotide variations (SNVs) (Cheng, Fei and Xiao, 2023). Consequently, PCR products were sent to GeneWiz (Azenta) for Sanger sequencing to determine the sequences of the CRISPR-Cas9 target sites in potential knockout cell lines. The 'Indigo: Rapid InDel discovery in Sanger chromatograms' software from Gear Genomics was then used to identify InDels within chromatograms. Sequences obtained from non-targeting sgRNA cell lines were aligned with the genome (*Homo sapiens* – GRCh38) to ensure that the non-targeting cell lines had no mutations within the target site. Non-targeting control sequences were then aligned with potential knockout cell line sequences to identify any mutations present.

The Sanger sequencing results for the Rab11A potential knockout cell lines are summarised in Table 4.1. Chromatograms could only be analysed for 14 out of 23 potential knockout cell lines (A12, B1, B7, B11, B12, C11, D3, D5, D6, E3, F4, F11, F12 and H8). The results supported those of the T7 endonuclease assay with 13 out of the 14 having two different mutations and the putative homozygote, A12 having a biallelic five nucleotide 'TCTCA' deletion. One cell line, D3, had an unmutated allele and a mutant allele, twelve cell lines had two different mutations. The chromatograms of nine cell lines could not be analysed. This was due to chromatogram nucleotides being unreadable despite multiple sequencing attempts.

For each of the cell lines which possessed mutations, the cDNA sequence was edited to input any InDels or single nucleotide variations identified through sequencing. The cDNA was then translated using the ExPASy translate tool

(web.expasy.org/translate/) to determine any amino acid alterations or the presence of any stop codons (Table 4.1.). This showed that all 14 potential cell lines whose chromatograms could be analysed had mutations which lead to a premature stop codon in at least one transcript. Of these, 10 (A12, B7, B11, B12, C11, D5, D6, F4, F12, H8) had genetic mutations that lead to a premature stop codon on both gene transcripts, suggesting that these 10 are all likely to be knockout cell lines. Two cell lines, B1 and F11 had one InDel which led to an alteration of the amino acid sequence and then resumption of the original amino acid sequence. D3 had one unedited transcript and one transcript with a two-nucleotide deletion. E3 had one transcript with an unidentified nucleotide and therefore could not be translated.

All *Rab40B* potential knockout cell lines were also sent for Sanger sequencing. However, due to the gene localising to isochromosome 17q (as mentioned in section 4.5.), more than two DNA traces appeared in most Sanger sequencing chromatograms. This meant that chromatograms were difficult to analyse and as the majority of InDel discovery tools, including Indigo, are designed to analyse chromatograms with a maximum of two traces, a different sequencing approach was required to characterise mutations within the target sites of *Rab40B* knockout cell lines.

Table 4.1. - Sanger sequencing and sequence translation results for Rab11A potential knockout cell lines *Red denotes a deletion mutation, green denotes an insertion mutation. 'nt' (nucleotides).*

ID	Number of mutated transcripts	InDel 1	InDel 2	Position of InDel	Amino acid alteration
A12	2	Deletion (5 nt)	Deletion (5 nt)	InDel 1: 5' GAGTGATCTACCGTCATCTCAGGG 3' InDel 2: 5' GAGTGATCTACCGTCATCTCAGGG 3'	InDel 1: T136X InDel 2: T136X
B1	2	Deletion (5 nt)	Insertion (9 nt)	InDel 1: 5' GAGTGATCTACCGTCATCTCAGGG 3' InDel 2: 5' GAGTGATCTACCGTCATCACTACTTCTTCAGGG 3'	InDel 1: T136X InDel 2: L131H, insertion of YFF 132-134
B7	2	Deletion (5 nt)	Insertion (1 nt)	InDel 1:5' GAGTGATCTACCGTCATCTCAGGG 3' InDel 2: 5' GAGTGATCTACCGTCATCCTCAGGG 3'	InDel 1: T136X InDel 2: E138X
B11	2	Deletion (5 nt)	Insertion (1 nt)	InDel 1: 5' GAGTGATCTACCGTCATCTCAGGG 3' InDel 2: 5' GAGTGATCTACCGTCATCCTCAGGG 3'	InDel 1: T136X InDel 2: E138X
B12	2	Deletion (5 nt)	Deletion (2 nt)	InDel 1: 5' GAGTGATCTACCGTCATCTCAGGG 3' InDel 2: 5' GAGTGATCTACCGTCATCTCAGGG 3'	InDel 1: T136X InDel 2: D137X
C11	2	Insertion (195 nt)	Insertion (195 nt)	InDel 1: 5' GAGTGATCTACCGTCATCTGGCGGCTCCTCCTAATGATGAAACAACTTTTGCTGGTTGTTGATGAGAATAACTTGATGATTCTTCTTACTGTGGCGTGTGGTGTTGATGATTCCTTCGGATAATAGTAAGATGTAATAATAGCTGAAAAGAAAACATGATGGCTGATTAAGAATAGTTGTTAAGATTGGTGATGAGTGCTGAGTATCACATATTCAGGG 3' InDel 2: 5' GAGTGATCTACCGTCATCCTCCGAATAGTTACAGCAGAAGCTGGAGGAGCTTTAACAGAGTACTAGTAGGTCTACCATATGATTTACCATCATTTTTTCCTGCTGTTTCACCATCCAATGAGGGGAAAAGTTTATTATCGTGTTATAGCGGTGGTAAACCATAATTCGCAACTTGTACTTTGTTAGAATTTTGTGCGTATATTGCAACAAATATCAGGG 3'	

Table 4.1. continued.

ID	Number of mutated transcripts	InDel 1	InDel 2	Position of InDel	Amino acid alteration
D3	1	N/A	Deletion (2 nt)	InDel 2: 5' GAGTGATCTACCGTCATCTCAGGG 3'	InDel 2: D137X
D5	2	Insertion (1 nt)	Insertion (1 nt)	InDel 1: 5' GAGTGATCTACCGTCATCCTCAGGG 3' InDel 1: 5' GAGTGATCTACCGTCATCTTCAGGG 3'	InDel 1: E138X InDel 2: E138X
D6	2	Insertion (1 nt)	Deletion (2 nt)	InDel 1: 5' GAGTGATCTACCGTCATCCTCAGGG 3' InDel 2: 5' GAGTGATCTACCGTCATCTCAGGG 3'	InDel 1: E138X InDel 2: D137X
E3	2	Insertion (1 nt)	Deletion (5 nt)	InDel 1: 5' GAGTGATCTACCGTCATCNTCAGGG 3' InDel 2: 5' GAGTGATCTACCGTCATCTCAGGG 3'	InDel 1: unable to determine InDel 2: T136X
F4	2	Deletion (5 nt)	Deletion (8 nt)	InDel 1: 5' GAGTGATCTACCGTCATCTCAGGG 3' InDel 2: 5' GAGTGATCTACCGTCATCTCAGGGCA 3'	InDel 1: T136X InDel 2: P135X
F11	2	Deletion (5 nt)	Deletion (6 nt)	InDel 1: 5' GAGTGATCTACCGTCATCTCAGGG 3' InDel 2: 5' GAGTGATCTACCGTCATCTCAGGG 3'	InDel 1: T136X InDel 2: H130Q, L131A, deletion of R132 and A133
F12	2	Deletion (2 nt)	Deletion (5 nt)	InDel 1: 5' GAGTGATCTACCGTCATCTCAGGG 3' InDel 2: 5' GAGTGATCTACCGTCATCTCAGGG 3'	InDel 1: D137X InDel 2: T136X
H8	2	Deletion (2 nt)	Deletion (19 nt)	InDel 1: 5' GAGTGATCTACCGTCATCTCAGGG 3' InDel 2: 5' GAGTGATCTACCGTCATCTCAGGGCAG 3'	InDel 1: D137X InDel 2: F150X

The HD-MB03 cell line used as the parental cell line for generation of the Rab knockout cell lines contains a chromosomal aberration, isochromosome 17q (i17q) (Milde et al., 2012). This is characterised by the duplication of the long q arm of the chromosome and the loss, or partial loss, of the short p arm of the chromosome (Pan et al., 2005) (Mendrzyk et al., 2006). The gene locus of Rab40B is 17q25.3 (ensembl.org) meaning that HD-MB03 cells possess three copies of the Rab40B gene (Figure 4.8.).
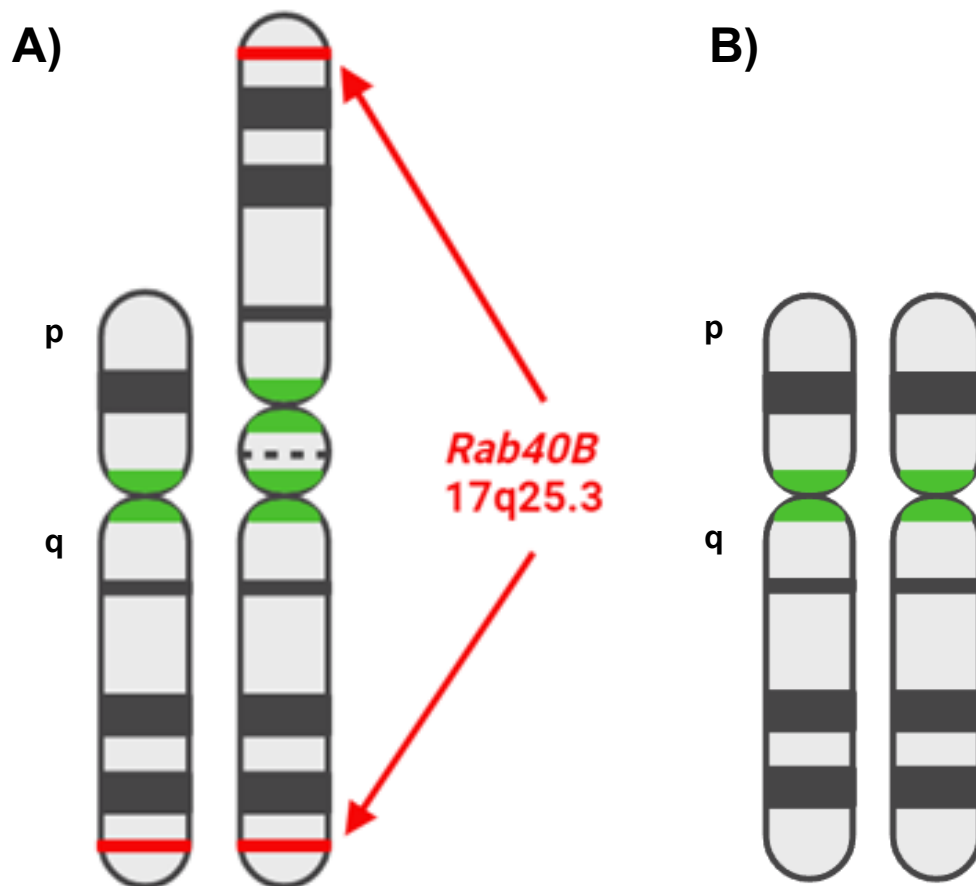
Figure 4.8. – Isochromosome 17q A) Isochromosome 17q is characterised by the presence of one chromosome with a long and a short arm (left) and a second chromosome with a duplication of the long arm and a small portion of the short arm leading to two centromeres (right). Sequence either side of the centromere is shown in green. The point of duplication of the short arm sequence is shown by a dotted line. Position of Rab40B is shown in red at q25.3. B) Chromosome 17 without isochromosome 17q. Centromere is also shown in green.

All *Rab40B* potential knockout cell lines were also sent for Sanger sequencing. However, due to the gene localising to isochromosome 17q, more than two DNA traces appeared in most chromatograms. This meant that chromatograms could not be analysed with available tools.

As Sanger sequencing and analysis algorithms were not suitable for characterising mutations within *Rab40B* knockout cell lines were sent for Oxford Nanopore sequencing at the University of Nottingham's Deep Seq facility.

Oxford Nanopore sequencing uses nanoscale protein pores (nanopores) which are embedded in an electrically resistant polymer membrane and act as biosensors. During the sequencing, a constant voltage is applied through the nanopore, generating an ionic current. Negatively charged DNA or RNA is then guided through the nanopore from the negatively charged 'cis' side to the positively charged 'trans' side by a motor protein in a stepwise manner. This motor protein has helicase activity and unwinds any double stranded DNA or RNA into single stranded DNA or RNA whilst guiding the nucleotides through the nanopore. Changes in the ionic current which correspond to the nucleotide sequence of the sample are detected by the sensing region of the nanopore and decoded using computation algorithms to give a sequencing trace or read (Figure 4.9.) (Yunhao Wang et al., 2021). Analysis can then be conducted on these reads to identify all genomic variants present within a sample regardless of the number of alleles present within it, making it suitable for the analysis of *Rab40B* variants within the potential knockout cell lines.

For this sequencing, PCR products generated from genomic DNA extracted from all ten potential knockout cell lines (identical to those sent to Sanger sequencing) were sent for analysis. Initial analysis on the results obtained from the nanopore was conducted by Dr Sonal Henson.

This analysis identified clusters of nucleotide fragments with identical sequences in each sample. These clusters were identified based on sequence reads which are the number of total DNA fragments detected within each sample (the number of sequence reads for each sample are shown in Appendix 1.8.). The number of clusters is not associated with the number of alleles present within the sample and instead the number of distinct genetic traces detected by the nanopore within the sample. Each non-targeting control cell line had one cluster. The number of clusters

identified in Rab40B knockout cell lines ranged from 1 to 8 with 40B E4 and 40B G11 possessing 1 and Rab40B H1 having 8 (Table 4.2.). Non-targeting control cell line sequences were compared with the genome and Rab40B potential knockout cell line clusters aligned with these to identify any mutations. Some clusters had poor alignment scores so analysis could not be conducted on these sequences.

As with the Sanger sequencing results, for each of the cell lines which possessed mutations the cDNA sequence of Rab40B was edited to include any InDels or single nucleotide variations present and the cDNA translated to identify any amino acid alterations (Table 4.2.).
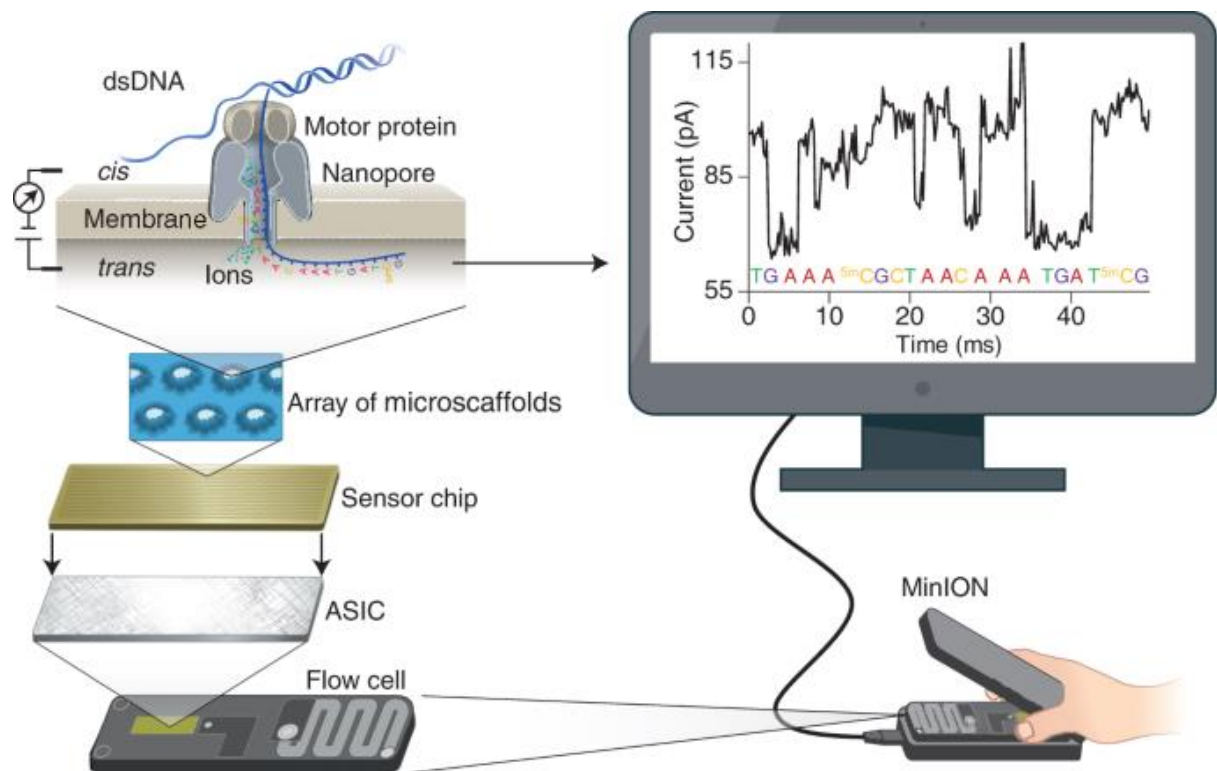
Figure 4.9. – Oxford nanopore sequencing summary *MinION flow cell containing 512 channels with 4 nanopores in each channel. Ionic current passes through the nanopore due to a constant voltage being applied across the membrane which has a cis (negatively charged) and a trans (positively charged) side. A motor protein unwinds double stranded DNA (dsDNA), and single stranded DNA is fed through the nanopore due to the voltage. The channels are in an electrically resistant polymer connected to microscaffolds and a sensor chip. Each channel has a separate electrode in the sensor chip with is controlled and measured by the application-specific integration circuit (ASIC). Each DNA or RNA base gives a characteristic current change which is measured and used to determine the sequence of the sample. Image reproduced from Wang et al., 2021.*

Table 4.2. – Oxford nanopore sequencing and sequence translation results for Rab40B potential knockout cell lines *Purple denotes a deletion mutation, yellow denotes an insertion mutation and light blue denotes a single nucleotide variation (SNV). All sequence clusters were identified using a 97% cluster identity threshold.*

Sample	Cluster	InDel	Amino acid alteration
40B A9	1	141 nt deletion: 5' TTGCAAGACCTCTGCTGCCGGGCGGTCGTGTCCTGCACGCCGGTGCACCTGGTGGACAAGCTCCCGCTCCCCATTGCCTTAAGA AGCCACCTCAAGTCCTTCTCGATGGCCAACGGCCTGAATGCCAGGATGATGCACGGCGG 3'	Deletion of L192 to G238
	2	7 nt deletion: 5' AATGCCAGGATGATGCACGGCGGT 3'	R255X
40B B4	1	7 nt deletion: 5' AATGCCAGGATGATGCACGGCGG 3'	R255X
	2	36 nt deletion: 5' GGCCTGAATGCCAGGATGATGCACGGCGGTTCCTAC 3'	Deletion of G230 to Y241
40B B10	1	*Poor alignment score*	
	2	8 nt deletion: 5' AATGCCAGGATGATGCACGGCGG 3'	M235R, alterations until K276L
	3	*Poor alignment score*	
	4	*Poor alignment score*	
40B C12	1	*Poor alignment score*	
	2	*Poor alignment score*	
	3	*Poor alignment score*	
40B E4	1	1 nt deletion: 5' AATGCCAGGATGATGCACGGCGG 3'	V257X

Table 4.2. continued.

Sample	Cluster	InDel	Amino acid alteration
40B F5	1	150 nt deletion: 5'CGGGCGGTTCGTGTCCTGCACGCCGGTGCACCTGGTGGACAAGCTCCCGCTCCCCATTGCCTTAAGAAGCCACCTCAAGT CCTTCTCGATGGCCAACGGCCTGAATGCCAGGATGATGCACGGCGGTTCCTACTCCTCACCACCAGCTCC3'	Deletion of R198 to S247
	2	61 nt deletion: 5'CTTAAGAAGCCACCTCAAGTCCTTCTCGATGGCCAACGGCCTGAATGCCAGGATGATGCACGGCGG3'	H237X
	3	44 nt deletion and SNV: 5' CCTTCTCGATGGCCAACGGCCTGAATGCCAGGATGATGCACGGCGG 3'	S224X
	4	26 nt deletion: 5' GAATGCCAGGATGATGCACGGCGGTT 3'	N232L, alterations until C270L
40B F9	1	1 nt insertion: 5' AATGCCAGGATGATGCAACGGCGG 3'	H237Q, alterations until X279L
	2	11 nt deletion: 5' AATGCCAGGATGATGCACGGCGGTT 3'	M236I, alterations until C275L
40B G8	1	182 nt deletion: 5' CAAGTCCTTCTCGATGGCCAACGGCCTGAATGCCAGGATGATGCACGGCGGTTCCTACTCCTCACCACCAGCTTCCTA CTCCCTCACCACCAGCTCCACCCACAAAAGGAGCAGCCTCCGCAAAGTGAAGCTCGTCCGCCCCCCCCAGAGCCCCCCCAAAAACTG CACCAGAAACAGCTGCAAAATTTCTTAAGGAACACT 3'	Truncation from H221
	2	1 nt deletion: 5' AATGCCAGGATGATGCACGGCGGTT 3'	V257X
	3	71 nt deletion: 5' TCAAGTCCTTCTCGATGGCCAACGGCCTGAATGCCAGGATGATGCACGGCGGTTCCTACTCCTCACCACC 3'	L222Q, alterations until R255L

143

Table 4.2. continued.

Sample	Cluster	InDel	Amino acid alteration
40B H1	1	*Poor alignment score*	
	2	*Poor alignment score*	
	3	1 nt insertion: 5' AATGCCAGGATGATGCA==A==CGGCGG 3'	H237Q, alterations until X279L
	4	*Poor alignment score*	
	5	*Poor alignment score*	
	6	*Poor alignment score*	
	7	301 nt deletion: 5' GCGGCAGGGCTTGCTGCATGTACAAGCCAGGGCCACGGGCGTCCGAGCCTGGGAGGGCGGGAGAACAGGTGGTGGGCACCACCCCTCATTCCCAGCCCAGGTGGGGACATCCACTAAGCAAGGTTTATCTTTTCTCTCCCAGTGCTGAGCTTGCAAGACCTCTGCTGCGGGCGGTTCGTGTCCTGCACGCCGGTGCACCTGGTGGACAAGCTCCCGCTCCCCATTGCCTTAAGAAGCCACCTCAAGTCCTTCTCGATGGCCAACGGCCTGAATGCCAGGATGATGCACGGCGGTTCCTAC 3'	R177P, alterations until P213L
	8	301 nt deletion: 5' GCGGCAGGGCTTGCTGCATGTACAAGCCAGGGCCACGGGCGTCCGAGCCTGGGAGGGCGGGAGAACAGGTGGTGGGCACCACCCCTCATTCCCAGCCCAGGTGGGGACATCCACTAAGCAAGGTTTATCTTTTCTCTCCCAGTGCTGAGCTTGCAAGACCTCTGCTGCGGGCGGTTCGTGTCCTGCACGCCGGTGCACCTGGTGGACAAGCTCCCGCTCCCCATTGCCTTAAGAAGCCACCTCAAGTCCTTCTCGATGGCCAACGGCCTGAATGCCAGGATGATGCACGGCGGTTCCTAC 3'	R177P alterations until P213L

Results showed that whilst most cell lines had clusters with amino acid alterations, of the ten potential knockout cell lines, after translation only 40B E4 and 40B G11 definitively had mutations which led to premature stop codons in all sequencing clusters. E4 and G11 both had a single cluster with a single nucleotide deletion, leading to the presence of a premature stop codon after translation. For E4 this supports the T7 endonuclease assay which identified this cell line as having one allele (section 4.5.).

Furthermore, most of the clusters for 40B B10 and 40B H1 and all of the clusters for 40B C12 had poor alignment so these cell lines could not be fully characterised. Whilst all four 40B F5 clusters had good alignment scores, the presence of four different genetic variations instead of the expected three leaves questions about the precise genetics of *Rab40B* within this cell line. Potentially this cell line could have arisen from a dividing cell which was not detected during FACS and consequently had more than three chromosomal arms with the *Rab40B* gene at the time of CRISPR-Cas9 gene editing.

Overall, this sequencing highlights the difficulty of characterising CRISPR-Cas9 knockouts for certain genes as ultimately despite using two different sequencing methods, most of the *Rab40B* potential knockout cell lines were not able to be characterised genetically.

4.7. Western blotting

To identify whether endogenous protein was expressed in each of the potential knockout cell lines, cell pellets for each cell line were lysed, protein concentration quantified and western blotting was used to determine the presence of Rab11A or Rab40B and calnexin used as a loading control. Endogenous protein was absent for seventeen out of the twenty-three Rab11A potential knockout cell lines (Figure 4.10.). For the remaining six, bands were present at approximately 24 kDa, the expected molecular weight for Rab11A. Of the seventeen which had no protein bands, seven could not be characterised by Sanger sequencing (Table 4.1.). Nine cell lines could be fully sequenced (A12, B7, B11, B12, C11, D5, D6, F4 and F12) and each had two InDels which resulted in the presence of premature stop codons.

One cell line (E3) had a 5 nucleotide deletion that could be characterised and a one nucleotide insertion that could not be so whilst it can be inferred that this InDel results in a premature stop codon, this could not be fully characterised.

Of the six which did have a protein band, two could not be characterised by sequencing (C3 and C10), one had a wildtype allele (D3), two had an InDel which was a multiple of three (B1 and F11) which resulted in amino acid changes and not a premature stop codon. Finally, one (H8) had two InDels, one of 2 nucleotides and the other of 20 but still had protein expression.

The epitope of the Rab11A antibody used lies C-terminal of the CRISPR-Cas9 gene editing site, within the C-terminal tail (although specific antibody residues are not specified by the manufacturer). Therefore, if a premature stop codon had been introduced and a truncated protein was translated within the cells, this antibody could not detect it. This truncated form of Rab11A is unlikely to be functional, however (as discussed in section 4.9.) and therefore this method still detects whether the cell line has a detectable functional form of Rab11A present.

Western blotting of *Rab40B* potential knockout cell lines indicated the presence of endogenous Rab40B in all ten cell lines (Appendix 1.9.). Western blot bands matched the expected molecular weight of 31 kDa and were consistent with untreated and non-targeting control cell lines. This did not support the sequencing conducted as cell lines E4 and G11 only had one sequence cluster with an InDel that in principle would result in a premature stop codon (section 4.6.2.). Thus, further exploration was conducted. The epitope of the Rab40B primary antibody used was within the C-terminus of the protein, this area of the protein has high sequence homology with the Rab40 isoform Rab40C (Neumann and Prekeris, 2023) and as such it was hypothesised that the bands observed on the Western blot were due to lack of specificity of the Rab40B antibody for Rab40B only. Joseph Allen, a PhD student, in the Hume lab, then conducted dot blotting on Rab40C-GFP HEK293T cell lysates and the Rab40B primary antibody (not shown). This showed that the Rab40B could detect the Rab40C-GFP conjugate protein and thus it was concluded that the Rab40B antibody was non-specific and unsuitable for detecting whether Rab40B endogenous protein was present within the knockout cell lines.

Due to time limitations of the project, an antibody which was specific to Rab40B was unable to be identified. Therefore, it could not be confirmed whether a *Rab40B* knockout cell line had been generated.
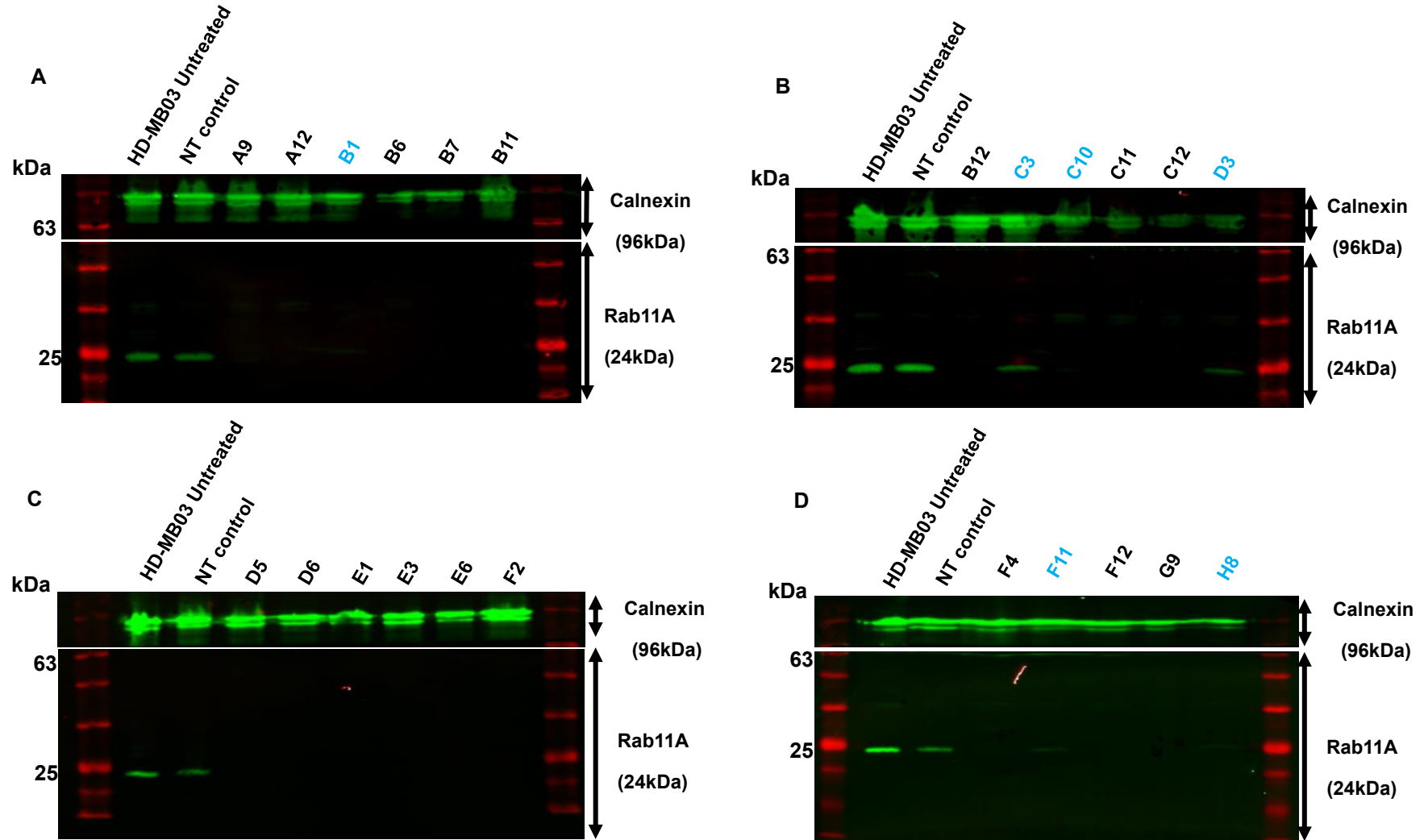
Figure 4.10. – Rab11A potential knockout cell lines Western blot *LI-COR Western blot images of Rab11A knockout cell lines (denoted by a letter and a number), non-targeting (NT) CRISPR-Control cell lines and untreated HD-MB03 cells. Membranes were cut at the 63kDa molecular weight marker (BLUeye pre-stained protein ladder, red) and stained with anti-calnexin and anti-Rab11A primary antibodies. Lanes with endogenous Rab11A protein bands are highlighted in light blue.*

4.8. Morphology of Rab11A knockout cell lines

As Rab40B potential knockout cell lines could not be fully validated, the focus was placed on further analysis of Rab11A cell lines. Initially it was decided to determine whether a particular InDel or group of InDels were indicative of a particular cellular morphology. All 23 potential knockout cell lines were examined using brightfield microscopy after culture in T-25 culture flasks and passaged twice.

This identified four morphological classes: A, B, C and D (Figure 4.11). Class A morphology appeared to be the most like wildtype with a largely adherent cell population, which have similar shape to wildtype cells, but with slightly larger clusters of semi-adherent cells. It included the cell lines B1 and H8. Class B were more semi-adherent than class A with small clusters of semi-adherent cells, it included the cell lines B12 and D5. Class C had a largely adherent population which grew in very dense round clusters of cells. Cultures had minimal semi-adherent cells and included A12, B11 and E3 Lastly, Class D were more suspension and included larger clusters of semi-adherent cells and fewer adherent cells. They were also much slower growing than other classes, cell lines with this morphology included C11 and D6. All other cell lines had a mixed morphology of multiple classes, were morphologically less well defined or were only observed in n = 1.

As no morphology was solely linked to a single InDel or group of InDels, it was concluded that cell morphology was not indicative of the type of CRISPR-Cas9 gene editing event. Therefore, any morphological changes are likely to be due to the cellular response to either being grown from a single cell or having undergone gene editing.
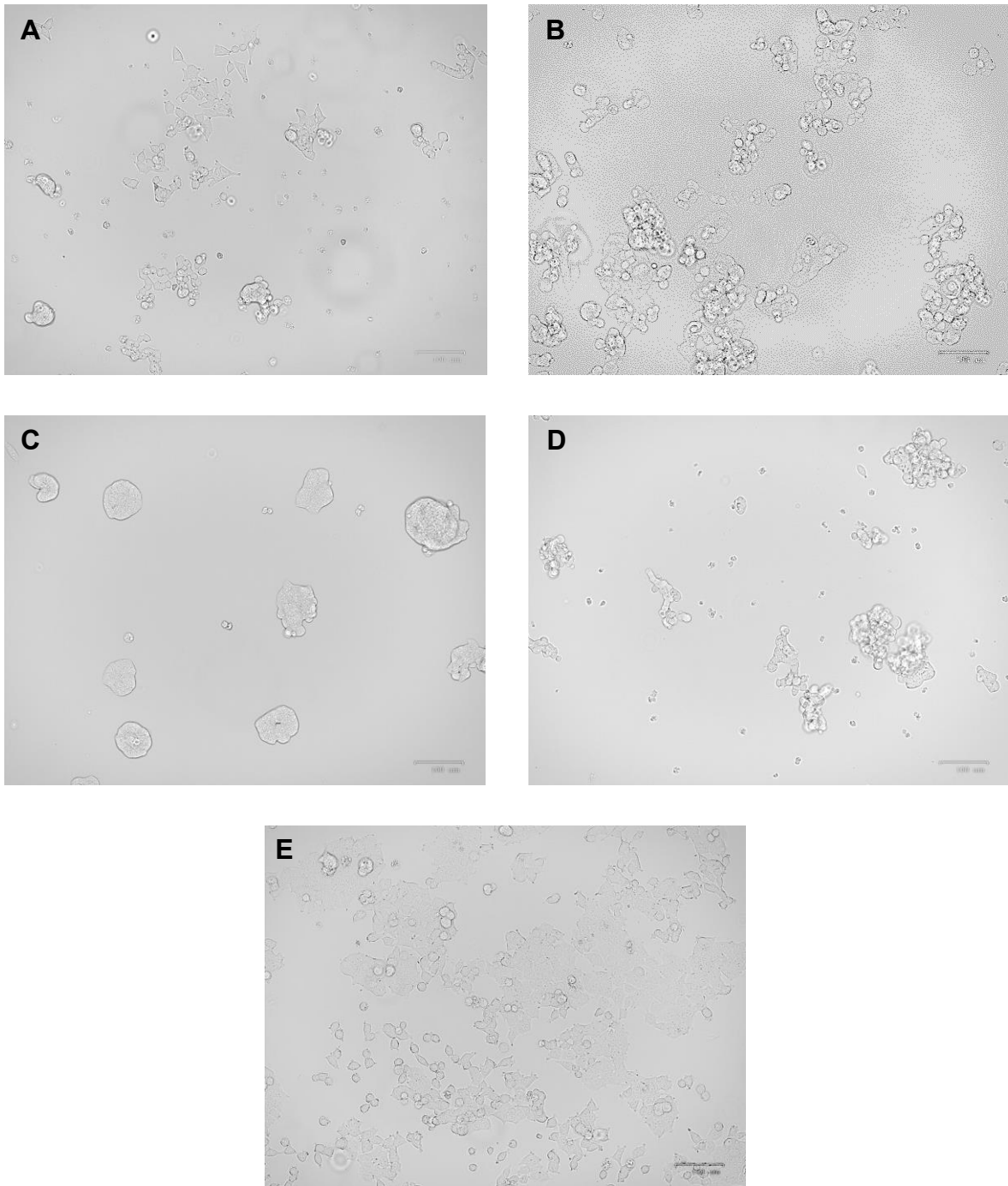
Figure 4.11. Cell morphologies of Rab11A knockout cell lines *Cell lines were divided into four classes (A-D) based on morphological characteristics after culture in a T-25 culture flask after two passages. Wildtype HD-MB03 cells (E) which had not undergone any gene editing or single cell sorting were cultured alongside all CRISPR lines and were used to make visual morphological comparisons. Brightfield images of cells in T-25 culture flasks were obtained using a BioRad ZOE fluorescent cell imager with a 20X magnification. Scale bars represent 100 μm.*

4.9. Analysis of Rab11A protein sequence in *Rab11A* knockout cell lines

In addition to assessing morphological changes in the Rab11A knockout cell lines. The effect of gene editing on the amino acid sequence compared to the wildtype and the corresponding impact to secondary structural elements was explored. As the most common mutation amongst Rab11A knockout cell lines was the 5-nucleotide 'TCTCA' deletion and the Rab11A cell line A12 was homozygous for this mutation, this is used as the example shown in Figure 4.12. The amino acid sequence was aligned to the wildtype Rab11A amino acid sequence using the UniProt align tool (www.uniprot.org/align). This resulted in a truncation of Rab11A from 216 amino acids to 135 amino acids with an altered amino acid sequence from H130.

```
Wildtype   MGTRDDEYDYLFKVVLIGDSGVGKSNLLSRFTRNEFNLESKSTIGVEFATRSIQVDGKTI   60
A12        MGTRDDEYDYLFKVVLIGDSGVGKSNLLSRFTRNEFNLESKSTIGVEFATRSIQVDGKTI   60
           ************************************************************

Wildtype   KAQIWDTAGQERYRAITSAYYRGAVGALLVYDIAKHLTYENVERWLKELRDHADSNIVIM   120
A12        KAQIWDTAGQERYRAITSAYYRGAVGALLVYDIAKHLTYENVERWLKELRDHADSNIVIM   120
           ************************************************************

Wildtype   LVGNKSDLRHLRAVPTDEARAFAEKNGLSFIETSALDSTNVEAAFQTILTEIYRIVSQKQ   180
A12        LVGNKSDLRQGSSYR---------------------------------------------   135
           *********:    :

Wildtype   MSDRRENDMSPSNNVVPIHVPPTTENKPKVQCCQNI   216
A12        ------------------------------------   135
```

***Figure 4.12. – Amino acid sequence alignment of Rab11A in mutant cell line compared to wildtype cell line** Wildtype amino acid sequence ('Wildtype', top row) and 11A A12 amino acid ('A12', bottom row). '*' denotes a fully aligned amino acid, '-' denotes absence of amino acids from one of the samples, ':' denotes the first four altered amino acids. Altered amino acids are highlighted in yellow. Alignments conducted using the UniProt Align software (www.uniprot.org/align).*

The position of the truncation was mapped onto the secondary structure and functional domains of the protein (Figure 4.13. A). This was to identify whether the truncation had caused the loss of any functional domains and therefore determine the likelihood of a functional but truncated form of Rab11A being retained by cells. There is also a possibility that whilst the truncated form may be translated, it is subsequently degraded by the proteasome as a misfolded protein. The secondary structure of Rab GTPases is characterised by a six-stranded beta sheet flanked by five alpha helices that form functional regions including the interswitch region that is responsible for GTP/GDP and effector protein binding (Figure 4.13. B). It also contains other alpha helices and beta sheets some of which are conserved amongst the Rab family members. This is followed by a C-terminal hypervariable region that has little recognised secondary structural elements and is the most unique sequence to each Rab.

The Cas9 target site where the genetic alterations caused by CRISPR-Cas9 gene editing is present, when translated, is present in the well-structured region containing beta strands and alpha helices. After translation, *in silico* results showed that the truncation caused the loss of two alpha helices, a beta sheet and a beta turn from the secondary structure (Figure 4.13.). This truncation likely affects effector binding as Rab11A is known to bind to Rabin8 at a non-canonical site between L128 and L131 (Vetter et al., 2015). This truncation also causes loss of the hypervariable domain in the C-terminal tail containing cysteine residues which require prenylation in order to associate with membranes (Duan and Lambright, 2019). Therefore, the absence of this C-terminal region in the truncated form means that this mutated Rab11A will be unable to associate with membranes, a critical part of its vesicle trafficking function. It should be noted that an AlphaFold model of the effects of gene editing on the structure of Rab11A was used instead of an experimental structure as this better allowed for highlighting of structural regions which would be affected by the presence of a premature stop codon.
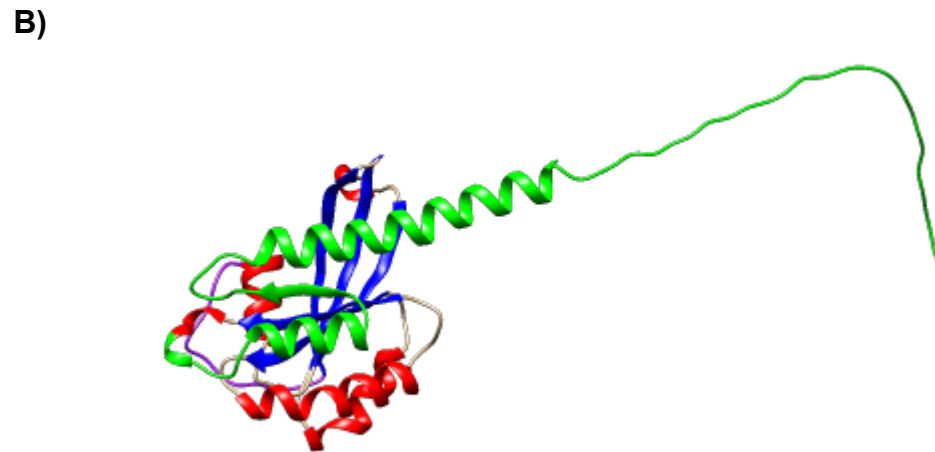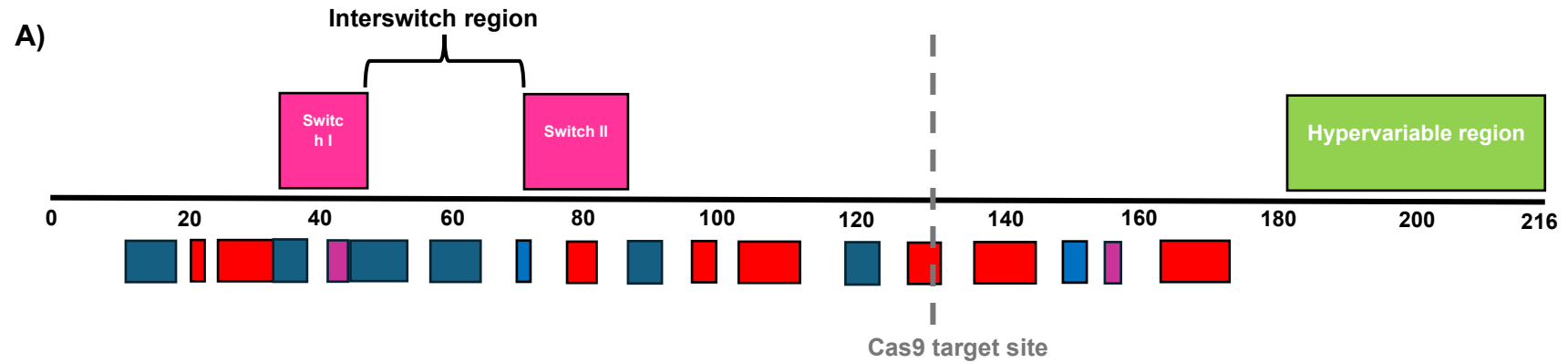
Figure 4.13. Structure of Rab11A protein *A) Schematic representation of secondary structural elements (below line) and functional regions (above line). Amino acid residue position is shown on a black line through the middle of the diagram with N-C terminus. Functional domains (above line) are shown in pink (switch region) and green (hypervariable region). Secondary structure elements (below line) are shown as rectangle with beta strands (blue), alpha helices (red) and beta turns (purple) shown. Length of rectangle corresponds to the approximate length of the secondary structural element. Position of the Cas9 target site in the amino acid sequence is highlighted in grey. (B) 3D structural model of Rab11A. Green indicates structure lost in knockout cell lines due to presence of a premature stop codon. Secondary structure features are coloured as detailed for (A). Model was obtained using AlphaFold (alphafold.ebi.ac.uk) and image coloured using the UCSF Chimera software (cgl.ucsf.edu/chimera/).*

153

4.10. Summary

In this chapter, HD-MB03 group 3 medulloblastoma cells were used as a model cell line for CRISPR-Cas9 gene editing to generate Rab11A and Rab40B protein knockout cell lines.

Here it was shown that HD-MB03 was a suitable cell line because cells survived nucleofection with a GFP plasmid and then survived nucleofection and single cell sorting. The ability to survive nucleofection and single cell sorting and then proliferate was critical in order to generate homogeneous, stable knockout cell lines. After CRISPR-Cas9 gene editing, three molecular techniques were then used to determine the presence of genetic alterations and full-length protein.

T7 endonuclease assay indicated that 22 potential Rab11A knockout cell lines had multiple alleles and one had one allele. It also showed that eight potential Rab40B knockout cell lines had multiple alleles and two had one allele. This suggests that for both Rabs, gene editing is likely to have occurred at the CRISPR-Cas9 sgRNA target site in multiple potential knockout cell lines.

Sequencing was then used to determine specific nucleotide changes within the CRISPR-Cas9 sgRNA target site. Sanger sequencing was used to analyse PCR products generated using primers specific to *Rab11A.* Chromatograms for 14 out of 23 potential knockout cell lines could be analysed using the Indigo InDel detection software. This showed that one cell line, A12, had a biallelic 'TCTCA' deletion, one cell line, D3, had an unmutated allele and a mutated allele and twelve cell lines had two different mutations. cDNA sequence for each of these cell lines was edited to take account of any mutations present and the ExPASy translate tool used to determine the presence of any amino acid alterations caused by the mutations. This showed that ten potential knockout cell lines (A12, B7, B11, B12, C11, D5, D6, F4, F12, H8) had genetic mutations that led to a premature stop codon on both gene transcripts suggesting that these ten are likely to have an absence of full length Rab11A protein and therefore be functional knockouts.

The HD-MB03 cell line used to generate the CRISPR-Cas9 knockouts contains a chromosomal aberration, isochromosome 17q. This means that there are three copies of the *Rab40B* gene being present within each cell. As such, Sanger sequencing

could not be used to characterise nucleotide variants within potential *Rab40B* knockout cell lines. Instead, Oxford nanopore sequencing was used to try to identify specific nucleotide changes. As with *Rab11A* potential knockout cell lines, the ExPASy translate was also used to determine the presence of amino acid alterations. Together this showed that only two cell lines, E4 and G11, had mutations which led to premature stop codons in all sequencing clusters.

Western blotting was then used to determine whether full length protein could be detected in each cell line. This showed that 17 out of 23 *Rab11A* potential knockout cell lines had absence of protein. This included the nine cell lines that were showed to have genetic mutations that led to a premature stop codon on both gene transcripts. Due to the lack of antibody specificity, the presence of full length Rab40B protein could not be determined in *Rab40B* potential knockout cell lines.

Therefore, as nine *Rab11A* potential cell lines could be fully characterised using all three molecular validation techniques, but full characterisation could not be completed on any of the Rab40B cell lines, the decision was made to proceed with functional analysis of Rab11A in the group 3 medulloblastoma HD-MB03 cell line. A summary of the results of all three validation techniques for the Rab11A knockout cell lines is shown in Table 4.3.

Cell morphology analysis of Rab11A cell lines in culture showed that knockout cell lines had four morphological categories, however none were attributed to a single InDel pattern.

Table 4.3. Summary of T7 endonuclease I mismatch detection assay, Sanger sequencing and Western blot results for Rab11A potential knockout cell lines *'nt' stands for nucleotide, 'WT' stands for wildtype allele.*

Rab11A cell line	Sequencing results			Western blot
	Phenotype	Mutation(s)	Amino acid alteration	
A9	Unable to sequence			No protein
A12	Homozygous	Two of the same 5 nt deletion	T136X	No protein
B1	Heterozygous	5 nt deletion, 9 nt insertion	T136X, L131H and insertion YFF 132-134	Protein
B6	Unable to sequence			No protein
B7	Heterozygous	5 nt deletion, 1 nt insertion	T136X, E138X	No protein
B11	Heterozygous	5 nt deletion, 1 nt insertion	T136X, E138X	No protein
B12	Heterozygous	5 nt deletion, 2 nt deletion	T136X, D137X	No protein
C3	Unable to sequence			Protein
C10	Unable to sequence			Protein
C11	Heterozygous	Two different 195 nt insertions		No protein
C12	Unable to sequence			No protein
D3	Heterozygous	WT, 2 nt deletion	D137X	Protein
D5	Heterozygous	Two different 1 nt insertions	Both E138X	No protein
D6	Heterozygous	1 nt insertion, 2 nt insertion	E138X, D137X	No protein

Table 4.3. continued

Rab11A cell line	Sequencing results			Western blot
	Phenotype	Mutation(s)	Amino acid alteration	
E1	*Unable to sequence*			No protein
E3	Heterozygous	1 nt insertion, 5 nt deletion	Unable to determine, T136X	No protein
E6	*Unable to sequence*			No protein
F2	*Unable to sequence*			No protein
F4	Heterozygous	5 nt deletion, 8 nt deletion	T136X, P135X	
F11	Heterozygous	5 nt deletion, 6 nt deletion	T136X, H130Q L131A deletion of R132 and A133	Protein
F12	Heterozygous	2 nt deletion, 5 nt deletion	D137X, T136X	No protein
G9	*Unable to sequence*			No protein
H8	Heterozygous	2 nt deletion, 19 nt deletion	D137X, F150X	Protein

Chapter 5:

Determining the function of Rab11A in group 3 medulloblastoma

5.1. Introduction

In Chapter 3, Rab11A and Rab40B were identified as Rab GTPase targets for functional analysis. To do this, CRISPR-Cas9 knockout HD-MB03 group 3 medulloblastoma cell lines were generated, with design, optimisation, and validation of nine Rab11A knockout cell lines described in Chapter 4. Whether a successful *Rab40B* knockout cell line had been generated could not be definitively determined. This chapter presents the first steps to decipher some of the functional roles of Rab11A in group 3 medulloblastoma using the knockout cell lines.

As with other members of the Rab GTPase family of proteins, Rab11A is a key regulator of vesicular trafficking (Stenmark, 2009). It is highly conserved amongst eukaryotes and is ubiquitously expressed in tissues throughout the body (Ullrich et al., 1996). It has been specifically implicated with roles in the endocytic recycling and exosome biogenesis pathways amongst others (Ullrich et al., 1996) (Bai et al., 2022).

Tripolitsioti et al. (2018) elucidated the role of endocytosis in the invasive behaviour of the SHH medulloblastoma subgroup, through the aberrant recycling of integrins to the cell membrane. Aberrant recycling of integrins and other apical transporter proteins has been associated with increased invasiveness of cancer cells (Vogel et al., 2017). There is no published work which currently deciphers the role of endocytic pathways in group 3 medulloblastoma pathogenesis. As Rab11A is associated with this pathway, it was hypothesised that the absence of Rab11A in HD-MB03 cells affects the endocytic recycling pathway. Additionally, Jackson et al. (2023) showed that metastatic medulloblastoma cell lines secrete more exosomes than non-metastatic cell lines, establishing a link between exosome secretion and metastatic phenotype in medulloblastoma cells. As HD-MB03 cells are known to be derived from a highly metastatic group 3 tumour (Lock and Stow, 2005; Milde et al., 2012a), and Rab11A is fundamentally involved in exosome biogenesis, it was hypothesised that a Rab11A knockout will affect EV characteristics e.g. number, size and contents.

In this chapter, the role of Rab11A in the endocytic recycling and extracellular vesicle biogenesis pathways was investigated. This was with a view to begin the determination of functional roles of Rab GTPases in metastatic medulloblastoma.

For functional analysis of Rab11A in group 3 medulloblastoma, three of the nine fully validated knockout cell lines were chosen. These all had different mutations which resulted in the presence of a premature stop codon in all alleles and undetectable Rab11A expression in western blots. To control for this, three non-targeting control cell lines were also used.

Cell lines used were 11A A12 (homozygous, 5 nucleotide deletion), 11A B11 (heterozygous, 5 nucleotide deletion and 1 nucleotide insertion) and 11A B12 (heterozygous, 5 nucleotide deletion and 2 nucleotide deletion). These cell lines represented two out of the four morphological categories (B and C) identified for the potential Rab11A knockout cell lines. Of the other two categories both had practical limitations, D was very slow growing and A contained a cell line, 11A H8, which had full length protein expression and therefore could not be entirely attributed to a full knockout phenotype.

Objectives of this chapter:

- Identify whether loss of Rab11A affects endocytic recycling.
- Quantify the effect of Rab11A knockout on extracellular vesicle size distribution and output.
- Identify whether Rab11A knockout results in altered cellular and extracellular vesicle proteomes.

5.2. Analysis of transferrin uptake by *Rab11A* knockout cells

Rab11A is a key regulator of the slow endocytic recycling pathway (Zulkefli et al., 2019) (Lock and Stow, 2005). In slow endocytic recycling, cargo such as tyrosine kinases and G-protein coupled receptors are transferred from early endosomes to the endocytic recycling compartment before transfer into recycling endosomes and trafficking to the plasma membrane (Allgood and Neunuebel, 2018) (O'Sullivan et al., 2020). Rab11A is localised to these recycling endosomes and therefore aids in the regulation of this endocytic recycling pathway (Zulkefli et al., 2019). The endosomal and lysosomal pathways are also connected through the early endosomal compartment. Inhibition of endocytic recycling members, such as Rab11A, has been shown to promote cargo degradation by lysosomes instead of recycling back to the plasma membrane (Bai et al., 2022). Studying the endocytic recycling pathway in *Rab11A* knockout cells, may therefore elucidate the potential contribution of Rab11A in group 3 medulloblastoma through the endocytic recycling pathway. It may also determine if there is dysregulation of lysosomal pathways also.

Transferrin is a marker of endocytic recycling and is commonly used to study the function of the pathway within cells. The mechanism of endocytic recycling of transferrin is shown in Figure 5.1. In this study, fluorescently tagged transferrin is used to identify whether the absence of Rab11A in Rab11A knockout cells leads to altered endocytic recycling compared to non-targeting CRISPR control cell lines. Experiments utilising fluorescent transferrin were n=1 for the most part, therefore analyses are exploratory.
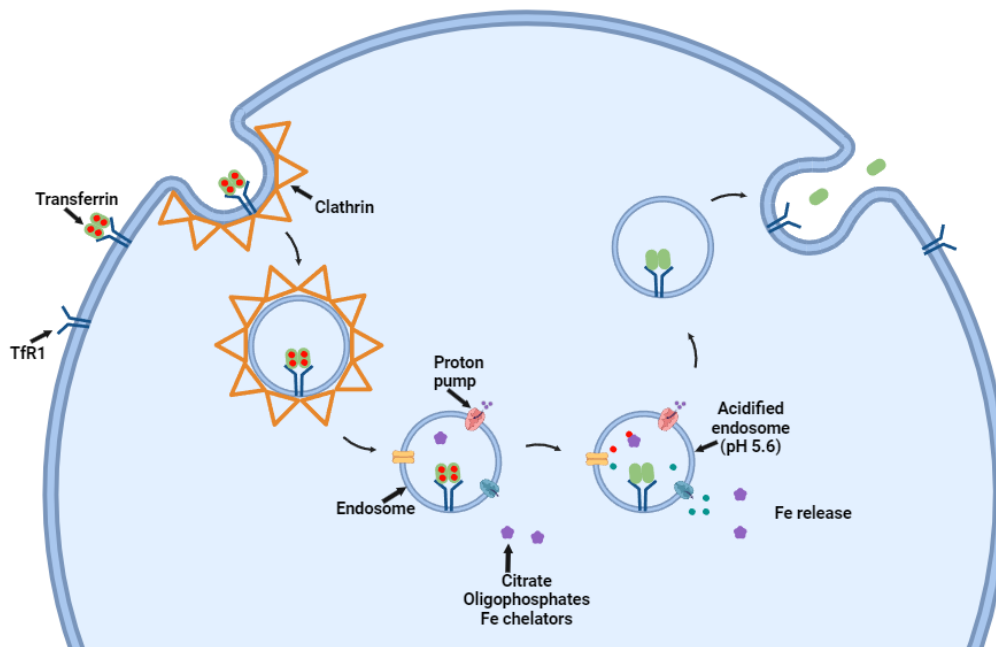
Figure 5.1. – Transferrin recycling through the cell *Iron (Fe)-bound transferrin binds to a transferrin receptor (TfR1) and is receptor mediated endocytosed in clathrin-coated vesicles before being recycled back to the plasma membrane. Image adapted from Silva et al., 2021 and created using BioRender.com.*

5.2.1. Transferrin uptake experiment optimisation

To visualise transferrin uptake by cells, an assay was developed using fluorescently tagged transferrin (Alexa Fluor™ 568). Initially, the wildtype HD-MB03 cell line was used to optimise conditions for the experiment. Cells were incubated with fluorescently tagged transferrin for up to 30 minutes and then fixed with paraformaldehyde (section 2.6.1.). Initial experiments confirmed that a 10–30-minute incubation period was sufficient to show intracellular accumulation of fluorescent transferrin (data not shown).

A second trial of the experiment was then conducted using the same protocol as used before. This second trial was designed to optimise imaging conditions and confocal microscopy was used with 63X magnification. Cells were stained after fixing using the nuclear stain DAPI and the lysosomal membrane marker LAMP-1 (lysosomal-associated membrane protein-1). Anti-LAMP-1 staining was included to see whether transferrin was being degraded by the lysosomal system instead of recycled back to the cell membrane.

Representative confocal microscopy images of the optimisation are shown in Figure 5.2. As fluorescence did not visibly change after a 20-minute incubation with transferrin, images of these cells are shown. All cells were positive for LAMP-1 and DAPI staining showing that these stains require no further optimisation. Transferrin appeared to be throughout the cytosol in small puncta which could be representative of intracellular vesicles. Anti-LAMP-1 was also within the cytoplasm and was located to larger intracellular structures than transferrin. These preliminary images also showed an overall lack of colocalisation between transferrin and LAMP-1, suggesting that transferrin is not being trafficked to lysosomes in the parental cell line.
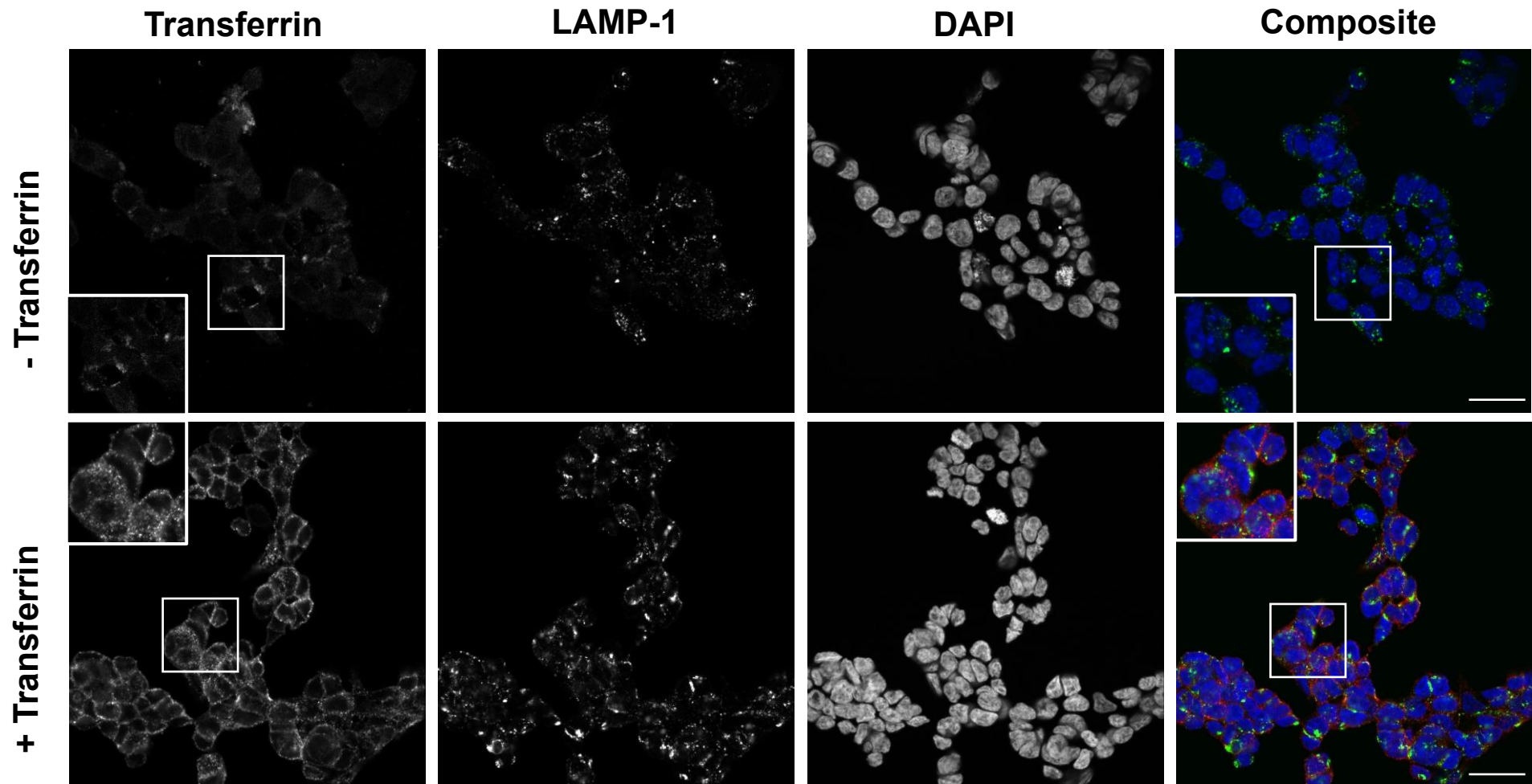
Figure 5.2. – Transferrin uptake assay imaging optimisation by confocal microscopy *Confocal images of HD-MB03 cells after a 20-minute incubation at 37oC with Alexa Fluor-568 conjugated transferrin and fixing with 4% paraformaldehyde. Cells were then stained using anti-LAMP-1 and DAPI before imaging at 63X magnification on a Zeiss LSM 710 confocal microscope. Scale bars represent 100 µm. Transferrin (left), anti-LAMP-1 (centre left), DAPI (centre right) and composite images are shown (right). Transferrin is shown in red, LAMP-1 in green and DAPI in blue on composite images.*

5.2.2. Use of microscopy to visualise transferrin uptake in Rab11A knockout cell lines to study endocytic recycling

After optimisation of the transferrin uptake assay was complete, the assay was then conducted on the Rab11A knockout cell lines A12, B11 and B12 and the non-targeting control cell lines F3, F11 and H4.

Confocal microscopy images of the cell lines 11A B11 and NT F3 after a 20-minute incubation with fluorescent transferrin show no obvious difference in fluorescent transferrin signal between the cell lines (Figure 5.3). They do however show the presence of fluorescent transferrin in both cell lines, suggesting that the endocytic mechanisms which facilitate transferrin uptake are not altered in either cell line. These results are from a single experiment, so this is an exploratory analysis and as such, any observations made are preliminary and require further experimental verification to confirm observations.

Fluorescence signal analysis of cells in microscopy images was conducted using Fiji ImageJ. This analysed the relative fluorescent signal obtained from transferrin and LAMP-1 images of the knockout and control cell lines. Images for each Rab11A knockout and non-targeting control cell line were analysed (three cell lines for each). The relative fluorescence was then plotted (Appendix 1.10.) this showed no difference in transferrin expression but did indicate a decrease in LAMP-1 in knockout cell lines compared to control cell lines. As a single experiment was conducted on each cell line, more experimentation, including more biological replicates are required to make any conclusions about transferrin and LAMP-1 expression in knockout cells. Further analysis is also required to identify whether there is any colocalisation between transferrin and lysosomes within each condition.
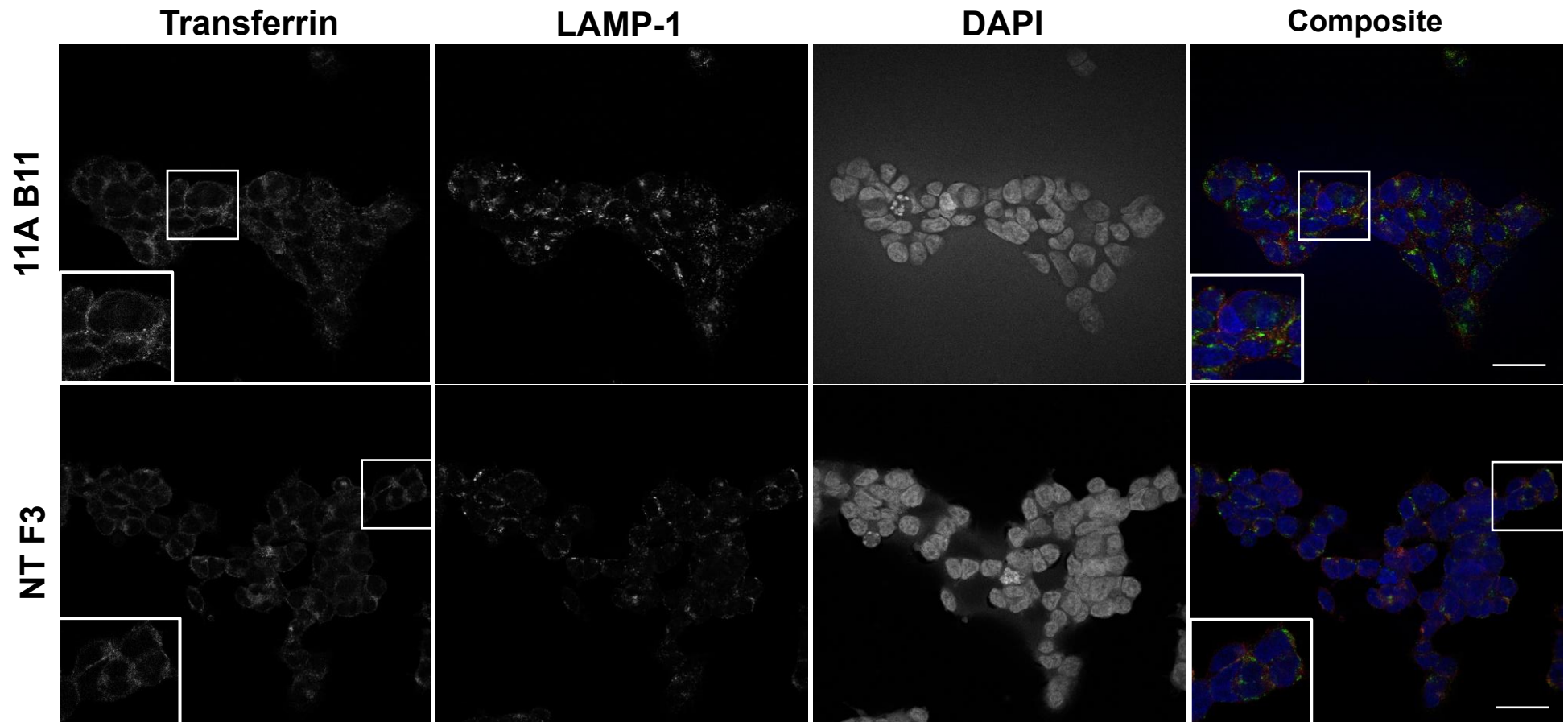
Figure 5.3. – Transferrin uptake by Rab11A knockout and non-targeting control cell lines *Confocal images of Rab11A knockout HD-MB03 cell line 11A B11 and non-targeting control cell line NT F3 after a 20-minute incubation at 37°C with Alexa Fluor-568 conjugated transferrin and fixing with 4% paraformaldehyde. Cells were then stained using anti-LAMP-1 and DAPI before imaging at 63X magnification on a Zeiss LSM 710 confocal microscope. Scale bars represent 100 μm. x63 magnification. Transferrin (left), anti-LAMP-1 (centre left), DAPI (centre right) and composite images are shown (right). Transferrin is shown in red, LAMP-1 in green and DAPI in blue on composite images.*

5.2.3. Analysis of transferrin uptake in Rab11A knockout cells by flow cytometry

To continue analysis of transferrin uptake by Rab11A knockout cells, flow cytometry was used. Wildtype, non-targeting cell line H4 and the Rab11A knockout cell line A12 were used for this experiment.

Cells were incubated with fluorescent transferrin for 10-30 minutes as highlighted throughout this section. Cells were then fixed and fluorescence measured using a flow cytometer. Cells were gated so only single cells with fluorescent levels above autofluorescence were analysed. Fluorescence was then plotted against cell count (Figure 5.4.).

Flow cytometry histograms (Figure 5.4.) showed a similar pattern of fluorescence intensity for all three cell lines at the 0-, 10- and 20-minute time points of the experiment. Most of the fluorescence uptake occurred between 0- and 10 minutes with a single, slightly shouldered fluorescence peak at 10^3-10^5 relative fluorescence units (RFU) which was sustained at 20 minutes.

For the wildtype cell line, this pattern is sustained at 30-minutes (bottom row of Figure 5.4.). Both the non-targeting and Rab11A control cell lines present differently to the wildtype at this timepoint. Analysis shows that both cell lines have two fluorescence peaks. The fluorescence profile of Rab11A knockout cells shows a larger fluorescence peak with a lower fluorescence than the smaller secondary peak. This is reversed for the non-targeting cell line and therefore suggests that there may be an effect on endocytic recycling in Rab11A knockout cells. This effect could be due to a switch from the utilisation of both the slow and fast endocytic pathways to the fast pathway only. Rab11A is a key regulator of the slow endocytic recycling pathway (as mentioned in section 5.2.), therefore knockout could lead to inhibition of this pathway and thus the fast recycling pathway used. In these cells, transferrin would be recycled back to the cell membrane more quickly, meaning that some would exhibit less fluorescence in this assay shown by a shift of the fluorescence peak to the left in Figure 5.4.

Combined with the confocal microscopy, despite the fact that any results are exploratory (n = 1), this suggests that there is a CRISPR-related phenotype that is worth further investigation.
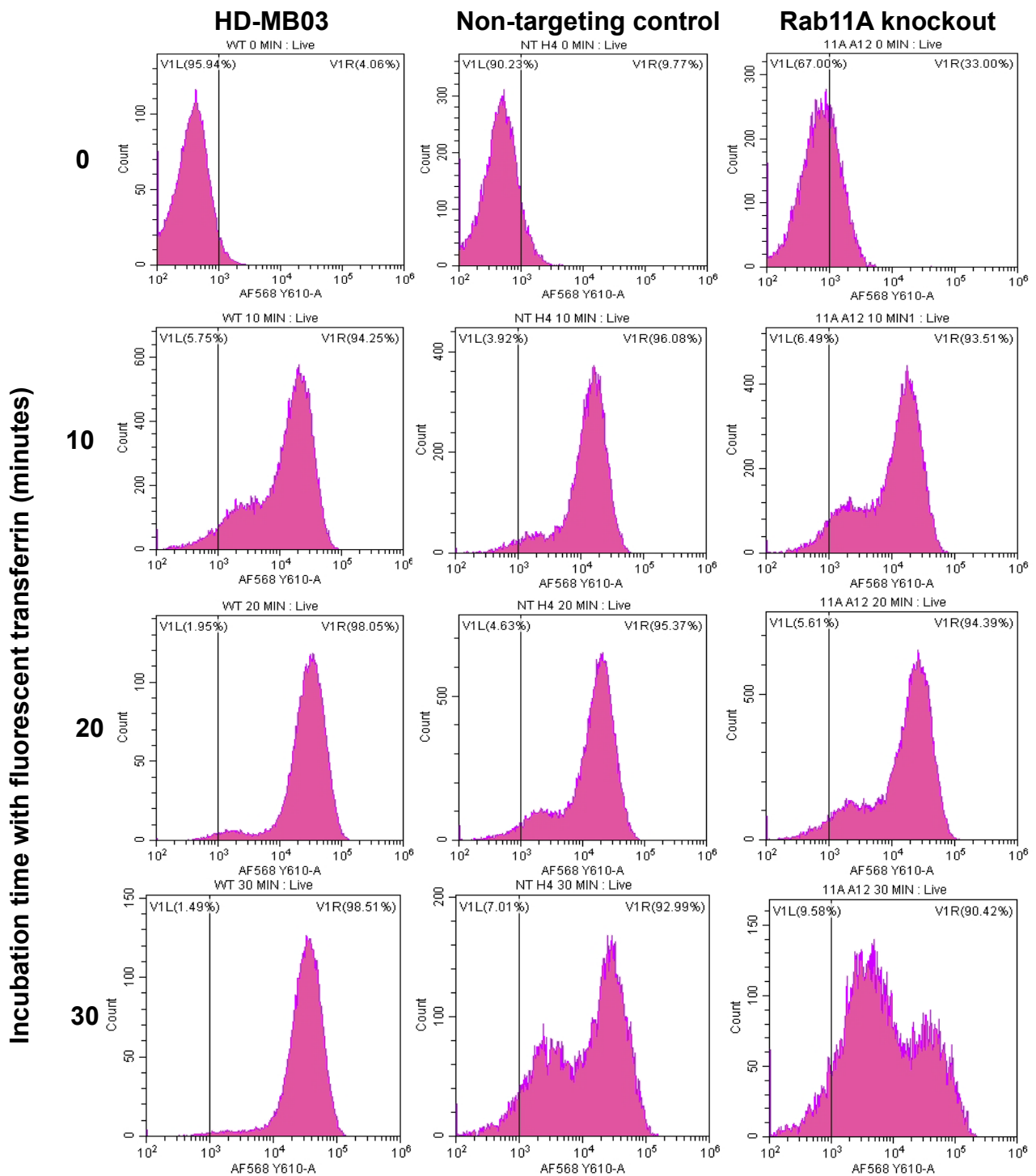
Figure 5.4. – Flow cytometry analysis of fluorescent transferrin uptake in Rab11A knockout, non-targeting control and wildtype HD-MB03 cells *Histograms showing fluorescence of Alexa-Fluor™ 568-tagged transferrin ('AF568 Y610-A'; x-axis) and cell count ('Count'; y-axis) of cells after incubation for 0-, 10-, 20- or 30-minutes at 37°C. HD-MB03 cells (WT; left), non-targeting (NT; centre) and Rab11A knockout (11A A12; right) are shown. A Y610 laser was used with a Cytoflex S flow cytometer. All graphs were generated using the Cytoflex S flow cytometer software. N = 1.*

5.3. Analysis of extracellular vesicle secretion by Rab11A knockout cells

In addition to being a regulator of the endocytic recycling pathway, Rab11A is also intricately involved in exosome biogenesis, hereafter referred to as small extracellular vesicles. For this reason, analysis of extracellular vesicle (EV) secretion, size and protein cargo was conducted.

5.3.1. Optimisation of extracellular vesicle fraction isolation

Extracellular vesicles were isolated from cell growth media using size exclusion chromatography and an Izon Automatic Fraction Collector (AFC). To separate EVs from protein components, Izon recommend collecting multiple 0.4 ml fractions during the isolation process. Seven 20% column volumes (0.4ml fractions) were then collected.

To quantify the number of particles present in each fraction, nanoparticle tracking analysis (NTA) using a ZetaView particle analyser was conducted. Upon particle concentration analysis for all seven cell lines analysed (wildtype HD-MB03, NT F3, NT F11, NT H4, 11A A12, 11A B11 and 11A B12), results showed that the second fraction (or 0.8 ml elution volume) had the highest concentration of particles, ranging from approximately 3,500-12,000 particles/ml) followed by either 1.2 ml or the 0.4 ml (Figure 5.5.). Therefore, to ensure the maximum number of particles are used for downstream analysis, the first four fractions (elution volumes 0.4-1.6 ml) were used. NTA of all seven fractions showed that the final fraction (2.8 ml) contained an almost undetectable number of particles (not shown) and this fraction was omitted from analyses. Exploratory analysis also indicated that wildtype cells secreted fewer particles than non-targeting or Rab11A knockout cell lines (Figure 5.5. G) but that there was no clear distinction between numbers of particle secreted Rab11A knockout cell lines and non-targeting cell lines overall. This suggests that absence of Rab11A does not affect numbers of EVs secreted from group 3 cells.
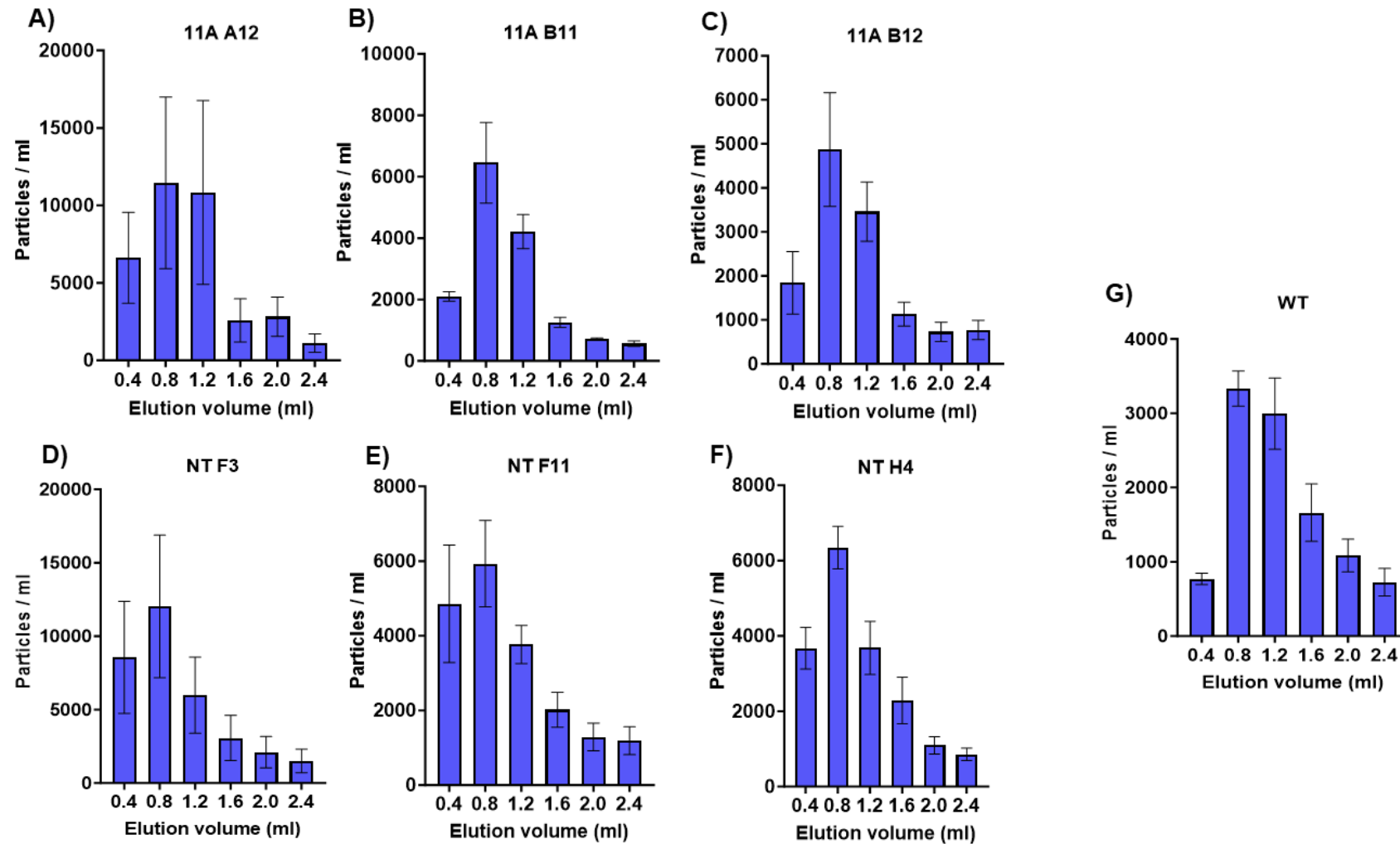
Figure 5.5. Quantification of number of particles in extracellular vesicle (EV) isolation fractions collected from Rab11A knockout, non-targeting control and wildtype HD-MB03 cells *Number of particles per ml in SEC purified fractions collected using Izon qEV 70 nm Gen2 collection columns from the Rab11A knockout cell lines A12 (A), B11 (B) and B12 (C), the non-targeting (NT) control cell lines F3 (D), F11 (E) and H4 (F), and the parental 'WT' cell line (G). Elution volume through the SEC column is shown. Each fraction collected was 0.4 ml in volume. EVs analysed in further experiments were in the first four fractions (1.6 ml eluted). Error bars represent standard error of the mean. N = 3. SEC = size exclusion chromatography.*

5.3.2. Analysis of size distribution of particles isolated from Rab11A knockout cells

Alongside particle concentration, analysis of the size distribution of particles in the fractions was conducted. As the first 1.6 ml eluted from the size exclusion column would be used for later analyses, the size distribution for these four fractions was collated (Figure 5.6). This showed that all seven cell lines (three non-targeting, three Rab11A knockout and wildtype HD-MB03) had the same size distribution profile with a single peak between 150-200 nm and an overall positive skew of the graph as most particles analysed were between 50-400 nm in diameter. Further analysis of the median particle diameter using Brown-Forsythe and Welch ANOVA tests with Dunnett's T3 multiple comparisons test (displayed on Figure 5.6.) showed no significant difference between the particle diameters of the non-targeting cell lines and the knockout cell lines (n=3), suggesting that Rab11A knockout does not affect the size of particles secreted by HD-MB03 cells.
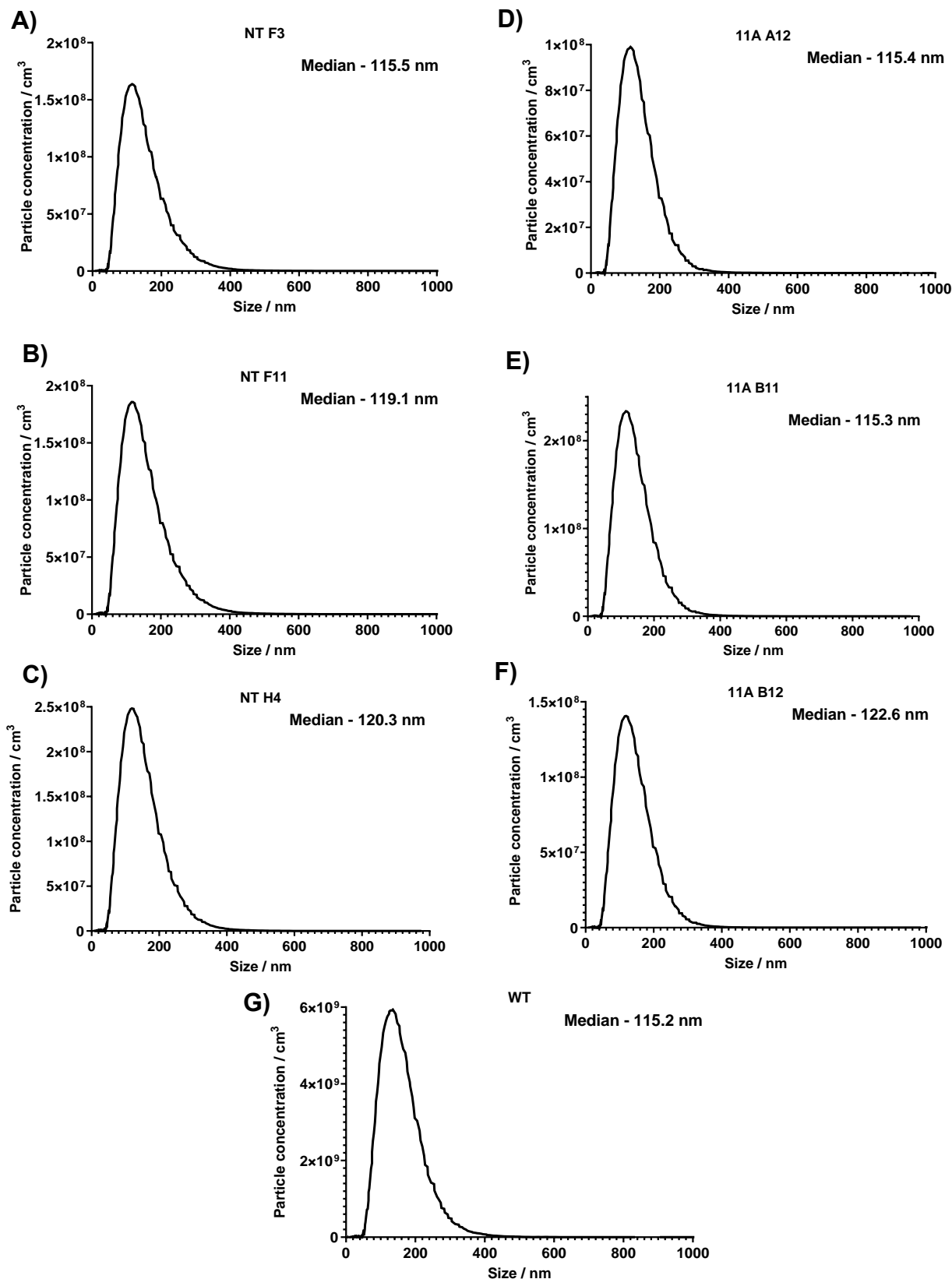
Figure 5.6. – Size distribution of extracellular vesicles isolated from wildtype, non-targeting and Rab11A knockout HD-MB03 cell lines *Nanoparticle tracking analysis (NTA) of the size distributions of particles in all extracellular vesicle fractions isolated from non-targeting (A-C), Rab11A knockout (D-F) and wildtype (WT; G) cell lines. N = 3. Graphs have undergone Savistsky-Golay smoothing using Graphpad Prism.*

5.4. SWATH Mass spectrometry analysis of cellular and extracellular vesicle proteomes

Mass spectrometry analysis was conducted to explore the protein content of cell lysates and extracellular vesicles from three biological replicates of seven cell lines (NT F3, NT F11, NT H4, 11A A12, 11A B11, 11A B12 and wildtype HD-MB03). This aimed to firstly, confirm that particles isolated in EV fractions isolated from cells were EVs through the identification of specific protein markers. Secondly, to determine whether there were any differences in the proteomes of *Rab11A* knockout cells compared to non-targeting control cells and thirdly, identify any differences in peptide cargo of extracellular vesicles secreted by *Rab11A* knockout cells and non-targeting control cells.

Mass spectrometry is a form of separation of ions based on charge to mass (m/z) ratios. Sequential Window Acquisition of all Theoretical Mass Spectra (SWATH-MS) is a quantitative form of mass spectrometry which is a variant of data-independent acquisition (DIA). DIA is a mode of data collection which focuses on the collection of mass spectrometry data using small mass windows (for example, 5-25 Daltons). The mass spectrometer acquires data for everything that can be detected within that window. The mass range of the window is then stepped up and data collected. This is repeated until the whole specified mass range of the experiment is completed (Wolf-Yadlin, Hu and Noble, 2016) (Gillet et al., 2012) This method allows for vast proteome coverage, allowing for the quantitative analysis of peptides in up to 9000 proteins with high quantitative consistency and accuracy (Gillet et al., 2012) (Ludwig et al., 2018).

In this technique, individual samples are fragmented into precursor ions which are then sorted into the pre-defined isolation mass windows (M. Li et al., 2022). In the mass spectrometer, these windows overlap by 1 Da to ensure full sample coverage. Each precursor isolation window (or SWATH) is consecutively scanned in a range of 400 – 1200 m/z giving 32 scans in total. The identity of peptides within the sample is then determined by analysing fragment ion signals, relative signal intensities, chromatographic concurrence and other information obtained from the mass spectrometer. These are then compared to DIA fragment ion maps which assess the similarity of data obtained by the mass spectrometer and known peptide fragments.

The data is also compared to spectral libraries of complete organisms and if peptide fragment data precisely matches a peptide in the database, a peptide identify is assigned (Gillet et al., 2012) (Figure 5.7.).

The total number of peptides detected in each sample is shown in Table 5.1.

Proteins detected by mass spectrometry analysis were filtered such that only those identified in at least two out of three biological replicates for each condition were included in further analysis.
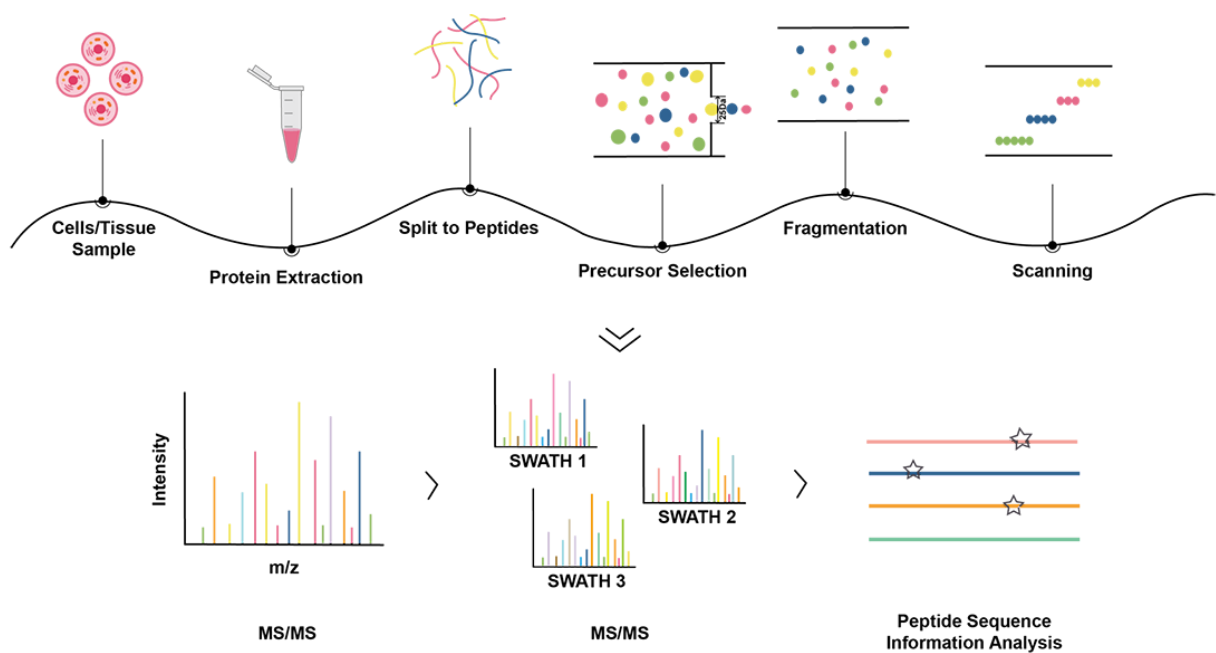
Figure 5.7. Workflow of SWATH-MS *Unlabelled samples are digested using trypsin to generate peptides of various lengths. Ions with a certain charge to mass ratio (m/z) are then selected in an unbiased fashion and fragmented. Typically, a single precursor ion spectrum is recorded followed by scanning of fragments which are analysed by the machine with a series of fragment ion spectra and recorded over a precursor isolation window (scanning range) of 25 Daltons (m/z). Through repeated cycling of consecutive precursor isolation windows, a data set is generated over a specified mass range. Each window or SWATH has a scanning time of approximately 100 ms with 32 scans in increments of 25 Da generally used in a 400-1200 m/z range. Peptide sequences obtained are then analysed through comparison with fragment ion maps and spectral libraries. Image obtained from www.creative-proteomics.com/ngpro/swath-ms.html.*

Table 5.1. Summary of total number of peptides identified in wildtype (WT), non-targeting control (NT) and Rab11A knockout (Rab11A KO) HD-MB03 cell lines through SWATH-MS analysis

Cell line	Sample type	Number of peptides
WT	Cell lysate	4643
WT	EV	2015
NT	Cell lysate	4554
NT	EV	1177
Rab11A KO	Cell lysate	4522
Rab11A KO	EV	1243

5.4.1. Analysis of extracellular vesicle markers in particles isolated from wildtype HD-MB03, non-targeting control and *Rab11A* knockout cell lines

In this study it was important to validate that EVs were the particles isolated from media using size exclusion chromatography. To do this, EV markers were identified in SWATH-MS data collected from Rab11A knockout, non-targeting control and wildtype HD-MB03 cells. These markers were identified by the international society of extracellular vesicles (ISEV) in the MISEV (minimal information for studies of extracellular vesicles) guidelines for best practices for the study of EVs. This includes a list of protein markers which were divided into five categories; membrane proteins, cytosolic proteins, lipoproteins and other contaminants, organelle proteins and secreted proteins (Théry et al., 2018). The abundance of these markers in EVs was compared to the lysates of cells that they were secreted from to show the comparative enrichment of them in EVs compared to cells (Figure 5.8.)

Results showed identified the presence of markers which were membrane, cytosolic and secreted proteins in EVs derived from all cell lines. This included the markers CD63 (Figure 5.8. A), Alix (PDCD6IP) and TSG101 (both Figure 5.8. B) and thereby confirmed that particles isolated were EVs. This was supported by the enrichment of organelle proteins, which are considered to be EV contaminants, in cell lysate compared to EV samples (Figure 5.8. D).
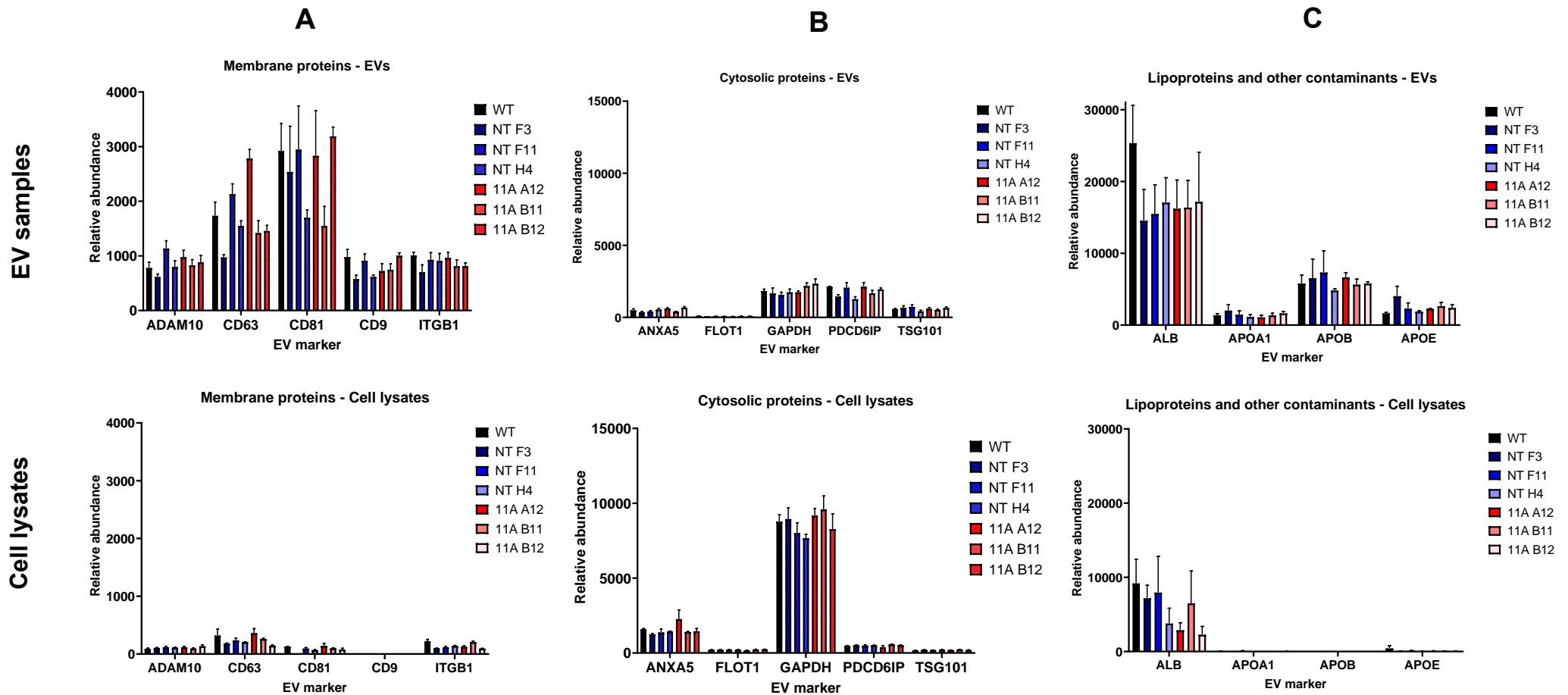
Figure 5.8. – Abundance of extracellular vesicle markers in extracellular vesicle and cell lysate samples *Graphical summary of the relative abundances (numbers from SWATH-MS) data of extracellular vesicle (EV) markers taken from the MISEV guidelines (Théry et al., 2018). (A) Category 1 – Membrane proteins (B) Category 2 – Cytosolic proteins (C) Category 3 – Lipoproteins and other contaminants (D) Category 4 – Organelle proteins (E) Category 5 – Secreted proteins. Wildtype (WT) cell samples shown in black, non-targeting (NT) shown in blue and 11A knockout (11A) shown in red. Relative abundance refers to numbers obtained following SWATH mass spectrometry analysis and indicates the relative abundance of a protein compared to other samples within the dataset. Error bars correspond to standard error of the mean based on three biological replicates per cell line.*

177

D

Organelle proteins - EVs

E

Secreted proteins - EVs

Organelle proteins - Cell lysates

Secreted proteins - Cell lysates

Figure 5.8. continued

Before making quantitative comparisons of the proteomic data, principal component analysis (PCA) was carried out. PCA is a method which reduces the dimensionality of large datasets by transforming large numbers of variables into a smaller number of principal components. It can therefore be used to cluster samples based on the similarity of values given for a wide range of unrelated factors. For the SWATH-MS data obtained in this study, the variables analysed were the expression values of the individual peptides identified by the mass spectrometer (Figure 5.9.).

Results showed a clear separation in protein expression profiles between cell lysate and EV samples. There was also no clear separation of Rab11A knockout, non-targeting control and wildtype EV samples with the exception of one biological replicate of the Rab11A knockout cell line B12. For cell lysate samples, Rab11A knockout and non-targeting control samples were not able to be distinguished, wildtype cells were distinct however. This suggests that from a proteome
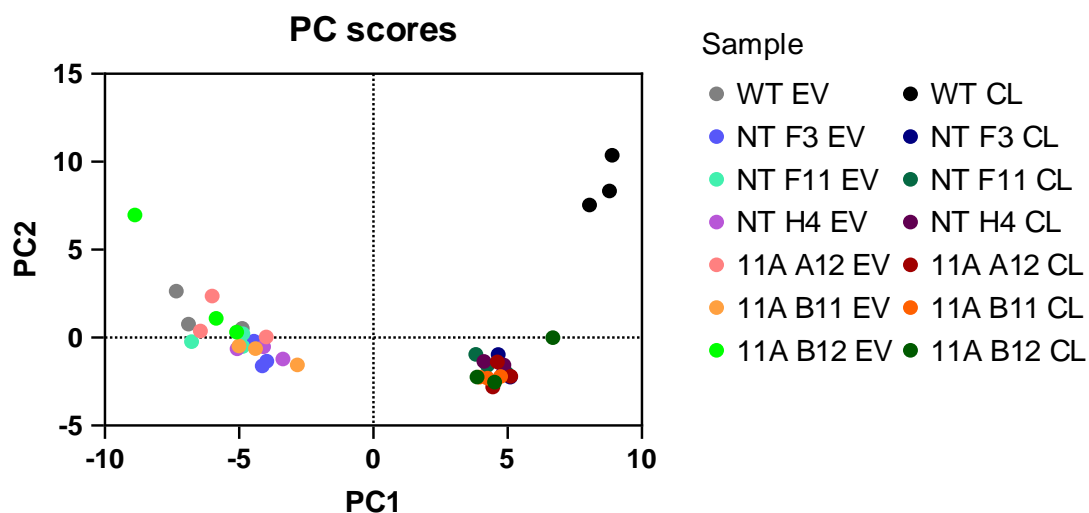
Figure 5.9. Principal component analysis of wildtype, non-targeting control and Rab11A HD-MB03 knockout cell lysates and extracellular vesicles *Expression of the 50 most expressed peptides within cell lysate and extracellular vesicle (EV) samples were compared in wildtype (WT, grey/black), non-targeting control ('NT' data, pink) and Rab11A knockout ('11A' data, teal) cell lines. Two principal components were derived, and PC (principal component) scores assigned. Analysis was conducted and graphs generated using GraphPad prism.*

perspective, the Rab11A knockout and non-targeting control conditions are more similar to each other than with the original wildtype cell line.

5.4.3. Quantitative differential protein expression analysis of *Rab11A* knockout cell lines compared to non-targeting control cell lines

An advantage of using SWATH-MS is that it is a quantitative form of mass spectrometry and therefore analysis can be conducted to identify changes in expression between sample conditions. PCA analysis conducted in section 5.4.2. showed proteome similarities between each of the Rab11A knockout and each of the non-targeting control cell conditions. As such, data for the three Rab11A knockout and three non-targeting control cell lines were pooled allowing for the general effect of a *Rab11A* knockout to be analysed. Spectral counts are used to infer the quantity of a particular peptide within in a sample. Some of these peptides are unique to a single protein, allowing for quantification of that protein to occur, or are common to multiple proteins.

For the expression analysis, the open-source software StatsPro (www.omicsolution.com/wukong/StatsPro/) was used with a LIMMA (linear models for microarray analysis) parametric test. This gave fold change and statistical significances of peptide expression which allowed for the identification of proteins which were upregulated or downregulated in the Rab11A knockout compared to non-targeting control cell lines.

To visualise the proteins which were up or downregulated, fold change and statistical significances of the data were arrayed on a volcano plot (Figure 5.10.). Cut-off thresholds of a $\log_2$(fold change) of ±0.3 and p-value value of 0.05 were also applied. This gave a total of 345 differentially regulated proteins in cell lysate samples, of which 260 were downregulated in Rab11A knockout cell lines compared to the non-targeting control and 85 were upregulated. In EV samples, 38 proteins were differentially regulated with 13 downregulated and 25 upregulated. Full lists of differentially regulated proteins are shown in Appendix 1.11.
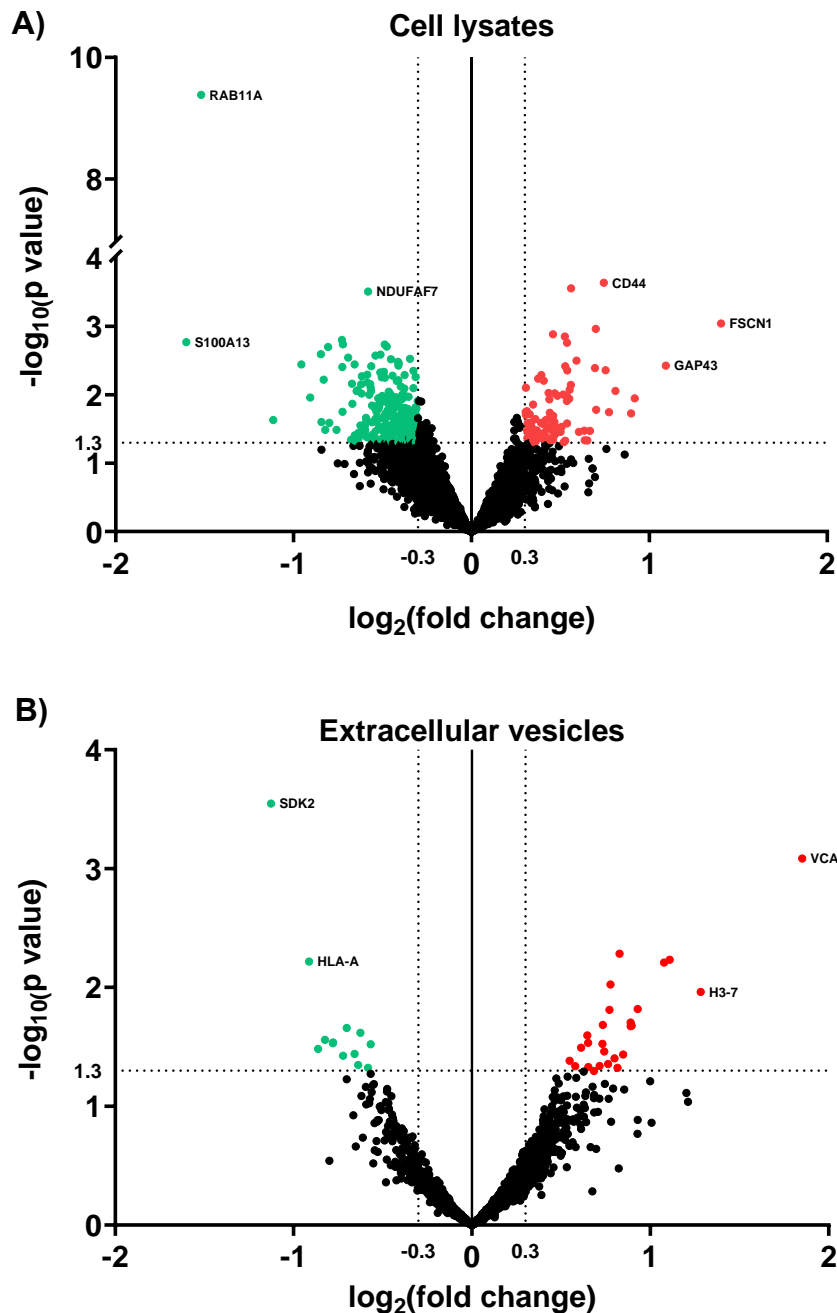
Figure 5.10. Differential protein expression analysis in Rab11A knockout cell lysates and extracellular vesicle samples compared to non-targeting control samples *A) Cell lysates and B) extracellular vesicles. Protein expression analysis conducted using a LIMMA test via the StatsPro analysis software to generate fold change and p values. Each fold change underwent a Log_2 transformation and each p value a – Log_{10} transformation. Cut off thresholds of log_2(fold change) = ±0.3 and p-value 0.05 (-Log_{10} 1.3) were applied (shown by dotted lines). Each dot represents one protein. Downregulated peptides are shown in teal, upregulated are shown in red. Gene notation of protein attributed to certain peptides identified are highlighted in black text next to their corresponding position on the graph.*

5.4.4. Functional pathway analysis of differentially expressed proteins in Rab11A knockout cell lines

To identify molecular pathways associated with differentially expressed proteins in the Rab11A knockout cell lines, the STRING (Search Tool for the Retrieval of Interacting Genes/proteins; string-db.org) and DAVID (the Database for Annotation, Visualisation and Integration Discovery; david.ncifcrf.gov) online bioinformatics tools were utilised. This was to begin the process of making associations between differentially expressed proteins in Rab11A knockout cell lines and functional pathways that could be regulated by Rab11A in these cells.

STRING was used to discover protein-protein interaction networks of up or downregulated proteins based on various resources including experimental data, computational predictions and public text collections. DAVID was used to generate KEGG (Kyoto Encyclopaedia of Genes and Genomes) pathways, which allowed for the identification of specific cellular processes and the specific positions of the differentially expressed proteins within them.

This analysis was conducted on upregulated and downregulated proteins within cell lysate samples and upregulated and downregulated proteins within EV samples.

5.4.4.1. Network analysis of proteins upregulated in Rab11A knockout cell lysates

The results of STRING and KEGG pathway analysis are shown in Figure 5.11. Of the 85 proteins that were significantly upregulated in Rab11A knockout cell lysates, 72 appeared in the STRING network (Figure 5.11. A, this network including Rab11A is shown in Appendix 1.13.). β-catenin (CTNNB1) had the most network associations with 28 proteins in total forming an association network. Other smaller networks comprising of 2 or 4 proteins were also present. KEGG pathway analysis identified 15 cellular processes that had significant pathway association (Figure 5.11. B). These can be broadly classified into 3 main groups: cancer, amino acid metabolism, and cellular response to pathogens. The most statistically significant process was bacterial invasion of epithelial cells. This pathway included upregulation of β-catenin and mostly had upregulation of proteins involved in actin polymerisation and

regulation of the actin cytoskeleton. Proteins upregulated in this pathway also included α-catenin (CTNNA1), Rac1, RHOA, Vinculin (VCL) and the Septins 2 and 11 (SEPTIN2, SEPTIN11) (Appendix 1.14.). This was unsurprising given the β-catenin centred STRING pathway network and the role of β-catenin in the regulation of cell adhesion. β-catenin binds to α-catenin which is able to bind directly to actin creating a complex link between the cadherin-catenin complex and the actin cytoskeleton. These dynamics are regulated by Rho GTPases, such as RhoA and vinculin both of which were also upregulated (Bachir et al., 2017).

Amino acid metabolism pathways included, amino acid biosynthesis and glycine, serine and threonine metabolism. Proteins that were commonly upregulated in these pathways included glutamine synthetase (GLUL), cystathionine beta synthase (CBS), cystathionine gamma-lyase (CTH), glycine cleavage system protein H (GCSH), carbolic anhydrase 14 (CA14) and enolase 2 (ENO2).

Cancer-related pathways included colorectal cancer, gastric cancer, adherens junctions, proteoglycans in cancer and WNT signalling pathway, and generally included the following proteins; β-catenin (CTNNB1), Mothers against decapentaplegic homolog 4 (SMAD4), Ras-related C3 botulinum toxin substrate 1 (RAC1), Ras Homolog Family Member A (RHOA) and Caspase 3 (CASP3). One of the processes identified was named 'pathways in cancer' and encompasses an overview of proteins associated with pathways believed to contribute to tumourigenesis (Figure 5.12.). These include adherens junction dynamics, WNT signalling pathway, apoptosis and cytokine-cytokine receptor interaction. The upregulation of proteins associated with the WNT signalling pathway, and more specifically β-catenin, is pertinent from a disease-specific context. The WNT medulloblastoma subgroup is named after this pathway which is dysregulated in patients (Bachir et al., 2017).
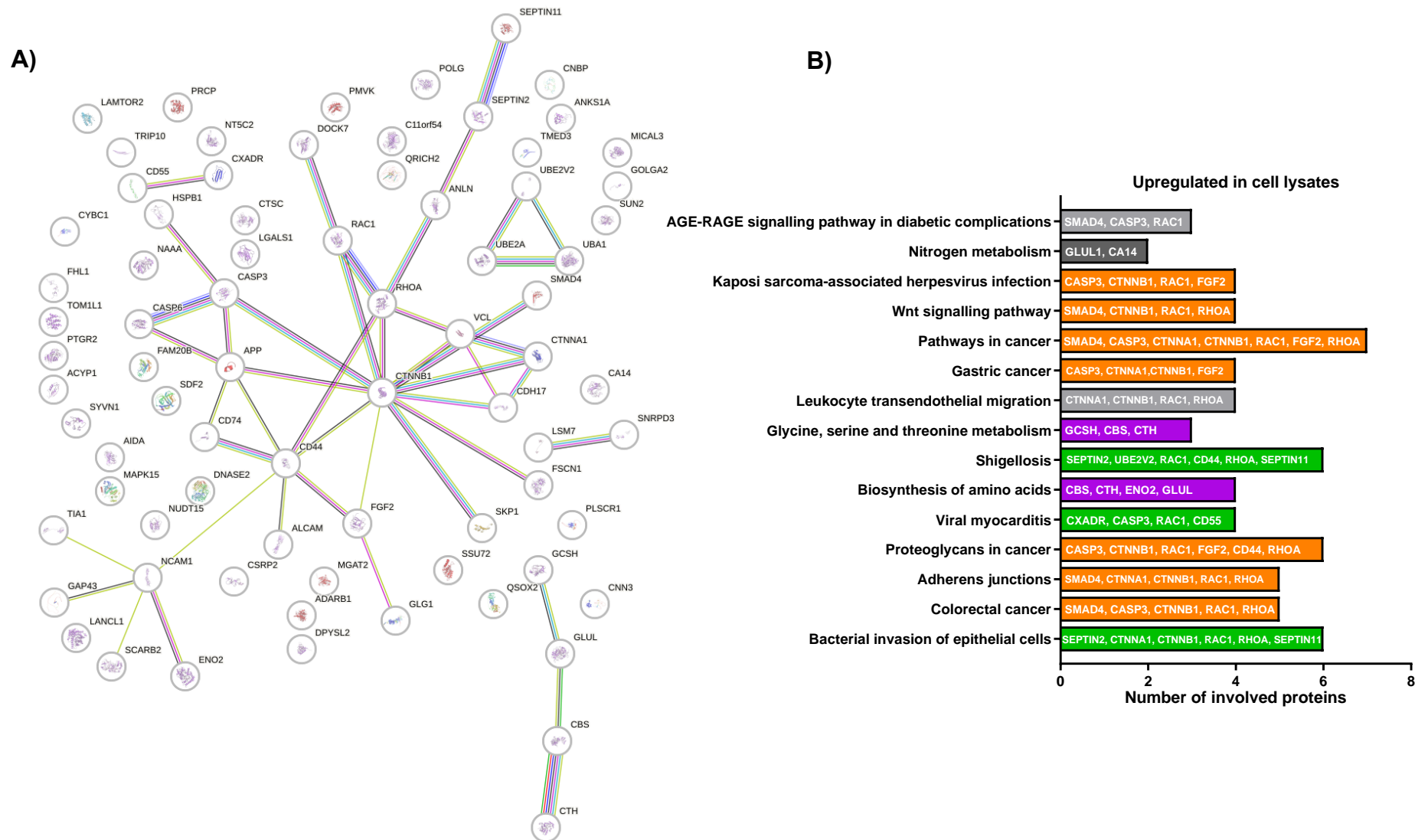
Figure 5.11. STRING and KEGG analysis of upregulated proteins in cell lysates derived from Rab11A knockout cells *A) STRING pathway analysis of protein-protein interactions. Analysis was conducted with a high confidence score of 0.7. Line colour and number between proteins indicate the source used to determine the interaction (light blue – from curated databases, pink – experimentally determined, green – predicted gene neighbourhood, red – gene fusions, dark blue – gene co-occurrence, light green – textmining, black – co-expression, lilac – protein homology). B) KEGG pathway analysis. Analysis was conducted using the bioinformatics tool DAVID (the Database for Annotation, Visualisation and Integration Discovery). Pathways included had a statistical significance of p≤0.05. Pathways are ordered from most statistically significant (closest to the x-axis) to least statistically significant (closest to graph title). Orange – cancer-associated pathways, purple – amino acid metabolism, green – cellular response to pathogen infection. STRING = Search Tool for the Retrieval of Interacting Genes/proteins. KEGG = Kyoto Encyclopaedia of Genes and Genomes*

184
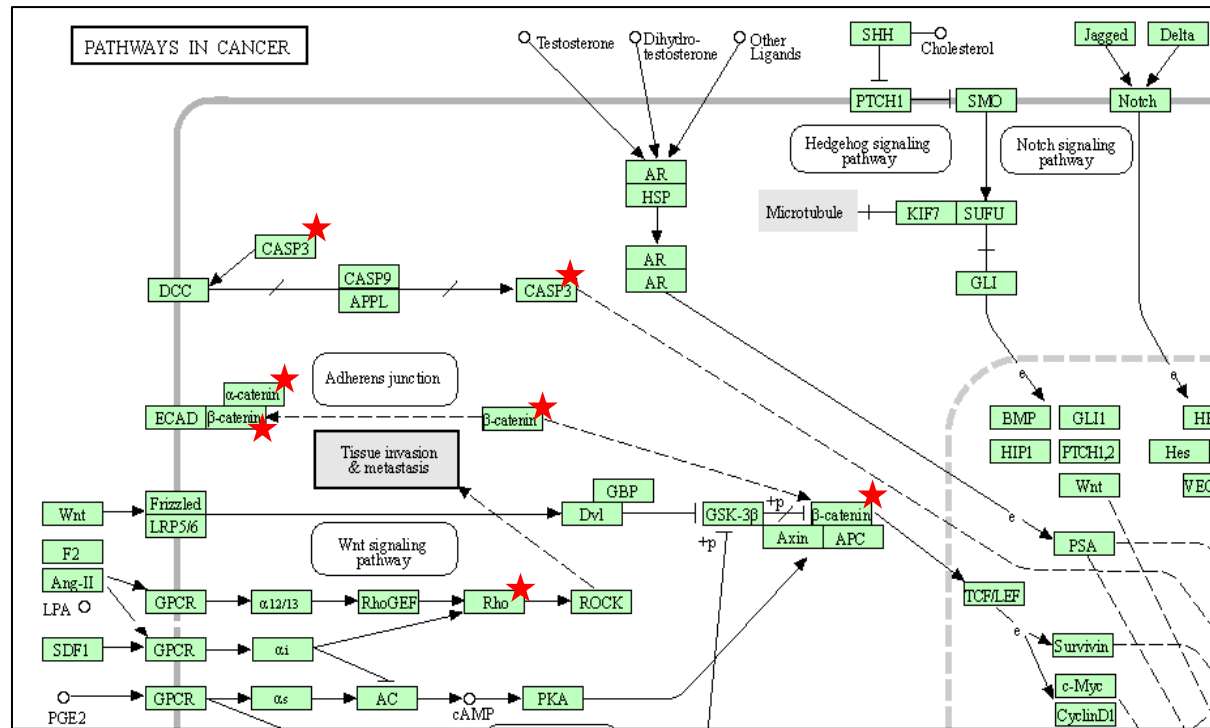
Figure 5.12. Pathways in cancer Kyoto Encyclopaedia of Genes and Genomes (KEGG) pathway with proteins upregulated in Rab11A knockout cells highlighted *Red stars indicate position of upregulated protein in the pathway. Red text indicates gene symbols from pathway analysis. Imaged adapted from analysis conducted using the online bioinformatics tool DAVID (the Database for Annotation, Visualisation and Integration Discovery). Rab11A does not appear in this KEGG pathway but knockout causes upregulation of multiple proteins in multiple pathways associated with tumourigenesis.*

5.4.4.2. Networks of proteins downregulated in Rab11A knockout cell lysates

Analysis of SWATH-MS data showed that there were 260 proteins significantly downregulated in Rab11A knockout compared to non-targeting control cell lysates. The STRING and KEGG pathway networks are shown in Figure 5.13 and the full list of downregulated proteins is shown in Appendix 1.15. Of the 260, 251 appeared in the STRING networks (Figure 5.13.A.). These networks presented with three main association clusters all of which were still interconnected. These focused around UTPs (U3 small nucleolar RNA-associated proteins), MRPSs (mitochondrial ribosomal proteins) and NDUFSs (NADH-ubiquinone oxidoreductases).

KEGG pathway analysis using DAVID identified 24 pathways with significantly downregulated proteins (Figure 5.13. B). General themes of pathways included mitochondria, metabolism and ribosomes which is consistent with the three main protein network clusters identified using STRING.

Rab11A is a key regulator of membrane transport, including the slow endocytic recycling pathway and as such is localised to recycling endosomes (Ullrich et al., 1996) (Zulkefli et al., 2019). Therefore, as expected after *Rab11A* knockout, the endocytosis KEGG pathway had statistically significant downregulation of proteins (Figure 5.14.). Analysis showed that nine proteins were downregulated; RUN and FYVE domain containing 1 (RUFY1), sorting nexin 2 (SNX2), EH domain-containing 4 (EHD4), charged multivesicular body protein 3 (CHMP3), neuronal precursor cell-expressed developmentally downregulated 4-like E3 ubiquitin protein ligase (NEDD4L), human leukocyte antigen G (HLA-G), adenosine diphosphate-ribosylation factor GTPase activating protein 1 (ARFGAP1), dynamin 1 (DNM1) and Rab11A. These proteins have been associated with various stages of endocytosis including both clathrin-dependent and clathrin-independent endocytosis as well as early endosomes and multivesicular body formation. Therefore, suggesting that Rab11A knockout affects multiple stages of endocytosis and is not restricted to affecting endocytic recycling only.

187

B)

Downregulated in cell lysates
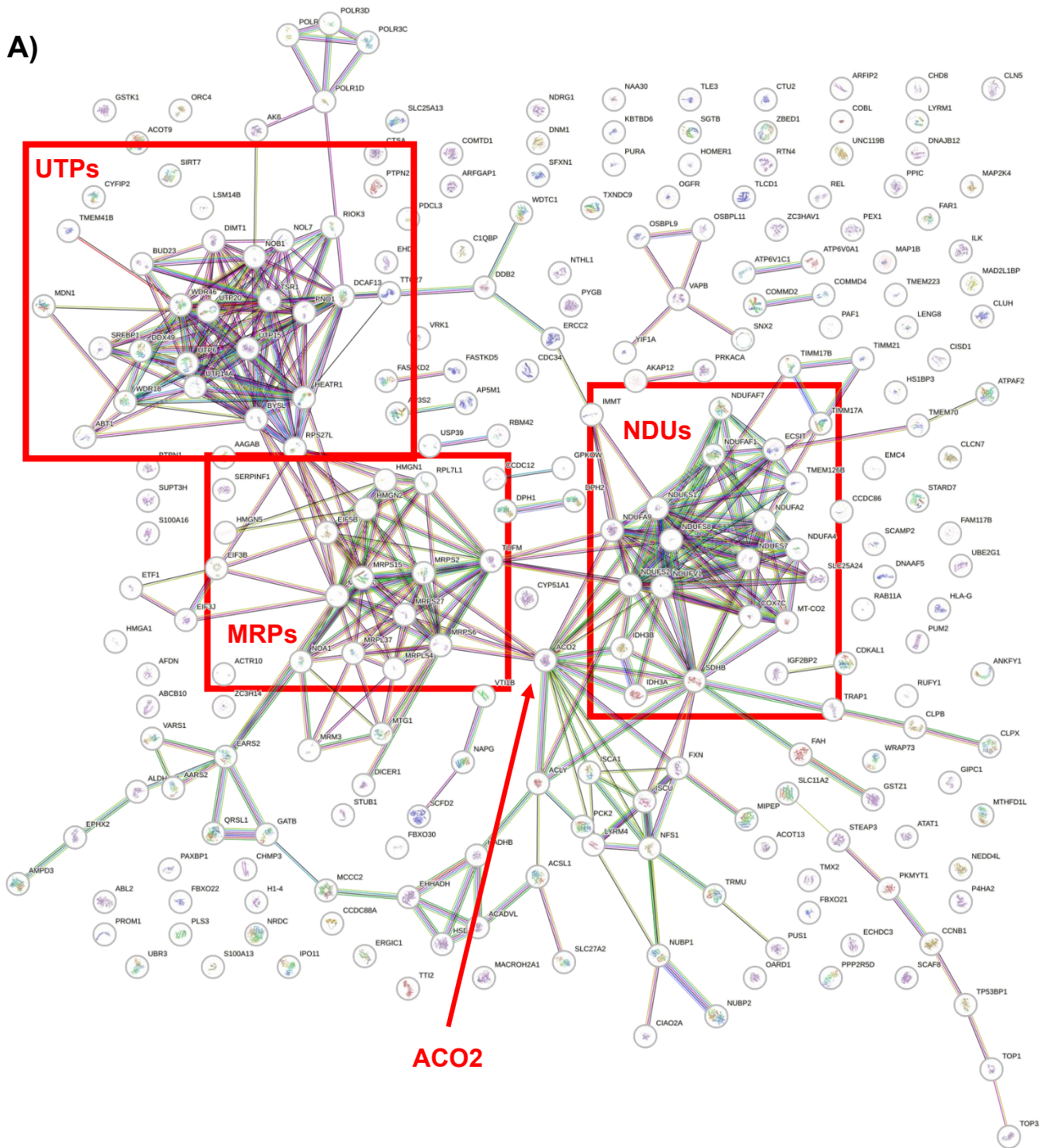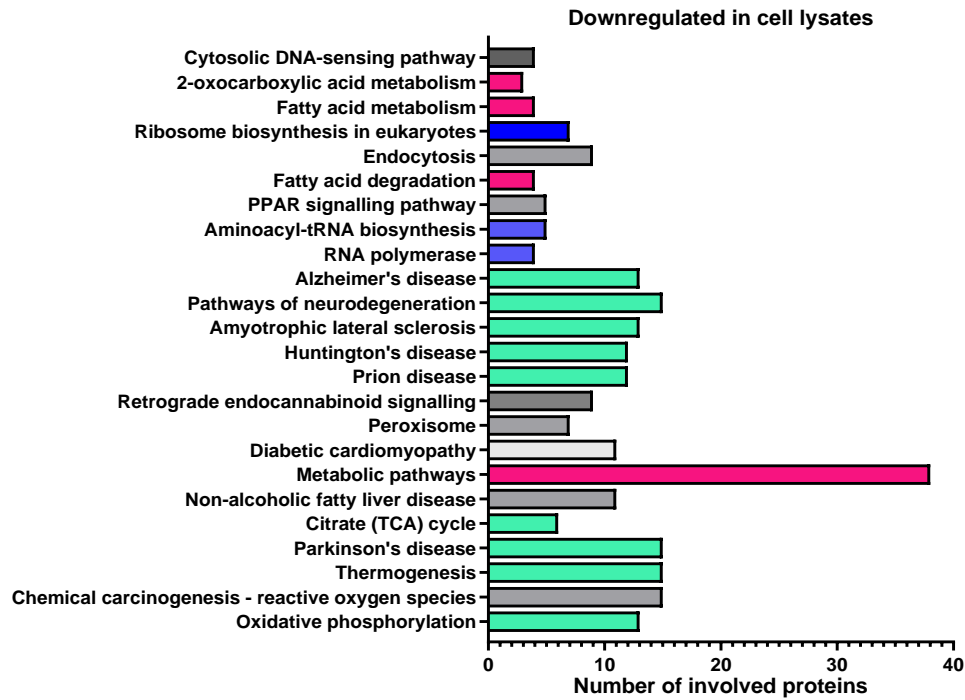
Figure 5.13. STRING and KEGG pathway analysis of downregulated proteins in cell lysates derived from Rab11A knockout compared to non-targeting control cells A) STRING pathway analysis of protein-protein interactions. Analysis was conducted with a high confidence score of 0.7. Line colour and number between proteins indicate the source used to determine the interaction (light blue – from curated databases, pink – experimentally determined, green – predicted gene neighbourhood, red – gene fusions, dark blue – gene co-occurrence, light green – textmining, black – co-expression, lilac – protein homology). B) KEGG pathway analysis. Analysis was conducted using the bioinformatics tool DAVID (the Database for Annotation, Visualisation and Integration Discovery). Pathways included had a statistical significance of p≤0.05. Pathways are ordered from most statistically significant (closest to the x-axis) to least statistically significant (closest to graph title). Light blue – mitochondrial dysfunction, pink – metabolism, blue – RNA/ribosomes. STRING = Search Tool for the Retrieval of Interacting Genes/proteins. KEGG = Kyoto Encyclopaedia of Genes and Genomes. UTP = U3 small nucleolar RNA-associated protein. MRPS = mitochrondrial ribosomal protein. NDU = NADH-ubiquinone oxidoreductase.

188
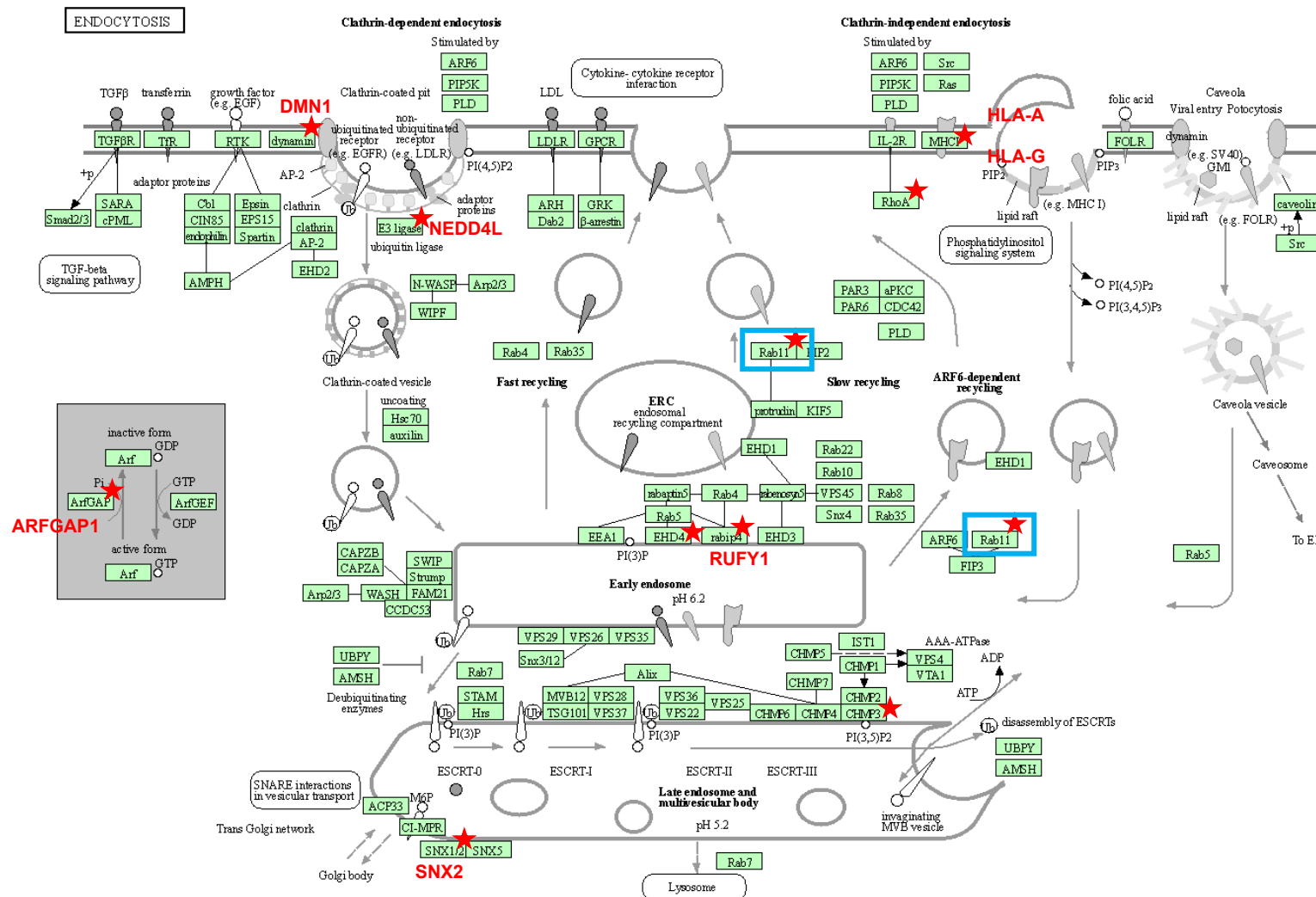
Figure 5.14. Endocytosis Kyoto Encyclopaedia of Genes and Genomes (KEGG) pathway with proteins downregulated in Rab11A knockout cells highlighted *Red stars indicate position of upregulated protein in the pathway. Red text indicates gene symbols of the protein from pathway analysis. Analysis conducted using the online bioinformatics tool DAVID (the Database for Annotation, Visualisation and Integration Discovery). Blue box indicates the position of Rab11 in the pathway.*

189

The pathway with the most statistically significant downregulation of proteins was oxidative phosphorylation with 13 downregulated proteins. These were NADH ubiquinone oxidoreductase subunits V1, S2, S1, S7, S8, A9, A4 and A2 (NDUFV1, S2, S1, S7, S8, A9, A2, A4), cytochrome C oxidase subunit 7C (COX7C), succinate dehydrogenase subunit B (SDHB), mitochondrially encoded cytochrome C oxidase II (MT-CO2), V-type proton ATPase subunit C1 (ATP6V1C1) and V-type proton ATPase subunit C1 (ATP6V0A1) (Figure 5.15.).

Other metabolism-associated pathways with significant protein downregulation included chemical carcinogenesis, TCA (tricarboxylic acid) cycle, fatty acid degradation and metabolism, and 2-oxocarboxylic acid metabolism. The specific proteins and the process they are associated with are shown in Appendix 1.15. A collection of downregulated proteins is seen in the TCA cycle primarily affecting the synthesis of cis-aconitate, isocitrate, α-ketoglutarate (2-oxoglutarate) and fumarate (Figure 5.16.). This is of interest because MYC amplified medulloblastoma cells show upregulation of the TCA cycle and oxidative phosphorylation compared to the normal brain (Pham et al., 2022) (Marabitti et al., 2022). The HD-MB03 cell line which the *Rab11A* knockout was conducted in has a MYC amplification (Milde et al., 2012) meaning that this cell line has high TCA cycle activity and high levels of oxidative phosphorylation ordinarily (Linke et al., 2023). As both of these pathways have statistically significant downregulation of proteins in the knockout cell lines compared to control cell lines, this could show that in the knockout cell lines there has been a metabolic change caused by a cascade of events due to the absence of Rab11A.

Additionally, Linke et al. (2023) showed that group 3 medulloblastoma HD-MB03 cells have low levels of isocitrate, glutamate and pyruvate, intermediate levels of α-ketoglutarate, high levels of succinate and very high levels of fumarate. This was proposed to be caused by blockages in the TCA cycle leading to the accumulation of fumarate as an onco-metabolite. Rab11A knockout HD-MB03 cells have downregulation of enzymes which synthesise isocitrate, α-ketoglutarate and fumarate which could lead to a difference in the concentration of these metabolites compared to wildtype and non-targeting control HD-MB03 cells. More specifically a downregulation of these metabolites, experimental verification is required, however, to determine the effect of Rab11A knockout on metabolite concentration.

Figure 5.15. Oxidative phosphorylation Kyoto Encyclopaedia of Genes and Genomes (KEGG) pathway with proteins downregulated in Rab11A knockout cells highlighted *Red stars indicate position of upregulated protein in the pathway. Red text indicates gene symbols from pathway analysis. Analysis conducted using the online bioinformatics tool DAVID (the Database for Annotation, Visualisation and Integration Discovery).*

191

Figure 5.16. Citrate (TCA; tricarboxylic acid) cycle Kyoto Encyclopaedia of Genes and Genomes (KEGG) pathway with proteins downregulated in Rab11A knockout cells highlighted *Red stars indicate position of downregulated protein in the pathway. Red text indicates gene symbols of the protein from pathway analysis. Analysis conducted using the online bioinformatics tool DAVID (the Database for Annotation, Visualisation and Integration Discovery).*

192

5.4.4.3. Protein networks of proteins upregulated in Rab11A knockout extracellular vesicles

Of the 38 dysregulated proteins in extracellular vesicles (EVs) secreted by Rab11A knockout cells compared to EVs secreted non-targeting control cells, 25 of them were upregulated. STRING pathway analysis (Appendix 1.16. A) only identified associations between two (ANXA2 and ANXA6). No pathways met KEGG pathway analysis statistical significance criteria so pathway association of proteins upregulated in Rab11A EVs compared to non-targeting control EVs could not be conducted.

5.4.4.4. Protein networks of proteins downregulated in Rab11A knockout extracellular vesicles

Thirteen proteins were downregulated in extracellular vesicles (EVs) secreted by Rab11A knockout compared to those secreted by non-targeting control cells. STRING and KEGG pathway analysis of these (Appendix 1.16. B and Appendix 1.17.) showed that two proteins have network associations. These were survival of motor neuron 1 (SMN1) and heterogeneous ribonuclear protein H (HNRNPH1), both of which are involved in RNA modification and pre-mRNA processing (Chari et al., 2008) (Pellizzoni et al., 1998) (M. Liu et al., 2021).

Whilst they were not identified to directly interact through STRING analysis, two downregulated proteins, hexokinase 2 (HK2) and phosphoenolpyruvate carboxykinase 2 (PCK2) have functions in metabolism. HK2 has an important role in cellular uptake and utilisation of glucose (R. Li et al., 2022) and PCK2 is catalyses the conversion of oxaloacetate to phophoenolpyruvate, which bridges the gap between glycolytic and TCA cycle intermediates in the mitochondria (Dong et al., 2021). These proteins were also the only downregulated proteins identified in KEGG pathways after DAVID analysis which connected them with the insulin secretion pathway and glycolysis / gluconeogenesis (not shown).

Finally, the most significantly downregulated protein was protein sidekick-2 (SDK2). SDK2 is an adhesion molecule which has primarily been associated with promoting

synaptic connections in the retina (Yamagata et al., 2002). It is of interest here because M. Li et al. (2022) identified SDK2 as a downstream effector gene of a super-enhancer driven transcriptional regulatory network of group 3 medulloblastoma. Smith et al., 2022 identified several retinal and photoreceptor gene sets that were common between group 3 tumours and the rhombic lip, the proposed cell type of origin of group 3 tumours. As sidekick proteins participate in the formation and/or maintenance of neural circuits in the retina (Yamagata, 2020), this generates a direct link between mechanisms of group 3 development and dysregulated proteins within Rab11A knockout EVs.

5.5. Summary

Amino acid analysis of Rab11A knockout cell lines A12, B11 and B12 showed a truncation from 216 amino acids to 135 amino acids (transcripts with a 5-nucleotide deletion), 137 amino acids (2-nucleotide deletion) or 138 amino acids (1-nucleotide insertion). This corresponds to the loss of two alpha helices, a beta sheet, a beta (Yamagata et al., 2022) turn and the hypervariable domain in the C-terminal tail meaning that if translated, the protein cannot bind to membranes and therefore is non-functional.

Preliminary transferrin uptake analysis using both immunofluorescence microscopy and flow cytometry indicates a potential effect of Rab11A knockout on endocytic recycling. More biological replicates are required, however, (as this experiment is n = 1 for all cell lines and techniques) in order to make any conclusions.

EV analysis of size distribution between Rab11A knockout and non-targeting control cell lines showed no significant difference in the overall size profile of particles isolated from each, thereby suggesting that Rab11A knockout does not affect the size of particles secreted by cells.

SWATH-MS was used to quantitatively determine the cargo of Rab11A knockout cells and EVs secreted by them. Initially this technique was used to characterise particles isolated from each cell line and determine whether they possessed any protein markers associated with extracellular vesicles so that the particles could be

referred to as such. Marker lists were obtained from the MISEV guidelines (Théry et al., 2018) and particles isolated from them contained markers from all five specified categories.

Differential protein expression analysis of Rab11A knockout cell lysates and EVs compared to non-targeting control cell lysates identified 345 differentially expressed proteins in cell lysate samples with 260 downregulated and 85 upregulated. In EVs 38 were differentially expressed with 13 downregulated and 25 upregulated.

Twenty-four cellular processes had statistically significant association with proteins downregulated in Rab11A knockout cell lysates. These were predominantly associated with ribosomal function and metabolism, with proteins associated with metabolism within mitochondria being commonly downregulated. Further analysis showed downregulation of proteins associated with complexes I, II, IV and V in the oxidative phosphorylation pathway and proteins within the TCA cycle responsible for the conversion of succinate to fumarate (succinate dehydrogenase subunit B), oxaloacetate and acetyl-CoA to citrate (ATP citrate lyase), citrate to isocitrate (acotinase 2) and isocitrate to α-ketoglutarate (isocitrate dehydrogenase). This may be of pathological importance because wildtype HD-MB03 cells generally have high TCA cycle activity and high levels of oxidative phosphorylation and a fumarate accumulation. Therefore, downregulation of proteins associated with these processes due to Rab11A knockout could mean there is an association of Rab11A with this high metabolic activity and thus a link between Rab11A and medulloblastoma pathology.

Whilst not present in any pathway, the protein sidekick 2 (SDK2) was the most statistically significantly downregulated protein in Rab11A knockout EVs compared to non-targeting EVs. Whilst little is known about the precise function of SDK2, aside from its association with promoting synaptic connections in the retina and its hypothesised participation in the formation of neural circuits, it has been identified as one of eleven downstream effectors of super-enhancer driven transcriptional regulation in group 3 medulloblastoma cells. With its potential association with Rab11A due to its downregulation in Rab11A knockout EVs and hypothesised role in the formation of neural circuits in the retina and retinal and photoreceptor gene sets common between group 3 medulloblastomas and its cell type of origin, this

generates a direct association between mechanisms of group 3 development and dysregulated proteins within Rab11A knockout EVs.

The abundance of peptides of interest from SWATH-MS analysis mentioned in this section in non-targeting and Rab11A knockout cell lysates and EV samples is shown in Appendix 1.18.

Chapter 6:
Discussion

6.1. Introduction

Rab GTPases are a family of small GTPase proteins known to regulate intracellular vesicle trafficking as well as vesicle budding, motility and fusion (Stenmark, 2009). Through their vesicle-related functions, they have been associated with oncogenic and tumour suppressive functions in adult cancers (Krishnan et al., 2020), the role of Rabs in paediatric tumours is yet unexplored. This study aimed to determine whether Rab GTPases (Rabs) could be contributing to the pathogenesis of the most common malignant paediatric brain tumour, medulloblastoma.

Medulloblastoma accounts for 20% of all paediatric brain tumours and 10% of paediatric cancer deaths (Medulloblastoma Statistics | medulloblastoma.org). It has four molecular subgroups; WNT, SHH, group 3 and group 4 (Northcott et al., 2019). WNT and SHH are named after the signalling pathways that are believed to play prominent pathogenic roles. Less is known about the mechanisms which underpin the pathogenesis of groups 3 and 4 which are consequently named generically (Cavalli et al., 2017) (Northcott et al., 2017). Of the four subgroups, group 3 and group 4 are associated with the worst patient prognosis (Kool et al., 2012) (Northcott et al., 2012), there is therefore a requirement to better understand the mechanisms which drive these molecular subgroups of medulloblastoma.

In this study, analysis of patient datasets and patient-derived cell lines was conducted to establish a baseline of Rab GTPase expression and the impact of this expression on patient survival. This was followed by generation of CRISPR-Cas9 knockout cell lines to generate a model for studying Rab function in medulloblastoma patient-derived cell lines. Finally, proteomics analysis of the knockout cell lines allowed for inferences to be made about potential pathways which were regulated by Rab11A in group 3 medulloblastoma. These techniques combined led to the proposal of a role for Rab11A in medulloblastoma pathogenesis through regulation of mitochondrial metabolism pathways.

6.2. Rab GTPase gene expression has prognostic significance in medulloblastoma patients

Despite the presence of 66 Rab GTPases in the human genome and an emerging role for Rab GTPases in oncogenic and tumour suppressive roles in adult cancers, there is a lack of literature elucidating a role of Rab GTPases in brain and CNS tumours. Published studies of Rab contribution to brain tumour pathogenesis tend to focus on identifying roles in glioblastoma multiforme. Kulasekaran et al. (2021) have proposed a tumour suppressor role for Rab35 in adult glioblastoma multiforme since Rab35 knockdown led to increased tumour growth. Additionally, J.K. Kim et al. (2014) identified an oncogenic role for Rab3A in glioma and glioblastoma multiforme through increased cyclin D1 expression which resulted in increased cell proliferation. As previously mentioned, there is an absence of studies connecting Rab GTPases with either tumour suppressive or oncogenic functions in paediatric cancers and more specifically paediatric brain cancers, creating a knowledge gap for this study. There have been studies, however, which implicate Rabs in pathways known to drive medulloblastoma. For example, Rab23 is a key inhibitor of SHH signalling during development, leading to shrinkage of hepatocellular carcinoma tumours (Mitra et al., 2011). The SHH pathway is a known driver of the SHH medulloblastoma subgroup, therefore, whilst Rabs have not been associated directly with medulloblastoma pathogenesis, there is a foundation to suggest that they may drive pathways which contribute to drive at least one of the medulloblastoma subgroups.

In the initial stages of this study, patient data sets were analysed for Rab GTPase expression. This included survival analysis of the Cavalli dataset of 763 medulloblastoma patients using the R2: Genomics analysis and visualisation platform. Expression of many different Rabs has been associated with poor overall survival in many adult cancer types cancer types. For example, Rabs 17 and 34 have been linked with poor overall and disease-free survival of colorectal cancer patients (Jiang et al., 2022). Neither of these Rabs, however, were shortlisted for patient data analysis in medulloblastoma as they did not appear to have prognostic significance. Of the target shortlist, Rabs associated with poor prognosis include Rab11A in non-small cell lung cancer patients (Dong et al., 2017), Rab7A in gastric cancer (H. Liu et al., 2020) and upregulation of Rab40B in hepatocellular carcinoma

patients (Shi et al., 2020). As section 3.5.2. shows, all medulloblastoma subgroups had poor patient survival associated with high expression of certain Rabs. Of the molecular subgroups, group 3 had the most Rabs associated with poor survival and for *Rab8B*, *Rab11A* and *Rab40B* this was a subgroup-specific effect. This shows that high expression of certain Rabs may be an independent predictor of survival of a subgroup. This study also shows, for the first time, a link between Rab GTPases and medulloblastoma pathogenesis.

Analysis of gene expression in patient-derived cell lines showed that survival outcome in a particular subgroup is not necessarily indicative of that subgroup having the highest expression of a particular Rab in patient-derived cell lines overall. For instance, high expression of Rab8B is associated with poor prognosis of group 3 patients only but RT-qPCR analysis showed that SHH cell lines had a significantly higher gene expression than group 3 cell lines (section 3.7.2.). Therefore, suggesting that for each Rab, there are subgroup-specific mechanisms that inform contribution of that Rab to patient prognosis.

Expression analyses, also of the Cavalli dataset, showed that for many Rabs there was not a significant difference in expression across the subgroups (section 3.5.1., Figure 3.4.). This supported patient-derived cell line expression analysis as, for example, Rab11A expression was similar across the subgroups upon gene or protein expression analysis. Additionally, after RT-qPCR analysis, whilst *Rab40B* had statistically significantly higher expression in the HD-MB03 cell line than both SHH cell lines, this was not a general effect across all group 3 cell lines studied. Only the D425 group 3 cell line also had statistically significant higher *Rab40B* expression than the DAOY SHH but no significance between the other group 3 cell lines and expression in SHH cell lines could be made.

6.3. Potential effect of Rab11A knockout on endocytic recycling

Rab11A is a key regulator of intracellular vesicle transport, including the regulation of the slow endocytic recycling pathway (Allgood and Neunuebel, 2018). In this study,

the potential role of Rab11A in endocytic recycling was explored through analysis of fluorescent transferrin uptake. Transferrin is widely used as a tool to characterise the function of endocytosis and endocytic recycling pathways in cells. The pathway in which transferrin is endocytosed and then recycled back to the cell membrane is well studied and as such, measuring transferrin is considered to be a good indicator of the function of these pathways (Mayle et al., 2012) (Harding et al., 1983).

Previous studies of the effect of a Rab11A knockout or knockdown on transferrin uptake, including that by Zulkefli et al. (2019) in HeLa cells, showed that Rab11A knockdown caused a reduction in cellular transferrin levels compared to control cell lines. The general trend when comparing all three Rab11A knockout cell lines studied using immunofluorescence imaging supports this, however it was not statistically significant (section 5.2.3, Appendix 1.10.). This was further examined by flow cytometry using one Rab11A knockout cell line and one non-targeting cell line where preliminary results supported immunofluorescence findings. Additionally, Zulkefli et al. (2019) also suggest that Rab11A knockout may lead to increased density of late endosomes/lysosomes. Therefore, in Rab11A knockout cells there could be a mechanism in which a blockage of the endocytic recycling pathway leads to increased trafficking to the lysosomes leading to degradation of transferrin instead of recycling back into the extracellular space (Figure 6.1.). Only one biological replicate was analysed for each cell line in each technique in this study, so more biological replicates are required before any conclusions can be drawn about the effect of Rab11A on endocytic recycling and the correctness of this proposed mechanism.

Dysregulation or dysfunction of the endocytic pathway in Rab11A knockout cells is supported, however, by proteomics analysis of the same Rab11A cell lines and shown in section 5.4.4.2. Differential protein expression analysis identified statistically significant downregulation of nine proteins within the endocytic pathway. This included downregulation of ARFGAP1 expression. ARFGAP1 interacts with mTORC1 (mechanistic target of rapamycin complex 1) which, when the cell has a low abundance of amino acids, inhibits lysosomal transport and activation (Meng et al., 2021). There was also downregulation of sorting nexin-2 (SNX2). SNX2 is involved in retrograde transport from the endosomes to the trans-Golgi network. Therefore, as described in the mechanism by Cullen and Steinberg (2018) (Figure 6.1.), this would lead to increased trafficking of cargo to the lysosomal compartment.
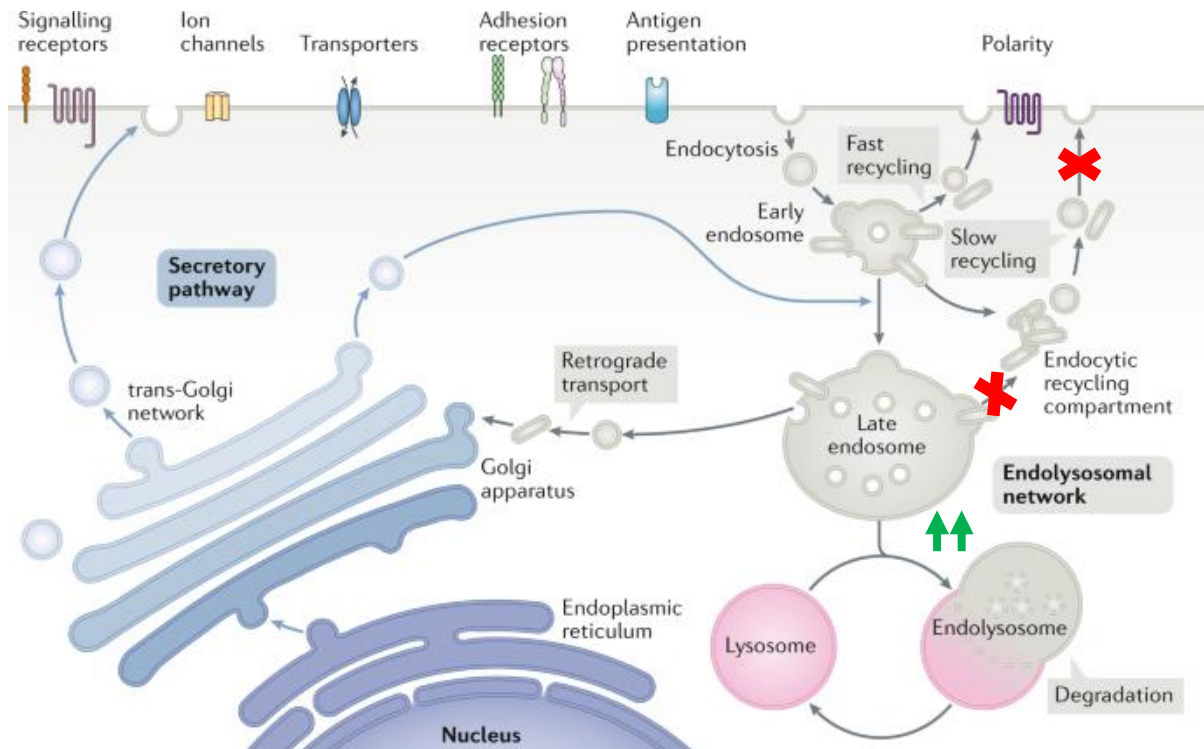
Figure 6.1. Proposed mechanism of alterations to the endocytic recycling pathway caused by Rab11A knockout *Rab11A regulates the endocytic recycling compartment. Upon Rab11A knockout, it is proposed that this compartment and the slow recycling pathway becomes blocked (red cross). This then leads to increased trafficking (green arrows) of cargo from the late endosomes to the lysosomes for degradation. Figure adapted from Cullen and Steinberg (2018).*

This provides another connection between the endocytic pathway and lysosomes and could help explain why there appears to be differences in the lysosomal population of Rab11A knockout cells compared to non-targeting control (section 5.2.2.).

Differential expression analysis of SWATH mass spectrometry data of Rab11A knockout extracellular vesicles also identified the lysosomal protein LAMP-2 (lysosomal-associated membrane protein-2) as being significantly downregulated (Appendix 1.16.). As with LAMP-1, LAMP-2 is a lysosomal membrane protein (Gowrishankar et al., 2020). It has also been implicated in tumour cell metastasis by promoting invasion pathways and upregulation of expression has been implicated in

the inhibition of apoptosis in glioblastoma (Onofre et al., 2021) (Yongjie Wang et al., 2021).

Combined, SWATH mass spectrometry analysis and preliminary fluorescent transferrin expression studies therefore show a dysregulation in proteins associated with the lysosomal and endocytic recycling compartments. They also indicate dysfunction of the endocytic recycling pathway due to Rab11A knockout.

Future work should include conducting further biological replicates of the transferrin uptake in Rab11A knockout and control cell lines. This could include both flow cytometry and immunofluorescence analysis and further LAMP-1 primary antibody staining to identify lysosomes. Lysosomal function could also be analysed using lysosomal hydrolytic assays.

6.4. Absence of Rab11A does not affect extracellular vesicle size or release

Rab11A forms a key part of the exosome biogenesis pathway, a class of small extracellular vesicle (Bai et al., 2022). There is an absence of published literature, however, describing the effect of Rab11A knockout or knockdown on the size or number of secreted particles. In this study, the size and concentration of particles secreted by Rab11A knockout and non-targeting control cell lines was examined (section 5.3.). Fractions collected after size exclusion chromatography underwent nanoparticle tracking analysis (NTA). This showed that there was no significant difference between the concentration of particles secreted or the median diameter of particles between the two conditions. Overall, this suggests that any contribution Rab11A may have to medulloblastoma is not through the alteration of EV morphology or secretion.

RT-qPCR analysis of the Rab11 family members Rab11B and Rab25 was then conducted on Rab11A knockout and control cell lines by Aleena Rahman of the Hume laboratory (not shown). This was to identify whether the lack of significant difference in the concentration and size of EVs secreted by Rab11A knockout cells could be attributed to dysregulation of other Rab11 proteins. This showed no

significant differences in their expression. Future work could be conducted to examine the expression of Rab27A and Rab35 in these cell lines, since both Rabs play a crucial role in exosome biogenesis alongside Rab11A (Blanc and Vidal, 2018). Exploration of these candidates would thus be useful to identify whether the lack of significant difference is due to compensation of the action of another Rab within the exosome biogenesis pathway.

SWATH-MS analysis was used to examine protein cargo of EVs secreted by knockout cells. The examination of medulloblastoma EVs using mass spectrometry has previously been conducted in two studies focusing on the SHH and group 3 subgroups (Bisaro et al., 2015) (Epple et al., 2012). The only Rab GTPase identified as cargo was Rab1B in the group 3 D283 cell line by Epple et al. There is a notable absence of published mass spectrometry studies on EVs derived from cell lines with Rab GTPase knockouts or knockdowns.

Differential protein expression analysis showed negligible pathway functional associations between proteins up- or downregulated in EVs from Rab11A knockout cells compared to non-targeting control cells. It did, however, identify some specific targets which are of note. The protein sidekick-2 (SDK2) is an adhesion molecule which promotes lamina-specific synapse connections in the retina (Yamagata et al., 2002). It was the most statistically significantly downregulated protein in Rab11A knockout EVs and had the greatest fold change difference in expression compared to non-targeting control cell lines (Figure 5.10. B). It has been previously identified as a protein in EVs derived from bone marrow mesenchymal stem cells, endothelial cells, platelets, squamous carcinoma cells and T-cells (Vesiclepedia) and as RNA in astrocyte EVs (Shanthi et al., 2023). None of these studies, however, identify a role for SDK2 in EVs and instead simply list it as cargo after -omics analysis.

SDK2 is of note in group 3 medulloblastoma cells because K. S. Smith et al. (2022) have identified the rhombic lip as the cell type of origin for group 3 tumours. In this study, Smith et al. analysed gene sets in common between group 3 and the rhombic lip and identified enrichment of several retinal and photoreceptor gene sets. This enrichment was not present in cells granule neurone precursor cells (SHH subgroup cell line of origin) or within rhombic lip progenitor cells which become the group 4 subgroup. As SDK2 is involved in the maintenance of neural circuits in the retina

(Krishnaswamy et al., 2015) and medulloblastoma tumours are considered to be of neuronal lineage (Sheng et al., 2024), this provides a further association between SDK2 and medulloblastoma. Additionally, *SDK2* was identified as a downstream effector gene of a super-enhancer driven transcriptional regulatory network of group 3 medulloblastoma (M. Li et al., 2022). One of these super-enhancers is *OTX2* which is a potent oncogene of group 3 medulloblastoma and has been identified as having a role in the generation of photoreceptors (Tegla et al., 2020) (Kaufman et al., 2021). Thereby providing an association between a protein significantly downregulated in Rab11A knockout group 3 medulloblastoma EVs, group 3 cell type of origin and a potent oncogene in group 3 cells. As such SDK2 could be helping to maintain neural circuits during the development of group 3 medulloblastoma. Its presence in EVs indicates a potential role in helping to develop a tumour niche at a secondary site for future metastasis. Future work is required, however, to determine the potential effect of Rab11A knockout on the metastatic potential of group 3 cells. Invasion and migration assays could be used in combination with EV treatment assays wherein wildtype HD-MB03 or another medulloblastoma cell line are treated with Rab11A knockout EVs to determine the effect of dysregulated cargo caused by the absence of Rab11A on recipient cells. Finally, large scale proximity-dependent biotinylation mapping of HEK293 cells by Go et al. (2021) identified an interaction between Rab11A and SDK2. Whilst SDK2 was not identified in SWATH-MS cell lysates from either non-targeting control or Rab11A knockout cell lines and so differences in SDK2 expression could not be examined, the finding by Go et al. suggests that an interaction between Rab11A and SDK2 may also be possible in medulloblastoma cells. As such SDK2 may be either a Rab11A effector or Rab11A may be directly involved in the packaging of SDK2 into EVs. Together this, identifies an association between a protein significantly downregulated in Rab11A knockout group 3 medulloblastoma EVs which interacts with Rab11A, group 3 cell type of origin and a potent oncogene in group 3 cells

The most significantly upregulated protein in Rab11A knockout EVs compared to non-targeting control cell line EVs was versican (VCAN). Versican is an extracellular matrix protein. Versican binds to hyaluronan, which is an important component of the brain extracellular matrix (ECM) (Novak and Kaye, 2000) and has been shown to accumulate as part of the early inflammatory response in many diseases, including

cancer (Ricciardelli et al., 2009). In cancer it has been shown to affect cancer cell motility, proliferation and metabolism and has been shown to reduce cell adhesive properties of prostate cancer cells (Ricciardelli et al., 2007) (Creighton et al., 2005) (Yee et al., 2007). Whilst versican has not been directly associated with pathogenesis in medulloblastoma, in glioma patients it has been associated with metastasis (Paulus et al., 1996) and it is enriched within the cerebellum of the brain (Human Protein Atlas), where medulloblastoma is localised. Taken together, this would suggest that increased versican expression could be a negative prognostic indicator of medulloblastoma. No significant association between expression and prognosis in medulloblastoma patients could be made, however, after patient dataset analysis using the Cavalli dataset on the R2: Genomics analysis and visualisation platform (Figure 6.2.). No association between expression of SDK2 and patient survival could be ascertained either. It should be noted that literature conclusions and the survival analysis is conducted on cells and not EVs so this only gives an indication about the potential effect of both proteins within medulloblastoma cells. More analysis is required to determine the effects of SDK2 and VCAN expression dysregulation within group 3 medulloblastoma EVs.

Whilst SWATH-MS analysis was not useful for functional pathway analysis of dysregulated proteins in EVs, it has allowed for the identification of specific targets, SDK2 and versican. Both SDK2 and versican have been associated with either pathways which are fundamental to the origins of medulloblastoma tumours or to pathways which have been associated with cancer progression.

Pathway analysis has also not highlighted any direct interactions between SDK2 or VCAN with Rab11A suggesting that dysregulation of both is likely due to the action of downstream effectors. Therefore, it is of interest to conduct further experiments to elucidate the specific roles of SDK2 and versican in medulloblastoma and to identify pathway associations in order to identify how Rab11A is affecting EV cargo and the effect that may have on medulloblastoma progression. This could include, firstly, using RT-qPCR to establish a baseline expression of *SDK2* and *VCAN* in Rab11A knockout and non-targeting control cell lines as neither was detected in cell lysates during SWATH-MS analysis.
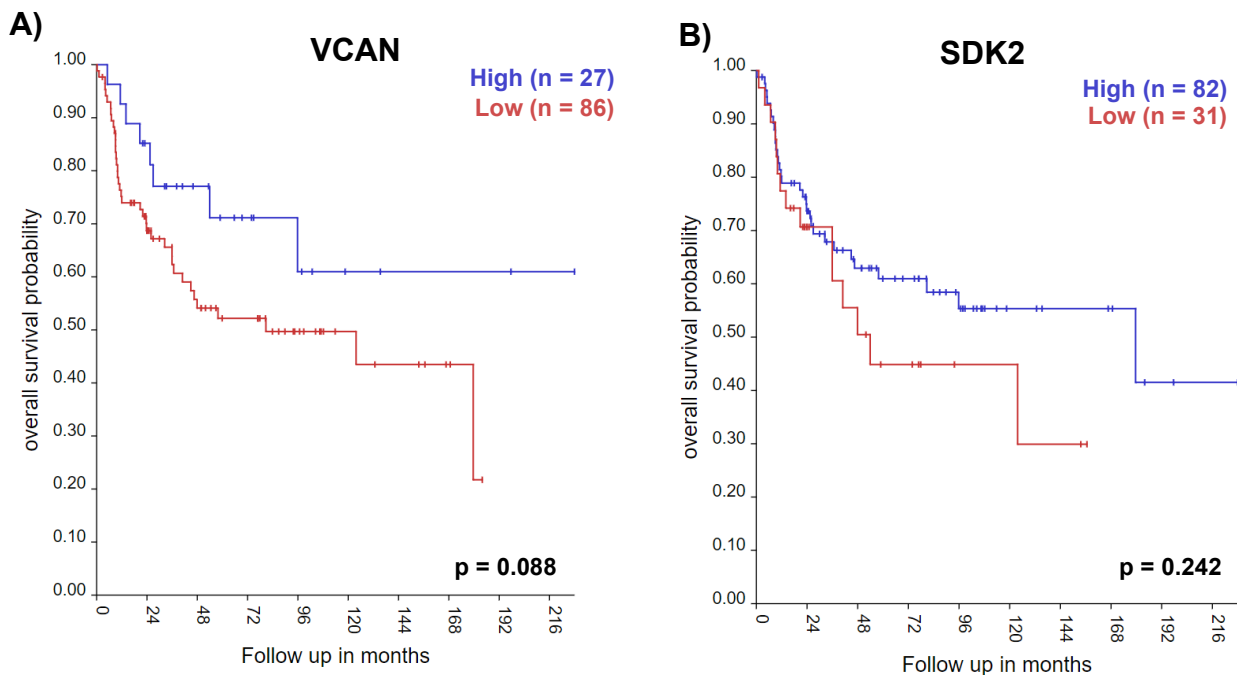
Figure 6.2. Survival prognosis of VCAN and SDK2 in group 3 patients *Gene expression-based survival curve analysis using the Cavalli dataset on the R2: Genomics analysis and visualisation platform. Survival analysis of versican (VCAN, A) and protein sidekick 2 (SDK2, B). Medulloblastoma patients from group 3 (n = 113). The R2:Kaplan Scan tool was used to generate survival curves. Statistical significance (p ≤ 0.05) between curves was determined using the log-rank (Mantel-Cox) test.*

6.5. Mass spectrometry analysis reveals function of Rab11A in multiple cellular pathways in group 3 medulloblastoma

Functional pathway analysis was conducted after differential protein expression analysis between Rab11A KO cells and non-targeting control cells after SWATH-MS analysis. In the literature, mass spectrometry techniques have been used to try and understand the proteome of medulloblastoma cell lines, for example Paine et al., (2019) Bakhshinyan et al., (2023) Clark et al., (2018). There is no published literature which aims to understand the regulatory landscape of Rabs in medulloblastoma.

As mentioned in sections 5.4.4.1. and 5.4.4.2., after KEGG pathway analysis of upregulated and downregulated proteins in cell lysates, there were some general themes of the dysregulated pathways. Pathways which had upregulation of proteins

were predominantly cancer-related, involved in amino acid metabolism and involved in the cellular response to pathogen infection. Pathways which had a downregulation of proteins were predominantly associated with mitochondrial dysfunction, metabolic dysfunction, and ribosomes. When examining the pathway associations, a lot of the pathways had proteins which were common (Figures 5.11. and 5.13.), indicating that dysregulation of a subset of proteins had led to changes in multiple cellular pathways. For example, upregulation was seen for α-catenin, β-catenin, RAC1 and RHOA. These were all present in the 'bacterial invasion of epithelial cells' pathway through their association with actin polymerisation, they are also involved in the 'pathways in cancer' and 'WNT' signalling pathways which have a more direct association to medulloblastoma.

6.5.1. Rab11A knockout leads to upregulation of β-catenin expression

When examining the pathway associations for upregulated proteins, the most common category was pathways in cancer, showing that Rab11A knockout dysregulated tumourigenic pathways. A pathway of interest in this category was the WNT signalling pathway. The WNT medulloblastoma molecular subgroup is named after this pathway which is dysregulated in patients with this subgroup (Mani et al., 2023). It has the most favourable survival outcomes of the subgroups with this being thought to be due to WNT signalling, which may contribute to the tumour's positive response to therapy (Pfaff et al., 2010). Whilst this pathway has subgroup-specific associations in medulloblastoma, mutations in *CTNNB1* which encodes β-catenin have been associated with pathogenesis of multiple cancer types including endometrial, liver and colorectal cancers (S. Kim and Jeong, 2019). Several studies exist, however, which identify anti-tumourigenic roles of β-catenin and the Wnt signalling pathway in other medulloblastoma subgroups, including group 3. In these studies, increased β-catenin has been associated with blockade of the G2/M phase of the cell cycle (Olmeda et al., 2003). This leads to a decrease of cells in G1 phase and triggers apoptosis (Davidson and Niehrs, 2010) (K. Kim et al., 2000). This has been observed through reduction in colony and neurosphere formation of cells deriving from SHH and group 3 and 4 patients respectively (Olmeda et al., 2003) (Manoranjan et al., 2020).

This leads to the hypothesis that in the non-WNT medulloblastoma subgroups, the WNT pathway has an anti-tumourigenic role. As such, whilst many pathways of tumourigenesis are upregulated in Rab11A knockout cells, the centering of these pathways around β-catenin upregulation, which is also shown in STRING pathway analysis (Figure 5.11.) may actually be having an anti-tumourigenic role in these cells. These cells also have an upregulation of the executioner caspase, caspase 3 suggesting that they also have apoptotic dysregulation, supporting the idea that upregulation of β-catenin is actually anti-tumourigenic in these cells. Dysregulation of β-catenin and caspase 3 expression is not sufficient, however, as expression does not confer functionality for either protein. β-catenin requires the presence of Wnt ligands and caspase 3 requires cleavage into its active form which allows it to act as an executioner caspase (Schunk et al., 2020) (P. F. Liu et al., 2017). Therefore, assays such as substrate utilisation assays are required to measure caspase activity and apoptosis and thereby determine whether this hypothesis is accurate.
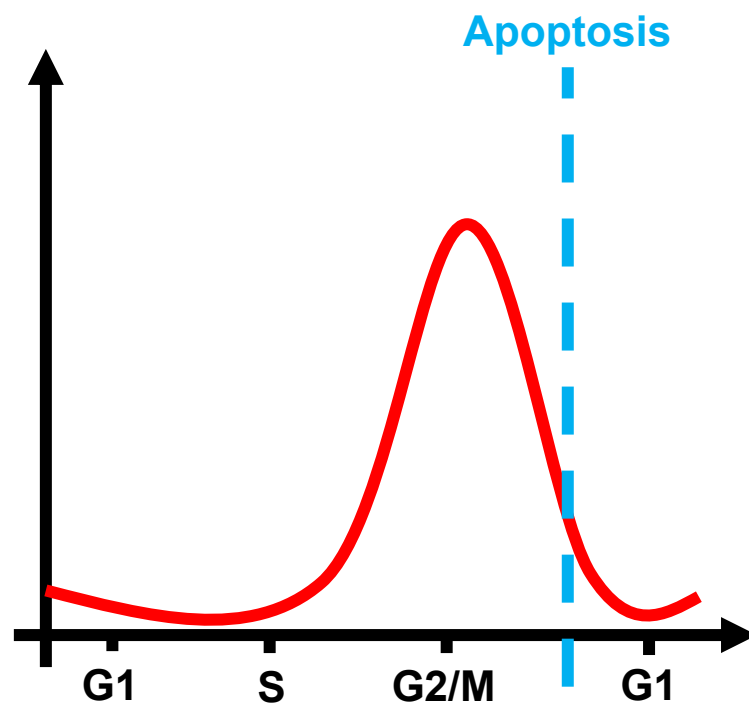
Figure 6.3. Schematic of β-catenin expression and the cell cycle *Cell cycle stage (x-axis) and beta catenin expression (y-axis). Red line represents β-catenin expression. Blue dotted line represents cell cycle blockade which leads to cellular apoptosis. Figure adapted from Davidson and Niehrs (2010).*

When examining cellular pathways which had downregulated proteins in Rab11A knockout cell lysates compared to non-targeting control cell lysates after SWATH-MS analysis, mitochondrial dysfunction, metabolic dysregulation and ribosomal were common themes.

Specific mechanisms which define Rab GTPase contribution to metabolic pathways are yet unexplored. Rabs, such as Rab10 and Rab14, have been implicated in the transport of membrane transporters such as GLUT4 (glucose transporter 4) to the cell membrane. This allows for cellular glucose uptake and metabolism thus implicating Rab10 and Rab14 in the facilitation of metabolic pathways (Chen et al., 2012).

The role of Rab11A specifically in metabolism is currently unexplored with an absence of literature associating it directly with any metabolic pathways. There is also a lack of literature directly associating Rab11A with mitochondrial function and any research associates Rab11A with mitophagy through endosomal compartments (Ravindran et al., 2021) (Puri et al., 2018) (Landry et al., 2014).

The reprogramming of cancer metabolism is now considered a hallmark of cancer (Hanahan, 2022). Cancer cells modulate their metabolism to promote survival and proliferation. It allows for cells to adapt to their changing environment and thus aids in the survival of tumour cells (Navarro et al., 2022). This is often observed as increased activity of the TCA cycle and oxidative phosphorylation, as well as concurrent phenomena such as the Warburg effect (which describes the utilisation of glycolysis as a metabolic pathway even when adequate oxygen concentrations are present) (Martínez-Reyes and Chandel, 2021) (Heiden et al., 2009) (Liberti and Locasale, 2016). In medulloblastoma, metabolic dysfunction appears to have a subgroup-specific prognostic significance. For example, reprogramming of the TCA cycle and upregulation of genes involved in oxidative phosphorylation and glycolysis are prognostically significant in group 3 patients (Kyung Park et al., 2019) (Funke et al., 2023). More specifically, group 3 cells with a *MYC* amplification showed upregulation of the TCA cycle and oxidative phosphorylation compared to the normal

brain (Pham et al., 2022) (Marabitti et al., 2022). Additionally, Linke et al., (2023) showed that the HD-MB03 group 3 medulloblastoma cell line, which possesses a *MYC* amplification (Milde et al., 2012), had multiple subpopulations of cells with increased expression of genes associated with oxidative phosphorylation and the TCA cycle.

In this study, HD-MB03 cells were used as a model cell line for Rab11A knockout. After mass spectrometry and differential protein expression analysis, downregulation of proteins within the TCA cycle and oxidative phosphorylation was observed (section 5.4.4.2., Figures 5.15. and 5.16.). This was as predicted because analysis of data obtained by Linke et al. (section 3.4.2.) identified *Rab11A* as an upregulated gene in subpopulations of cells which also had upregulation of metabolic genes. Therefore, creating an association between upregulation of mitochondrial metabolism pathways when *Rab11A* is upregulated and downregulation of these pathways in the absence of Rab11A.

Furthermore, this downregulation involved proteins associated with complexes I, II, IV and V of oxidative phosphorylation and enzymes in the TCA cycle responsible for the conversion of succinate to fumarate, oxaloacetate and acetyl-CoA to citrate, citrate to isocitrate and isocitrate to α-ketoglutarate. Therefore, Rab11A knockout cells have dysregulation of adjacent enzymes within metabolic pathways which have prognostic significance in group 3 medulloblastoma. This downregulation may be associated with the reduced formation of coenzymes, such as NADH, leading to further downstream reduction in metabolic capabilities of the cell and thus ATP production.

Additionally, Linke et al. (2023) observed fumarate accumulation and proposed fumarate to be an oncometabolite in group 3 medulloblastoma. The downregulation in Rab11A knockout cells of succinate dehydrogenase subunit B (SDHB) which is responsible for the conversion of succinate to fumarate may therefore lead to a lack of this accumulation, inhibiting its oncometabolite function and increasing patient survival outcomes. Furthermore, the downregulation of enzymes involved in citrate, isocitrate and α-ketoglutarate synthesis may lead to a reduction in cellular α-ketoglutarate levels which would have a downstream effect on firstly the biosynthesis of other metabolites in the TCA cycle and secondly the oxidation of fatty acids, amino

acids and glucose of which α-ketoglutarate is a key regulator (L. He et al., 2015) (Naeini et al., 2023). A summary of the proposed effects of Rab11A knockout on the TCA cycle is shown in Figure 6.4. Additional exploration is therefore required to determine the levels of these metabolites within Rab11A knockout cells, through metabolomic studies, to explore the potential effect of downregulation of enzymes within the TCA cycle on their accumulation within cells.
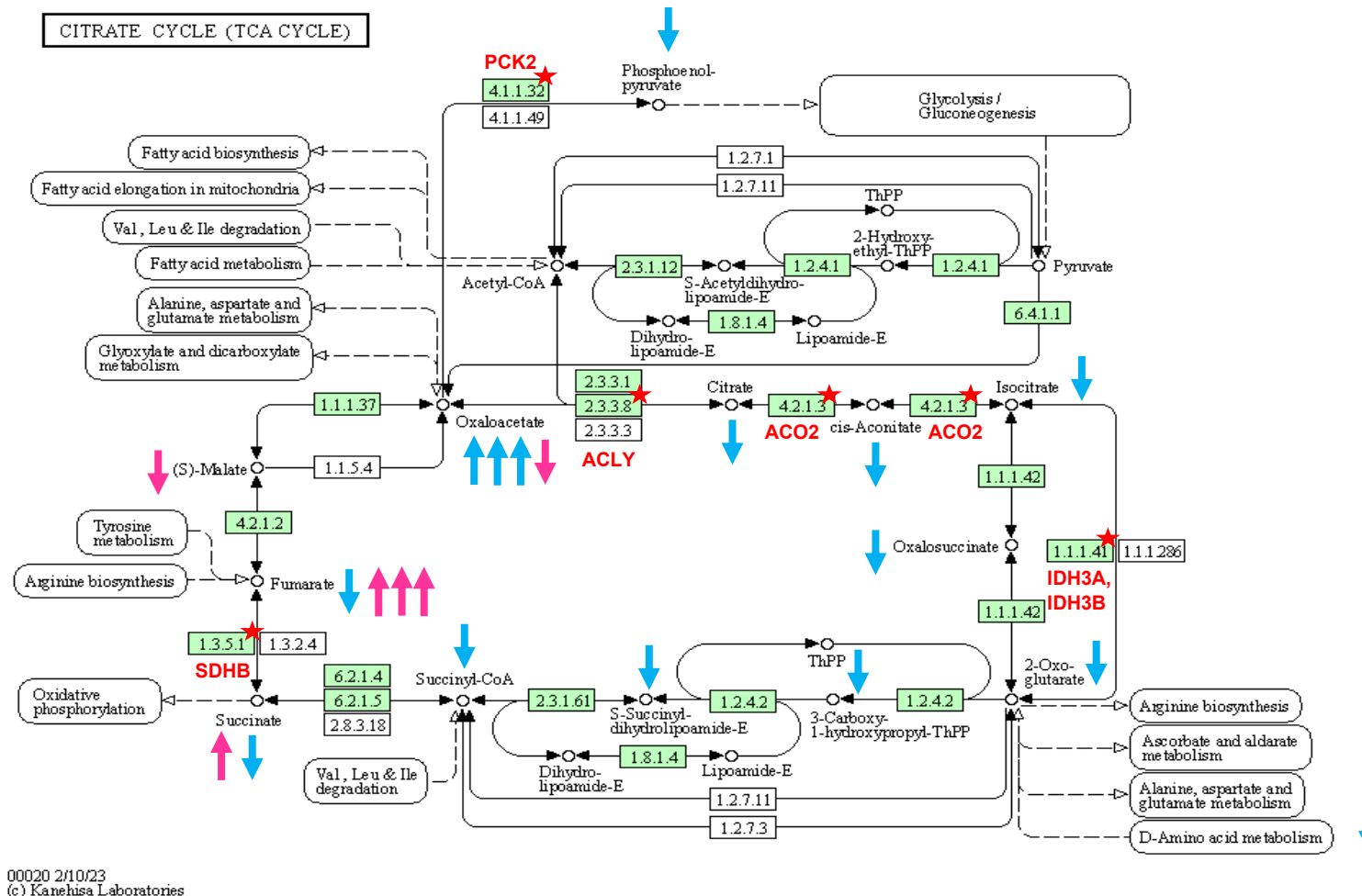
Figure 6.4. Proposed effect of Rab11A knockout on the tricarboxylic acid (TCA) cycle *Kyoto Encyclopaedia of Genes and Genomes (KEGG) pathway is shown. Blue arrows indicate the proposed effect of Rab11A knockout on parts of the pathway. Pink arrows indicate findings observed by Linke et al. (2023). Red stars indicate position of upregulated protein in the pathway. Red text indicates gene symbols of the protein from pathway analysis. Analysis conducted and KEGG pathway image generated using the online bioinformatics tool DAVID (the Database for Annotation, Visualisation and Integration Discovery).*

214

Downregulation of two of the subunits (α and β) of isocitrate dehydrogenase 3 (IDH3) which catalyses the decarboxylation of isocitrate into α-ketoglutarate in the TCA cycle within the mitochondria is seen in Rab11A knockout cells. IDH1 catalyses the same reaction but within the cytosol. Mutations which cause dysregulation of IDH1 are associated with long-term survival in patients with high-grade glioma (HGG) (Kaminska et al., 2019), therefore it is hypothesised that dysregulation of IDH3 may also lead to increased survival for medulloblastoma patients.

Downregulation of PCK2 was observed in both cell lysates and EVs deriving from Rab11A knockout cells. PCK2 is responsible for the regulation of metabolic adaptation, enabling glucose-independent tumour growth. It is generally active and more highly expressed in low glucose states where it catalyses the conversion of oxaloacetate into phosphoenol pyruvate in the mitochondria (Leithner et al., 2014).

Reduction in PCK2 expression combined with the downregulation of ATP citrate lyase (ACLY) which catalyses the conversion of oxaloacetate to citrate within the TCA cycle, may lead to oxaloacetate accumulation within Rab11A knockout cells. The effect of this could therefore be something to be explored. It should be noted that oxaloacetate is a metabolic intermediate in several metabolic pathways (Hakimi et al., 2007). Changes in oxaloacetate concentrations can therefore affect many stages of metabolism. Wilkins et al., (2014) suggest that oxaloacetate-induced metabolic changes produce an overall pro-mitochondrial effect, indirectly activating mitochondrial biogenesis and adding to the overall mitochondrial dysfunction of Rab11A knockout cells.

Mitochondria are unique organelles which consist of an out membrane and a folded inner membrane separated by an intermembrane space. It is within this inner membrane that respiratory complexes exist, facilitating oxidative phosphorylation. The TCA cycle occurs within the mitochondrial matrix which also houses the mitochondrial genome (Kühlbrandt, 2015). The mitochondrial genome is distinct from the nuclear genome of the cell and is a circular DNA molecule of about 16kb in humans (Cooper, 2000). It contains 37 genes which encode 13 proteins, 22 tRNAs (transfer ribonucleic acids) and 2 rRNAs (ribosomal ribonucleic acids) (Anderson et al., 1981). The proteins encode proteins of the oxidative phosphorylation pathway (Chinnery and Hudson, 2013). None of these proteins were downregulated in

Rab11A knockout cells, however, meaning that all of the proteins identified as dysregulated in Rab11A knockout cells were nuclear encoded gene products. The nuclear genome is responsible for encoding the majority of the oxidative phosphorylation pathway as well as encoding proteins which modulate mitochondrial biogenesis, replication and mitophagy. The balance between mitochondrial biogenesis and mitophagy is a crucial part of maintaining cellular homeostasis, for example, dysregulation of mitophagy has been connected to illnesses such as cancer, neurological disorders and metabolic diseases (Klionsky et al., 2021) The process of oxidative phosphorylation is responsible for the generation of most of the ATP within cells (D. F. Wilson, 2017). Downregulation of enzymes within the oxidative phosphorylation pathway in Rab11A knockout cells could therefore result in decreased ATP production which could affect mitochondrial membrane potential (Higgins and Coughlan, 2014), leading to the triggering of mitophagy and affect the balance between mitophagy and mitochondrial biogenesis within the cells.

As dysregulation of oxidative phosphorylation has been associated with decreased ATP production, it has also been linked with increased oxidative stress (Schütt et al., 2012). Oxidative DNA damage is a consequence of oxidative stress leading to hydrolysis of DNA bases as a consequence. This can lead to impaired cell growth among other effects due to the altering of the physiological transcriptomic profile of the cells which in itself causes gene mutations (Valko et al., 2004) (Pizzino et al., 2017) (Salmon et al., 2004). This may help explain why multiple morphologies were observed for Rab11A knockout cells (section 4.8.) and why, as mentioned in section 5.1. some cell lines were slower growing than others. Quantitative analysis of knockout cell line growth would therefore be beneficial to identify whether there is a statistically significant cellular proliferation impairment within Rab11A knockout cell lines. This could be used to ascertain whether oxidative stress is causing cellular quiescence or an overall slowing of the cell line. This could be complemented by cell cycle analysis which would allow for the amount of Rab11A knockout cells within the population in each stage of the cell cycle to be established.

6.6. Use of CRISPR-Cas9 as a method for protein knockout and evaluation of the sensitivity of knockout validation techniques

As mentioned in Chapter 4, in order to fully validate potential CRISPR knockouts, the absence of endogenous protein needed to be confirmed. Western blotting is a common approach for validating the absence of target protein expression after CRISPR-Cas9 gene editing. With a fully optimised primary antibody, western blotting can detect picogram amounts of protein within a sample (Ghosh et al., 2014). Mass spectrometry is a highly sensitive technique which can also be used to detect protein within a sample. It has an advantage over antibody-based methods in the sense that it offers greater specificity, reproducibility and can detect protein concentrations as small as femtomoles (Jayasena et al., 2016).

When conducting statistical analysis of data obtained by SWATH-MS, in order for a protein to be considered up- or downregulated it has to be present within both samples. Rab11A was the most significantly downregulated protein in cell lysate samples, therefore it had to be present in both Rab11A knockout and non-targeting control samples. The mass spectrometer detects peptide fragments, the knockout site is present 130 amino acids into the sequence, therefore, if the truncated protein was still present in the cells as it had not undergone degradation, it is plausible that fragments may still be present.

The amino acid sequence of peptides identified by the mass spectrometer can be obtained from the mass spectrometry results. One Rab11A-specific peptide was identified, this was aligned with the unedited Rab11A sequence using the ExPASy translate tool. This showed that the peptide identified was downstream (C-terminal) of the target site meaning that full length Rab11A was likely still present within the cells (Figure 6.5). When looking at raw expression values, however, this showed that the expression of this peptide within Rab11A knockout cells was significantly reduced (Figure 6.6) and therefore, cells still had reduced Rab11A expression due to the CRISPR-Cas9 gene editing process (approximately 30% of the level observed in non-targeting control cells). Therefore, despite the presence of a Rab11A peptide, due to the significant reduction in expression compared to control cells, the protein dysregulation observed through SWATH-MS analysis can still be attributed to the effects of Rab11A expression depletion within the cells.
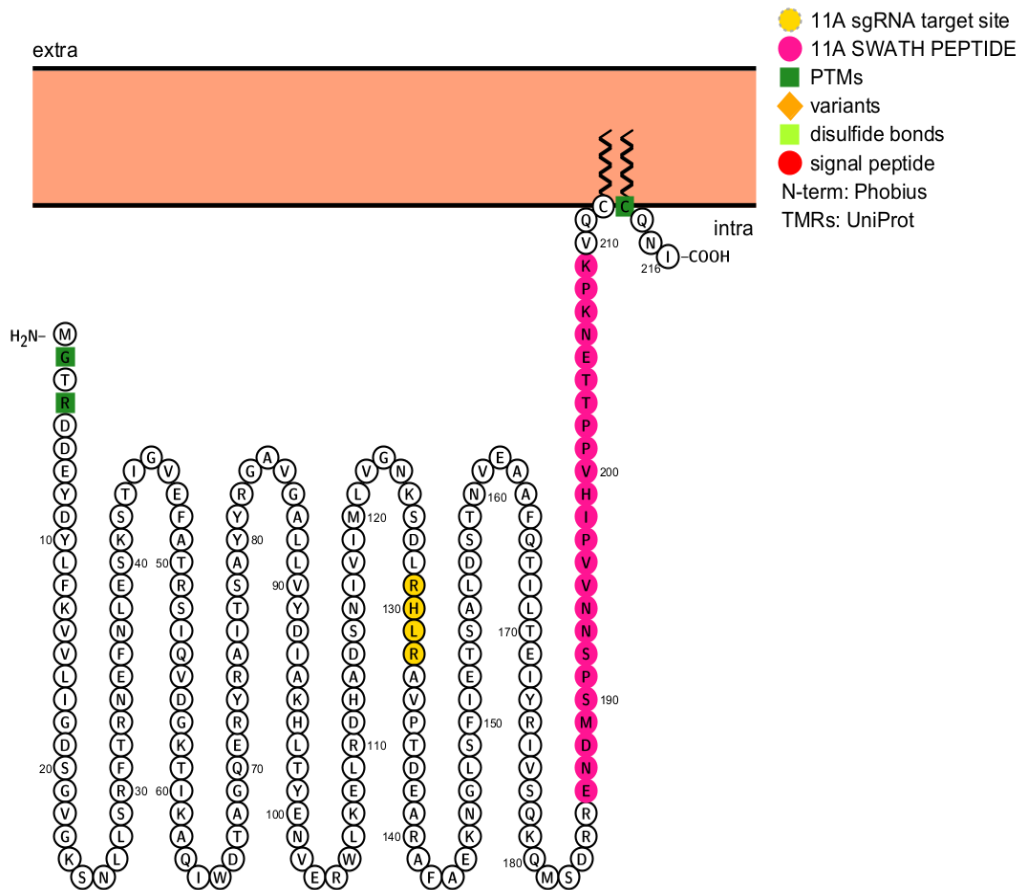
Figure 6.5. Amino acid sequence of Rab11A with peptide fragment from SWATH-MS analysis highlighted *Letters correspond to the one letter amino acid code. Numbers alongside correspond to position of the amino acid within the whole sequence. Amino acids at the translated location of the CRISPR-Cas9 gene editing site are highlighted in yellow. Amino acids from the peptide fragment detected during SWATH-MS is highlighted in pink. Image shows Rab11A with post-translational modifications attached to a membrane. Green amino acids represent these post-translational modifications. 'Intra' stands for intracellular. 'Extra' stands for extracellular. Image was generated using the protein feature visualisation tool Protter (wlab.ethz.ch/protter/).*
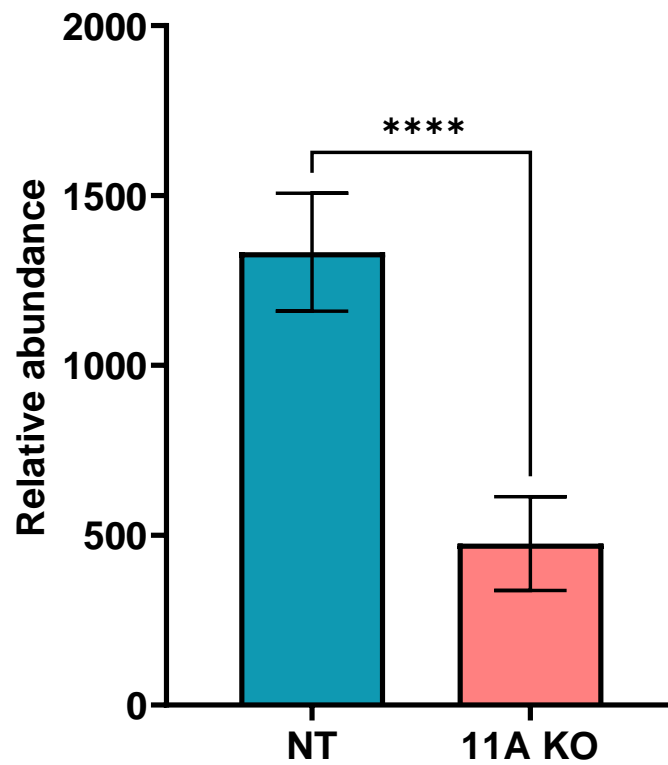
Figure 6.6. Relative abundance of Rab11A peptide in non-targeting and Rab11A knockout cell lysate samples *Relative abundance of the number of the peptide detected using SWATH-MS. Relative abundance was calculated by comparing the number of peptides detected to the amount of protein in the lysate sample. The statistical significance of abundance of the peptide in non-targeting (NT) samples compared to Rab11A knockout (11A KO) was calculated using Welch's t-test and Graphpad Prism. '****' represents p value < 0.0001.*

A potential explanation for this continued expression is defective protein synthesis termination. Termination of protein synthesis is not completely efficient meaning that in some cases, termination suppression occurs. This can happen naturally due to ribosomal frameshifting, be due to a phenomenon known as ribosomal readthrough or due the presence of suppressor tRNAs (Weiss et al., 1990) (Fearon et al., 1994) (Beier and Grimm, 2001) (Dabrowski et al., 2015). These suppressor tRNAs are aminoacylated and possess anticodons which are complementary to stop codons in mRNA (Beier and Grimm, 2001). As shown through SWATH-MS KEGG pathway analysis, Rab11A knockout cells have dysregulation of the aminoacyl-tRNA biosynthesis pathway (section 5.4.4.2.), supporting the hypothesis that the cells have dysfunction in DNA replication pathways. Additionally, there is evidence to suggest that under conditions of cell stress, cells can also induce ribosomal readthrough. Ribosomal readthrough is a phenomenon in which a ribosome passes through a stop codon and continues to translate a protein sequence. In conditions of cellular stress, it is believed that cells can purposefully induce this in order to produce proteins which may help alleviate this cellular stress and prevent apoptosis (Tyedmers et al., 2008) (Gerashchenko et al., 2012) (C. Li and Zhang, 2019). This phenomenon has been shown to be widespread amongst species and within specific tissues with research showing that it can occur during between 0.1% and 31% of transcription events (C. Li and Zhang, 2019) (Biziaev et al., 2022) (Loughran et al., 2014).

As Rab11A was detected during SWATH-MS analysis but not during western blot analysis, it highlights the increased sensitivity for protein detection of techniques such as mass spectrometry over immunoblotting.

It should also be noted that the only peptide which was detected that was specific to Rab11A was the peptide highlighted in Figure 6.5. within the C-terminus. Therefore, the mass spectrometer could not detect any unique N-terminal peptides. This stresses the limitations of studying endogenous Rab GTPase family members as high levels of sequence similarity mean that detection methods have to identify a specific region of the protein. These difficulties were also highlighted in Chapter 3 wherein there were issues obtaining antibodies which were specific to Rab family members.

6.7. Rab40B as a therapeutic target in group 3 medulloblastoma

Throughout this study the difficulty identifying reagents which are specific to the Rab GTPase targets has been highlighted. As mentioned in Chapter 4, there was an attempt to generate and fully validate a Rab40B HD-MB03 group 3 medulloblastoma cell line. Due to issues obtaining an antibody which was specific to Rab40B, however, the ten potential knockout cell lines created could not be fully validated (section 4.7.). Oxford Nanopore sequencing identified the cell lines E4 and G11 as having mutations in all alleles which would lead to premature termination of Rab40B and thus protein knockout (section 4.6.2.). Therefore, it would be worthwhile identifying or generating a primary antibody which is specific to Rab40B so that knockout cell lines could be fully validated.

The biology of Rab40B is relatively unexplored in the literature with an absence of studies identifying a potential role for it in paediatric cancer. Interestingly, *Rab40B* is positioned at 17q25.3, meaning that the gene is present on the most common chromosomal aberration in medulloblastoma patients, isochromosome 17q (Figure 4.8.). Previous work also associates Rab40B with trafficking of MMP-2 and MMP-9 to invadopodia during tumour migration (Jacob et al., 2013). MMP-2 and MMP-9 have been associated with poor prognosis and recurrence in glioma patients (Zhou et al., 2019). Additionally, MMP-2 has been identified as a promigratory factor in medulloblastoma (Jackson et al., 2023), creating a disease-specific association between Rab40B and a potential mechanism in which it could contribute to medulloblastoma pathogenesis. This combined with analysis conducted in section 3.5.2. wherein high expression of *Rab40B* was associated with highly statistically significant poor prognosis in group 3 patients, makes Rab40B an exciting novel target in group 3 medulloblastoma. Therefore, it would be worthwhile continuing to explore Rab40B as a target and explore its potential role in group 3 metastasis.

6.8. Conclusions

This study aimed to identify whether Rab GTPases were contributing to medulloblastoma pathogenesis. Analysis of medulloblastoma patient survival data showed that Rab expression is indicative of prognosis. For some Rabs, such as Rab11A, this was subgroup specific. Other Rabs, such as Rab1B, were prognostically significant in multiple subgroups. This showed for the first time that from a genetic perspective, Rabs could be contributing to medulloblastoma pathogenesis. Further patient dataset analysis showed that generally there was no subgroup-specific enrichment of Rab expression. This was supported by gene and protein expression analysis on patient-derived cell lines.

CRISPR-Cas9 technology was then used to generate Rab11A knockout cell lines. Functional analysis showed a potential effect of Rab11A knockout on the endocytic recycling and lysosomal compartments; however, further replicates are required to confirm this. Analysis of extracellular vesicles isolated from these cell lines showed no significant difference in size or concentration compared to control cell lines. Analysis of cargo using SWATH-MS did indicate the differential expression of proteins within EVs such as SDK2 and versican which may lead to downstream effects including modulation of the tumour microenvironment.

SWATH-MS was also used to conduct differential protein expression and cellular pathway analysis on cell lysate samples. This showed an upregulation of β-catenin expression which led to dysregulation of other tumourigenic pathways. For proteins which were downregulated, mitochondrial dysfunction and metabolism were common themes. This included the downregulation of proteins associated with the complexes in oxidative phosphorylation and enzymes within the TCA cycle which catalyse the metabolism of substates and the redox of coenzymes such as NAD which are utilised in other metabolic pathways. These findings were in contrast to previous studies which identified HD-MB03 cells as having high TCA cycle and oxidative phosphorylation activity. It also identified an upregulation of Rab11A expression within these cells. Therefore, as previously stated, the decreased expression of enzymes within mitochondrial metabolism pathways may mean that Rab11A is involved in increased TCA cycle and oxidative phosphorylation activity. As such, it could be targeted to reduce metabolic activity within group 3 cells.

222

Combined, this research elucidates a novel role of Rab11A of regulating mitochondrial metabolism pathways in group 3 medulloblastoma cells. A summary of the proposed contributions of Rab11A to medulloblastoma pathogenesis is highlighted in Figure 6.7.

Figure 6.7. Overview of potential roles of Rab11A in medulloblastoma pathogenesis identified by this study ↑ = increased or upregulated, ↓ = decreased or downregulated. MB = medulloblastoma. TCA cycle and oxidative phosphorylation figure adapted from Martinez-Reyes and Chandel, 2020. Endocytic recycling figure adapted from Cullen and Steinberg, 2018.

Bibliography

Aboubakr, H., Lavanya, S., Thirupathi, M., Rohini, R., Sarita, R., Uma, V., 2016. Human Rab8b Protein as a Cancer Target-An In Silico Study. J Comput Sci Syst Biol Aboubakr 9, 132–149. https://doi.org/10.4172/jcsb.1000231

Abounit, S., Zurzolo, C., 2012. Wiring through tunneling nanotubes - from electrical signals to organelle transfer. J Cell Sci 125, 1089–1098. https://doi.org/10.1242/jcs.083279

Adamson, D.C., Shi, Q., Wortham, M., Northcott, P.A., Di, C., Duncan, C.G., Li, J., McLendon, R.E., Bigner, D.D., Taylor, M.D., Yan, H., 2010. OTX2 is critical for the maintenance and progression of Shh-independent medulloblastomas. Cancer Res 70, 181–191. https://doi.org/10.1158/0008-5472.CAN-09-2331

Agarwal, R., Jurisica, I., Mills, G.B., Cheng, K.W., 2009. The emerging role of the RAB25 small GTPase in cancer. Traffic. https://doi.org/10.1111/j.1600-0854.2009.00969.x

Agola, J.O., Jim, P.A., Ward, H.H., Basuray, S., Wandinger-Ness, A., 2011. Rab GTPases as regulators of endocytosis, targets of disease and therapeutic opportunities. Clin Genet. https://doi.org/10.1111/j.1399-0004.2011.01724.x

Akavia, U.D., Litvin, O., Kim, J., Sanchez-Garcia, F., Kotliar, D., Causton, H.C., Pochanard, P., Mozes, E., Garraway, L.A., Pe'Er, D., 2010. An integrated approach to uncover drivers of cancer. Cell 143, 1005–1017. https://doi.org/10.1016/j.cell.2010.11.013

Albright, A.L., Wisoff, J.H., Zeltzer, P.M., Boyett, J.M., Rorke, L.B., Stanley, P., 1996. Effects of Medulloblastoma Resections on Outcome in Children: A Report from the Children's Cancer Group. Neurosurgery 38, 265–271. https://doi.org/10.1097/00006123-199602000-00007

Allgood, S.C., Neunuebel, M.R., 2018a. The recycling endosome and bacterial pathogens. Cell Microbiol 20, e12857. https://doi.org/10.1111/CMI.12857

Allgood, S.C., Neunuebel, M.R., 2018b. The recycling endosome and bacterial pathogens. Cell Microbiol 20, e12857. https://doi.org/10.1111/CMI.12857

Al-Nedawi, K., Meehan, B., Micallef, J., Lhotak, V., May, L., Guha, A., Rak, J., 2008. Intercellular transfer of the oncogenic receptor EGFRvIII by microvesicles derived from tumour cells. Nat Cell Biol 10, 619–624. https://doi.org/10.1038/ncb1725

Archer, T.C., Mahoney, E.L., Pomeroy, S.L., 2017. Medulloblastoma: Molecular Classification-Based Personal Therapeutics. Neurotherapeutics. https://doi.org/10.1007/s13311-017-0526-y

Armingol, E., Officer, A., Harismendy, O., Lewis, N.E., 2020. Deciphering cell–cell interactions and communication from gene expression. Nature Reviews Genetics 2020 22:2 22, 71–88. https://doi.org/10.1038/s41576-020-00292-x

Arya, S.B., Collie, S.P., Parent, C.A., 2024. The ins-and-outs of exosome biogenesis, secretion, and internalization. Trends Cell Biol 34, 90–108. https://doi.org/10.1016/J.TCB.2023.06.006

Bachir, A.I., Horwitz, A.R., Nelson, W.J., Bianchini, J.M., 2017. Actin-Based Adhesion Modules Mediate Cell Interactions with the Extracellular Matrix and Neighboring Cells. Cold Spring Harb Perspect Biol 9. https://doi.org/10.1101/CSHPERSPECT.A023234

Bai, S., Hou, W., Yao, Y., Meng, J., Wei, Y., Hu, F., Hu, X., Wu, J., Zhang, N., Xu, R., Tian, F., Wang, B., Liao, H., Du, Y., Fang, H., He, W., Liu, Y., Shen, B., Du, J., 2022a. Exocyst controls exosome biogenesis via Rab11a. Mol Ther Nucleic Acids 27, 535. https://doi.org/10.1016/J.OMTN.2021.12.023

Bai, S., Hou, W., Yao, Y., Meng, J., Wei, Y., Hu, F., Hu, X., Wu, J., Zhang, N., Xu, R., Tian, F., Wang, B., Liao, H., Du, Y., Fang, H., He, W., Liu, Y., Shen, B., Du, J., 2022b. Exocyst controls exosome biogenesis via Rab11a. Molecular Therapy: Nucleic Acid 27, 535–546. https://doi.org/10.1016/j.omtn.2021.12.023

Baietti, M.F., Zhang, Z., Mortier, E., Melchior, A., Degeest, G., Geeraerts, A., Ivarsson, Y., Depoortere, F., Coomans, C., Vermeiren, E., Zimmermann, P., David, G., 2012. Syndecan-syntenin-ALIX regulates the biogenesis of exosomes. Nat Cell Biol 14, 677–685. https://doi.org/10.1038/ncb2502

Bailey, C.C., Gnekow, A., Wellek, S., Jones, M., Round, C., Brown, J., Phillips, A., Neidhardt, M.K., 1995. Prospective randomised trial of chemotherapy given before radiotherapy in childhood medulloblastoma. International society of paediatric oncology (SIOP) and the (German) society of paediatric oncology (GPO): SIOP II. Med Pediatr Oncol 25, 166–178. https://doi.org/10.1002/mpo.2950250303

Bakhshinyan, D., Suk, Y., Kuhlman, L., Adile, A.A., Ignatchenko, V., Custers, S., Gwynne, W.D., Mackling, A., Venugopal, C., Kislinger, T., Singh, S.K., 2023. Dynamic profiling of medulloblastoma surfaceome. Acta Neuropathol Commun 11, 1–14. https://doi.org/10.1186/S40478-023-01609-7/FIGURES/5

Bale, S.J., Falk, R.T., Rogers, G.R., 1998. Patching Together the Genetics of Gorlin Syndrome. https://doi.org/10.1177/120347549800300109 3, 31–34. https://doi.org/10.1177/120347549800300109

Barr, F., Lambright, D.G., 2010. Rab GEFs and GAPs. Curr Opin Cell Biol 22, 461. https://doi.org/10.1016/J.CEB.2010.04.007

Bayraktar, R., Van Roosbroeck, K., Calin, G.A., 2017. Cell-to-cell communication: microRNAs as hormones. Mol Oncol 11, 1673. https://doi.org/10.1002/1878-0261.12144

Beier, H., Grimm, M., 2001. Misreading of termination codons in eukaryotes by natural nonsense suppressor tRNAs. Nucleic Acids Res 29, 4767–4782. https://doi.org/10.1093/NAR/29.23.4767

Bisaro, B., Mandili, G., Poli, A., Piolatto, A., Papa, V., Novelli, F., Cenacchi, G., Forni, M., Zanini, C., 2015a. Proteomic analysis of extracellular vesicles from medullospheres reveals a role for iron in the cancer progression of medulloblastoma. Mol Cell Ther 3. https://doi.org/10.1186/s40591-015-0045-3

Bisaro, B., Mandili, G., Poli, A., Piolatto, A., Papa, V., Novelli, F., Cenacchi, G., Forni, M., Zanini, C., 2015b. Proteomic analysis of extracellular vesicles from medullospheres reveals a role for iron in the cancer progression of medulloblastoma. https://doi.org/10.1186/s40591-015-0045-3

Biziaev, N., Sokolova, E., Yanvarev, D. V., Toropygin, I.Y., Shuvalov, A., Egorova, T., Alkalaeva, E., 2022. Recognition of 3′ nucleotide context and stop codon readthrough are determined during mRNA translation elongation. J Biol Chem 298. https://doi.org/10.1016/J.JBC.2022.102133

Blanc, L., Vidal, M., 2018. New insights into the function of Rab GTPases in the context of exosomal secretion. Small GTPases. https://doi.org/10.1080/21541248.2016.1264352

Bobrie, A., Krumeich, S., Reyal, F., Recchi, C., Moita, L.F., Seabra, M.C., Ostrowski, M., Théry, C., 2012. Rab27a supports exosome-dependent and -independent mechanisms that modify the tumor microenvironment and can promote tumor progression. Cancer Res 72, 4920–4930. https://doi.org/10.1158/0008-5472.CAN-12-0925/650455/AM/RAB27A-SUPPORTS-EXOSOME-DEPENDENT-AND-INDEPENDENT

Bravo-Cordero, J.J., Marrero-Diaz, R., Megías, D., Genís, L., García-Grande, A., García, M.A., Arroyo, A.G., Montoya, M.C., 2007. MT1-MMP proinvasive activity is regulated by a novel Rab8-dependent exocytic pathway. EMBO Journal 26, 1499–1510. https://doi.org/10.1038/sj.emboj.7601606

Carroll, K.S., Hanna, J., Simon, I., Krise, J., Barbero, P., Pfeffer, S.R., 2001. Role of Rab9 GTPase in facilitating receptor recruitment by TIP47. Science (1979) 292, 1373–1376. https://doi.org/10.1126/science.1056791

Casanova, J.E., Wang, X., Kumar, R., Bhartur, S.G., Navarre, J., Woodrum, J.E., Altschuler, Y., Ray, G.S., Goldenring, J.R., 1999. Association of Rab25 and Rab11a with the Apical Recycling System of Polarized Madin–Darby Canine Kidney Cells. Mol Biol Cell 10, 47. https://doi.org/10.1091/MBC.10.1.47

Caswell, P.T., Spence, H.J., Parsons, M., White, D.P., Clark, K., Cheng, K.W., Mills, G.B., Humphries, M.J., Messent, A.J., Anderson, K.I., McCaffrey, M.W., Ozanne, B.W., Norman, J.C., 2007. Rab25 Associates with α5β1 Integrin to Promote Invasive Migration in 3D Microenvironments. Dev Cell 13, 496–510. https://doi.org/10.1016/J.DEVCEL.2007.08.012

Cavalli, F.M.G., Remke, M., Rampasek, L., Peacock, J., Shih, D.J.H., Luu, B., Garzia, L., Torchia, J., Nor, C., Morrissy, A.S., Agnihotri, S., Thompson, Y.Y., Kuzan-Fischer, C.M., Farooq, H., Isaev, K., Daniels, C., Cho, B.K., Kim, S.K., Wang, K.C., Lee, J.Y., Grajkowska, W.A., Perek-Polnik, M., Vasiljevic, A., Faure-Conter, C., Jouvet, A., Giannini, C., Nageswara Rao, A.A., Li, K.K.W., Ng, H.K.,

Eberhart, C.G., Pollack, I.F., Hamilton, R.L., Gillespie, G.Y., Olson, J.M., Leary, S., Weiss, W.A., Lach, B., Chambless, L.B., Thompson, R.C., Cooper, M.K., Vibhakar, R., Hauser, P., van Veelen, M.L.C., Kros, J.M., French, P.J., Ra, Y.S., Kumabe, T., López-Aguilar, E., Zitterbart, K., Sterba, J., Finocchiaro, G., Massimino, M., Van Meir, E.G., Osuka, S., Shofuda, T., Klekner, A., Zollo, M., Leonard, J.R., Rubin, J.B., Jabado, N., Albrecht, S., Mora, J., Van Meter, T.E., Jung, S., Moore, A.S., Hallahan, A.R., Chan, J.A., Tirapelli, D.P.C., Carlotti, C.G., Fouladi, M., Pimentel, J., Faria, C.C., Saad, A.G., Massimi, L., Liau, L.M., Wheeler, H., Nakamura, H., Elbabaa, S.K., Perezpeña-Diazconti, M., Chico Ponce de León, F., Robinson, S., Zapotocky, M., Lassaletta, A., Huang, A., Hawkins, C.E., Tabori, U., Bouffet, E., Bartels, U., Dirks, P.B., Rutka, J.T., Bader, G.D., Reimand, J., Goldenberg, A., Ramaswamy, V., Taylor, M.D., 2017a. Intertumoral Heterogeneity within Medulloblastoma Subgroups. Cancer Cell 31, 737-754.e6. https://doi.org/10.1016/j.ccell.2017.05.005

Cavalli, F.M.G., Remke, M., Rampasek, L., Peacock, J., Shih, D.J.H., Luu, B., Garzia, L., Torchia, J., Nor, C., Morrissy, A.S., Agnihotri, S., Thompson, Y.Y., Kuzan-Fischer, C.M., Farooq, H., Isaev, K., Daniels, C., Cho, B.K., Kim, S.K., Wang, K.C., Lee, J.Y., Grajkowska, W.A., Perek-Polnik, M., Vasiljevic, A., Faure-Conter, C., Jouvet, A., Giannini, C., Nageswara Rao, A.A., Li, K.K.W., Ng, H.K., Eberhart, C.G., Pollack, I.F., Hamilton, R.L., Gillespie, G.Y., Olson, J.M., Leary, S., Weiss, W.A., Lach, B., Chambless, L.B., Thompson, R.C., Cooper, M.K., Vibhakar, R., Hauser, P., van Veelen, M.L.C., Kros, J.M., French, P.J., Ra, Y.S., Kumabe, T., López-Aguilar, E., Zitterbart, K., Sterba, J., Finocchiaro, G., Massimino, M., Van Meir, E.G., Osuka, S., Shofuda, T., Klekner, A., Zollo, M., Leonard, J.R., Rubin, J.B., Jabado, N., Albrecht, S., Mora, J., Van Meter, T.E., Jung, S., Moore, A.S., Hallahan, A.R., Chan, J.A., Tirapelli, D.P.C., Carlotti, C.G., Fouladi, M., Pimentel, J., Faria, C.C., Saad, A.G., Massimi, L., Liau, L.M., Wheeler, H., Nakamura, H., Elbabaa, S.K., Perezpeña-Diazconti, M., Chico Ponce de León, F., Robinson, S., Zapotocky, M., Lassaletta, A., Huang, A., Hawkins, C.E., Tabori, U., Bouffet, E., Bartels, U., Dirks, P.B., Rutka, J.T., Bader, G.D., Reimand, J., Goldenberg, A., Ramaswamy, V., Taylor, M.D., 2017b. Intertumoral Heterogeneity within Medulloblastoma Subgroups. Cancer Cell 31, 737-754.e6. https://doi.org/10.1016/j.ccell.2017.05.005

Cervenakova, L., Saá, P., Yakovleva, O., Vasilyeva, I., de Castro, J., Brown, P., Dodd, R., 2016. Are prions transported by plasma exosomes? Transfusion and Apheresis Science. https://doi.org/10.1016/j.transci.2016.07.013

Chalmin, F., Ladoire, S., Mignot, G., Vincent, J., Bruchard, M., Remy-Martin, J.P., Boireau, W., Rouleau, A., Simon, B., Lanneau, D., De Thonel, A., Multhoff, G., Hamman, A., Martin, F., Chauffert, B., Solary, E., Zitvogel, L., Garrido, C., Ryffel, B., Borg, C., Apetoh, L., Rébé, C., Ghiringhelli, F., 2010. Membrane-associated Hsp72 from tumor-derived exosomes mediates STAT3-dependent immunosuppressive function of mouse and human myeloid-derived suppressor cells. Journal of Clinical Investigation 120, 457–471. https://doi.org/10.1172/JCI40483

Chang, C.H., Housepian, E.M., Herbert, C., 1969. An operative staging system and a megavoltage radiotherapeutic technic for cerebellar medulloblastomas. Radiology 93, 1351–1359. https://doi.org/10.1148/93.6.1351

Chari, A., Golas, M.M., Klingenhäger, M., Neuenkirchen, N., Sander, B., Englbrecht, C., Sickmann, A., Stark, H., Fischer, U., 2008. An Assembly Chaperone Collaborates with the SMN Complex to Generate Spliceosomal SnRNPs. Cell 135, 497–509. https://doi.org/10.1016/J.CELL.2008.09.020

Chavrier, P., Parton, R.G., Hauri, H.P., Simons, K., Zerial, M., 1990. Localization of low molecular weight GTP binding proteins to exocytic and endocytic compartments. Cell 62, 317–329. https://doi.org/10.1016/0092-8674(90)90369-P

Cheng, K.W., Agarwal, R., Mitra, S., Lee, J.S., Carey, M., Gray, J.W., Mills, G.B., 2012. Rab25 increases cellular ATP and glycogen stores protecting cancer cells from bioenergetic stress. EMBO Mol Med 4, 125. https://doi.org/10.1002/EMMM.201100193

Chevignard, M., Câmara-Costa, H., Doz, F., Dellatolas, G., 2017. Core deficits and quality of survival after childhood medulloblastoma: a review. Neurooncol Pract 4, 82. https://doi.org/10.1093/NOP/NPW013

Childhood cancer – IARC [WWW Document], n.d. URL https://www.iarc.who.int/cancer-type/childhood-cancer/ (accessed 3.21.24).

Chung, Y.C., Wei, W.C., Hung, C.N., Kuo, J.F., Hsu, C.P., Chang, K.J., Chao, W.T., 2016. Rab11 collaborates E-cadherin to promote collective cell migration and indicates a poor prognosis in colorectal carcinoma. Eur J Clin Invest 46, 1002–1011. https://doi.org/10.1111/ECI.12683

Clark, A.R., Calligaris, D., Regan, M.S., Pomeranz Krummel, D., Agar, J.N., Kallay, L., MacDonald, T., Schniederjan, M., Santagata, S., Pomeroy, S.L., Agar, N.Y.R., Sengupta, S., 2018. Rapid discrimination of pediatric brain tumors by mass spectrometry imaging. J Neurooncol 140, 269. https://doi.org/10.1007/S11060-018-2978-2

Clifford, S.C., Lusher, M.E., Lindsey, J.C., Langdon, J.A., Gilbertson, R.J., Straughton, D., Ellison, D.W., 2006. Wnt/Wingless pathway activation and chromosome 6 loss characterize a distinct molecular sub-group of medulloblastomas associated with a favorable prognosis. Cell Cycle 5, 2666–2670. https://doi.org/10.4161/CC.5.22.3446

Cocucci, E., Meldolesi, J., 2015. Ectosomes and exosomes: shedding the confusion between extracellular vesicles. Trends Cell Biol 25, 364–372. https://doi.org/10.1016/J.TCB.2015.01.004

Cocucci, E., Meldolesi, J., 2011. Ectosomes. Current Biology 21, R940–R941. https://doi.org/10.1016/J.CUB.2011.10.011

Cocucci, E., Racchetti, G., Meldolesi, J., 2009. Shedding microvesicles: artefacts no more. Trends Cell Biol 19, 43–51. https://doi.org/10.1016/J.TCB.2008.11.003

Cohen, S.B., 1982. Familial polyposis coli and its extracolonic manifestations. J Med Genet 19, 193–203. https://doi.org/10.1136/jmg.19.3.193

Colombo, M., Moita, C., Van Niel, G., Kowal, J., Vigneron, J., Benaroch, P., Manel, N., Moita, L.F., Théry, C., Raposo, G., 2013. Analysis of ESCRT functions in exosome biogenesis, composition and secretion highlights the heterogeneity of extracellular vesicles. J Cell Sci 126, 5553–5565. https://doi.org/10.1242/jcs.128868

Colombo, M., Raposo, G., Théry, C., 2014. Biogenesis, Secretion, and Intercellular Interactions of Exosomes and Other Extracellular Vesicles. Annu Rev Cell Dev Biol 30, 255–289. https://doi.org/10.1146/annurev-cellbio-101512-122326

Coluccia, D., Figuereido, C., Isik, S., Smith, C., Rutka, J.T., 2016. Medulloblastoma: Tumor biology and relevance to treatment and prognosis paradigm. Curr Neurol Neurosci Rep. https://doi.org/10.1007/s11910-016-0644-7

Corcoran, C., Rani, S., O'Brien, K., O'Neill, A., Prencipe, M., Sheikh, R., Webb, G., McDermott, R., Watson, W., Crown, J., O'Driscoll, L., 2012. Docetaxel-Resistance in Prostate Cancer: Evaluating Associated Phenotypic Changes and Potential for Resistance Transfer via Exosomes. PLoS One 7. https://doi.org/10.1371/journal.pone.0050999

Crawford, J.R., MacDonald, T.J., Packer, R.J., 2007. Medulloblastoma in childhood: new biological advances. Lancet Neurology. https://doi.org/10.1016/S1474-4422(07)70289-2

Creighton, C.J., Bromberg-White, J.L., Misek, D.E., Monsma, D.J., Brichory, F., Kuick, R., Giordano, T.J., Gao, W., Omenn, G.S., Webb, C.P., Hanash, S.M., 2005. Analysis of tumor-host interactions by gene expression profiling of lung adenocarcinoma xenografts identifies genes involved in tumor formation. Mol Cancer Res 3, 119–129. https://doi.org/10.1158/1541-7786.MCR-04-0189

Crescitelli, R., Lässer, C., Szabó, T.G., Kittel, A., Eldh, M., Dianzani, I., Buzás, E.I., Lötvall, J., 2013. Distinct RNA profiles in subpopulations of extracellular vesicles: apoptotic bodies, microvesicles and exosomes. J Extracell Vesicles 2. https://doi.org/10.3402/JEV.V2I0.20677

Cullen, P.J., Steinberg, F., 2018. To degrade or not to degrade: mechanisms and significance of endocytic recycling. Nature Reviews Molecular Cell Biology 2018 19:11 19, 679–696. https://doi.org/10.1038/s41580-018-0053-7

Dabrowski, M., Bukowy-Bieryllo, Z., Zietkiewicz, E., 2015. Translational readthrough potential of natural termination codons in eucaryotes – The impact of RNA sequence. RNA Biol 12, 950. https://doi.org/10.1080/15476286.2015.1068497

Dai, X., Ahn, K.S., Wang, L.Z., Kim, C., Deivasigamni, A., Arfuso, F., Um, J.Y., Kumar, A.P., Chang, Y.C., Kumar, D., Kundu, G.C., Magae, J., Goh, B.C., Hui, K.M., Sethi, G., 2016. Ascochlorin Enhances the Sensitivity of Doxorubicin Leading to the Reversal of Epithelial-to-Mesenchymal Transition in

Hepatocellular Carcinoma. Mol Cancer Ther 15, 2966–2976. https://doi.org/10.1158/1535-7163.MCT-16-0391

Davidson, G., Niehrs, C., 2010. Emerging links between CDK cell cycle regulators and Wnt signaling. Trends Cell Biol 20, 453–460. https://doi.org/10.1016/j.tcb.2010.05.002

Deatheragea, B.L., Cooksona, B.T., 2012. Membrane vesicle release in bacteria, eukaryotes, and archaea: A conserved yet underappreciated aspect of microbial life. Infect Immun. https://doi.org/10.1128/IAI.06014-11

Demir, K., Kirsch, N., Beretta, C.A., Erdmann, G., Ingelfinger, D., Moro, E., Argenton, F., Carl, M., Niehrs, C., Boutros, M., 2013. RAB8B Is Required for Activity and Caveolar Endocytosis of LRP6. Cell Rep 4, 1224–1234. https://doi.org/10.1016/j.celrep.2013.08.008

Deng, Z. Bin, Liu, Y., Liu, C., Xiang, X., Wang, J., Cheng, Z., Shah, S. V., Zhang, S., Zhang, L., Zhuang, X., Michalek, S., Grizzle, W.E., Zhang, H.G., 2009. Immature myeloid cells induced by a high-fat diet contribute to liver inflammation. Hepatology 50, 1412–1420. https://doi.org/10.1002/hep.23148

Diao, A., Frost, L., Morohashi, Y., Lowe, M., 2008. Coordination of Golgin Tethering and SNARE Assembly: GM130 BINDS SYNTAXIN 5 IN A p115-REGULATED MANNER. Journal of Biological Chemistry 283, 6957–6967. https://doi.org/10.1074/JBC.M708401200

Diao, B., Huang, X., Yang, C., Guo, S., Fei, L., Chen, Y., Wu, Y., 2016. Original Article Rab13 silencing causes inhibition of growth and induction of apoptosis in human glioma cells. Int J Clin Exp Pathol 9, 3007–3014.

Dolo, V., D'Ascenzo, S., Violini, S., Pompucci, L., Festuccia, C., Ginestra, A., Vittorelli, M.L., Canevari, S., Pavan, A., 1999. Matrix-degrading proteinases are shed in membrane vesicles by ovarian cancer cells in vivo and in vitro. Clin Exp Metastasis 17, 131–140. https://doi.org/10.1023/A:1006500406240

Dolo, V., Ginestra, A., Cassare, D., Violini, S., Lucania, G., Torrisi, M.R., Nagase, H., Canevari, S., Pavan, A., Vittorelli2, M.L., 1998. Selective Localization of Matrix Metalloproteinase 9, ÃŸ, Integrins, and Human Lymphocyte Antigen Class I Molecules on Membrane Vesicles Shed by 8701-BC Breast Carcinoma Cells1, CANCER RESEARCH.

Dong, H., Feng, Y., Yang, Y., Hu, Y., Jia, Y., Yang, S., Zhao, N., Zhao, R., 2021. A Novel Function of Mitochondrial Phosphoenolpyruvate Carboxykinase as a Regulator of Inflammatory Response in Kupffer Cells. Front Cell Dev Biol 9, 726931. https://doi.org/10.3389/FCELL.2021.726931/BIBTEX

Dong, Q., Fu, L., Zhao, Y., Du, Y., Li, Q., Qiu, X., Wang, E., 2017. Rab11a promotes proliferation and invasion through regulation of YAP in non-small cell lung cancer. Oncotarget 8, 27800–27811. https://doi.org/10.18632/oncotarget.15359

Dong, W., Qin, G., Shen, R., 2016. Rab11-FIP2 promotes the metastasis of gastric cancer cells. Int J Cancer 138, 1680–1688. https://doi.org/10.1002/IJC.29899

Doussouki, M. El, Gajjar, A., Chamdine, O., 2019. Molecular genetics of medulloblastoma in children: diagnostic, therapeutic and prognostic implications. Future Neurol 14, FNL8. https://doi.org/10.2217/fnl-2018-0030

Dufour, C., Beaugrand, A., Pizer, B., Micheli, J., Aubelle, M.S., Fourcade, A., Couanet, D., Laplanche, A., Kalifa, C., Grill, J., 2012. Metastatic medulloblastoma in childhood: Chang's classification revisited. Int J Surg Oncol 2012. https://doi.org/10.1155/2012/245385

Durcin, M., Fleury, A., Taillebois, E., Hilairet, G., Krupova, Z., Henry, C., Truchet, S., Trötzmüller, M., Köfeler, H., Mabilleau, G., Hue, O., Andriantsitohaina, R., Martin, P., Lay, S. Le, 2017. Characterisation of adipocyte-derived extracellular vesicle subtypes identifies distinct protein and lipid signatures for large and small extracellular vesicles. J Extracell Vesicles 6. https://doi.org/10.1080/20013078.2017.1305677

Dvorak, H.F., 2015. Tumors: Wounds that do not heal-redux. Cancer Immunol Res 3, 1–11. https://doi.org/10.1158/2326-6066.CIR-14-0209

Eberhart, C.G., Kepner, J.L., Goldthwaite, P.T., Kun, L.E., Duffner, P.K., Friedman, H.S., Strother, D.R., Burger, P.C., 2002. Histopathologic grading of medulloblastomas: a Pediatric Oncology Group study. Cancer 94, 552–560. https://doi.org/10.1002/CNCR.10189

Eberhart, C.G., Tihan, T., Burger, P.C., 2000. Nuclear Localization and Mutation of β-Catenin in Medulloblastomas. J Neuropathol Exp Neurol 59, 333–337. https://doi.org/10.1093/jnen/59.4.333

Eggenschwiler, J.T., Espinoza, E., Anderson, K. V., 2001. Rab23 is an essential negative regulator of the mouse Sonic hedgehog signalling pathway. Nature 412, 194–198. https://doi.org/10.1038/35084089

El Andaloussi, S., Mäger, I., Breakefield, X.O., Wood, M.J.A., 2013. Extracellular vesicles: biology and emerging therapeutic opportunities. Nature Reviews Drug Discovery 2013 12:5 12, 347–357. https://doi.org/10.1038/nrd3978

Ellison, D.W., Dalton, J., Kocak, M., Nicholson, S.L., Fraga, C., Neale, G., Kenney, A.M., Brat, D.J., Perry, A., Yong, W.H., Taylor, R.E., Bailey, S., Clifford, S.C., Gilbertson, R.J., 2011a. Medulloblastoma: Clinicopathological correlates of SHH, WNT, and non-SHH/WNT molecular subgroups. Acta Neuropathol 121, 381–396. https://doi.org/10.1007/s00401-011-0800-8

Ellison, D.W., Dalton, J., Kocak, M., Nicholson, S.L., Fraga, C., Neale, G., Kenney, A.M., Brat, D.J., Perry, A., Yong, W.H., Taylor, R.E., Bailey, S., Clifford, S.C., Gilbertson, R.J., 2011b. Medulloblastoma: Clinicopathological correlates of SHH, WNT, and non-SHH/WNT molecular subgroups. Acta Neuropathol 121, 381–396. https://doi.org/10.1007/s00401-011-0800-8

Epple, L.M., Griffiths, S.G., Dechkovskaia, A.M., Dusto, N.L., White, J., Ouellette, R.J., Anchordoquy, T.J., Bemis, L.T., Graner, M.W., 2012. Medulloblastoma

exosome proteomics yield functional roles for extracellular vesicles. PLoS One 7. https://doi.org/10.1371/journal.pone.0042064

Evans, G., Burnell, L., Campbell, R., Gattamaneni, H.R., Birch, J., 1993. Congenital anomalies and genetic syndromes in 173 cases of medulloblastoma. Med Pediatr Oncol 21, 433–434. https://doi.org/10.1002/mpo.2950210608

Fabbri, M., Paone, A., Calore, F., Galli, R., Gaudio, E., Santhanam, R., Lovat, F., Fadda, P., Mao, C., Nuovo, G.J., Zanesi, N., Crawford, M., Ozer, G.H., Wernicke, D., Alder, H., Caligiuri, M.A., Nana-Sinkam, P., Perrotti, D., Croce, C.M., 2012. MicroRNAs bind to Toll-like receptors to induce prometastatic inflammatory response. Proc Natl Acad Sci U S A 109, E2110. https://doi.org/10.1073/pnas.1209414109

Fearon, K., Mcclendon, V., Bonetti, B., Bedwell$, D.M., 1994. THE JOURNAl. OF BIOl.OGICAl. CHEMISTRY Premature Translation Termination Mutations Are Efficiently Suppressed in a Highly Conserved Region of Yeast SteGp, a Member of the ATP-binding Cassette (ABC) Transporter Family* 269, 17802–17808. https://doi.org/10.1016/S0021-9258(17)32379-7

Fidler, I.J., 2003. The pathogenesis of cancer metastasis: The "seed and soil" hypothesis revisited. Nat Rev Cancer. https://doi.org/10.1038/nrc1098

Forget, A., Martignetti, L., Barillot, E., Remke, M., Ayrault, O., 2018. Aberrant ERBB4-SRC Signaling as a Hallmark of Group 4 Medulloblastoma Revealed by Integrative Phosphoproteomic Profiling. Cancer Cell 34, 379-395.e7. https://doi.org/10.1016/j.ccell.2018.08.002

Formentin, C., Joaquim, A.F., Ghizoni, E., 2023. Posterior fossa tumors in children: current insights. European Journal of Pediatrics 2023 182:11 182, 4833–4850. https://doi.org/10.1007/S00431-023-05189-5

Fröhlich, D., Kuo, W.P., Frühbeis, C., Sun, J.J., Zehendner, C.M., Luhmann, H.J., Pinto, S., Toedling, J., Trotter, J., Krämer-Albers, E.M., 2014. Multifaceted effects of oligodendroglial exosomes on neurons: Impact on neuronal firing rate, signal transduction and gene regulation. Philosophical Transactions of the Royal Society B: Biological Sciences 369. https://doi.org/10.1098/rstb.2013.0510

Frühbeis, C., Fröhlich, D., Kuo, W.P., Amphornrat, J., Thilemann, S., Saab, A.S., Kirchhoff, F., Möbius, W., Goebbels, S., Nave, K.A., Schneider, A., Simons, M., Klugmann, M., Trotter, J., Krämer-Albers, E.M., 2013. Neurotransmitter-Triggered Transfer of Exosomes Mediates Oligodendrocyte-Neuron Communication. PLoS Biol 11. https://doi.org/10.1371/journal.pbio.1001604

Fukuda, M., 2011. TBC proteins: GAPs for mammalian small GTPase Rab? Biosci Rep 31, 159–168. https://doi.org/10.1042/BSR20100112

Funke, V.L.E., Walter, C., Melcher, V., Wei, L., Sandmann, S., Hotfilder, M., Varghese, J., Jäger, N., Kool, M., Jones, D.T.W., Pfister, S.M., Milde, T., Mynarek, M., Rutkowski, S., Seggewiss, J., Jeising, D., de Faria, F.W., Marquardt, T., Albert, T.K., Schüller, U., Kerl, K., 2023. Group-specific cellular

metabolism in Medulloblastoma. J Transl Med 21, 1–16. https://doi.org/10.1186/S12967-023-04211-6/FIGURES/5

Gajjar, A., Chintagumpala, M., Ashley, D., Kellie, S., Kun, L.E., Merchant, T.E., Woo, S., Wheeler, G., Ahern, V., Krasin, M.J., Fouladi, M., Broniscer, A., Krance, R., Hale, G.A., Stewart, C.F., Dauser, R., Sanford, R.A., Fuller, C., Lau, C., Boyett, J.M., Wallace, D., Gilbertson, R.J., 2006. Risk-adapted craniospinal radiotherapy followed by high-dose chemotherapy and stem-cell rescue in children with newly diagnosed medulloblastoma (St Jude Medulloblastoma-96): long-term results from a prospective, multicentre trial. Lancet Oncology 7, 813–820. https://doi.org/10.1016/S1470-2045(06)70867-1

Gajjar, A.J., Robinson, G.W., 2014. Medulloblastoma - Translating discoveries from the bench to the bedside. Nat Rev Clin Oncol. https://doi.org/10.1038/nrclinonc.2014.181

Gandola, L., Massimino, M., Cefalo, G., Solero, C., Spreafico, F., Pecori, E., Riva, D., Collini, P., Pignoli, E., Giangaspero, F., Luksch, R., Berretta, S., Poggi, G., Biassoni, V., Ferrari, A., Pollo, B., Favre, C., Sardi, I., Terenziani, M., Fossati-Bellani, F., 2009. Hyperfractionated accelerated radiotherapy in the Milan strategy for metastatic medulloblastoma. J Clin Oncol 27, 566–71. https://doi.org/10.1200/JCO.2008.18.4176

Gao, F., Fan, Y., Zhou, B., Guo, W., Jiang, X., Shi, J., Ren, C., 2020. The functions and properties of cullin-5, a potential therapeutic target for cancers. Am J Transl Res 12, 618.

Garzia, L., Kijima, N., Morrissy, A.S., De Antonellis, P., Guerreiro-Stucklin, A., Holgado, B.L., Wu, X., Wang, X., Parsons, M., Zayne, K., Manno, A., Kuzan-Fischer, C., Nor, C., Donovan, L.K., Liu, J., Qin, L., Garancher, A., Liu, K.W., Mansouri, S., Luu, B., Thompson, Y.Y., Ramaswamy, V., Peacock, J., Farooq, H., Skowron, P., Shih, D.J.H., Li, A., Ensan, S., Robbins, C.S., Cybulsky, M., Mitra, S., Ma, Y., Moore, R., Mungall, A., Cho, Y.J., Weiss, W.A., Chan, J.A., Hawkins, C.E., Massimino, M., Jabado, N., Zapotocky, M., Sumerauer, D., Bouffet, E., Dirks, P., Tabori, U., Sorensen, P.H.B., Brastianos, P.K., Aldape, K., Jones, S.J.M., Marra, M.A., Woodgett, J.R., Wechsler-Reya, R.J., Fults, D.W., Taylor, M.D., 2018. A Hematogenous Route for Medulloblastoma Leptomeningeal Metastases. Cell 172, 1050-1062.e14. https://doi.org/10.1016/j.cell.2018.01.038

Ge, J., Chen, Q., Liu, B., Wang, L., Zhang, S., Ji, B., 2017. Knockdown of Rab21 inhibits proliferation and induces apoptosis in human glioma cells. Cell Mol Biol Lett 22. https://doi.org/10.1186/S11658-017-0062-0

Gerashchenko, M. V., Lobanov, A. V., Gladyshev, V.N., 2012. Genome-wide ribosome profiling reveals complex translational regulation in response to oxidative stress. Proc Natl Acad Sci U S A 109, 17394–17399. https://doi.org/10.1073/PNAS.1120799109/-/DCSUPPLEMENTAL

Ghosh, R., Gilda, J.E., Gomes, A. V., 2014. The necessity of and strategies for improving confidence in the accuracy of western blots. Expert Rev Proteomics 11, 549. https://doi.org/10.1586/14789450.2014.939635

Gibson, P., Tong, Y., Robinson, G., Thompson, M.C., Currle, D.S., Eden, C., Kranenburg, T.A., Hogg, T., Poppleton, H., Martin, J., Finkelstein, D., Pounds, S., Weiss, A., Patay, Z., Scoggins, M., Ogg, R., Pei, Y., Yang, Z.J., Brun, S., Lee, Y., Zindy, F., Lindsey, J.C., Taketo, M.M., Boop, F.A., Sanford, R.A., Gajjar, A., Clifford, S.C., Rousse, M.F., McKinnon, P.J., Gutmann, D.H., Ellison, D.W., Wechsler-Reya, R., Gilbertson, R.J., 2010. Subtypes of medulloblastoma have distinct developmental origins. Nature 468, 1095. https://doi.org/10.1038/NATURE09587

Gilbertson, R.J., Ellison, D.W., 2008. The Origins of Medulloblastoma Subtypes. Annual Review of Pathology: Mechanisms of Disease 3, 341–365. https://doi.org/10.1146/annurev.pathmechdis.3.121806.151518

Gillet, L.C., Navarro, P., Tate, S., Röst, H., Selevsek, N., Reiter, L., Bonner, R., Aebersold, R., 2012. Targeted data extraction of the MS/MS spectra generated by data-independent acquisition: a new concept for consistent and accurate proteome analysis. Mol Cell Proteomics 11. https://doi.org/10.1074/MCP.O111.016717

Gillingham, A.K., Sinka, R., Torres, I.L., Lilley, K.S., Munro, S., 2014a. Toward a Comprehensive Map of the Effectors of Rab GTPases. Dev Cell 31, 358. https://doi.org/10.1016/j.devcel.2014.10.007

Gillingham, A.K., Sinka, R., Torres, I.L., Lilley, K.S., Munro, S., 2014b. Toward a Comprehensive Map of the Effectors of Rab GTPases. Dev Cell 31, 358–373. https://doi.org/10.1016/J.DEVCEL.2014.10.007

Giordana, M.T., Schiffer, P., Lanotte, M., Girardi, P., Chio, A., 1999. Epidemiology of adult medulloblastoma. Int J Cancer 80, 689–692. https://doi.org/10.1002/(SICI)1097-0215(19990301)80:5<689::AID-IJC10>3.0.CO;2-G

Gowrishankar, S., Cologna, S.M., Givogri, M.I., Bongarzone, E.R., 2020. Deregulation of signalling in genetic conditions affecting the lysosomal metabolism of cholesterol and galactosyl-sphingolipids. Neurobiol Dis 146, 105142. https://doi.org/10.1016/J.NBD.2020.105142

Grange, C., Tapparo, M., Collino, F., Vitillo, L., Damasco, C., Deregibus, M.C., Tetta, C., Bussolati, B., Camussi, G., 2011. Microvesicles released from human renal cancer stem cells stimulate angiogenesis and formation of lung premetastatic niche. Cancer Res 71, 5346–5356. https://doi.org/10.1158/0008-5472.CAN-11-0241

Graves, L.E., Ariztia, E. V., Navari, J.R., Matzel, H.J., Stack, M.S., Fishman, D.A., 2004. Proinvasive properties of ovarian cancer ascites-derived membrane vesicles. Cancer Res 64, 7045–7049. https://doi.org/10.1158/0008-5472.CAN-04-1800

Grill, J., Sainte-Rose, C., Jouvet, A., Gentet, J.C., Lejars, O., Frappaz, D., Doz, F., Rialland, X., Pichon, F., Bertozzi, A.I., Chastagner, P., Couanet, D., Habrand, J.L., Raquin, M.A., Le Deley, M.C., Kalifa, C., 2005. Treatment of medulloblastoma with postoperative chemotherapy alone: An SFOP prospective trial in young children. Lancet Oncology 6, 573–580. https://doi.org/10.1016/S1470-2045(05)70252-7

Grimmelikhuijzen, C.J.P., Hauser, F., 2012. Mini-review: The evolution of neuropeptide signaling. Regul Pept. https://doi.org/10.1016/j.regpep.2012.05.001

Grivennikov, S.I., Greten, F.R., Karin, M., 2010. Immunity, Inflammation, and Cancer. Cell. https://doi.org/10.1016/j.cell.2010.01.025

Guise, T., 2010. Examining the metastatic niche: targeting the microenvironment. Semin Oncol. https://doi.org/10.1053/j.seminoncol.2010.10.007

Guo, D., Lui, G.Y.L., Lai, S.L., Wilmott, J.S., Tikoo, S., Jackett, L.A., Quek, C., Brown, D.L., Sharp, D.M., Kwan, R.Y.Q., Chacon, D., Wong, J.H., Beck, D., van Geldermalsen, M., Holst, J., Thompson, J.F., Mann, G.J., Scolyer, R.A., Stow, J.L., Weninger, W., Haass, N.K., Beaumont, K.A., 2019. RAB27A promotes melanoma cell invasion and metastasis via regulation of pro-invasive exosomes. Int J Cancer 144, 3070–3085. https://doi.org/10.1002/ijc.32064

Gupta, S., Knowlton, A.A., 2007. HSP60 trafficking in adult cardiac myocytes: Role of the exosomal pathway. Am J Physiol Heart Circ Physiol 292. https://doi.org/10.1152/ajpheart.01355.2006

Gurung, S., Perocheau, D., Touramanidou, L., Baruteau, J., 2021. The exosome journey: from biogenesis to uptake and intracellular signalling. Cell Communication and Signaling 2021 19:1 19, 1–19. https://doi.org/10.1186/S12964-021-00730-1

György, B., Szabó, T.G., Pásztói, M., Pál, Z., Misják, P., Aradi, B., László, V., Pállinger, É., Pap, E., Kittel, Á., Nagy, G., Falus, A., Buzás, E.I., 2011. Membrane vesicles, current state-of-the-art: Emerging role of extracellular vesicles. Cellular and Molecular Life Sciences. https://doi.org/10.1007/s00018-011-0689-3

Haas, A.K., Yoshimura, S.I., Stephens, D.J., Preisinger, C., Fuchs, E., Barr, F.A., 2007. Analysis of GTPase-activating proteins: Rab1 and Rab43 are key Rabs required to maintain a functional Golgi complex in human cells. J Cell Sci 120, 2997–3010. https://doi.org/10.1242/jcs.014225

Haider, T., Pandey, V., Nagma Banjare, ·, Gupta, P.N., Soni, V., 2020. Drug resistance in cancer: mechanisms and tackling strategies 1, 3. https://doi.org/10.1007/s43440-020-00138-7

Hakimi, P., Yang, J., Casadesus, G., Massillon, D., Tolentino-Silva, F., Nye, C.K., Cabrera, M.E., Hagen, D.R., Utter, C.B., Baghdy, Y., Johnson, D.H., Wilson, D.L., Kirwan, J.P., Kalhan, S.C., Hanson, R.W., 2007. Overexpression of the

Cytosolic Form of Phosphoenolpyruvate Carboxykinase (GTP) in Skeletal Muscle Repatterns Energy Metabolism in the Mouse. J Biol Chem 282, 32844. https://doi.org/10.1074/JBC.M706127200

Halkein, J., Tabruyn, S.P., Ricke-Hoch, M., Haghikia, A., Nguyen, N.Q.N., Scherr, M., Castermans, K., Malvaux, L., Lambert, V., Thiry, M., Sliwa, K., Noel, A., Martial, J.A., Hilfiker-Kleiner, D., Struman, I., 2013. MicroRNA-146a is a therapeutic target and biomarker for peripartum cardiomyopathy. Journal of Clinical Investigation 123, 2143–2154. https://doi.org/10.1172/JCI64365

Hanahan, D., 2022. Hallmarks of Cancer: New Dimensions. Cancer Discov 12, 31–46. https://doi.org/10.1158/2159-8290.CD-21-1059

Hanahan, D., Weinberg, R.A., 2011. Hallmarks of cancer: The next generation. Cell. https://doi.org/10.1016/j.cell.2011.02.013

Harding, C., Heuser, J., Stahl, P., 1983a. Receptor-mediated endocytosis of transferrin and recycling of the transferrin receptor in rat reticulocytes. J Cell Biol 97, 329–339. https://doi.org/10.1083/jcb.97.2.329

Harding, C., Heuser, J., Stahl, P., 1983b. Receptor-mediated endocytosis of transferrin and recycling of the transferrin receptor in rat reticulocytes. J Cell Biol 97, 329–339. https://doi.org/10.1083/jcb.97.2.329

Harding, C. V., Heuser, J.E., Stahl, P.D., 2013. Exosomes: Looking back three decades and into the future. Journal of Cell Biology. https://doi.org/10.1083/jcb.201212113

Hartmann, A., Muth, C., Dabrowski, O., Krasemann, S., Glatzel, M., 2017. Exosomes and the prion protein: More than one truth. Front Neurosci. https://doi.org/10.3389/fnins.2017.00194

Hatten, M.E., Roussel, M.F., 2011. Development and cancer of the cerebellum. Trends Neurosci. https://doi.org/10.1016/j.tins.2011.01.002

He, L., Xu, Z., Yao, K., Wu, G., Yin, Y., Nyachoti, C., Kim, S., 2015. The Physiological Basis and Nutritional Function of Alpha-ketoglutarate. Curr Protein Pept Sci 16, 576–581. https://doi.org/10.2174/1389203716666150630140157

Heiden, M.G.V., Cantley, L.C., Thompson, C.B., 2009. Understanding the Warburg Effect: The Metabolic Requirements of Cell Proliferation. Science 324, 1029. https://doi.org/10.1126/SCIENCE.1160809

Hendrix, A., Ciccone, C., Gespach, C., Bracke, M., De, O., Westbroek, W., 2013. Rab27B-Mediated Metabolic Reprogramming Induces Secretome Acidification and Chemoresistance in Breast Cancer Cells. Exosomes Microvesicles 1. https://doi.org/10.5772/56521

Higgins, G.C., Coughlan, M.T., 2014. Mitochondrial dysfunction and mitophagy: the beginning and end to diabetic nephropathy? Br J Pharmacol 171, 1917. https://doi.org/10.1111/BPH.12503

Homma, Y., Hiragi, S., Fukuda, M., 2021. Rab family of small GTPases: an updated view on their regulation and functions. FEBS J 288, 36. https://doi.org/10.1111/FEBS.15453

Hood, J.L., San Roman, S., Wickline, S.A., 2011. Exosomes released by melanoma cells prepare sentinel lymph nodes for tumor metastasis. Cancer Res 71, 3792–3801. https://doi.org/10.1158/0008-5472.CAN-10-4455

Hopkins, A.L., Groom, C.R., 2002. The druggable genome. Nature Reviews Drug Discovery 2002 1:9 1, 727–730. https://doi.org/10.1038/nrd892

Hoshino, A., Costa-Silva, B., Shen, T.L., Rodrigues, G., Hashimoto, A., Tesic Mark, M., Molina, H., Kohsaka, S., Di Giannatale, A., Ceder, S., Singh, S., Williams, C., Soplop, N., Uryu, K., Pharmer, L., King, T., Bojmar, L., Davies, A.E., Ararso, Y., Zhang, T., Zhang, H., Hernandez, J., Weiss, J.M., Dumont-Cole, V.D., Kramer, K., Wexler, L.H., Narendran, A., Schwartz, G.K., Healey, J.H., Sandstrom, P., Jørgen Labori, K., Kure, E.H., Grandgenett, P.M., Hollingsworth, M.A., De Sousa, M., Kaur, S., Jain, M., Mallya, K., Batra, S.K., Jarnagin, W.R., Brady, M.S., Fodstad, O., Muller, V., Pantel, K., Minn, A.J., Bissell, M.J., Garcia, B.A., Kang, Y., Rajasekhar, V.K., Ghajar, C.M., Matei, I., Peinado, H., Bromberg, J., Lyden, D., 2015. Tumour exosome integrins determine organotropic metastasis. Nature 527, 329–335. https://doi.org/10.1038/nature15756

Hou, Q., Yong, H.W., Grabsch, H., Zhu, Y., Siew, H.L., Ganesan, K., Cross, D., Lay, K.T., Tao, J., Gopalakrishnan, V., Bor, L.T., Oi, L.K., Tan, P., 2008. Integrative genomics identifies RAB23 as an invasion mediator gene in diffuse-type gastric cancer. Cancer Res 68, 4623–4630. https://doi.org/10.1158/0008-5472.CAN-07-5870

Huang, W., Yan, Y., Liu, Y., Lin, M., Ma, J., Zhang, W., Dai, J., Li, J., Guo, Q., Chen, H., Makabel, B., Liu, H., Su, C., Bi, H., Zhang, J., 2020. Exosomes with low miR-34c-3p expression promote invasion and migration of non-small cell lung cancer by upregulating integrin α2β1. Signal Transduction and Targeted Therapy 2020 5:1 5, 1–13. https://doi.org/10.1038/s41392-020-0133-y

Hutagalung, A.H., Novick, P.J., 2011. Role of Rab GTPases in membrane traffic and cell physiology. Physiol Rev. https://doi.org/10.1152/physrev.00059.2009

Hyvola, N., Diao, A., McKenzie, E., Skippen, A., Cockcroft, S., Lowe, M., 2006. Membrane targeting and activation of the Lowe syndrome protein OCRL1 by rab GTPases. EMBO J 25, 3750. https://doi.org/10.1038/SJ.EMBOJ.7601274

Iero, M., Valenti, R., Huber, V., Filipazzi, P., Parmiani, G., Fais, S., Rivoltini, L., 2008. Tumour-released exosomes and their implications in cancer immunity. Cell Death Differ. https://doi.org/10.1038/sj.cdd.4402237

Ihara, T., Yamamoto, T., Sugamata, M., Okumura, H., Ueno, Y., 1998. The process of ultrastructural changes from nuclei to apoptotic body. Virchows Archiv 433, 443–447. https://doi.org/10.1007/S004280050272/METRICS

Isola, A., Chen, S., 2016. Exosomes: The Messengers of Health and Disease. Curr Neuropharmacol 15, 157–165. https://doi.org/10.2174/1570159x14666160825160421

Itoh, T., Satoh, M., Kanno, E., Fukuda, M., 2006. Screening for target Rabs of TBC (Tre-2/Bub2/Cdc16) domain-containing proteins based on their Rab-binding activity. Genes to Cells 11, 1023–1037. https://doi.org/10.1111/J.1365-2443.2006.00997.X

Jackson, H.K., 2021. Analysing the role of medulloblastoma exosomes as biomarkers and their functional contribution to metastasis. PhD thesis. University of Nottingham.

Jackson, H.K., Mitoko, C., Linke, F., Macarthur, D., Kerr, I.D., Coyle, B., 2023. Extracellular Vesicles Potentiate Medulloblastoma Metastasis in an EMMPRIN and MMP-2 Dependent Manner. Cancers (Basel) 15. https://doi.org/10.3390/CANCERS15092601/S1

Jacob, A., Jing, J., Lee, J., Schedin, P., Gilbert, S.M., Peden, A.A., Junutula, J.R., Prekeris, R., 2013a. Rab40b regulates trafficking of MMP2 and MMP9 during invadopodia formation and invasion of breast cancer cells. J Cell Sci 126, 4647–4658. https://doi.org/10.1242/jcs.126573

Jacob, A., Jing, J., Lee, J., Schedin, P., Gilbert, S.M., Peden, A.A., Junutula, J.R., Prekeris, R., 2013b. Rab40b regulates trafficking of MMP2 and MMP9 during invadopodia formation and invasion of breast cancer cells. J Cell Sci 126, 4647–4658. https://doi.org/10.1242/jcs.126573

Jacob, A., Linklater, E., Bayless, B.A., Lyons, T., Prekeris, R., 2016. The role and regulation of Rab40b-Tks5 complex during invadopodia formation and cancer cell invasion. J Cell Sci 129, 4341–4353. https://doi.org/10.1242/jcs.193904

Jadli, A.S., Ballasy, N., Edalat, P., Patel, V.B., 2020. Inside(sight) of tiny communicator: exosome biogenesis, secretion, and uptake. Mol Cell Biochem 467, 77–94. https://doi.org/10.1007/S11010-020-03703-Z

Jayasena, T., Poljak, A., Braidy, N., Zhong, L., Rowlands, B., Muenchhoff, J., Grant, R., Smythe, G., Teo, C., Raftery, M., Sachdev, P., 2016. Application of Targeted Mass Spectrometry for the Quantification of Sirtuins in the Central Nervous System. Scientific Reports 2016 6:1 6, 1–11. https://doi.org/10.1038/srep35391

Jeppesen, D.K., Zhang, Q., Franklin, J.L., Coffey, R.J., 2023. Extracellular vesicles and nanoparticles: emerging complexities. Trends Cell Biol 33, 667–681. https://doi.org/10.1016/J.TCB.2023.01.002

Jiang, X., Yang, L., Gao, Q., Liu, Y., Feng, X., Ye, S., Yang, Z., 2022. The Role of RAB GTPases and Its Potential in Predicting Immunotherapy Response and Prognosis in Colorectal Cancer. Front Genet 13, 60. https://doi.org/10.3389/FGENE.2022.828373/BIBTEX

Jin, J., Wu, Y., Zhou, D., Sun, Q., Wang, W., 2018. miR-448 targets Rab2B and is pivotal in the suppression of pancreatic cancer. Oncol Rep 40, 1379. https://doi.org/10.3892/OR.2018.6562

Johnson, J.E.C., 2023. Investigating the role of tumour-deposited extracellular matrix in medulloblastoma progression. PhD Thesis. University of Nottingham.

Johnston, D.L., Keene, D., Kostova, M., Strother, D., Lafay-Cousin, L., Fryer, C., Scheinemann, K., Carret, A.S., Fleming, A., Percy, V., Afzal, S., Wilson, B., Bowes, L., Zelcer, S., Mpofu, C., Silva, M., Larouche, V., Brossard, J., Bouffet, E., 2014. Incidence of medulloblastoma in Canadian children. J Neurooncol 120, 575–579. https://doi.org/10.1007/s11060-014-1588-x

Johnstone, R.M., Adam, M., Hammond, J.R., Orr, L., Turbide, C., 1987. Vesicle formation during reticulocyte maturation. Association of plasma membrane activities with released vesicles (exosomes). Journal of Biological Chemistry 262, 9412–9420.

Jones, D.T.W., Jäger, N., Kool, M., Zichner, T., Hutter, B., Sultan, M., Cho, Y.J., Pugh, T.J., Hovestadt, V., Stütz, A.M., Rausch, T., Warnatz, H.J., Ryzhova, M., Bender, S., Sturm, D., Pleier, S., Cin, H., Pfaff, E., Sieber, L., Wittmann, A., Remke, M., Witt, H., Hutter, S., Tzaridis, T., Weischenfeldt, J., Raeder, B., Avci, M., Amstislavskiy, V., Zapatka, M., Weber, U.D., Wang, Q., Lasitschka, B., Bartholomae, C.C., Schmidt, M., von Kalle, C., Ast, V., Lawerenz, C., Eils, J., Kabbe, R., Benes, V., van Sluis, P., Koster, J., Volckmann, R., Shih, D., Betts, M.J., Russell, R.B., Coco, S., Tonini, G.P., Schüller, U., Hans, V., Graf, N., Kim, Y.J., Monoranu, C., Roggendorf, W., Unterberg, A., Herold-Mende, C., Milde, T., Kulozik, A.E., von Deimling, A., Witt, O., Maass, E., Rössler, J., Ebinger, M., Schuhmann, M.U., Frühwald, M.C., Hasselblatt, M., Jabado, N., Rutkowski, S., von Bueren, A.O., Williamson, D., Clifford, S.C., Mc Cabe, M.G., Collins, V.P., Wolf, S., Wiemann, S., Lehrach, H., Brors, B., Scheurlen, W., Felsberg, J., Reifenberger, G., Northcott, P.A., Taylor, M.D., Meyerson, M., Pomeroy, S.L., Yaspo, M.L., Korbel, J.O., Korshunov, A., Eils, R., Pfister, S.M., Lichter, P., 2012. Dissecting the genomic complexity underlying medulloblastoma. Nature 488, 100–105. https://doi.org/10.1038/nature11284

Joyce, J.A., Pollard, J.W., 2009. Microenvironmental regulation of metastasis. Nat Rev Cancer. https://doi.org/10.1038/nrc2618

Kaminska, B., Czapski, B., Guzik, R., Król, S.K., Gielniewski, B., 2019. Consequences of IDH1/2 Mutations in Gliomas and an Assessment of Inhibitors Targeting Mutated IDH Proteins. Molecules 24. https://doi.org/10.3390/MOLECULES24050968

Kanehisa, M., Goto, S., 2000. KEGG: Kyoto Encyclopedia of Genes and Genomes. Nucleic Acids Res 28, 27. https://doi.org/10.1093/NAR/28.1.27

Kaufman, M.L., Goodson, N.B., Park, K.U., Schwanke, M., Office, E., Schneider, S.R., Abraham, J., Hensley, A., Jones, K.L., Brzezinski, J.A., 2021. Initiation of Otx2 expression in the developing mouse retina requires a unique enhancer and

either Ascl1 or Neurog2 activity. Development 148. https://doi.org/10.1242/DEV.199399

Kawauchi, D., Robinson, G., Uziel, T., Gibson, P., Rehg, J., Gao, C., Finkelstein, D., Qu, C., Pounds, S., Ellison, D.W., Gilbertson, R.J., Roussel, M.F., 2012. A mouse model of the most aggressive subgroup of human medulloblastoma. Cancer Cell 21, 168. https://doi.org/10.1016/J.CCR.2011.12.023

Keller, S., Ridinger, J., Rupp, A.K., Janssen, J.W.G., Altevogt, P., 2011. Body fluid derived exosomes as a novel template for clinical diagnostics. J Transl Med 9, 86. https://doi.org/10.1186/1479-5876-9-86

Kerleroux, B., Cottier, J.P., Janot, K., Listrat, A., Sirinelli, D., Morel, B., 2020. Posterior fossa tumors in children: Radiological tips & tricks in the age of genomic tumor classification and advance MR technology. Journal of Neuroradiology 47, 46–53. https://doi.org/10.1016/j.neurad.2019.08.002

Khorkova, O., Stahl, J., Joji, A., Volmar, C.H., Wahlestedt, C., 2023. Amplifying gene expression with RNA-targeted therapeutics. Nature Reviews Drug Discovery 2023 22:7 22, 539–561. https://doi.org/10.1038/s41573-023-00704-7

Kim, J.-K., Lee, S.-Y., Park, C.-W., Park, S.-H., Yin, J., Kim, J., Park, J.-B., Lee, J.-Y., Kim, H., Kim, S.-C., 2014. Rab3a promotes brain tumor initiation and progression. Mol Biol Rep 41, 5903–11. https://doi.org/10.1007/s11033-014-3465-2

Kim, K., Ka Ming Pang, Evans, M., Hay, E.D., 2000. Overexpression of β-Catenin Induces Apoptosis Independent of Its Transactivation Function with LEF-1 or the Involvement of Major G1 Cell Cycle Regulators. Mol Biol Cell 11, 3509. https://doi.org/10.1091/MBC.11.10.3509

Kim, S., Jeong, S., 2019. Mutation Hotspots in the β-Catenin Gene: Lessons from the Human Cancer Genome Databases. Mol Cells 42, 8. https://doi.org/10.14348/MOLCELLS.2018.0436

Kiral, F.R., Kohrs, F.E., Jin, E.J., Hiesinger, P.R., 2018. Rab GTPases and Membrane Trafficking in Neurodegeneration. Current Biology. https://doi.org/10.1016/j.cub.2018.02.010

Klionsky, D.J., Petroni, G., Amaravadi, R.K., Baehrecke, E.H., Ballabio, A., Boya, P., Pedro, J.M.B., Cadwell, K., Cecconi, F., Choi, A.M.K., Choi, M.E., Chu, C.T., Codogno, P., Colombo, M.I., Cuervo, A.M., Deretic, V., Dikic, I., Elazar, Z., Eskelinen, E., Fimia, G.M., Gewirtz, D.A., Green, D.R., Hansen, M., Jäättelä, M., Johansen, T., Juhász, G., Karantza, V., Kraft, C., Kroemer, G., Ktistakis, N.T., Kumar, S., Lopez-Otin, C., Macleod, K.F., Madeo, F., Martinez, J., Meléndez, A., Mizushima, N., Münz, C., Penninger, J.M., Perera, R.M., Piacentini, M., Reggiori, F., Rubinsztein, D.C., Ryan, K.M., Sadoshima, J., Santambrogio, L., Scorrano, L., Simon, H., Simon, A.K., Simonsen, A., Stolz, A., Tavernarakis, N., Tooze, S.A., Yoshimori, T., Yuan, J., Yue, Z., Zhong, Q., Galluzzi, L., Pietrocola, F., 2021. Autophagy in major human diseases. EMBO J 40, 108863. https://doi.org/10.15252/EMBJ.2021108863

Klöpper, T.H., Kienle, N., Fasshauer, D., Munro, S., 2012. Untangling the evolution of Rab G proteins: implications of a comprehensive genomic analysis. BMC Biol 10, 71. https://doi.org/10.1186/1741-7007-10-71

Koczkodaj, D., Muzyka-Kasietczuk, J., Chocholska, S., Podhorecka, M., 2021. Prognostic significance of isochromosome 17q in hematologic malignancies. Oncotarget 12, 708. https://doi.org/10.18632/ONCOTARGET.27914

Köhler, K., Louvard, D., Zahraoui, A., 2004. Rab13 regulates PKA signaling during tight junction assembly. Journal of Cell Biology 165, 175–180. https://doi.org/10.1083/jcb.200312118

Kool, M., Jones, D.T.W., Jäger, N., Northcott, P.A., Pugh, T.J., Hovestadt, V., Piro, R.M., Esparza, L.A., Markant, S.L., Remke, M., Milde, T., Bourdeaut, F., Ryzhova, M., Sturm, D., Pfaff, E., Stark, S., Hutter, S., Sxeker-Cin, H., Johann, P., Bender, S., Schmidt, C., Rausch, T., Shih, D., Reimand, J., Sieber, L., Wittmann, A., Linke, L., Witt, H., Weber, U.D., Zapatka, M., König, R., Beroukhim, R., Bergthold, G., Van Sluis, P., Volckmann, R., Koster, J., Versteeg, R., Schmidt, S., Wolf, S., Lawerenz, C., Bartholomae, C.C., Von Kalle, C., Unterberg, A., Herold-Mende, C., Hofer, S., Kulozik, A.E., Von Deimling, A., Scheurlen, W., Felsberg, J., Reifenberger, G., Hasselblatt, M., Crawford, J.R., Grant, G.A., Jabado, N., Perry, A., Cowdrey, C., Croul, S., Zadeh, G., Korbel, J.O., Doz, F., Delattre, O., Bader, G.D., McCabe, M.G., Collins, V.P., Kieran, M.W., Cho, Y.J., Pomeroy, S.L., Witt, O., Brors, B., Taylor, M.D., Schüller, U., Korshunov, A., Eils, R., Wechsler-Reya, R.J., Lichter, P., Pfister, S.M., 2014. Genome sequencing of SHH medulloblastoma predicts genotype-related response to smoothened inhibition. Cancer Cell 25, 393–405. https://doi.org/10.1016/j.ccr.2014.02.004

Kool, M., Korshunov, A., Remke, M., Jones, D.T.W., Schlanstein, M., Northcott, P.A., Cho, Y.-J., Koster, J., Schouten-van Meeteren, A., van Vuurden, D., Clifford, S.C., Pietsch, T., von Bueren, A.O., Rutkowski, S., McCabe, M., Collins, V.P., Bäcklund, M.L., Haberler, C., Bourdeaut, F., Delattre, O., Doz, F., Ellison, D.W., Gilbertson, R.J., Pomeroy, S.L., Taylor, M.D., Lichter, P., Pfister, S.M., 2012a. Molecular subgroups of medulloblastoma: an international meta-analysis of transcriptome, genetic aberrations, and clinical data of WNT, SHH, Group 3, and Group 4 medulloblastomas. Acta Neuropathol 123, 473–484. https://doi.org/10.1007/s00401-012-0958-8

Kool, M., Korshunov, A., Remke, M., Jones, D.T.W., Schlanstein, M., Northcott, P.A., Cho, Y.-J., Koster, J., Schouten-van Meeteren, A., van Vuurden, D., Clifford, S.C., Pietsch, T., von Bueren, A.O., Rutkowski, S., McCabe, M., Collins, V.P., Bäcklund, M.L., Haberler, C., Bourdeaut, F., Delattre, O., Doz, F., Ellison, D.W., Gilbertson, R.J., Pomeroy, S.L., Taylor, M.D., Lichter, P., Pfister, S.M., 2012b. Molecular subgroups of medulloblastoma: an international meta-analysis of transcriptome, genetic aberrations, and clinical data of WNT, SHH, Group 3, and Group 4 medulloblastomas. Acta Neuropathol 123, 473–484. https://doi.org/10.1007/s00401-012-0958-8

Kool, M., Koster, J., Bunt, J., Hasselt, N.E., Lakeman, A., van Sluis, P., Troost, D., Meeteren, N.S., Caron, H.N., Cloos, J., Mršić, A., Ylstra, B., Grajkowska, W., Hartmann, W., Pietsch, T., Ellison, D., Clifford, S.C., Versteeg, R., 2008. Integrated Genomics Identifies Five Medulloblastoma Subtypes with Distinct Genetic Profiles, Pathway Signatures and Clinicopathological Features. PLoS One 3, e3088. https://doi.org/10.1371/journal.pone.0003088

Krishnan, P.D.G., Golden, E., Woodward, E.A., Pavlos, N.J., Blancafort, P., 2020. Rab gtpases: Emerging oncogenes and tumor suppressive regulators for the editing of survival pathways in cancer. Cancers (Basel). https://doi.org/10.3390/cancers12020259

Krishnaswamy, A., Yamagata, M., Duan, X., Hong, Y.K., Sanes, J.R., 2015. SIDEKICK 2 DIRECTS FORMATION OF A RETINAL CIRCUIT THAT DETECTS DIFFERENTIAL MOTION. Nature 524, 466. https://doi.org/10.1038/NATURE14682

Kulasekaran, G., Chaineau, M., Crescenzo Piscopo, V.E., Verginelli, F., Fotouhi, M., Girard, M., Tang, Y., Dali, R., Lo, R., Stifani, S., McPherson, P.S., 2021. An Arf/Rab cascade controls the growth and invasiveness of glioblastoma. Journal of Cell Biology 220. https://doi.org/10.1083/JCB.202004229/211682

Kuzan-Fischer, C.M., Juraschka, K., Taylor, M.D., 2018. Medulloblastoma in the molecular era. J Korean Neurosurg Soc. https://doi.org/10.3340/jkns.2018.0028

Kyung Park, A., Yeoun Lee, J., Cheong, H., Ramaswamy, V., Park, S.-H., Kool, M., Hoon Phi, J., Ah Choi, S., Cavalli, F., Taylor, M.D., Kim, S.-K., n.d. Subgroup-specific prognostic signaling and metabolic pathways in pediatric medulloblastoma. https://doi.org/10.1186/s12885-019-5742-x

Landry, M.C., Champagne, C., Boulanger, M.C., Jetté, A., Fuchs, M., Dziengelewski, C., Lavoie, J.N., 2014. A Functional Interplay between the Small GTPase Rab11a and Mitochondria-shaping Proteins Regulates Mitochondrial Positioning and Polarization of the Actin Cytoskeleton Downstream of Src Family Kinases. J Biol Chem 289, 2230. https://doi.org/10.1074/JBC.M113.516351

Lau, A.S.N., Mruk, D.D., 2003. Rab8B GTPase and Junction Dynamics in the Testis. Endocrinology 144, 1549–1563. https://doi.org/10.1210/en.2002-220893

Leithner, K., Hrzenjak, A., Trötzmüller, M., Moustafa, T., Köfeler, H.C., Wohlkoenig, C., Stacher, E., Lindenmann, J., Harris, A.L., Olschewski, A., Olschewski, H., 2014. PCK2 activation mediates an adaptive response to glucose depletion in lung cancer. Oncogene 2015 34:8 34, 1044–1050. https://doi.org/10.1038/onc.2014.47

Leung, K.F., Baron, R., Seabra, M.C., 2006. Geranylgeranylation of Rab GTPases. J Lipid Res. https://doi.org/10.1194/jlr.R500017-JLR200

Li, C., Zhang, J., 2019. Stop-codon read-through arises largely from molecular errors and is generally nonadaptive. PLoS Genet 15. https://doi.org/10.1371/JOURNAL.PGEN.1008141

Li, G., Marlin, M.C., 2015. Rab Family of GTPases. Methods Mol Biol 1298, 1. https://doi.org/10.1007/978-1-4939-2569-8_1

Li, M., Han, Y., Wang, C., Kang, W., Jiang, W., Zhang, L., Tang, Y., 2022. Dissecting super-enhancer driven transcriptional dependencies reveals novel therapeutic strategies and targets for group 3 subtype medulloblastoma. J Exp Clin Cancer Res 41. https://doi.org/10.1186/S13046-022-02506-Y

Li, R., Mei, S., Ding, Q., Wang, Q., Yu, L., Zi, F., 2022. A pan-cancer analysis of the role of hexokinase II (HK2) in human tumors. Scientific Reports 2022 12:1 12, 1–11. https://doi.org/10.1038/s41598-022-23598-8

Li, W., Hu, Y., Jiang, T., Han, Y., Han, G., Chen, J., Li, X., 2014. Rab27A regulates exosome secretion from lung adenocarcinoma cells A549: involvement of EPI64. APMIS 122, n/a-n/a. https://doi.org/10.1111/apm.12261

Li, Z., Wang, Xiaoling, Wang, Xiaoxing, Yi, X., Wong, Y.K., Wu, J., Xie, F., Hu, D., Wang, Q., Wang, J., Zhong, T., 2023. Research progress on the role of extracellular vesicles in neurodegenerative diseases. Translational Neurodegeneration 2023 12:1 12, 1–19. https://doi.org/10.1186/S40035-023-00375-9

Liberti, M. V., Locasale, J.W., 2016. The Warburg Effect: How Does it Benefit Cancer Cells? Trends Biochem Sci 41, 211–218. https://doi.org/10.1016/J.TIBS.2015.12.001

Linke, F., Johnson, J.E.C., Kern, S., Bennett, C.D., Lourdusamy, A., Lea, D., Clifford, S.C., Merry, C.L.R., Stolnik, S., Alexander, M.R., Peet, A.C., Scurr, D.J., Griffiths, R.L., Grabowska, A.M., Kerr, I.D., Coyle, B., 2023. Identifying new biomarkers of aggressive Group 3 and SHH medulloblastoma using 3D hydrogel models, single cell RNA sequencing and 3D OrbiSIMS imaging. Acta Neuropathol Commun 11, 1–18. https://doi.org/10.1186/S40478-022-01496-4/FIGURES/7

Linklater, E.S., Duncan, E.D., Han, K.-J., Kaupinis, A., Valius, M., Lyons, T.R., Prekeris, R., n.d. Rab40/Cullin5 complex regulates EPLIN and actin cytoskeleton dynamics during cell migration and invasion. https://doi.org/10.1101/2021.04.01.438077

Liu, D., Kou, X., Chen, C., Liu, S., Liu, Y., Yu, W., Yu, T., Yang, R., Wang, R., Zhou, Y., Shi, S., 2018. Circulating apoptotic bodies maintain mesenchymal stem cell homeostasis and ameliorate osteopenia via transferring multiple cellular factors. Cell Res 28, 918. https://doi.org/10.1038/S41422-018-0070-2

Liu, H., Xu, J., Yao, Q., Zhang, Z., Guo, Q., Lin, J., 2020. Rab7 Is Associated with Poor Prognosis of Gastric Cancer and Promotes Proliferation, Invasion, and Migration of Gastric Cancer Cells. Med Sci Monit 26, e922217-1. https://doi.org/10.12659/MSM.922217

Liu, J., Wu, S., Zheng, X., Zheng, P., Fu, Y., Wu, C., Lu, B., Ju, J., Jiang, J., 2020. Immune suppressed tumor microenvironment by exosomes derived from gastric

cancer cells via modulating immune functions. Scientific Reports 2020 10:1 10, 1–12. https://doi.org/10.1038/s41598-020-71573-y

Liu, M., Yang, L., Liu, X., Nie, Z., Zhang, X., Lu, Y., Pan, Y., Wang, X., Luo, J., 2021. HNRNPH1 Is a Novel Regulator Of Cellular Proliferation and Disease Progression in Chronic Myeloid Leukemia. Front Oncol 11, 682859. https://doi.org/10.3389/FONC.2021.682859/BIBTEX

Liu, P.F., Hu, Y.C., Kang, B.H., Tseng, Y.K., Wu, P.C., Liang, C.C., Hou, Y.Y., Fu, T.Y., Liou, H.H., Hsieh, I.C., Ger, L.P., Shu, C.W., 2017. Expression levels of cleaved caspase-3 and caspase-3 in tumorigenesis and prognosis of oral tongue squamous cell carcinoma. PLoS One 12. https://doi.org/10.1371/JOURNAL.PONE.0180620

Liu, X.N., Zhang, C. Bin, Lin, H., Tang, X.Y., Zhou, R., Wen, H.L., Li, J., 2021. microRNA-204 shuttled by mesenchymal stem cell-derived exosomes inhibits the migration and invasion of non-small-cell lung cancer cells via the KLF7/AKT/HIF-1α axis. Neoplasma 68, 719–731. https://doi.org/10.4149/NEO_2021_201208N1328

Liu, Y., Xiao, B., Li, S., Liu, J., 2022. Risk Factors for Survival in Patients With Medulloblastoma: A Systematic Review and Meta-Analysis. Front Oncol 12. https://doi.org/10.3389/FONC.2022.827054/FULL

Lock, J.G., Stow, J.L., 2005. Rab11 in recycling endosomes regulates the sorting and basolateral transport of E-cadherin. Mol Biol Cell 16, 1744–1755. https://doi.org/10.1091/mbc.E04-10-0867

Loughran, G., Chou, M.Y., Ivanov, I.P., Jungreis, I., Kellis, M., Kiran, A.M., Baranov, P. V., Atkins, J.F., 2014. Evidence of efficient stop codon readthrough in four mammalian genes. Nucleic Acids Res 42, 8928. https://doi.org/10.1093/NAR/GKU608

Louis, D.N., Perry, A., Reifenberger, G., von Deimling, A., Figarella-Branger, D., Cavenee, W.K., Ohgaki, H., Wiestler, O.D., Kleihues, P., Ellison, D.W., 2016. The 2016 World Health Organization Classification of Tumors of the Central Nervous System: a summary. Acta Neuropathol. https://doi.org/10.1007/s00401-016-1545-1

Louis, D.N., Perry, A., Wesseling, P., Brat, D.J., Cree, I.A., Figarella-Branger, D., Hawkins, C., Ng, H.K., Pfister, S.M., Reifenberger, G., Soffietti, R., Von Deimling, A., Ellison, D.W., 2021a. The 2021 WHO Classification of Tumors of the Central Nervous System: a summary. Neuro Oncol 23, 1231. https://doi.org/10.1093/NEUONC/NOAB106

Louis, D.N., Perry, A., Wesseling, P., Brat, D.J., Cree, I.A., Figarella-Branger, D., Hawkins, C., Ng, H.K., Pfister, S.M., Reifenberger, G., Soffietti, R., Von Deimling, A., Ellison, D.W., 2021b. The 2021 WHO Classification of Tumors of the Central Nervous System: a summary. Neuro Oncol 23, 1231. https://doi.org/10.1093/NEUONC/NOAB106

Luga, V., Zhang, L., Viloria-Petit, A.M., Ogunjimi, A.A., Inanlou, M.R., Chiu, E., Buchanan, M., Hosein, A.N., Basik, M., Wrana, J.L., 2012. Exosomes mediate stromal mobilization of autocrine Wnt-PCP signaling in breast cancer cell migration. Cell 151, 1542–1556. https://doi.org/10.1016/j.cell.2012.11.024

Lv, M. meng, Zhu, X. ya, Chen, W. xian, Zhong, S. liang, Hu, Q., Ma, T. fei, Zhang, J., Chen, L., Tang, J. hai, Zhao, J. hua, 2014. Exosomes mediate drug resistance transfer in MCF-7 breast cancer cells and a probable mechanism is delivery of P-glycoprotein. Tumor Biology 35, 10773–10779. https://doi.org/10.1007/S13277-014-2377-Z/FIGURES/6

Lyu, L., Wang, H., Li, B., Qin, Q., Qi, L., Nagarkatti, M., Nagarkatti, P., Janicki, J.S., Wang, X.L., Cui, T., 2015. A critical role of cardiac fibroblast-derived exosomes in activating renin angiotensin system in cardiomyocytes. J Mol Cell Cardiol 89, 268–279. https://doi.org/10.1016/j.yjmcc.2015.10.022

Mani, S., Chatterjee, A., Dasgupta, A., Shirsat, N., Epari, S., Chinnaswamy, G., Gupta, T., 2023. WNT-pathway medulloblastoma: what constitutes low-risk and how low can one go? Oncotarget 14, 105. https://doi.org/10.18632/ONCOTARGET.28360

Manoranjan, B., Venugopal, C., Bakhshinyan, D., Adile, A.A., Richards, L., Kameda-Smith, M.M., Whitley, O., Dvorkin-Gheva, A., Subapanditha, M., Savage, N., Tatari, N., McKenna, D., Bassey-Archibong, B., Winegarden, N., Hallett, R., Provias, J.P., Yarascavitch, B., Ajani, O., Fleming, A., Bader, G.D., Pugh, T.J., Doble, B.W., Singh, S.K., 2020. Wnt activation as a therapeutic strategy in medulloblastoma. Nature Communications 2020 11:1 11, 1–12. https://doi.org/10.1038/s41467-020-17953-4

Marabitti, V., Giansanti, M., De Mitri, F., Gatto, F., Mastronuzzi, A., Nazio, F., 2022a. Pathological implications of metabolic reprogramming and its therapeutic potential in medulloblastoma. Front Cell Dev Biol 10. https://doi.org/10.3389/FCELL.2022.1007641

Marabitti, V., Giansanti, M., De Mitri, F., Gatto, F., Mastronuzzi, A., Nazio, F., 2022b. Pathological implications of metabolic reprogramming and its therapeutic potential in medulloblastoma. Front Cell Dev Biol 10. https://doi.org/10.3389/FCELL.2022.1007641

Marat, A.L., Dokainish, H., McPherson, P.S., 2011. DENN Domain Proteins: Regulators of Rab GTPases. J Biol Chem 286, 13791. https://doi.org/10.1074/JBC.R110.217067

Martínez-Reyes, I., Chandel, N.S., 2021. Cancer metabolism: looking forward. Nature Reviews Cancer 2021 21:10 21, 669–680. https://doi.org/10.1038/s41568-021-00378-6

Marzesco, A.M., Dunia, I., Pandjaitan, R., Recouvreur, M., Dauzonne, D., Benedetti, E.L., Louvard, D., Zahraoui, A., 2002. The small GTPase Rab13 regulates assembly of functional tight junctions in epithelial cells. Mol Biol Cell 13, 1819–1831. https://doi.org/10.1091/mbc.02-02-0029

Mashouri, L., Yousefi, H., Aref, A.R., Ahadi, A.M., Molaei, F., Alahari, S.K., 2019. Exosomes: composition, biogenesis, and mechanisms in cancer metastasis and drug resistance. Mol Cancer 18. https://doi.org/10.1186/S12943-019-0991-5

Massimino, M., Biassoni, V., Gandola, L., Garrè, M.L., Gatta, G., Giangaspero, F., Poggi, G., Rutkowski, S., 2016a. Childhood medulloblastoma. Crit Rev Oncol Hematol 105, 35–51. https://doi.org/10.1016/J.CRITREVONC.2016.05.012

Massimino, M., Biassoni, V., Gandola, L., Garrè, M.L., Gatta, G., Giangaspero, F., Poggi, G., Rutkowski, S., 2016b. Childhood medulloblastoma. Crit Rev Oncol Hematol. https://doi.org/10.1016/j.critrevonc.2016.05.012

Mathivanan, S., Simpson, R.J., 2009. ExoCarta: A compendium of exosomal proteins and RNA. Proteomics 9, 4997–5000. https://doi.org/10.1002/pmic.200900351

Mayle, K.M., Le, A.M., Kamei, D.T., 2012. The Intracellular Trafficking Pathway of Transferrin. Biochim Biophys Acta 1820, 264. https://doi.org/10.1016/J.BBAGEN.2011.09.009

Medulloblastoma | Children's brain tumours | Cancer Research UK [WWW Document], n.d. URL https://www.cancerresearchuk.org/about-cancer/childrens-cancer/brain-tumours/types/medulloblastoma (accessed 6.21.20).

Medulloblastoma | Children's brain tumours [WWW Document], n.d. URL https://www.cancerresearchuk.org/about-cancer/childrens-cancer/brain-tumours/types/medulloblastoma (accessed 3.21.24).

Medulloblastoma Statistics | medulloblastoma.org [WWW Document], n.d. URL https://medulloblastoma.org/medulloblastoma-statistics/ (accessed 3.18.24a).

Medulloblastoma Statistics | medulloblastoma.org [WWW Document], n.d. URL https://medulloblastoma.org/medulloblastoma-statistics/ (accessed 3.12.24b).

Mei, K., Guo, W., 2018. The exocyst complex. Current Biology 28, R922–R925. https://doi.org/10.1016/J.CUB.2018.06.042

Ménasché, G., Pastural, E., Feldmann, J., Certain, S., Ersoy, F., Dupuis, S., Wulffraat, N., Bianchi, D., Fischer, A., Le Deist, F., De Saint Basile, G., 2000. Mutations in RAB27A cause Griscelli syndrome associated with haemophagocytic syndrome. Nat Genet 25, 173–176. https://doi.org/10.1038/76024

Mendrzyk, F., Korshunov, A., Toedt, G., Schwarz, F., Korn, B., Joos, S., Hochhaus, A., Schoch, C., Lichter, P., Radlwimmer, B., 2006. Isochromosome breakpoints on 17p in medulloblastoma are flanked by different classes of DNA sequence repeats. Genes Chromosomes Cancer 45, 401–410. https://doi.org/10.1002/GCC.20304

Meng, D., Yang, Q., Melick, C.H., Park, B.C., Hsieh, T., Curukovic, A., Jeong, M., Zhang, J., James, N.G., Jewell, J.L., 2021. ArfGAP1 inhibits mTORC1 lysosomal localization and activation. EMBO J 40.

https://doi.org/10.15252/EMBJ.2020106412/SUPPL_FILE/EMBJ2020106412-SUP-0002-EVFIGS.PDF

Menyhárt, O., Giangaspero, F., Gyorffy, B., 2019. Molecular markers and potential therapeutic targets in non-WNT/non-SHH (group 3 and group 4) medulloblastomas. J Hematol Oncol. https://doi.org/10.1186/s13045-019-0712-y

Mignogna, M.L., D'Adamo, P., 2018. Critical importance of RAB proteins for synaptic function. Small GTPases. https://doi.org/10.1080/21541248.2016.1277001

Milde, T., Lodrini, M., Savelyeva, L., Korshunov, A., Kool, M., Brueckner, L.M., Antunes, A.S.L.M., Oehme, I., Pekrun, A., Pfister, S.M., Kulozik, A.E., Witt, O., Deubzer, H.E., 2012a. HD-MB03 is a novel Group 3 medulloblastoma model demonstrating sensitivity to histone deacetylase inhibitor treatment. J Neurooncol 110, 335–348. https://doi.org/10.1007/S11060-012-0978-1/FIGURES/5

Milde, T., Lodrini, M., Savelyeva, L., Korshunov, A., Kool, M., Brueckner, L.M., Antunes, A.S.L.M., Oehme, I., Pekrun, A., Pfister, S.M., Kulozik, A.E., Witt, O., Deubzer, H.E., 2012b. HD-MB03 is a novel Group 3 medulloblastoma model demonstrating sensitivity to histone deacetylase inhibitor treatment. J Neurooncol 110, 335–348. https://doi.org/10.1007/s11060-012-0978-1

Millard, N.E., De Braganca, K.C., 2016. Medulloblastoma. J Child Neurol 31, 1341–1353. https://doi.org/10.1177/0883073815600866

Mitra, S., Cheng, K.W., Mills, G.B., 2011. Rab GTPases implicated in inherited and acquired disorders. Semin Cell Dev Biol 22, 57. https://doi.org/10.1016/J.SEMCDB.2010.12.005

Morimoto, S., Nishimura, N., Terai, T., Manabe, S., Yamamoto, Y., Shinahara, W., Miyake, H., Tashiro, S., Shimada, M., Sasaki, T., 2005. Rab13 mediates the continuous endocytic recycling of occludin to the cell surface. Journal of Biological Chemistry 280, 2220–2228. https://doi.org/10.1074/jbc.M406906200

Morrissy, A.S., Garzia, L., Shih, D.J.H., Zuyderduyn, S., Huang, X., Skowron, P., Remke, M., Cavalli, F.M.G., Ramaswamy, V., Lindsay, P.E., Jelveh, S., Donovan, L.K., Wang, X., Luu, B., Zayne, K., Li, Y., Mayoh, C., Thiessen, N., Mercier, E., Mungall, K.L., Ma, Y., Tse, K., Zeng, T., Shumansky, K., Roth, A.J.L., Shah, S., Farooq, H., Kijima, N., Holgado, B.L., Lee, J.J.Y., Matan-Lithwick, S., Liu, J., Mack, S.C., Manno, A., Michealraj, K.A., Nor, C., Peacock, J., Qin, L., Reimand, J., Rolider, A., Thompson, Y.Y., Wu, X., Pugh, T., Ally, A., Bilenky, M., Butterfield, Y.S.N., Carlsen, R., Cheng, Y., Chuah, E., Corbett, R.D., Dhalla, N., He, A., Lee, D., Li, H.I., Long, W., Mayo, M., Plettner, P., Qian, J.Q., Schein, J.E., Tam, A., Wong, T., Birol, I., Zhao, Y., Faria, C.C., Pimentel, J., Nunes, S., Shalaby, T., Grotzer, M., Pollack, I.F., Hamilton, R.L., Li, X.N., Bendel, A.E., Fults, D.W., Walter, A.W., Kumabe, T., Tominaga, T., Collins, V.P., Cho, Y.J., Hoffman, C., Lyden, D., Wisoff, J.H., Garvin, J.H., Stearns, D.S., Massimi, L., Schüller, U., Sterba, J., Zitterbart, K., Puget, S., Ayrault, O., Dunn, S.E., Tirapelli, D.P.C., Carlotti, C.G., Wheeler, H., Hallahan, A.R., Ingram, W., MacDonald, T.J., Olson,

J.J., Van Meir, E.G., Lee, J.Y., Wang, K.C., Kim, S.K., Cho, B.K., Pietsch, T., Fleischhack, G., Tippelt, S., Ra, Y.S., Bailey, S., Lindsey, J.C., Clifford, S.C., Eberhart, C.G., Cooper, M.K., Packer, R.J., Massimino, M., Garre, M.L., Bartels, U., Tabori, U., Hawkins, C.E., Dirks, P., Bouffet, E., Rutka, J.T., Wechsler-Reya, R.J., Weiss, W.A., Collier, L.S., Dupuy, A.J., Korshunov, A., Jones, D.T.W., Kool, M., Northcott, P.A., Pfister, S.M., Largaespada, D.A., Mungall, A.J., Moore, R.A., Jabado, N., Bader, G.D., Jones, S.J.M., Malkin, D., Marra, M.A., Taylor, M.D., 2016. Divergent clonal selection dominates medulloblastoma at recurrence. Nature 529, 351–357. https://doi.org/10.1038/nature16478

Müller, M.P., Goody, R.S., 2018. Molecular control of Rab activity by GEFs, GAPs and GDI. Small GTPases 9, 5. https://doi.org/10.1080/21541248.2016.1276999

Muralidharan-Chari, V., Clancy, J.W., Sedgwick, A., D'Souza-Schorey, C., 2010. Microvesicles: Mediators of extracellular communication during cancer progression. J Cell Sci. https://doi.org/10.1242/jcs.064386

Musi, A., Bongiovanni, L., 2023. Extracellular Vesicles in Cancer Drug Resistance: Implications on Melanoma Therapy. Cancers (Basel) 15. https://doi.org/10.3390/CANCERS15041074

Naeini, S.H., Mavaddatiyan, L., Kalkhoran, Z.R., Taherkhani, S., Talkhabi, M., 2023. Alpha-ketoglutarate as a potent regulator for lifespan and healthspan: Evidences and perspectives. Exp Gerontol 175, 112154. https://doi.org/10.1016/J.EXGER.2023.112154

Navarro, C., Ortega, Á., Santeliz, R., Garrido, B., Chacín, M., Galban, N., Vera, I., De Sanctis, J.B., Bermúdez, V., 2022. Metabolic Reprogramming in Cancer Cells: Emerging Molecular Mechanisms and Novel Therapeutic Approaches. Pharmaceutics 14. https://doi.org/10.3390/PHARMACEUTICS14061303

Nederveen, J.P., Warnier, G., Di Carlo, A., Nilsson, M.I., Tarnopolsky, M.A., 2021. Extracellular Vesicles and Exosomes: Insights From Exercise Science. Front Physiol 11. https://doi.org/10.3389/FPHYS.2020.604274/FULL

Niedziółka, S.M., Datta, S., Uśpieński, T., Baran, B., Skarżyńska, W., Humke, E.W., Rohatgi, R., Niewiadomski, P., 2024. The exocyst complex and intracellular vesicles mediate soluble protein trafficking to the primary cilium. Communications Biology 2024 7:1 7, 1–19. https://doi.org/10.1038/s42003-024-05817-2

Northcott, P.A., Buchhalter, I., Morrissy, A.S., Hovestadt, V., Weischenfeldt, J., Ehrenberger, T., Gröbner, S., Segura-Wang, M., Zichner, T., Rudneva, V.A., Warnatz, H.J., Sidiropoulos, N., Phillips, A.H., Schumacher, S., Kleinheinz, K., Waszak, S.M., Erkek, S., Jones, D.T.W., Worst, B.C., Kool, M., Zapatka, M., Jäger, N., Chavez, L., Hutter, B., Bieg, M., Paramasivam, N., Heinold, M., Gu, Z., Ishaque, N., Jäger-Schmidt, C., Imbusch, C.D., Jugold, A., Hübschmann, D., Risch, T., Amstislavskiy, V., Gonzalez, F.G.R., Weber, U.D., Wolf, S., Robinson, G.W., Zhou, X., Wu, G., Finkelstein, D., Liu, Y., Cavalli, F.M.G., Luu, B., Ramaswamy, V., Wu, X., Koster, J., Ryzhova, M., Cho, Y.J., Pomeroy, S.L.,

Herold-Mende, C., Schuhmann, M., Ebinger, M., Liau, L.M., Mora, J., McLendon, R.E., Jabado, N., Kumabe, T., Chuah, E., Ma, Y., Moore, R.A., Mungall, A.J., Mungall, K.L., Thiessen, N., Tse, K., Wong, T., Jones, S.J.M., Witt, O., Milde, T., Von Deimling, A., Capper, D., Korshunov, A., Yaspo, M.L., Kriwacki, R., Gajjar, A., Zhang, J., Beroukhim, R., Fraenkel, E., Korbel, J.O., Brors, B., Schlesner, M., Eils, R., Marra, M.A., Pfister, S.M., Taylor, M.D., Lichter, P., 2017. The whole-genome landscape of medulloblastoma subtypes. Nature 547, 311–317. https://doi.org/10.1038/nature22973

Northcott, P.A., Dubuc, A.M., Pfister, S., Taylor, M.D., 2012a. Molecular subgroups of medulloblastoma. Expert Rev Neurother. https://doi.org/10.1586/ern.12.66

Northcott, P.A., Jones, D.T.W., Kool, M., Robinson, G.W., Gilbertson, R.J., Cho, Y.J., Pomeroy, S.L., Korshunov, A., Lichter, P., Taylor, M.D., Pfister, S.M., 2012b. Medulloblastomics: The End of the Beginning. Nat Rev Cancer 12, 818. https://doi.org/10.1038/NRC3410

Northcott, P.A., Korshunov, A., Witt, H., Hielscher, T., Eberhart, C.G., Mack, S., Bouffet, E., Clifford, S.C., Hawkins, C.E., French, P., Rutka, J.T., Pfister, S., Taylor, M.D., 2011. Medulloblastoma Comprises Four Distinct Molecular Variants. Journal of Clinical Oncology 29, 1408. https://doi.org/10.1200/JCO.2009.27.4324

Northcott, P.A., Robinson, G.W., Kratz, C.P., Mabbott, D.J., Pomeroy, S.L., Clifford, S.C., Rutkowski, S., Ellison, D.W., Malkin, D., Taylor, M.D., Gajjar, A., Pfister, S.M., 2019a. Medulloblastoma. Nat Rev Dis Primers 5. https://doi.org/10.1038/s41572-019-0063-6

Northcott, P.A., Robinson, G.W., Kratz, C.P., Mabbott, D.J., Pomeroy, S.L., Clifford, S.C., Rutkowski, S., Ellison, D.W., Malkin, D., Taylor, M.D., Gajjar, A., Pfister, S.M., 2019b. Medulloblastoma. Nat Rev Dis Primers 5. https://doi.org/10.1038/s41572-019-0063-6

Novak, U., Kaye, A.H., 2000. Extracellular matrix and the brain: components and function. Journal of Clinical Neuroscience 7, 280–290. https://doi.org/10.1054/JOCN.1999.0212

Oggero, S., Austin-Williams, S., Norling, L.V., 2019. The contrasting role of extracellular vesicles in vascular inflammation and tissue repair. Front Pharmacol. https://doi.org/10.3389/fphar.2019.01479

Olmeda, D., Castel, S., Vilaró, S., Cano, A., 2003. β-Catenin Regulation during the Cell Cycle: Implications in G2/M and Apoptosis. Mol Biol Cell 14, 2844. https://doi.org/10.1091/MBC.E03-01-0865

Onofre, T.S., Rodrigues, J.P.F., Shio, M.T., Macedo, S., Juliano, M.A., Yoshida, N., 2021. Interaction of Trypanosoma cruzi Gp82 With Host Cell LAMP2 Induces Protein Kinase C Activation and Promotes Invasion. Front Cell Infect Microbiol 11, 1. https://doi.org/10.3389/FCIMB.2021.627888/FULL

Orellana, J.A., Schalper, K.A., Figueroa, V., Sánchez, H.A., Sáez, J.C., 2012. Regulation of intercellular calcium signaling through calcium interactions with connexin-based channels. Adv Exp Med Biol 740, 777–794. https://doi.org/10.1007/978-94-007-2888-2_34

Orr, B.A., 2020a. Pathology, diagnostics, and classification of medulloblastoma. Brain Pathology 30, 664. https://doi.org/10.1111/BPA.12837

Orr, B.A., 2020b. Pathology, diagnostics, and classification of medulloblastoma. Brain Pathology 30, 664. https://doi.org/10.1111/BPA.12837

Ostenfeld, M.S., Jeppesen, D.K., Laurberg, J.R., Boysen, A.T., Bramsen, J.B., Primdal-Bengtson, B., Hendrix, A., Lamy, P., Dagnaes-Hansen, F., Rasmussen, M.H., Bui, K.H., Fristrup, N., Christensen, E.I., Nordentoft, I., Morth, J.P., Jensen, J.B., Pedersen, J.S., Beck, M., Theodorescu, D., Borre, M., Howard, K.A., Dyrskjøt, L., Ørntoft, T.F., 2014. Cellular disposal of miR23b by RAB27-dependent exosome release is linked to acquisition of metastatic properties. Cancer Res 74, 5758–5771. https://doi.org/10.1158/0008-5472.CAN-13-3512

Ostrom, Q.T., Gittleman, H., Liao, P., Vecchione-Koval, T., Wolinsky, Y., Kruchko, C., Barnholtz-Sloan, J.S., 2017. Neuro-Oncology CBTRUS Statistical Report: Primary brain and other central nervous system tumors diagnosed in the United Introduction 1–88. https://doi.org/10.1093/neuonc/nox158

Ostrowski, M., Carmo, N.B., Krumeich, S., Fanget, I., Raposo, G., Savina, A., Moita, C.F., Schauer, K., Hume, A.N., Freitas, R.P., Goud, B., Benaroch, P., Hacohen, N., Fukuda, M., Desnos, C., Seabra, M.C., Darchen, F., Amigorena, S., Moita, L.F., Thery, C., 2010. Rab27a and Rab27b control different steps of the exosome secretion pathway. Nat Cell Biol 12, 19–30. https://doi.org/10.1038/ncb2000

Otero-Ortega, L., Laso-García, F., Gómez-de Frutos, M.C., Fuentes, B., Diekhorst, L., Díez-Tejedor, E., Gutiérrez-Fernández, M., 2019. Role of Exosomes as a Treatment and Potential Biomarker for Stroke. Transl Stroke Res. https://doi.org/10.1007/s12975-018-0654-7

Overmeyer, J.H., Wilson, A.L., Erdman, R.A., Maltese, W.A., 1998. The putative "Switch 2" domain of the ras-related GTpase, Rab1b, plays an essential role in the interaction with Rab escort protein. Mol Biol Cell 9, 223–235. https://doi.org/10.1091/mbc.9.1.223

Paine, M.R.L., Liu, J., Huang, D., Ellis, S.R., Trede, D., Kobarg, J.H., Heeren, R.M.A., Fernández, F.M., MacDonald, T.J., 2019. Three-Dimensional Mass Spectrometry Imaging Identifies Lipid Markers of Medulloblastoma Metastasis. Scientific Reports 2019 9:1 9, 1–10. https://doi.org/10.1038/s41598-018-38257-0

Palma, M., Hansson, L., Choudhury, A., Näsman-Glaser, B., Eriksson, I., Adamson, L., Rossmann, E., Widén, K., Horváth, R., Kokhaei, P., Vertuani, S., Mellstedt, H., Österborg, A., 2012. Vaccination with dendritic cells loaded with tumor apoptotic bodies (Apo-DC) in patients with chronic lymphocytic leukemia: effects

of various adjuvants and definition of immune response criteria. Cancer Immunol Immunother 61, 865–879. https://doi.org/10.1007/S00262-011-1149-5

Pan, E., Pellarin, M., Holmes, E., Smirnov, I., Misra, A., Eberhart, C.G., Burger, P.C., Biegel, J.A., Feuerstein, B.G., Mason, S., 2005. Isochromosome 17q Is a Negative Prognostic Factor in Poor-Risk Childhood Medulloblastoma Patients. Clinical Cancer Research 11, 4733–4740. https://doi.org/10.1158/1078-0432.CCR-04-0465

Paulus, W., Baur, I., Dours-Zimmermann, M.T., Zimmermann, D.R., 1996. Differential Expression of Versican Isoforms in Brain Tumors. J Neuropathol Exp Neurol 55, 528–533. https://doi.org/10.1097/00005072-199605000-00005

Pegtel, D.M., Gould, S.J., 2019. Annual Review of Biochemistry Exosomes. https://doi.org/10.1146/annurev-biochem-013118

Peinado, H., Alečković, M., Lavotshkin, S., Matei, I., Costa-Silva, B., Moreno-Bueno, G., Hergueta-Redondo, M., Williams, C., García-Santos, G., Ghajar, C.M., Nitadori-Hoshino, A., Hoffman, C., Badal, K., Garcia, B.A., Callahan, M.K., Yuan, J., Martins, V.R., Skog, J., Kaplan, R.N., Brady, M.S., Wolchok, J.D., Chapman, P.B., Kang, Y., Bromberg, J., Lyden, D., 2012. Melanoma exosomes educate bone marrow progenitor cells toward a pro-metastatic phenotype through MET. Nat Med 18, 883–891. https://doi.org/10.1038/nm.2753

Pellinen, T., Arjonen, A., Vuoriluoto, K., Kallio, K., Fransen, J.A.M., Ivaska, J., 2006. Small GTPase Rab21 regulates cell adhesion and controls endosomal traffic of β1-integrins. Journal of Cell Biology 173, 767–780. https://doi.org/10.1083/jcb.200509019

Pellizzoni, L., Kataoka, N., Charroux, B., Dreyfuss, G., 1998. A Novel Function for SMN, the Spinal Muscular Atrophy Disease Gene Product, in Pre-mRNA Splicing. Cell 95, 615–624. https://doi.org/10.1016/S0092-8674(00)81632-3

Pereira-Leal, J.B., Seabra, M.C., 2000. The mammalian Rab family of small GTPases: definition of family and subfamily sequence motifs suggests a mechanism for functional specificity in the Ras superfamily. J Mol Biol 301, 1077–1087. https://doi.org/10.1006/JMBI.2000.4010

Perreault, S., Ramaswamy, V., Achrol, A.S., Chao, K., Liu, T.T., Shih, D., Remke, M., Schubert, S., Bouffet, E., Fisher, P.G., Partap, S., Vogel, H., Taylor, M.D., Cho, Y.J., Yeom, K.W., 2014. MRI surrogates for molecular subgroups of medulloblastoma. American Journal of Neuroradiology 35, 1263–1269. https://doi.org/10.3174/ajnr.A3990

Pfaff, E., Remke, M., Sturm, D., Benner, A., Witt, H., Milde, T., Von Bueren, A.O., Wittmann, A., Schöttler, A., Jorch, N., Graf, N., Kulozik, A.E., Witt, O., Scheurlen, W., Von Deimling, A., Rutkowski, S., Taylor, M.D., Tabori, U., Lichter, P., Korshunov, A., Pfister, S.M., 2010. TP53 mutation is frequently associated with CTNNB1 mutation or MYCN amplification and is compatible with long-term survival in medulloblastoma. Journal of Clinical Oncology 28, 5188–5196.

https://doi.org/10.1200/JCO.2010.31.1670/ASSET/IMAGES/ZLJ9991006720004.JPEG

Pfeffer, S.R., 2005. Structural clues to rab GTPase functional diversity. Journal of Biological Chemistry. https://doi.org/10.1074/jbc.R500003200

Pham, K., Hanaford, A.R., Poore, B.A., Maxwell, M.J., Sweeney, H., Parthasarathy, A., Alt, J., Rais, R., Slusher, B.S., Eberhart, C.G., Raabe, E.H., 2022a. Comprehensive Metabolic Profiling of MYC-Amplified Medulloblastoma Tumors Reveals Key Dependencies on Amino Acid, Tricarboxylic Acid and Hexosamine Pathways. Cancers (Basel) 14. https://doi.org/10.3390/CANCERS14051311/S1

Pham, K., Hanaford, A.R., Poore, B.A., Maxwell, M.J., Sweeney, H., Parthasarathy, A., Alt, J., Rais, R., Slusher, B.S., Eberhart, C.G., Raabe, E.H., 2022b. Comprehensive Metabolic Profiling of MYC-Amplified Medulloblastoma Tumors Reveals Key Dependencies on Amino Acid, Tricarboxylic Acid and Hexosamine Pathways. Cancers (Basel) 14. https://doi.org/10.3390/CANCERS14051311/S1

Pietsch, T., Schmidt, R., Remke, M., Korshunov, A., Hovestadt, V., Jones, D.T.W., Felsberg, J., Kaulich, K., Goschzik, T., Kool, M., Northcott, P.A., von Hoff, K., von Bueren, A.O., Friedrich, C., Mynarek, M., Skladny, H., Fleischhack, G., Taylor, M.D., Cremer, F., Lichter, P., Faldum, A., Reifenberger, G., Rutkowski, S., Pfister, S.M., 2014. Prognostic significance of clinical, histopathological, and molecular characteristics of medulloblastomas in the prospective HIT2000 multicenter clinical trial cohort. Acta Neuropathol 128, 137–149. https://doi.org/10.1007/s00401-014-1276-0

Pizer, B.L., Clifford, S.C., 2009. The potential impact of tumour biology on improved clinical practice for medulloblastoma: Progress towards biologically driven clinical trials. Br J Neurosurg. https://doi.org/10.1080/02688690903121807

Pizzino, G., Irrera, N., Cucinotta, M., Pallio, G., Mannino, F., Arcoraci, V., Squadrito, F., Altavilla, D., Bitto, A., 2017. Oxidative Stress: Harms and Benefits for Human Health. Oxid Med Cell Longev 2017. https://doi.org/10.1155/2017/8416763

Pollack, I.F., Agnihotri, S., Broniscer, A., 2019. Childhood brain tumors: Current management, biological insights, and future directions. J Neurosurg Pediatr. https://doi.org/10.3171/2018.10.PEDS18377

Posterior Fossa Syndrome - Together by St. Jude™ [WWW Document], n.d. URL https://together.stjude.org/en-us/diagnosis-treatment/side-effects/posterior-fossa-syndrome.html (accessed 7.25.24).

Prashar, A., Schnettger, L., Bernard, E.M., Gutierrez, M.G., 2017. Rab GTPases in immunity and inflammation. Front Cell Infect Microbiol. https://doi.org/10.3389/fcimb.2017.00435

Proia, P., Schiera, G., Mineo, M., Ingrassia, A.M.R., Santoro, G., Savettieri, G., Di Liegro, I., 2008. Astrocytes shed extracellular vesicles that contain fibroblast growth factor-2 and vascular endothelial growth factor. Int J Mol Med 21, 63–67. https://doi.org/10.3892/ijmm.21.1.63

Puri, C., Vicinanza, M., Ashkenazi, A., Gratian, M.J., Zhang, Q., Bento, C.F., Renna, M., Menzies, F.M., Rubinsztein, D.C., 2018. The RAB11A-Positive Compartment Is a Primary Platform for Autophagosome Assembly Mediated by WIPI2 Recognition of PI3P-RAB11A. Dev Cell 45, 114. https://doi.org/10.1016/J.DEVCEL.2018.03.008

Pylypenko, O., Hammich, H., Yu, I.M., Houdusse, A., 2018. Rab GTPases and their interacting protein partners: Structural insights into Rab functional diversity. Small GTPases. https://doi.org/10.1080/21541248.2017.1336191

Ramaswamy, V., Remke, M., Bouffet, E., Bailey, S., Clifford, S.C., Doz, F., Kool, M., Dufour, C., Vassal, G., Milde, T., Witt, O., von Hoff, K., Pietsch, T., Northcott, P.A., Gajjar, A., Robinson, G.W., Padovani, L., André, N., Massimino, M., Pizer, B., Packer, R., Rutkowski, S., Pfister, S.M., Taylor, M.D., Pomeroy, S.L., 2016. Risk stratification of childhood medulloblastoma in the molecular era: the current consensus. Acta Neuropathol 131, 821–831. https://doi.org/10.1007/s00401-016-1569-6

Ramaswamy, V., Remke, M., Bouffet, E., Faria, C.C., Perreault, S., Cho, Y.J., Shih, D.J., Luu, B., Dubuc, A.M., Northcott, P.A., Schüller, U., Gururangan, S., McLendon, R., Bigner, D., Fouladi, M., Ligon, K.L., Pomeroy, S.L., Dunn, S., Triscott, J., Jabado, N., Fontebasso, A., Jones, D.T.W., Kool, M., Karajannis, M.A., Gardner, S.L., Zagzag, D., Nunes, S., Pimentel, J., Mora, J., Lipp, E., Walter, A.W., Ryzhova, M., Zheludkova, O., Kumirova, E., Alshami, J., Croul, S.E., Rutka, J.T., Hawkins, C., Tabori, U., Codispoti, K.E.T., Packer, R.J., Pfister, S.M., Korshunov, A., Taylor, M.D., 2013. Recurrence patterns across medulloblastoma subgroups: An integrated clinical and molecular analysis. Lancet Oncol 14, 1200–1207. https://doi.org/10.1016/S1470-2045(13)70449-2

Ramaswamy, V., Remke, M., Shih, D., Wang, X., Northcott, P.A., Faria, C.C., Raybaud, C., Tabori, U., Hawkins, C., Rutka, J., Taylor, M.D., Bouffet, E., 2014. Duration of the pre-diagnostic interval in medulloblastoma is subgroup dependent. Pediatr Blood Cancer 61, 1190–1194. https://doi.org/10.1002/pbc.25002

Ramteke, A., Ting, H., Agarwal, C., Mateen, S., Somasagara, R., Hussain, A., Graner, M., Frederick, B., Agarwal, R., Deep, G., 2015. Exosomes secreted under hypoxia enhance invasiveness and stemness of prostate cancer cells by targeting adherens junction molecules. Mol Carcinog 54, 554–565. https://doi.org/10.1002/mc.22124

Rani, S., Lai, A., Nair, S., Sharma, S., Handberg, A., Carrion, F., Möller, A., Salomon, C., 2023a. Extracellular vesicles as mediators of cell-cell communication in ovarian cancer and beyond – A lipids focus. Cytokine Growth Factor Rev 73, 52–68. https://doi.org/10.1016/J.CYTOGFR.2023.06.004

Rani, S., Lai, A., Nair, S., Sharma, S., Handberg, A., Carrion, F., Möller, A., Salomon, C., 2023b. Extracellular vesicles as mediators of cell-cell communication in ovarian cancer and beyond – A lipids focus. Cytokine Growth Factor Rev 73, 52–68. https://doi.org/10.1016/J.CYTOGFR.2023.06.004

Rapalino, O., Batchelor, T., González, R.G., 2016. Intra-axial brain tumors. Handb Clin Neurol 135, 253–274. https://doi.org/10.1016/B978-0-444-53485-9.00014-3

Raposo, G., Nijman, H.W., Stoorvogel, W., Leijendekker, R., Harding, C. V., Melief, C.J.M., Geuze, H.J., 1996. B lymphocytes secrete antigen-presenting vesicles. Journal of Experimental Medicine 183, 1161–1172. https://doi.org/10.1084/jem.183.3.1161

Raposo, G., Stoorvogel, W., 2013. Extracellular vesicles: Exosomes, microvesicles, and friends. Journal of Cell Biology. https://doi.org/10.1083/jcb.201211138

Ratajczak, J., Miekus, K., Kucia, M., Zhang, J., Reca, R., Dvorak, P., Ratajczak, M.Z., 2006. Embryonic stem cell-derived microvesicles reprogram hematopoietic progenitors: Evidence for horizontal transfer of mRNA and protein delivery. Leukemia 20, 847–856. https://doi.org/10.1038/sj.leu.2404132

Ravindran, R., Velikkakath, A.K.G., Narendradev, N.D., Chandrasekharan, A., Santhoshkumar, T.R., Srinivasula, S.M., 2021. Endosomes facilitate mitochondrial clearance by enhancing Parkin recruitment to mitochondria. bioRxiv 2020.02.19.955880. https://doi.org/10.1101/2020.02.19.955880

Ricciardelli, C., Russell, D.L., Ween, M.P., Mayne, K., Suwiwat, S., Byers, S., Marshall, V.R., Tilley, W.D., Horsfall, D.J., 2007. Formation of hyaluronan- and versican-rich pericellular matrix by prostate cancer cells promotes cell motility. J Biol Chem 282, 10814–10825. https://doi.org/10.1074/JBC.M606991200

Ricciardelli, C., Sakko, A.J., Ween, M.P., Russell, D.L., Horsfall, D.J., 2009. The biological role and regulation of versican levels in cancer. Cancer and Metastasis Reviews 28, 233–245. https://doi.org/10.1007/S10555-009-9182-Y/FIGURES/3

Robinson, D.G., Ding, Y., Jiang, L., 2016. Unconventional protein secretion in plants: a critical assessment. Protoplasma. https://doi.org/10.1007/s00709-015-0887-1

Roland, J.T., Bryant, D.M., Datta, A., Itzen, A., Mostov, K.E., Goldenring, J.R., 2011. Rab GTPase-Myo5B complexes control membrane recycling and epithelial polarization. Proc Natl Acad Sci U S A 108, 2789–2794. https://doi.org/10.1073/pnas.1010754108

Roma-Rodrigues, C., Fernandes, A.R., Baptista, P.V., 2014. Exosome in Tumour Microenvironment: Overview of the Crosstalk between Normal and Cancer Cells. Biomed Res Int 2014. https://doi.org/10.1155/2014/179486

Ruben, J.M., Van Den Ancker, W., Bontkes, H.J., Westers, T.M., Hooijberg, E., Ossenkoppele, G.J., De Gruijl, T.D., Van De Loosdrecht, A.A., 2014. Apoptotic blebs from leukemic cells as a preferred source of tumor-associated antigen for dendritic cell-based vaccines. Cancer Immunology, Immunotherapy 63, 335–345. https://doi.org/10.1007/S00262-013-1515-6/FIGURES/6

Salmon, T.B., Evert, B.A., Song, B., Doetsch, P.W., 2004. Biological consequences of oxidative stress-induced DNA damage in Saccharomyces cerevisiae. Nucleic Acids Res 32, 3712. https://doi.org/10.1093/NAR/GKH696

Saman, Sudad, Kim, W.H., Raya, M., Visnick, Y., Miro, S., Saman, Sarmad, Jackson, B., McKee, A.C., Alvarez, V.E., Lee, N.C.Y., Hall, G.F., 2012. Exosome-associated tau is secreted in tauopathy models and is selectively phosphorylated in cerebrospinal fluid in early Alzheimer disease. Journal of Biological Chemistry 287, 3842–3849. https://doi.org/10.1074/jbc.M111.277061

Sancho-Albero, M., Navascués, N., Mendoza, G., Sebastián, V., Arruebo, M., Martín-Duque, P., Santamaría, J., 2019. Exosome origin determines cell targeting and the transfer of therapeutic nanoparticles towards target cells. J Nanobiotechnology 17, 16. https://doi.org/10.1186/s12951-018-0437-z

Sato, M., Sato, K., Liou, W., Pant, S., Harada, A., Grant, B.D., 2008. Regulation of endocytic recycling by C. elegans Rab35 and its regulator RME-4, a coated-pit protein. EMBO J 27, 1183. https://doi.org/10.1038/EMBOJ.2008.54

Savina, A., Vidal, M., Colombo, M.I., 2002. The exosome pathway in K562 cells is regulated by Rab11. J Cell Sci 115, 2505–2515.

Schorey, J.S., Bhatnagar, S., 2008. Exosome function: From tumor immunology to pathogen biology. Traffic. https://doi.org/10.1111/j.1600-0854.2008.00734.x

Schunk, S.J., Floege, J., Fliser, D., Speer, T., 2020. WNT–β-catenin signalling — a versatile player in kidney injury and repair. Nature Reviews Nephrology 2020 17:3 17, 172–184. https://doi.org/10.1038/s41581-020-00343-w

Schütt, F., Aretz, S., Auffarth, G.U., Kopitz, J., 2012. Moderately Reduced ATP Levels Promote Oxidative Stress and Debilitate Autophagic and Phagocytic Capacities in Human RPE Cells. Invest Ophthalmol Vis Sci 53, 5354–5361. https://doi.org/10.1167/IOVS.12-9845

Schwalbe, E.C., Lindsey, J.C., Nakjang, S., Crosier, S., Smith, A.J., Hicks, D., Rafiee, G., Hill, R.M., Iliasova, A., Stone, T., Pizer, B., Michalski, A., Joshi, A., Wharton, S.B., Jacques, T.S., Bailey, S., Williamson, D., Clifford, S.C., 2017. Novel molecular subgroups for clinical classification and outcome prediction in childhood medulloblastoma: a cohort study. Lancet Oncol 18, 958. https://doi.org/10.1016/S1470-2045(17)30243-7

Seabra, M.C., Mules, E.H., Hume, A.N., 2002. Rab GTPases, intracellular traffic and disease. Trends Mol Med. https://doi.org/10.1016/S1471-4914(01)02227-4

Seo, M., Kim, S.M., Woo, E.Y., Han, K.C., Park, E.J., Ko, S., Wook Choi, E., Jang, M., 2018. Stemness-Attenuating miR-503-3p as a Paracrine Factor to Regulate Growth of Cancer Stem Cells. Stem Cells Int 2018. https://doi.org/10.1155/2018/4851949

Shah, R., Patel, T., Freedman, J.E., 2018. Circulating extracellular vesicles in human disease. New England Journal of Medicine. https://doi.org/10.1056/NEJMra1704286

Shanthi, K.B., Fischer, D., Sharma, A., Kiviniemi, A., Kaakinen, M., Vainio, S.J., Bart, G., 2023. Human Adult Astrocyte Extracellular Vesicle Transcriptomics Study

Identifies Specific RNAs Which Are Preferentially Secreted as EV Luminal Cargo. Genes (Basel) 14. https://doi.org/10.3390/GENES14040853/S1

Sharma, T., Schwalbe, E.C., Williamson, D., Sill, M., Hovestadt, V., Mynarek, M., Rutkowski, S., Robinson, G.W., Gajjar, A., Cavalli, F., Ramaswamy, V., Taylor, M.D., Lindsey, J.C., Hill, R.M., Jäger, N., Korshunov, A., Hicks, D., Bailey, S., Kool, M., Chavez, L., Northcott, P.A., Pfister, S.M., Clifford, S.C., 2019. Second-generation molecular subgrouping of medulloblastoma: an international meta-analysis of Group 3 and Group 4 subtypes. Acta Neuropathol 138, 309–326. https://doi.org/10.1007/s00401-019-02020-0

Shen, D.W., Gottesman, M.M., 2012. RAB8 Enhances TMEM205-Mediated Cisplatin Resistance. Pharm Res 29, 643. https://doi.org/10.1007/S11095-011-0562-Y

Sheng, H., Li, H., Zeng, H., Zhang, B., Lu, Y., Liu, X., Xu, Z., Zhang, J., Zhang, L., 2024. Heterogeneity and tumoral origin of medulloblastoma in the single-cell era. Oncogene 2024 1–12. https://doi.org/10.1038/s41388-024-02967-9

Sheta, M., Taha, E.A., Lu, Y., Eguchi, T., 2023. Extracellular Vesicles: New Classification and Tumor Immunosuppression. Biology (Basel) 12. https://doi.org/10.3390/BIOLOGY12010110

Shi, L.-W., Zhao, Z.-B., Zhong, L., Gao, J., Gong, J.-P., Chen, H., Min, Y., Zhang, Y.-Y., Li, Z., 2020. Overexpression of Rab40b Promotes Hepatocellular Carcinoma Cell Proliferation and Metastasis via PI3K/AKT Signaling Pathway. https://doi.org/10.2147/CMAR.S255870

Shih, D.J.H., Northcott, P.A., Remke, M., Korshunov, A., Ramaswamy, V., Kool, M., Luu, B., Yao, Y., Wang, X., Dubuc, A.M., Garzia, L., Peacock, J., Mack, S.C., Wu, X., Rolider, A., Morrissy, A.S., Cavalli, F.M.G., Jones, D.T.W., Zitterbart, K., Faria, C.C., Schüller, U., Kren, L., Kumabe, T., Tominaga, T., Ra, Y.S., Garami, M., Hauser, P., Chan, J.A., Robinson, S., Bognár, L., Klekner, A., Saad, A.G., Liau, L.M., Albrecht, S., Fontebasso, A., Cinalli, G., De Antonellis, P., Zollo, M., Cooper, M.K., Thompson, R.C., Bailey, S., Lindsey, J.C., Di Rocco, C., Massimi, L., Michiels, E.M.C., Scherer, S.W., Phillips, J.J., Gupta, N., Fan, X., Muraszko, K.M., Vibhakar, R., Eberhart, C.G., Fouladi, M., Lach, B., Jung, S., Wechsler-Reya, R.J., Fèvre-Montange, M., Jouvet, A., Jabado, N., Pollack, I.F., Weiss, W.A., Lee, J.Y., Cho, B.K., Kim, S.K., Wang, K.C., Leonard, J.R., Rubin, J.B., De Torres, C., Lavarino, C., Mora, J., Cho, Y.J., Tabori, U., Olson, J.M., Gajjar, A., Packer, R.J., Rutkowski, S., Pomeroy, S.L., French, P.J., Kloosterhof, N.K., Kros, J.M., Van Meir, E.G., Clifford, S.C., Bourdeaut, F., Delattre, O., Doz, F.F., Hawkins, C.E., Malkin, D., Grajkowska, W.A., Perek-Polnik, M., Bouffet, E., Rutka, J.T., Pfister, S.M., Taylor, M.D., 2014. Cytogenetic prognostication within medulloblastoma subgroups. Journal of Clinical Oncology 32, 886–896. https://doi.org/10.1200/JCO.2013.50.9539

Sidhu, S.S., Mengistab, A.T., Tauscher, A.N., LaVail, J., Basbaum, C., 2004. The microvesicle as a vehicle for EMMPRin in tumor-stromal interactions. Oncogene 23, 956–963. https://doi.org/10.1038/sj.onc.1207070

Siegel, R.L., Miller, K.D., Jemal, A., 2018. Cancer statistics, 2018. CA Cancer J Clin 68, 7–30. https://doi.org/10.3322/caac.21442

Simons, M., Raposo, G., 2009. Exosomes - vesicular carriers for intercellular communication. Curr Opin Cell Biol. https://doi.org/10.1016/j.ceb.2009.03.007

Sivars, U., Aivazian, D., Pfeffer, S.R., 2003. Yip3 catalyses the dissociation of endosomal Rab–GDI complexes. Nature 2003 425:6960 425, 856–859. https://doi.org/10.1038/nature02057

Skog, J., Würdinger, T., van Rijn, S., Meijer, D.H., Gainche, L., Curry, W.T., Carter, B.S., Krichevsky, A.M., Breakefield, X.O., 2008. Glioblastoma microvesicles transport RNA and proteins that promote tumour growth and provide diagnostic biomarkers. Nat Cell Biol 10, 1470–1476. https://doi.org/10.1038/ncb1800

Smith, K.S., Bihannic, L., Gudenas, B.L., Haldipur, P., Tao, R., Gao, Q., Li, Y., Aldinger, K.A., Iskusnykh, I.Y., Chizhikov, V. V., Scoggins, M., Zhang, S., Edwards, A., Deng, M., Glass, I.A., Overman, L.M., Millman, J., Sjoboen, A.H., Hadley, J., Golser, J., Mankad, K., Sheppard, H., Onar-Thomas, A., Gajjar, A., Robinson, G.W., Hovestadt, V., Orr, B.A., Patay, Z., Millen, K.J., Northcott, P.A., 2022a. Unified rhombic lip origins of group 3 and group 4 medulloblastoma. Nature 2022 609:7929 609, 1012–1020. https://doi.org/10.1038/s41586-022-05208-9

Smith, K.S., Bihannic, L., Gudenas, B.L., Haldipur, P., Tao, R., Gao, Q., Li, Y., Aldinger, K.A., Iskusnykh, I.Y., Chizhikov, V. V., Scoggins, M., Zhang, S., Edwards, A., Deng, M., Glass, I.A., Overman, L.M., Millman, J., Sjoboen, A.H., Hadley, J., Golser, J., Mankad, K., Sheppard, H., Onar-Thomas, A., Gajjar, A., Robinson, G.W., Hovestadt, V., Orr, B.A., Patay, Z., Millen, K.J., Northcott, P.A., 2022b. Unified rhombic lip origins of group 3 and group 4 medulloblastoma. Nature 2022 609:7929 609, 1012–1020. https://doi.org/10.1038/s41586-022-05208-9

Smith, M.J., Beetz, C., Williams, S.G., Bhaskar, S.S., O'Sullivan, J., Anderson, B., Daly, S.B., Urquhart, J.E., Bholah, Z., Oudit, D., Cheesman, E., Kelsey, A., McCabe, M.G., Newman, W.G., Evans, D.G.R., 2014. Germline mutations in SUFU cause Gorlin syndrome-associated childhood medulloblastoma and redefine the risk associated with PTCH1 mutations. J Clin Oncol 32, 4155–61. https://doi.org/10.1200/JCO.2014.58.2569

Smoll, N.R., Drummond, K.J., 2012. The incidence of medulloblastomas and primitive neurectodermal tumours in adults and children. Journal of Clinical Neuroscience 19, 1541–1544. https://doi.org/10.1016/j.jocn.2012.04.009

Sobajima, T., Yoshimura, S.I., Iwano, T., Kunii, M., Watanabe, M., Atik, N., Mushiake, S., Morii, E., Koyama, Y., Miyoshi, E., Harada, A., 2015. Rab11a is required for apical protein localisation in the intestine. Biol Open 4, 86–94. https://doi.org/10.1242/BIO.20148532/-/DC1

Stenmark, H., 2009. Rab GTPases as coordinators of vesicle traffic. Nat Rev Mol Cell Biol. https://doi.org/10.1038/nrm2728

Stenmark, H., Olkkonen, V.M., 2001. The Rab GTPase family. Genome Biol. https://doi.org/10.1186/gb-2001-2-5-reviews3007

Stoorvogel, W., Strous, G.J., Geuze, H.J., Oorschot, V., Schwartzt, A.L., 1991. Late endosomes derive from early endosomes by maturation. Cell 65, 417–427. https://doi.org/10.1016/0092-8674(91)90459-C

Sui, Y., Zheng, X., Zhao, D., 2015. Rab31 promoted hepatocellular carcinoma (HCC) progression via inhibition of cell apoptosis induced by PI3K/AKT/Bcl-2/BAX pathway. Tumor Biology 36, 8661–8670. https://doi.org/10.1007/S13277-015-3626-5/FIGURES/6

Svalina, M.N., Kikuchi, K., Abraham, J., Lal, S., Davare, M.A., Settelmeyer, T.P., Young, M.C., Peckham, J.L., Cho, Y.J., Michalek, J.E., Hernandez, B.S., Berlow, N.E., Jackson, M., Guillaume, D.J., Selden, N.R., Bigner, D.D., Nazemi, K.J., Green, S.C., Corless, C.L., Gultekin, S., Mansoor, A., Rubin, B.P., Woltjer, R., Keller, C., 2016. IGF1R as a Key Target in High Risk, Metastatic Medulloblastoma. Sci Rep 6, 1–14. https://doi.org/10.1038/srep27012

Szklarczyk, D., Gable, A.L., Lyon, D., Junge, A., Wyder, S., Huerta-Cepas, J., Simonovic, M., Doncheva, N.T., Morris, J.H., Bork, P., Jensen, L.J., Von Mering, C., 2019. STRING v11: protein–protein association networks with increased coverage, supporting functional discovery in genome-wide experimental datasets. Nucleic Acids Res 47, D607. https://doi.org/10.1093/NAR/GKY1131

Tai, Y.L., Chen, K.C., Hsieh, J.T., Shen, T.L., 2018. Exosomes in cancer development and clinical applications. Cancer Sci 109, 2364. https://doi.org/10.1111/CAS.13697

Takahashi, R.H., Milner, T.A., Li, F., Nam, E.E., Edgar, M.A., Yamaguchi, H., Beal, M.F., Xu, H., Greengard, P., Gouras, G.K., 2002. Intraneuronal Alzheimer Aβ42 accumulates in multivesicular bodies and is associated with synaptic pathology. American Journal of Pathology 161, 1869–1879. https://doi.org/10.1016/S0002-9440(10)64463-X

Tamai, K., Shiina, M., Tanaka, N., Nakano, T., Yamamoto, A., Kondo, Y., Kakazu, E., Inoue, J., Fukushima, K., Sano, K., Ueno, Y., Shimosegawa, T., Sugamura, K., 2012. Regulation of hepatitis C virus secretion by the Hrs-dependent exosomal pathway. Virology 422, 377–385. https://doi.org/10.1016/j.virol.2011.11.009

Taylor, D.D., Gerçel-Taylor, C., 2005. Tumour-derived exosomes and their role in cancer-associated T-cell signalling defects. Br J Cancer 92, 305–311. https://doi.org/10.1038/sj.bjc.6602316

Taylor, M.D., Northcott, P.A., Korshunov, A., Remke, M., Cho, Y.J., Clifford, S.C., Eberhart, C.G., Parsons, D.W., Rutkowski, S., Gajjar, A., Ellison, D.W., Lichter, P., Gilbertson, R.J., Pomeroy, S.L., Kool, M., Pfister, S.M., 2012. Molecular subgroups of medulloblastoma: The current consensus. Acta Neuropathol 123, 465–472. https://doi.org/10.1007/s00401-011-0922-z

Tegla, M.G.G., Buenaventura, D.F., Kim, D.Y., Thakurdin, C., Gonzalez, K.C., Emerson, M.M., 2020. OTX2 represses sister cell fate choices in the developing retina to promote photoreceptor specification. Elife 9. https://doi.org/10.7554/ELIFE.54279

Théry, C., Boussac, M., Véron, P., Ricciardi-Castagnoli, P., Raposo, G., Garin, J., Amigorena, S., 2001. Proteomic Analysis of Dendritic Cell-Derived Exosomes: A Secreted Subcellular Compartment Distinct from Apoptotic Vesicles. The Journal of Immunology 166, 7309–7318. https://doi.org/10.4049/JIMMUNOL.166.12.7309

Théry, C., Duban, L., Segura, E., Væron, P., Lantz, O., Amigorena, S., 2002. Indirect activation of naïve CD4+ T cells by dendritic cell–derived exosomes. Nature Immunology 2002 3:12 3, 1156–1162. https://doi.org/10.1038/ni854

Théry, C., Witwer, K.W., Aikawa, E., Alcaraz, M.J., Anderson, J.D., Andriantsitohaina, R., Antoniou, A., Arab, T., Archer, F., Atkin-Smith, G.K., Ayre, D.C., Bach, J.M., Bachurski, D., Baharvand, H., Balaj, L., Baldacchino, S., Bauer, N.N., Baxter, A.A., Bebawy, M., Beckham, C., Bedina Zavec, A., Benmoussa, A., Berardi, A.C., Bergese, P., Bielska, E., Blenkiron, C., Bobis-Wozowicz, S., Boilard, E., Boireau, W., Bongiovanni, A., Borràs, F.E., Bosch, S., Boulanger, C.M., Breakefield, X., Breglio, A.M., Brennan, M., Brigstock, D.R., Brisson, A., Broekman, M.L.D., Bromberg, J.F., Bryl-Górecka, P., Buch, S., Buck, A.H., Burger, D., Busatto, S., Buschmann, D., Bussolati, B., Buzás, E.I., Byrd, J.B., Camussi, G., Carter, D.R.F., Caruso, S., Chamley, L.W., Chang, Y.T., Chaudhuri, A.D., Chen, C., Chen, S., Cheng, L., Chin, A.R., Clayton, A., Clerici, S.P., Cocks, A., Cocucci, E., Coffey, R.J., Cordeiro-da-Silva, A., Couch, Y., Coumans, F.A.W., Coyle, B., Crescitelli, R., Criado, M.F., D'Souza-Schorey, C., Das, S., de Candia, P., De Santana, E.F., De Wever, O., del Portillo, H.A., Demaret, T., Deville, S., Devitt, A., Dhondt, B., Di Vizio, D., Dieterich, L.C., Dolo, V., Dominguez Rubio, A.P., Dominici, M., Dourado, M.R., Driedonks, T.A.P., Duarte, F. V., Duncan, H.M., Eichenberger, R.M., Ekström, K., EL Andaloussi, S., Elie-Caille, C., Erdbrügger, U., Falcón-Pérez, J.M., Fatima, F., Fish, J.E., Flores-Bellver, M., Försönits, A., Frelet-Barrand, A., Fricke, F., Fuhrmann, G., Gabrielsson, S., Gámez-Valero, A., Gardiner, C., Gärtner, K., Gaudin, R., Gho, Y.S., Giebel, B., Gilbert, C., Gimona, M., Giusti, I., Goberdhan, D.C.I., Görgens, A., Gorski, S.M., Greening, D.W., Gross, J.C., Gualerzi, A., Gupta, G.N., Gustafson, D., Handberg, A., Haraszti, R.A., Harrison, P., Hegyesi, H., Hendrix, A., Hill, A.F., Hochberg, F.H., Hoffmann, K.F., Holder, B., Holthofer, H., Hosseinkhani, B., Hu, G., Huang, Y., Huber, V., Hunt, S., Ibrahim, A.G.E., Ikezu, T., Inal, J.M., Isin, M., Ivanova, A., Jackson, H.K., Jacobsen, S., Jay, S.M., Jayachandran, M., Jenster, G., Jiang, L., Johnson, S.M., Jones, J.C., Jong, A., Jovanovic-Talisman, T., Jung, S., Kalluri, R., Kano, S. ichi, Kaur, S., Kawamura, Y., Keller, E.T., Khamari, D., Khomyakova, E., Khvorova, A., Kierulf, P., Kim, K.P., Kislinger, T., Klingeborn, M., Klinke, D.J., Kornek, M., Kosanović, M.M., Kovács, Á.F., Krämer-Albers, E.M., Krasemann, S., Krause, M., Kurochkin, I. V., Kusuma, G.D., Kuypers, S., Laitinen, S., Langevin, S.M., Languino, L.R., Lannigan, J., Lässer, C., Laurent, L.C., Lavieu, G., Lázaro-Ibáñez, E., Le Lay, S., Lee, M.S.,

Lee, Y.X.F., Lemos, D.S., Lenassi, M., Leszczynska, A., Li, I.T.S., Liao, K., Libregts, S.F., Ligeti, E., Lim, R., Lim, S.K., Linē, A., Linnemannstöns, K., Llorente, A., Lombard, C.A., Lorenowicz, M.J., Lörincz, Á.M., Lötvall, J., Lovett, J., Lowry, M.C., Loyer, X., Lu, Q., Lukomska, B., Lunavat, T.R., Maas, S.L.N., Malhi, H., Marcilla, A., Mariani, J., Mariscal, J., Martens-Uzunova, E.S., Martin-Jaular, L., Martinez, M.C., Martins, V.R., Mathieu, M., Mathivanan, S., Maugeri, M., McGinnis, L.K., McVey, M.J., Meckes, D.G., Meehan, K.L., Mertens, I., Minciacchi, V.R., Möller, A., Møller Jørgensen, M., Morales-Kastresana, A., Morhayim, J., Mullier, F., Muraca, M., Musante, L., Mussack, V., Muth, D.C., Myburgh, K.H., Najrana, T., Nawaz, M., Nazarenko, I., Nejsum, P., Neri, C., Neri, T., Nieuwland, R., Nimrichter, L., Nolan, J.P., Nolte-'t Hoen, E.N.M., Noren Hooten, N., O'Driscoll, L., O'Grady, T., O'Loghlen, A., Ochiya, T., Olivier, M., Ortiz, A., Ortiz, L.A., Osteikoetxea, X., Ostegaard, O., Ostrowski, M., Park, J., Pegtel, D.M., Peinado, H., Perut, F., Pfaffl, M.W., Phinney, D.G., Pieters, B.C.H., Pink, R.C., Pisetsky, D.S., Pogge von Strandmann, E., Polakovicova, I., Poon, I.K.H., Powell, B.H., Prada, I., Pulliam, L., Quesenberry, P., Radeghieri, A., Raffai, R.L., Raimondo, S., Rak, J., Ramirez, M.I., Raposo, G., Rayyan, M.S., Regev-Rudzki, N., Ricklefs, F.L., Robbins, P.D., Roberts, D.D., Rodrigues, S.C., Rohde, E., Rome, S., Rouschop, K.M.A., Rughetti, A., Russell, A.E., Saá, P., Sahoo, S., Salas-Huenuleo, E., Sánchez, C., Saugstad, J.A., Saul, M.J., Schiffelers, R.M., Schneider, R., Schøyen, T.H., Scott, A., Shahaj, E., Sharma, S., Shatnyeva, O., Shekari, F., Shelke, G.V., Shetty, A.K., Shiba, K., Siljander, P.R.M., Silva, A.M., Skowronek, A., Snyder, O.L., Soares, R.P., Sódar, B.W., Soekmadji, C., Sotillo, J., Stahl, P.D., Stoorvogel, W., Stott, S.L., Strasser, E.F., Swift, S., Tahara, H., Tewari, M., Timms, K., Tiwari, S., Tixeira, R., Tkach, M., Toh, W.S., Tomasini, R., Torrecilhas, A.C., Tosar, J.P., Toxavidis, V., Urbanelli, L., Vader, P., van Balkom, B.W.M., van der Grein, S.G., Van Deun, J., van Herwijnen, M.J.C., Van Keuren-Jensen, K., van Niel, G., van Royen, M.E., van Wijnen, A.J., Vasconcelos, M.H., Vechetti, I.J., Veit, T.D., Vella, L.J., Velot, É., Verweij, F.J., Vestad, B., Viñas, J.L., Visnovitz, T., Vukman, K. V., Wahlgren, J., Watson, D.C., Wauben, M.H.M., Weaver, A., Webber, J.P., Weber, V., Wehman, A.M., Weiss, D.J., Welsh, J.A., Wendt, S., Wheelock, A.M., Wiener, Z., Witte, L., Wolfram, J., Xagorari, A., Xander, P., Xu, J., Yan, X., Yáñez-Mó, M., Yin, H., Yuana, Y., Zappulli, V., Zarubova, J., Žėkas, V., Zhang, J. ye, Zhao, Z., Zheng, L., Zheutlin, A.R., Zickler, A.M., Zimmermann, P., Zivkovic, A.M., Zocco, D., Zuba-Surma, E.K., 2018. Minimal information for studies of extracellular vesicles 2018 (MISEV2018): a position statement of the International Society for Extracellular Vesicles and update of the MISEV2014 guidelines. J Extracell Vesicles 7. https://doi.org/10.1080/20013078.2018.1535750

Thomas, A., Noël, G., 2019. Medulloblastoma: Optimizing care with a multidisciplinary approach. J Multidiscip Healthc 12, 335–347. https://doi.org/10.2147/JMDH.S167808

Thomou, T., Mori, M.A., Dreyfuss, J.M., Konishi, M., Sakaguchi, M., Wolfrum, C., Rao, T.N., Winnay, J.N., Garcia-Martin, R., Grinspoon, S.K., Gorden, P., Kahn,

C.R., 2017. Adipose-derived circulating miRNAs regulate gene expression in other tissues. Nature 542, 450–455. https://doi.org/10.1038/nature21365

Thompson, M.C., Fuller, C., Hogg, T.L., Dalton, J., Finkelstein, D., Lau, C.C., Chintagumpala, M., Adesina, A., Ashley, D.M., Kellie, S.J., Taylor, M.D., Curran, T., Gajjar, A., Gilbertson, R.J., 2006. Genomics identifies medulloblastoma subgroups that are enriched for specific genetic alterations. Journal of Clinical Oncology 24, 1924–1931. https://doi.org/10.1200/JCO.2005.04.4974/SUPPL_FILE/APPENDIX_TABLE_3.XLS

Tischkowitz, M.D., Chisholm, J., Gaze, M., Michalski, A., Rosser, E.M., 2004. Medulloblastoma as a first presentation of fanconi anemia. J Pediatr Hematol Oncol 26, 52–55. https://doi.org/10.1097/00043426-200401000-00016

Tong, M., Chan, K.W., Bao, J.Y.J., Wong, K.Y., Chen, J.N., Kwan, P.S., Tang, K.H., Fu, L., Qin, Y.R., Lok, S., Guan, X.Y., Ma, S., 2012. Rab25 is a tumor suppressor gene with antiangiogenic and anti-invasive activities in esophageal squamous cell carcinoma. Cancer Res 72, 6024–6035. https://doi.org/10.1158/0008-5472.CAN-12-1269/650493/AM/RAB25-IS-A-TUMOR-SUPPRESSOR-GENE-WITH-ANTI

Trams, E.G., Lauter, C.J., Norman Salem, J., Heine, U., 1981. Exfoliation of membrane ecto-enzymes in the form of micro-vesicles. BBA - Biomembranes 645, 63–70. https://doi.org/10.1016/0005-2736(81)90512-5

Tripolitsioti, D., Kumar, K.S., Neve, A., Migliavacca, J., Capdeville, C., Rushing, E.J., Ma, M., Kijima, N., Sharma, A., Pruschy, M., McComb, S., Taylor, M.D., Grotzer, M.A., Baumgartner, M., 2018. MAP4K4 controlled integrin β1 activation and c-Met endocytosis are associated with invasive behavior of medulloblastoma cells. Oncotarget 9, 23220. https://doi.org/10.18632/ONCOTARGET.25294

Tyedmers, J., Madariaga, M.L., Lindquist, S., 2008. Prion Switching in Response to Environmental Stress. PLoS Biol 6, 2605–2613. https://doi.org/10.1371/JOURNAL.PBIO.0060294

Tzeng, H.T., Wang, Y.C., 2016. Rab-mediated vesicle trafficking in cancer. J Biomed Sci 23, 1–7. https://doi.org/10.1186/s12929-016-0287-7

Uddin, F., Rudin, C.M., Sen, T., 2020. CRISPR Gene Therapy: Applications, Limitations, and Implications for the Future. Front Oncol 10, 1387. https://doi.org/10.3389/FONC.2020.01387

Ullrich, O., Reinsch, S., Urbé, S., Zerial, M., Parton, R.G., 1996. Rab11 regulates recycling through the pericentriolar recycling endosome. J Cell Biol 135, 913. https://doi.org/10.1083/JCB.135.4.913

Valko, M., Izakovic, M., Mazur, M., Rhodes, C.J., Telser, J., 2004. Role of oxygen radicals in DNA damage and cancer incidence. Mol Cell Biochem 266, 37–56. https://doi.org/10.1023/B:MCBI.0000049134.69131.89

Van Niel, G., D'Angelo, G., Raposo, G., 2018. Shedding light on the cell biology of extracellular vesicles. Nat Rev Mol Cell Biol. https://doi.org/10.1038/nrm.2017.125

Veleri, S., Punnakkal, P., Dunbar, G.L., Maiti, P., 2018. Molecular Insights into the Roles of Rab Proteins in Intracellular Dynamics and Neurodegenerative Diseases. Neuromolecular Med. https://doi.org/10.1007/s12017-018-8479-9

Veneroni, L., Boschetti, L., Barretta, F., Clerici, C.A., Simonetti, F., Schiavello, E., Biassoni, V., Spreafico, F., Gandola, L., Pecori, E., Diletto, B., Poggi, G., Gariboldi, F., Sensi, R., Massimino, M., 2017. Quality of life in long-term survivors treated for metastatic medulloblastoma with a hyperfractionated accelerated radiotherapy (HART) strategy. Child's Nervous System 33, 1969–1976. https://doi.org/10.1007/s00381-017-3548-1

Verbeek, M.M., Otte-Höller, I., Fransen, J.A.M., de Waal, R.M.W., 2002. Accumulation of the Amyloid-β Precursor Protein in Multivesicular Body-like Organelles. Journal of Histochemistry & Cytochemistry 50, 681–690. https://doi.org/10.1177/002215540205000509

Vetter, I.R., 2014. The structure of the G domain of the Ras superfamily. Ras Superfamily Small G Proteins: Biology and Mechanisms 1: General Features, Signaling 25–50. https://doi.org/10.1007/978-3-7091-1806-1_2/COVER

Viaud, S., Terme, M., Flament, C., Taieb, J., André, F., Novault, S., Escudier, B., Robert, C., Caillat-Zucman, S., Tursz, T., Zitvogel, L., Chaput, N., 2009. Dendritic Cell-Derived Exosomes Promote Natural Killer Cell Activation and Proliferation: A Role for NKG2D Ligands and IL-15Rα. PLoS One 4, 4942. https://doi.org/10.1371/JOURNAL.PONE.0004942

Vogel, G.F., Janecke, A.R., Krainer, I.M., Gutleben, K., Witting, B., Mitton, S.G., Mansour, S., Ballauff, A., Roland, J.T., Engevik, A.C., Cutz, E., Müller, T., Goldenring, J.R., Huber, L.A., Hess, M.W., 2017. Abnormal Rab11-Rab8-vesicles cluster in enterocytes of patients with Microvillus Inclusion Disease. Traffic 18, 453. https://doi.org/10.1111/TRA.12486

Vong, S., Kalluri, R., 2011. The Role of Stromal Myofibroblast and Extracellular Matrix in Tumor Angiogenesis. Genes Cancer. https://doi.org/10.1177/1947601911423940

Vrijsen, K.R., Sluijter, J.P.G., Schuchardt, M.W.L., van Balkom, B.W.M., Noort, W.A., Chamuleau, S.A.J., Doevendans, P.A.F.M., 2010. Cardiomyocyte progenitor cell-derived exosomes stimulate migration of endothelial cells. J Cell Mol Med. https://doi.org/10.1111/j.1582-4934.2010.01081.x

Waldenström, A., Gennebäck, N., Hellman, U., Ronquist, G., 2012. Cardiomyocyte microvesicles contain DNA/RNA and convey biological messages to target cells. PLoS One 7. https://doi.org/10.1371/journal.pone.0034653

Wandinger-Ness, A., Zerial, M., 2014. Rab Proteins and the Compartmentalization of the Endosomal System. Cold Spring Harb Perspect Biol 6, a022616. https://doi.org/10.1101/CSHPERSPECT.A022616

Wang, S., Shi, Y., 2022. Exosomes Derived from Immune Cells: The New Role of Tumor Immune Microenvironment and Tumor Therapy. Int J Nanomedicine 17, 6527. https://doi.org/10.2147/IJN.S388604

Wang, Yongjie, Zhang, B., Wang, J., Wu, H., Xu, S., Zhang, J., Wang, L., 2021. Discovery of LAMP-2A as potential biomarkers for glioblastoma development by modulating apoptosis through N-CoR degradation. Cell Commun Signal 19, 40. https://doi.org/10.1186/S12964-021-00729-8

Wang, Yunhao, Zhao, Y., Bollas, A., Wang, Yuru, Au, K.F., 2021. Nanopore sequencing technology, bioinformatics and applications. Nature Biotechnology 2021 39:11 39, 1348–1365. https://doi.org/10.1038/s41587-021-01108-x

Waszak, S.M., Northcott, P.A., Buchhalter, I., Robinson, G.W., Sutter, C., Groebner, S., Grund, K.B., Brugières, L., Jones, D.T.W., Pajtler, K.W., Morrissy, A.S., Kool, M., Sturm, D., Chavez, L., Ernst, A., Brabetz, S., Hain, M., Zichner, T., Segura-Wang, M., Weischenfeldt, J., Rausch, T., Mardin, B.R., Zhou, X., Baciu, C., Lawerenz, C., Chan, J.A., Varlet, P., Guerrini-Rousseau, L., Fults, D.W., Grajkowska, W., Hauser, P., Jabado, N., Ra, Y.S., Zitterbart, K., Shringarpure, S.S., De La Vega, F.M., Bustamante, C.D., Ng, H.K., Perry, A., MacDonald, T.J., Hernáiz Driever, P., Bendel, A.E., Bowers, D.C., McCowage, G., Chintagumpala, M.M., Cohn, R., Hassall, T., Fleischhack, G., Eggen, T., Wesenberg, F., Feychting, M., Lannering, B., Schüz, J., Johansen, C., Andersen, T. V., Röösli, M., Kuehni, C.E., Grotzer, M., Kjaerheim, K., Monoranu, C.M., Archer, T.C., Duke, E., Pomeroy, S.L., Shelagh, R., Frank, S., Sumerauer, D., Scheurlen, W., Ryzhova, M. V., Milde, T., Kratz, C.P., Samuel, D., Zhang, J., Solomon, D.A., Marra, M., Eils, R., Bartram, C.R., von Hoff, K., Rutkowski, S., Ramaswamy, V., Gilbertson, R.J., Korshunov, A., Taylor, M.D., Lichter, P., Malkin, D., Gajjar, A., Korbel, J.O., Pfister, S.M., 2018. Spectrum and prevalence of genetic predisposition in medulloblastoma: a retrospective genetic study and prospective validation in a clinical trial cohort. Lancet Oncol 19, 785. https://doi.org/10.1016/S1470-2045(18)30242-0

Waszak, S.M., Robinson, G.W., Gudenas, B.L., Smith, K.S., Forget, A., Kojic, M., Garcia-Lopez, J., Hadley, J., Hamilton, K. V., Indersie, E., Buchhalter, I., Kerssemakers, J., Jäger, N., Sharma, T., Rausch, T., Kool, M., Sturm, D., Jones, D.T.W., Vasilyeva, A., Tatevossian, R.G., Neale, G., Lombard, B., Loew, D., Nakitandwe, J., Rusch, M., Bowers, D.C., Bendel, A., Partap, S., Chintagumpala, M., Crawford, J., Gottardo, N.G., Smith, A., Dufour, C., Rutkowski, S., Eggen, T., Wesenberg, F., Kjaerheim, K., Feychting, M., Lannering, B., Schüz, J., Johansen, C., Andersen, T. V., Röösli, M., Kuehni, C.E., Grotzer, M., Remke, M., Puget, S., Pajtler, K.W., Milde, T., Witt, O., Ryzhova, M., Korshunov, A., Orr, B.A., Ellison, D.W., Brugieres, L., Lichter, P., Nichols, K.E., Gajjar, A., Wainwright, B.J., Ayrault, O., Korbel, J.O., Northcott,

P.A., Pfister, S.M., 2020. Germline Elongator mutations in sonic hedgehog medulloblastoma. Nature 580, 396. https://doi.org/10.1038/S41586-020-2164-5

Webber, J., Steadman, R., Mason, M.D., Tabi, Z., Clayton, A., 2010. Cancer exosomes trigger fibroblast to myofibroblast differentiation. Cancer Res 70, 9621–9630. https://doi.org/10.1158/0008-5472.CAN-10-1722

Weiss, R.B., Dunn, D.M., Atkins, J.F., Gesteland, R.F., 1990. Ribosomal frameshifting from -2 to +50 nucleotides. Prog Nucleic Acid Res Mol Biol 39, 159–183. https://doi.org/10.1016/S0079-6603(08)60626-1

Wheeler, D.B., Zoncu, R., Root, D.E., Sabatini, D.M., Sawyers, C.L., 2015. Identification of an Oncogenic RAB Protein. Science 350, 211. https://doi.org/10.1126/SCIENCE.AAA4903

Wilkins, H.M., Harris, J.L., Carl, S.M., E, L., Lu, J., Eva Selfridge, J., Roy, N., Hutfles, L., Koppel, S., Morris, J., Burns, J.M., Michaelis, M.L., Michaelis, E.K., Brooks, W.M., Swerdlow, R.H., 2014. Oxaloacetate activates brain mitochondrial biogenesis, enhances the insulin pathway, reduces inflammation and stimulates neurogenesis. Hum Mol Genet 23, 6528–6541. https://doi.org/10.1093/HMG/DDU371

Wilson, D.F., 2017. Oxidative phosphorylation: regulation and role in cellular and tissue metabolism. J Physiol 595, 7023. https://doi.org/10.1113/JP273839

Wilson, G.M., Fielding, A.B., Simon, G.C., Yu, X., Andrews, P.D., Haines, R.S., Frey, A.M., Peden, A.A., Gould, G.W., Prekeris, R., 2005. The FIP3-Rab11 protein complex regulates recycling endosome targeting to the cleavage furrow during late cytokinesis. Mol Biol Cell 16, 849–860. https://doi.org/10.1091/mbc.E04-10-0927

Wittinghofer, A., Vetter, I.R., 2011. Structure-Function Relationships of the G Domain, a Canonical Switch Motif. https://doi.org/10.1146/annurev-biochem-062708-134043 80, 943–971. https://doi.org/10.1146/ANNUREV-BIOCHEM-062708-134043

World Cancer Day 2023: Close the care gap - PAHO/WHO | Pan American Health Organization [WWW Document], n.d. URL https://www.paho.org/en/campaigns/world-cancer-day-2023-close-care-gap (accessed 3.21.24).

Wu, L., Xu, D., Zhou, L., Xie, B., Yu, L., Yang, H., Huang, L., Ye, J., Deng, H., Yuan, Y.A., Chen, S., Li, P., 2014. Rab8a-AS160-MSS4 Regulatory Circuit Controls Lipid Droplet Fusion and Growth. Dev Cell 30, 378–393. https://doi.org/10.1016/J.DEVCEL.2014.07.005

Wu, X., Northcott, P.A., Croul, S., Taylor, M.D., 2011. Mouse models of medulloblastoma. Chin J Cancer 30, 442. https://doi.org/10.5732/CJC.011.10040

Wu, X., Northcott, P.A., Dubuc, A., Dupuy, A.J., Shih, D.J.H., Witt, H., Croul, S., Bouffet, E., Fults, D.W., Eberhart, C.G., Garzia, L., Van Meter, T., Zagzag, D.,

Jabado, N., Schwartzentruber, J., Majewski, J., Scheetz, T.E., Pfister, S.M., Korshunov, A., Li, X.N., Scherer, S.W., Cho, Y.J., Akagi, K., MacDonald, T.J., Koster, J., McCabe, M.G., Sarver, A.L., Collins, V.P., Weiss, W.A., Largaespada, D.A., Collier, L.S., Taylor, M.D., 2012a. Clonal selection drives genetic divergence of metastatic medulloblastoma. Nature 482, 529–533. https://doi.org/10.1038/nature10825

Wu, X., Northcott, P.A., Dubuc, A., Dupuy, A.J., Shih, D.J.H., Witt, H., Croul, S., Bouffet, E., Fults, D.W., Eberhart, C.G., Garzia, L., Van Meter, T., Zagzag, D., Jabado, N., Schwartzentruber, J., Majewski, J., Scheetz, T.E., Pfister, S.M., Korshunov, A., Li, X.N., Scherer, S.W., Cho, Y.J., Akagi, K., MacDonald, T.J., Koster, J., McCabe, M.G., Sarver, A.L., Collins, V.P., Weiss, W.A., Largaespada, D.A., Collier, L.S., Taylor, M.D., 2012b. Clonal selection drives genetic divergence of metastatic medulloblastoma. Nature 482, 529–533. https://doi.org/10.1038/nature10825

Wu, X., Zheng, T., Zhang, B., 2017. Exosomes in Parkinson's Disease. Neurosci Bull. https://doi.org/10.1007/s12264-016-0092-z

Xiaoshuai, L., Qiushi, W., Rui, W., 2022. Advantages of CRISPR-Cas9 combined organoid model in the study of congenital nervous system malformations. Front Bioeng Biotechnol 10. https://doi.org/10.3389/FBIOE.2022.932936

Xu, Shouying, Cao, B., Xuan, G., Xu, Shu, An, Z., Zhu, C., Li, L., Tang, C., 2024. Function and regulation of Rab GTPases in cancers. Cell Biology and Toxicology 2024 40:1 40, 1–21. https://doi.org/10.1007/S10565-024-09866-5

Yakimchuk, K., 2015. Exosomes: isolation methods and specific markers. Materials and Methods 5. https://doi.org/10.13070/mm.en.5.1450

Yamagata, M., Weiner, J.A., Sanes, J.R., 2002a. Sidekicks: Synaptic Adhesion Molecules that Promote Lamina-Specific Connectivity in the Retina. Cell 110, 649–660. https://doi.org/10.1016/S0092-8674(02)00910-8

Yamagata, M., Weiner, J.A., Sanes, J.R., 2002b. Sidekicks: Synaptic Adhesion Molecules that Promote Lamina-Specific Connectivity in the Retina. Cell 110, 649–660. https://doi.org/10.1016/S0092-8674(02)00910-8

Yáñez-Mó, M., R-M Siljander, P., Andreu, Z., Bedina Zavec, A., Borràs, F.E., Buzas, E.I., Buzas, K., Casal, E., Cappello, F., Carvalho, J., Colás, E., Cordeiro-da Silva, A., Fais, S., Falcon-Perez, J.M., Ghobrial, I.M., Giebel, B., Gimona, M., Graner, M., Gursel, I., Gursel, M., H Heegaard, N.H., Hendrix, A., Kierulf, P., Kokubun, K., Kosanovic, M., Kralj-Iglic, V., Krämer-Albers, E.-M., Laitinen, S., Lässer, C., Lener, T., Ligeti, E., Linē, A., Lipps, G., Llorente, A., Lötvall, J., Manček-Keber, M., Marcilla, A., Mittelbrunn, M., Nazarenko, I., Nolte-, E.N., Nyman, T.A., Olivan, M., Oliveira, C., Pállinger, É., del Portillo, H.A., Reventós, J., Rigau, M., Rohde, E., Sammar, M., Sánchez-Madrid, F., Santarém, N., Schallmoser, K., Stampe Ostenfeld, M., Stoorvogel, W., Stukelj, R., Van der Grein, S.G., Helena Vasconcelos, M., M Wauben, M.H., De Wever, O., 2015.

Biological properties of extracellular vesicles and their physiological functions. J Extracell Vesicles. https://doi.org/10.3402/jev.v4.27066

Yang, R., Liu, G., Han, L., Qiu, Y., Wang, L., Wang, M., 2021. MiR-365a-3p-Mediated Regulation of HELLS/GLUT1 Axis Suppresses Aerobic Glycolysis and Gastric Cancer Growth. Front Oncol 11. https://doi.org/10.3389/FONC.2021.616390/FULL

Yee, A.J., Akens, M., Yang, B.L., Finkelstein, J., Zheng, P.-S., Deng, Z., Yang, B., 2007. The effect of versican G3 domain on local breast cancer invasiveness and bony metastasis. Breast Cancer Res 9. https://doi.org/10.1186/BCR1751

Yoon, S.O., Shin, S., Mercurio, A.M., 2005. Hypoxia Stimulates Carcinoma Invasion by Stabilizing Microtubules and Promoting the Rab11 Trafficking of the α6β4 Integrin. Cancer Res 65, 2761–2769. https://doi.org/10.1158/0008-5472.CAN-04-4122

Yoshimura, S.I., Gerondopoulos, A., Linford, A., Rigden, D.J., Barr, F.A., 2010. Family-wide characterization of the DENN domain Rab GDP-GTP exchange factors. Journal of Cell Biology 191, 367–381. https://doi.org/10.1083/jcb.201008051

Yousaf, M., Ali, M., 2020. Modulation of ABCG2 surface expression by Rab5 and Rab21 to overcome multidrug resistance in cancer cells. Xenobiotica 50, 988–996. https://doi.org/10.1080/00498254.2020.1716107

Yu, L., Zhu, G., Zhang, Z., Yu, Y., Zeng, L., Xu, Z., Weng, J., Xia, J., Li, J., Pathak, J.L., 2023. Apoptotic bodies: bioactive treasure left behind by the dying cells with robust diagnostic and therapeutic application potentials. Journal of Nanobiotechnology 2023 21:1 21, 1–26. https://doi.org/10.1186/S12951-023-01969-1

Zagrean, A.M., Hermann, D.M., Opris, I., Zagrean, L., Popa-Wagner, A., 2018. Multicellular crosstalk between exosomes and the neurovascular unit after cerebral ischemia. therapeutic implications. Front Neurosci. https://doi.org/10.3389/fnins.2018.00811

Zapotocky, M., Mata-Mbemba, D., Sumerauer, D., Liby, P., Lassaletta, A., Zamecnik, J., Krskova, L., Kyncl, M., Stary, J., Laughlin, S., Arnoldo, A., Hawkins, C., Tabori, U., Taylor, M.D., Bouffet, E., Raybaud, C., Ramaswamy, V., 2018. Differential patterns of metastatic dissemination across medulloblastoma subgroups. J Neurosurg Pediatr 21, 145–152. https://doi.org/10.3171/2017.8.PEDS17264

Zerial, M., McBride, H., 2001. Rab proteins as membrane organizers. Nat Rev Mol Cell Biol. https://doi.org/10.1038/35052055

Zhang, X.M., Ellis, S., Sriratana, A., Mitchell, C.A., Rowe, T., 2004. Sec15 Is an Effector for the Rab11 GTPase in Mammalian Cells. Journal of Biological Chemistry 279, 43027–43034. https://doi.org/10.1074/JBC.M402264200

Zhen, Y., Stenmark, H., 2015. Cellular functions of Rab GTPases at a glance. J Cell Sci 128, 3171–3176. https://doi.org/10.1242/JCS.166074/260447/AM/CELLULAR-FUNCTIONS-OF-RAB-GTPASES-AT-A-GLANCE

Zheng, Y., Campbell, E.C., Lucocq, J., Riches, A., Powis, S.J., 2013. Monitoring the Rab27 associated exosome pathway using nanoparticle tracking analysis. Exp Cell Res 319, 1706–1713. https://doi.org/10.1016/j.yexcr.2012.10.006

Zulkefli, K.L., Houghton, F.J., Gosavi, P., Gleeson, P.A., 2019. A role for Rab11 in the homeostasis of the endosome-lysosomal pathway. Exp Cell Res 380, 55–68. https://doi.org/10.1016/J.YEXCR.2019.04.010

Appendix

Appendix 1.1. Summary of pathways with gene upregulation after single cell RNA sequencing cluster analysis in HD-MB03 cells *Figure adapted from Linke et al., 2023.*

		HD-MB03								
		Cluster 1	Cluster 2	Cluster 3	Cluster 4	Cluster 5	Cluster 6	Cluster 7	Cluster 8	Cluster 9
Cell cycle	Ribosome		■							
	Translation		■							
	RNA splicing			■			■			
	Biosynthesis of amino acids	■		■			■			
	S phase			■			■			
	G2M transition			■						
	% G1	93.1	91.1	1.3	48.8	28.0	9.9	43.8	78.0	96.5
	% S	5.5	6.9	44.5	26.6	33.7	56.3	34.1	13.7	2.2
	% G2M	1.4	2.0	54.2	24.6	38.3	33.8	22.2	8.3	1.3
Metabolism	OxPhos	■		■	■			■		
	TCA cycle	■		■	■			■		
	Glycolysis	■		■						
	Purine/pyrimidine metabolism			■			■			
	Valine, leucine and isoleucine degradation	■		■						
	Tryptophan metabolism	■		■						
	Glutathione metabolism	■		■						
	Abnormal CSF lactate level			■						
ECM interaction	ECM receptor interaction									
	Collagen biosynthesis									
	Laminin interactions									
	Adherens junctions			■						
	Gap junctions									
	Tight junctions			■						
	Focal adhesion		■							
	p53 signalling pathway	■		■						
	cAMP signalling pathway									
	Ras signalling pathway			■						
	Insulin/IGF1 signalling pathway			■						
	PI3K signalling									
	WNT signalling	■								
	FOXO signalling	■								
	EC exosome	■		■						
	Glioma			■						
	Non-small cell lung cancer							■		

271

Appendix 1.2. Summary Kaplan-Meier survival curves of potential Rab GTPase targets in WNT, SHH and group 4 medulloblastoma *Overall survival probability of both non-metastatic and metastatic patients was determined using the Cavalli medulloblastoma dataset from the R2: Genomics Analysis and Visualisation Platform. (A) WNT (M0 + M+): n=63, (B) SHH (M0 + M+): n=172, SHH (M+): n=22, (C) group 4 (M0 + M+): n=264, group 4 (M+): n=92. M0 denotes patients that were not metastatic and diagnosis. WNT M+ data is not present because there were too few patients to generate the survival curve. M+ denotes patients that were metastatic at diagnosis. Shaded green – high expression has a statistically significant (p≤ 0.05) better outcome. Shaded red – high expression has a statistically significant poorer outcome.*

A)

Rab GTPase	n		WNT (M0 + M+)
	High	Low	p value
Rab1A	54	9	0.0032
Rab1B	35	28	0.124
Rab3A	52	11	0.185
Rab3C	36	27	0.077
Rab7A	53	10	0.085
Rab8B	39	24	0.083
Rab10	38	25	0.032
Rab11A	43	20	0.157
Rab11B	14	49	0.249
Rab13	48	15	0.13
Rab27A	13	50	0.272
Rab37	54	9	0.020
Rab40B	45	18	0.411

B)	Rab GTPase	n		SHH (M0 + M+) p value	n		SHH (M+) p value
		High	Low		High	Low	
	Rab1A	162	10	0.00028	13	9	0.526
	Rab1B	164	8	0.029	13	9	0.146
	Rab3A	66	106	0.084	9	13	0.056
	Rab3C	14	158	0.057	9	13	0.0066
	Rab6A	157	15	0.019	11	11	0.528
	Rab7A	126	46	0.041	10	12	0.408
	Rab8B	113	59	0.011	11	11	0.232
	Rab10	17	155	0.00056	12	10	0.362
	Rab11A	164	8	0.00054	8	14	0.306
	Rab11B	160	12	0.018	13	9	0.202
	Rab13	70	102	0.0069	8	14	0.088
	Rab27A	95	77	0.120	10	12	0.148
	Rab37	12	160	0.080	9	13	0.0046
	Rab40B	134	38	0.021	11	11	0.560

C)

Rab GTPase	n		Group 4 (M0 + M+) p value	n		Group 4 (M+) p value
	High	Low		High	Low	
Rab1A	145	119	0.0023	46	46	0.037
Rab1B	58	206	0.03	19	73	0.022
Rab3A	32	232	0.0036	71	21	0.019
Rab3C	244	20	0.0011	41	51	0.00056
Rab7A	10	254	0.0012	10	82	0.388
Rab8B	85	179	0.061	29	63	0.026
Rab10	27	237	0.17	84	8	0.000013
Rab11A	190	74	0.168	69	23	0.134
Rab11B	214	50	0.0017	27	65	0.057
Rab13	209	55	0.003	73	19	0.051
Rab27A	185	79	0.0069	63	29	0.148
Rab37	52	212	0.057	13	79	0.087
Rab40B	125	139	0.063	31	61	0.164

Appendix 1.3. Roles of predicted Rab GTPase functional partners identified by STRING pathway analysis. *All functional information of proteins provided was found on the STRING platform (Szklarczyk et al., 2018).*

Rab GTPase	Interactor(s)	Function
Rab1B	Rab1A, Rab11B	Members of the Rab GTPase family of small GTPase proteins which are key regulators of intracellular membrane trafficking.
	GDI1, GDI2	Regulates GDP/GTP exchange from Rab proteins by inhibiting the dissociation of GDP from them and subsequent binding of GTP to them.
	TBC1 domain family member 20 (TBC120)	GTPase-activating protein specific for Rab1 and Rab2 GTPase families.
	Golgin subfamily A member 2 (GOLGA2)	Peripheral membrane component of the cis-Golgi stack that acts as a membrane skeleton which maintains the structure of the Golgi apparatus, and as a vesicle tether that facilitates vesicle fusion to the Golgi membrane.
	Trafficking protein particle complex subunit 8, 12 and 13 (TRAPPC8, TRAPPC12, TRAPPC13)	Involved in endoplasmic reticulum to Golgi apparatus trafficking, role in chromosome and kinetochore assembly and stability.
	Rab proteins geranylgeranyltransferase component A 1 (CHM)	Substrate-binding subunit of the Rab geranylgeranyltransferase (GGTase) complex.
Rab8B	Rab1B Rab8A	Member(s) of the Rab GTPase family of small GTPase proteins which are key regulators of intracellular membrane trafficking.
	GDI1 GDI2	Regulates GDP/GTP exchange from Rab proteins by inhibiting the dissociation of GDP from them and subsequent binding of GTP to them.
	Rab-3A-interacting protein (Rab3IP)	Guanine nucleotide exchange factor thought to activate Rab8A and Rab8B. Promotes exchange of GDP for GTP, converting the Rab from a GDP-bound inactive to a GTP-bound active form.
	Rab3IL1	Guanine nucleotide exchange factor for Rab3A, activating it.
	DENN domain-containing protein 1C (DENND1C)	Guanine nucleotide exchange factor which may activate Rab8A, Rab13 and Rab35.

| Rab GTPase	Interactor(s)	Function
Rab8B	MICAL-like protein 2 (MICALL2)	Effector of small Rab GTPases. Involved in junctional complex assembly through regulation of cell adhesion molecule transport to the plasma membrane.
	PEX5-related protein (PEX5L)	Accessory subunit of hyperpolarisation-activated cyclic nucleotide-gated channels, regulating their cell-surface expression and cyclic nucleotide dependence.
	Otoferlin (OTOF)	Calcium ion sensor involved in calcium ion-associated synaptic vesicle-plasma membrane fusion.
Rab11A	Myosin Va (MYO5A)	Part of the unconventional myosins group. Helps transport melanosomes.
	Myosin Vb (MYO5B)	Involved in vesicular trafficking through association with the CART complex.
	Rab11 family-interacting proteins 1, 2 and 5 (Rab11FIP1, Rab11FIP2, Rab11FIP5)	Involved in endosomal recycling through regulation of trafficking of vesicles from the endosomal recycling compartment to the plasma membrane.
	Exocyst complex component 6 (EXOC6)	Part of the exocyst complex involved in docking of exocytic vesicles with fusion sites on the plasma membrane.
	Phosphatidylinositol 4-kinase beta (PI4KB)	Phosphorylates phosphatidyl inositol in the first step in the production of inositol-1,4,5-triphosphate.
	Optineurin (OPTN)	Role in maintenance of the Golgi complex, membrane trafficking and exocytosis through interaction with myosin VI and Rab8A.
Rab13	Exocyst complex component 2, 4, 6, 7 and 8 (EXOC2, 4, 6, 7 and 8)	Part of the exocyst complex involved in docking of exocytic vesicles with fusion sites on the plasma membrane.
	MICAL-like protein 2 (MICALL2)	Effector of small Rab GTPases. Involved in junctional complex assembly through regulation of cell adhesion molecule transport to the plasma membrane.
	DENN domain-containing protein 1C (DENND1C)	Guanine nucleotide exchange factor which may activate Rab8A, Rab13 and Rab35.

| Rab GTPase	Interactor(s)	Function
Rab13	TBC1 domain family member 1 (TBC1D1)	GTPase-activating protein for Rab family proteins. Involved in the trafficking and translocation of GLUT4-containing vesicles.
	TBC1 domain family member 4 (TBC1D4)	GTPase-activating protein for Rabs 2A, 8A, 10 and 14. Promotes insulin-induced glucose transporter (SLC2A4/GLUT4) translocation to the plasma membrane.
Rab40B	Cullin 5 (CUL5)	Core component of multiple Elongin-Cullin 2/5-SOCS-box protein E3 ubiquitin-protein ligase complexes which regulate the ubiquitination of protein targets.
	Elongin C (TCEB1)	Transcription elongation factor which increases RNA polymerase II transcription elongation past arresting sites.
	Rab40C Rab40A-like protein (Rab40AL)	Substrate-recognition components of the Elongin-Cullin-SOCS-box protein E3 ubiquitin ligase complex.
	SAP domain-containing ribonucleoprotein (SARNP)	Binds ssDNA and dsDNA with specificity for scaffold/matrix attachment region DNA.
	Homeobox protein cut-like 1 and 2 (CUX1, CUX2)	Broad roles in mammalian development as repressors of developmentally regulated gene expression. May be involved in neural specification.
	Metalloproteinase inhibitor 2 (TIMP2)	Complexes with metalloproteinases and irreversibly inactivates them.
	Pericentrin (PCNT)	Component of the filamentous matrix of the centrosome involves in the establishment of microtubule arrays in mitosis and meiosis.
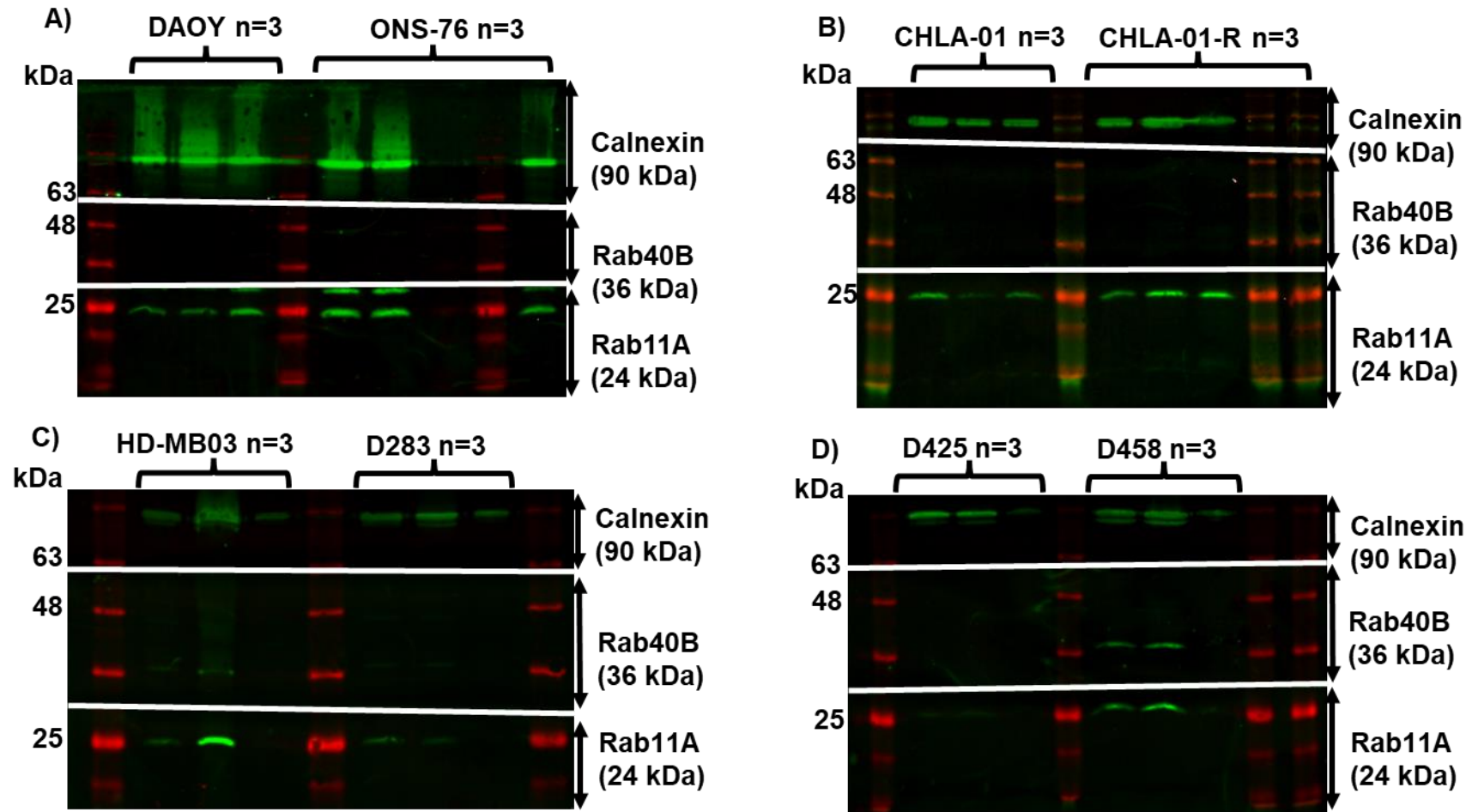
Appendix 1.4. – Full length Western blots of Rab11A endogenous protein expression analysis *Full length blots highlighting expression within SHH cell lines (A) group 4 cell lines (B) and group 3 cell lines (C, D). Imaged using a LI-COR imaging system. Blots were probed with anti-calnexin, anti-Rab40B and anti-Rab11A. BLUeye prestained protein ladder can be seen in red in each image. Molecular weights corresponding to the markers on the ladder in kilodaltons (kDa) can be seen on the left of each image.*
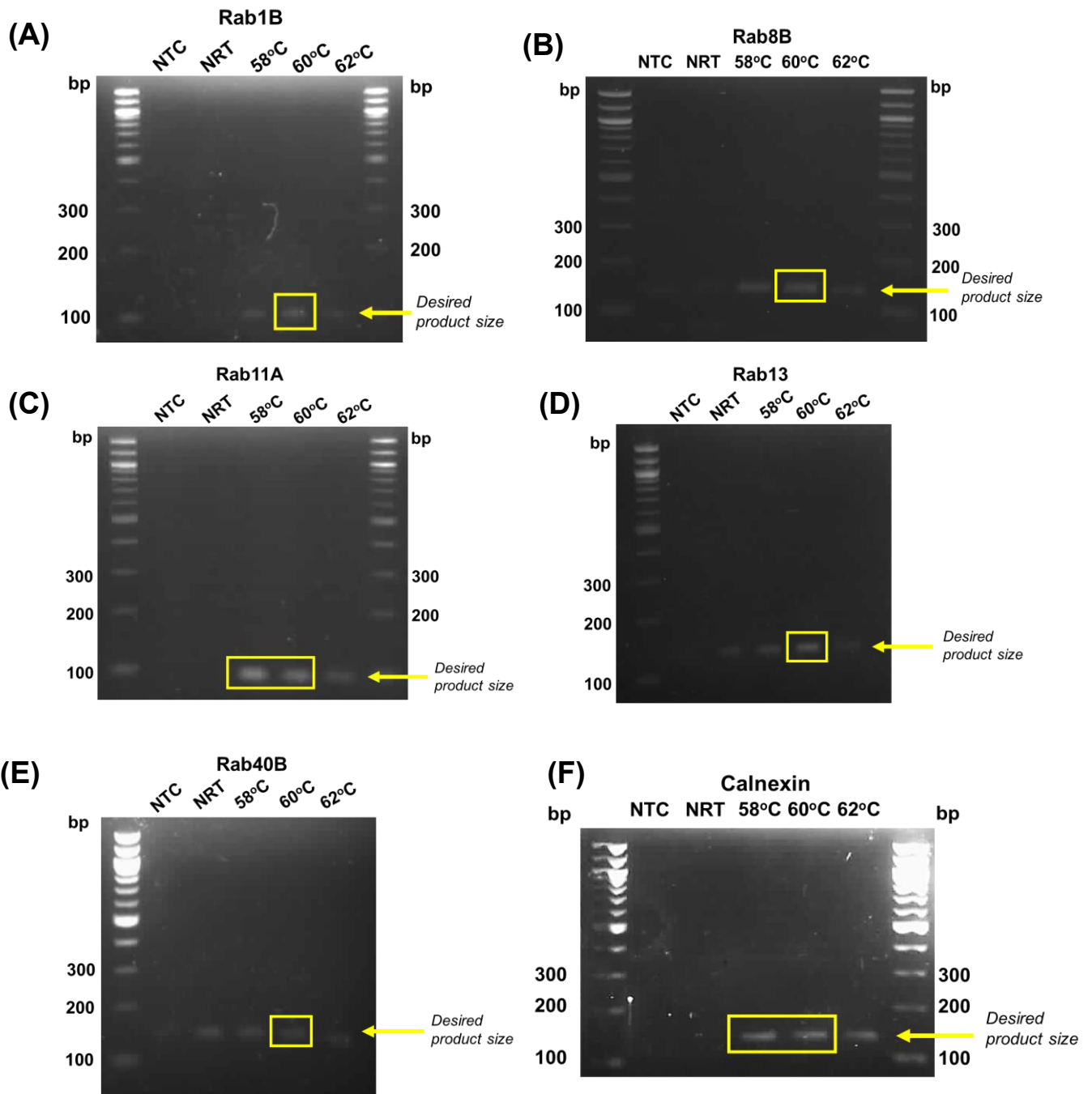
Appendix 1.5. – Annealing temperature optimisation of primers used for RT-qPCR Rab1B (A), Rab8B (B), Rab11A (C), Rab13 (D), Rab40B (E) and Calnexin (F). Primers were cycled between annealing temperatures of $58^oC – 62^oC$ and PCR products run on an agarose gel with 100bp ladder. Optimal annealing temperature of each primer is highlighted by the yellow box. Desired PCR product size is indicated by the yellow arrow. NTC – no transcript control. NRT – no reverse transcriptase control. bp – base pairs donated by 100bp ladder.
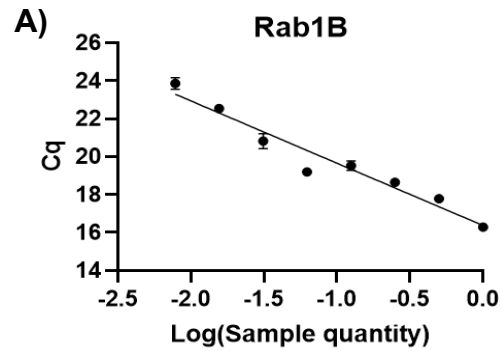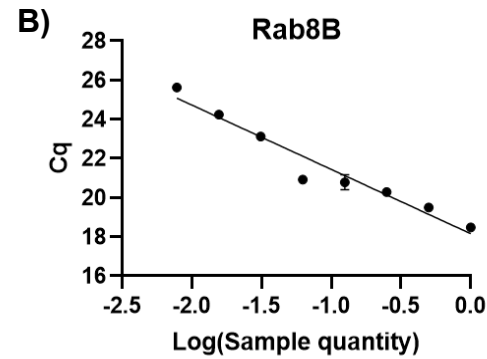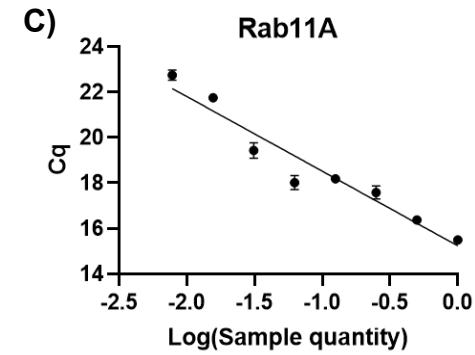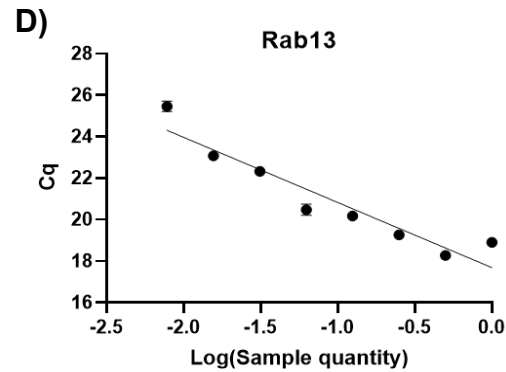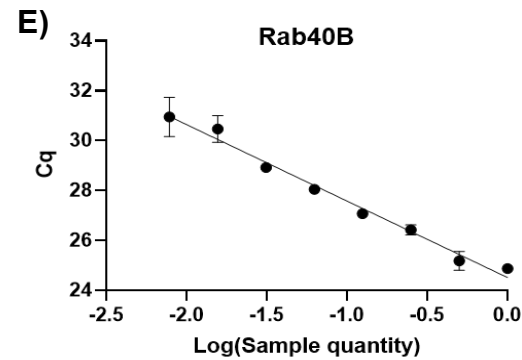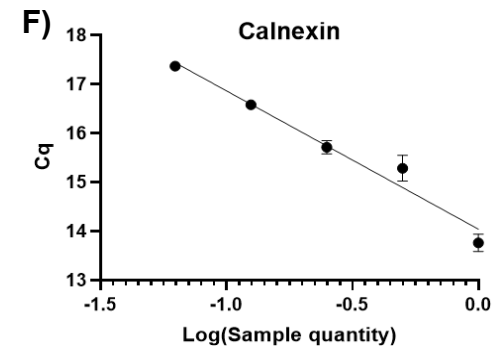
Appendix 1.6. – Primer efficiencies for RT-qPCR primer optimisation *Log$_2$ standard curve of D425 cDNA (ng/µl) plotted against Cq values (quantification cycle) used to calculate primer efficiencies. Efficiencies of primers designed for Rab1B (A), Rab8B (B), Rab11A (C), Rab13 (D), Rab40B (E) and Calnexin (F) were calculated. Slope, R^2 and efficiency calculated using GraphPad Prism.*
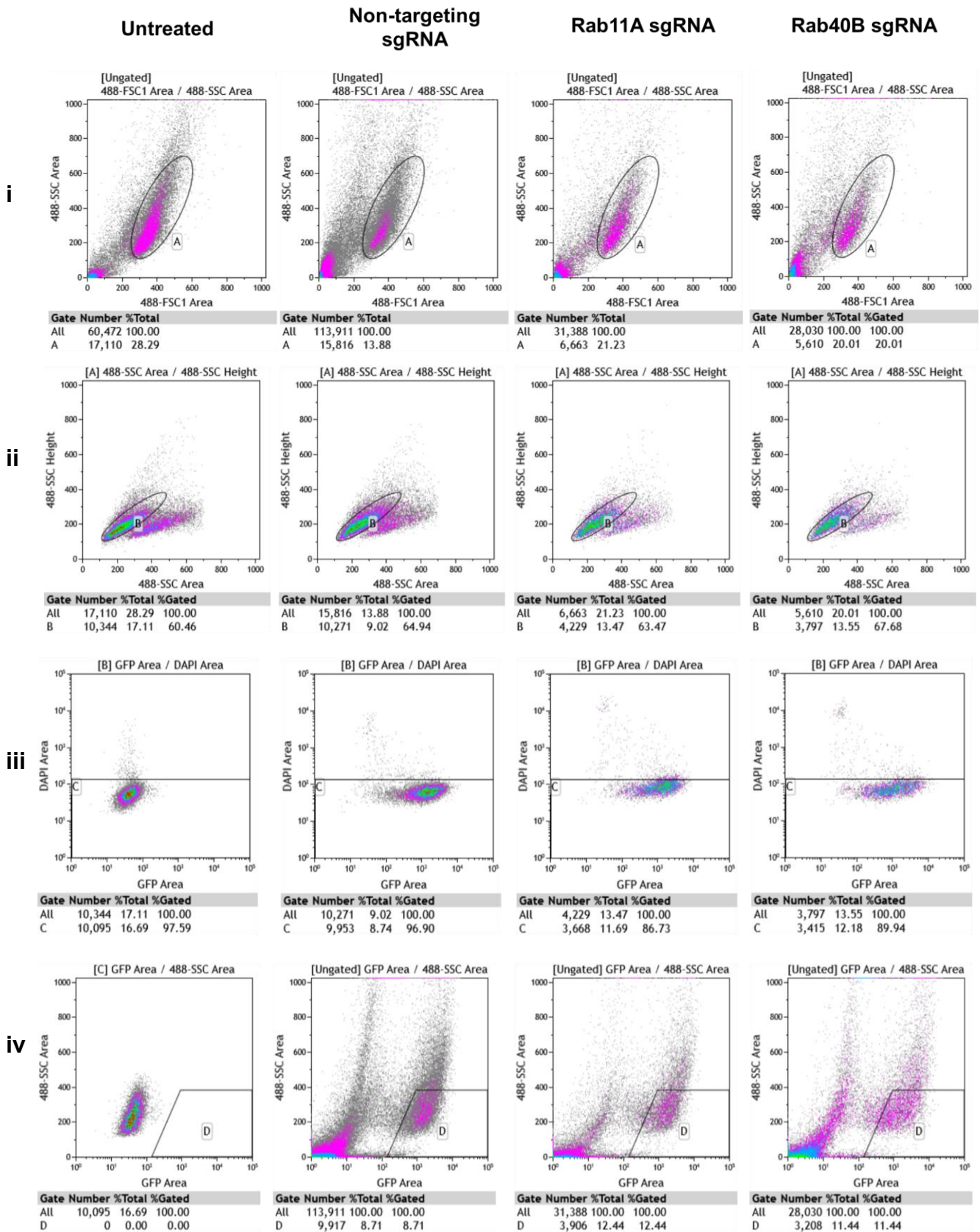
Appendix 1.7. Flow cytometry gating scatter plots of untreated HD-MB03 cells and HD-MB03 cells eletroporated with non-targeting, Rab11A or Rab40B sgRNA *i*) *Side scatter (SSC) and forward scatter (FSC) plot of whole content of samples, gate (A) represents cells. ii) SSC height and SSC area, gate (B) represents single cells. iii) DAPI and GFP signal plot, gate (C) represents live single cells (DAPI negative). iv) SSC and GFP plot, gate (D) represents live single cells with GFP expression. All gate parameters were set based on the untreated condition. The total number cells within each gate is given below each scatter plot. Analysis and graphs were generated using the Kaluza software.*

281

Appendix 1.8. – Non-targeting and Rab40B knockout cell line Oxford Nanopore sequencing read and cluster analysis summary

Sample ID	cluster_id	Raw number of reads	% of total reads
NT1 A2	1	40791	39%
NT1 A10	1	30466	40%
NT1 H7	1	57569	42%
40B A9	1	9378	7%
	2	19389	15%
40B B4	1	47350	30%
	2	14320	9%
40B B10	1	8042	9%
	2	10343	12%
	3	5495	6%
	5	5757	6%
40B C12	1	39443	22%
	2	29539	17%
	3	15810	9%
40B E4	1	41406	34%
40B F5	1	20843	10%
	2	17080	9%
	3	16647	8%
	4	16612	8%
40B F9	1	38798	33%
	2	5212	4%
40B G8	1	10717	7%
	2	32162	20%
	3	5667	3%
40B G11	1	29896	30%
40B H1	1	10872	9%
	3	6279	5%
	5	16886	14%
	6	5845	5%
	7	1081	1%
	9	6720	5%
	10	66	0%
	12	111	0%
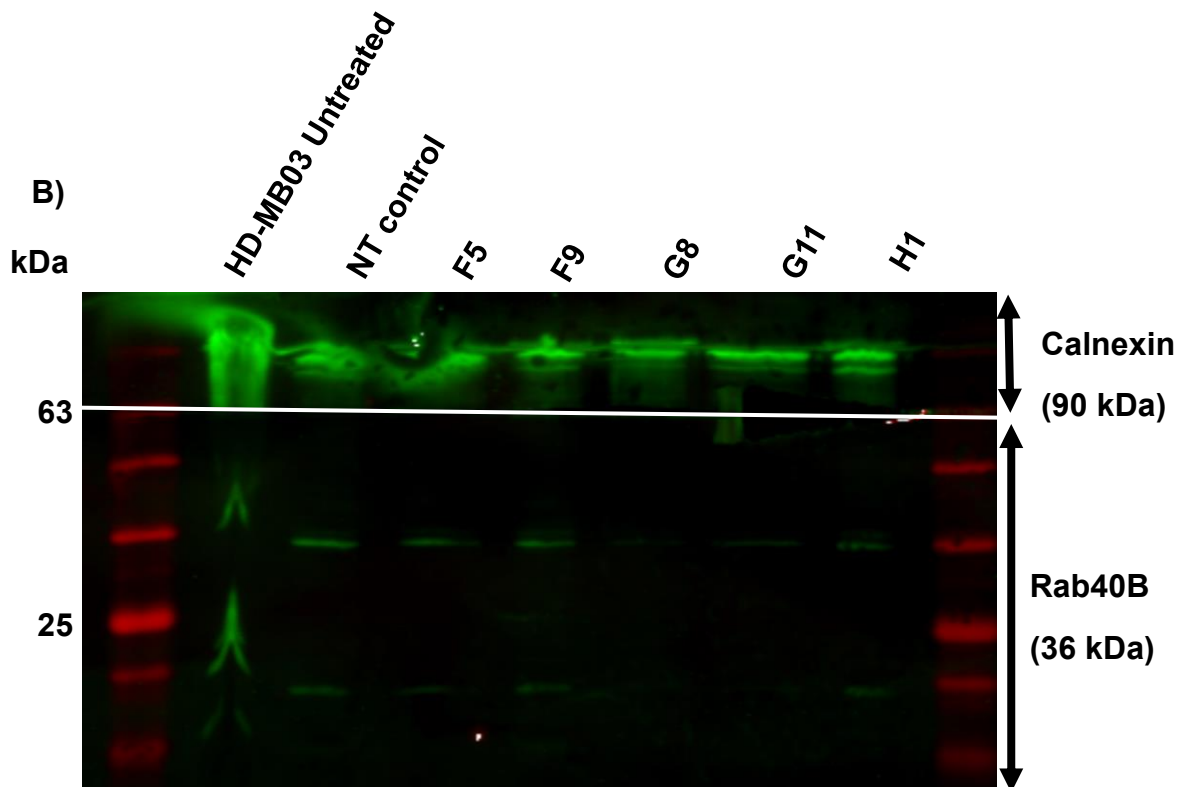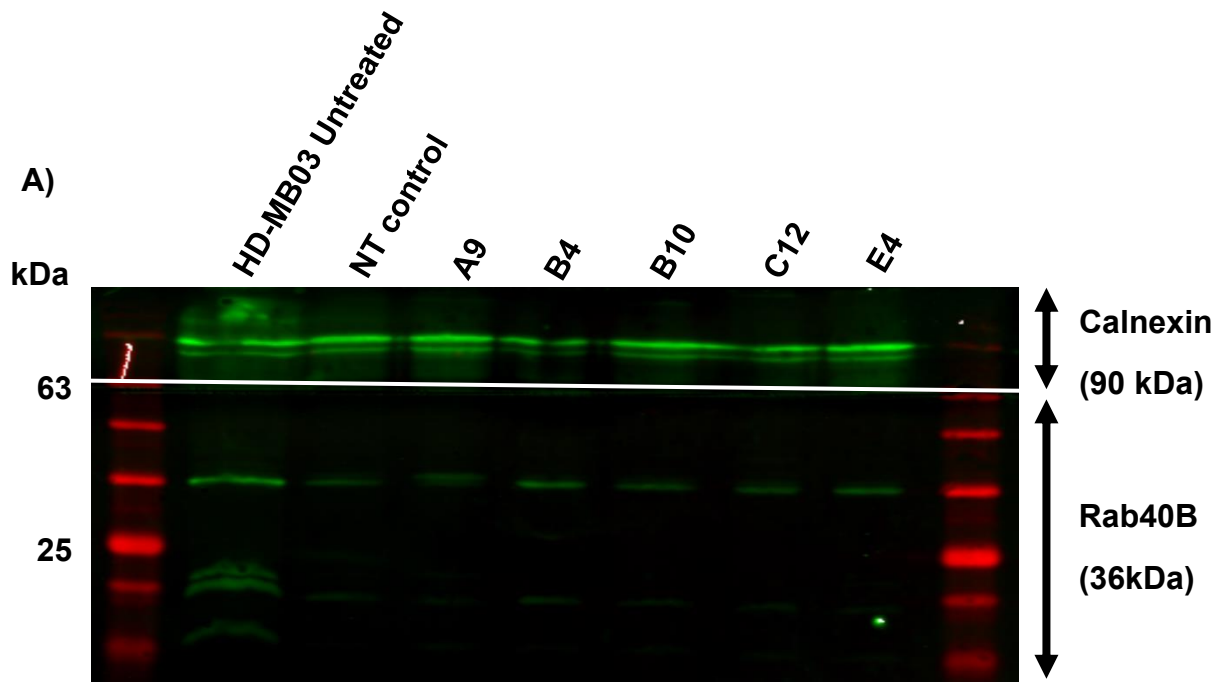
Appendix 1.9. – Rab40B potential knockout cell lines Western blot *LI-COR Western blot images of Rab40B knockout cell lines (denoted by a letter and a number), non-targeting (NT) CRISPR-Control cell lines and untreated HD-MB03 cells. Membranes were cut at the 63kDa molecular weight marker (BLUeye pre-stained protein ladder, red) and stained with anti-calnexin (90 kDa) and anti-Rab40B (36 kDa) primary antibodies.*
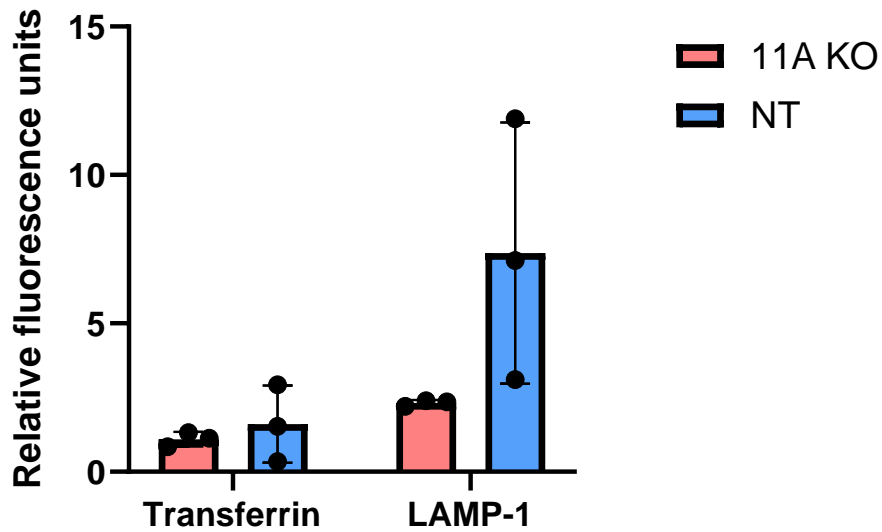
Appendix 1.10. Transferrin and LAMP-1 expression after transferrin uptake assay in Rab11A knockout and non-targeting control HD-MB03 cells
Fluorescence microscopy image analysis of Rab11A knockout (11A KO) and non-targeting control (NT) cells after 20-minute incubation at 37^oC with Alexa-Fluor 568-tagged transferrin. Relative fluorescence was calculated by comparing raw fluorescence values of cells exposed to transferrin and not exposed to transferrin. LAMP-1 relative fluorescence was calculated by comparing raw fluorescence to a no secondary antibody control. The Rab11A knockout cell lines A12, B11 and B12 and non-targeting control cell lines F3, F11 and H4 were analysed to generate this bar graph. Dots represent relative fluorescence units of individual cell lines. Error bars represent mean with standard deviation.

Appendix 1.11. List of proteins upregulated in Rab11A cell lysates compared to non-targeting control cell lysates *Fold change values are given as log2(fold change). Statistical analysis was conducted using a LIMMA test on the StatsPro platform. Peptides are listed from highest to lowest fold change.*

Peptide	log pvalue	fold.change	Peptide	log pvalue	fold.change	Peptide	log pvalue	fold.change	Peptide	log pvalue	fold.change
FSCN1	3.042718	1.403082	CYBC1	1.457351	0.604323	APLP2;APP	1.530276	0.506572	GCSH	1.931086	0.437699
GAP43	2.424849	1.092574	CASP6	2.50005	0.589936	MGAT2	1.457136	0.501186	CTN1	2.026848	0.433239
ENO2;ENO3	1.948309	0.918158	DPYSL2	3.555942	0.560462	SUN2	1.984564	0.48364	NT5C2	1.512421	0.428867
CA14	1.726694	0.897048	CSRP2	2.145225	0.558369	RAC1;RAC3	1.438212	0.476534	UBE2A	1.640034	0.426638
MT1E;MT1G;MT1M;MT1X;MT2A	2.054795	0.80903	CTNNB1;JUP	2.073601	0.552543	TRIP10	1.522383	0.475792	RHOA;RHOC	1.379065	0.422521
PAPSS1;PAPSS2	1.743891	0.773351	AIDA	1.940247	0.549291	ENO2	2.020384	0.468829	TOM1L1	1.626668	0.416646
CTNNB1	2.358818	0.753626	APP	2.355891	0.539032	POLG	1.604747	0.466455	MAPK15	1.341599	0.415733
CD44	3.637136	0.743469	QSOX2	2.759254	0.536883	CELF1;CELF2	1.397622	0.464076	TIA1	1.600351	0.41317
ALCAM	1.779919	0.701031	CBS	1.908394	0.535856	TMT1B	1.693289	0.459002	GLUL	1.450528	0.411033
C11orf54	2.962648	0.699033	ADARB1	1.978173	0.535833	UBA1	2.881927	0.458551	GOLGA2	2.205583	0.406379
ACYP1	2.390372	0.694348	DSE2	2.415927	0.52687	CDC42BPA;CDC42BPB	1.339974	0.457106	AA	1.373671	0.405666
NCAM1	1.472834	0.665671	LGALS1	1.326818	0.526699	SSU72	1.475494	0.453703	LSM7	1.571275	0.403293
PPP2CA;PPP2CB;PPP4C	1.330947	0.651719	CD55	2.850243	0.525508	FGF2	1.538019	0.451858	RHOA	1.365651	0.395048
PTBP1;PTBP3	1.334435	0.636747	NUDT15	1.308161	0.519524	QRICH2	1.338124	0.442654	FAM20B	2.28901	0.393411
FHL1	1.47466	0.634137	PRCP	2.004352	0.51588	TMED3	1.735541	0.439858	PMVK	1.58942	0.391182

Appendix 1.11. continued

Peptide	log pvalue	fold.change	Peptide	log pvalue	fold.change
GLG1	2.233555	0.374979	CTSC	1.585848	0.315663
ANKS1A	1.384129	0.37327	LAMTOR2	1.369678	0.315147
CTH	1.407113	0.372928	CNN3	1.477428	0.312537
SCARB2	1.478301	0.36763	PLSCR1	1.759471	0.311571
MICAL3	1.322502	0.362235	DST;MACF1	1.70766	0.306249
SMAD4	1.64467	0.358998	SEPTIN2	2.103257	0.305691
ANLN	1.302857	0.354791	LANCL1	1.746884	0.30456
PTGR2	1.363845	0.349812			
SEPTIN11	1.857366	0.346337			
HSPB1	1.338662	0.346072			
CXADR	1.377915	0.345987			
RAC1	1.515899	0.340776			
SUMO2;SUMO3	1.435504	0.34056			
CASP3	1.594857	0.336402			
UBE2V2	1.714899	0.327058			
SDF2	1.570982	0.32292			
SYVN1	1.364833	0.316648			

286

Appendix 1.12. List of proteins downregulated in Rab11A cell lysates compared to non-targeting control cell lysates *Fold change values are given as log2(fold change). Statistical analysis was conducted using a LIMMA test on the StatsPro platform. Peptides are listed from highest to lowest fold change.*

Peptide	log pvalue	fold.change	Peptide	log pvalue	fold.change	Peptide	log pvalue	fold.change	Peptide	log pvalue	fold.change
S100A13	2.767649	-1.60298	AMPD3	1.365608	-0.63458	CCDC12	1.362151	-0.54608	RBM42	1.348223	-0.49315
RAB11A	9.383478	-1.51985	SLC11A2	1.550247	-0.62418	TIMM17B	1.80106	-0.54185	ORC4	2.33383	-0.49246
A2M;PZP	1.629772	-1.114	H1-4	2.151406	-0.62001	NDUFA4	2.571987	-0.53986	TIMM21	1.644318	-0.48906
MACROH2A1	2.444276	-0.95657	UTP15	2.018183	-0.61753	CTU2	1.647226	-0.53949	MTHFD1L	1.467963	-0.48793
TLCD1	1.959676	-0.90612	MAD2L1BP	2.268669	-0.6161	AK6	1.46674	-0.53924	EIF5B	1.428423	-0.48792
P4HA2	2.591862	-0.84645	COX7C	1.431071	-0.61058	DDB2	1.750674	-0.53442	PTPN1	2.734916	-0.48732
SCFD2	1.600254	-0.84364	PPIC	1.462195	-0.60101	DIMT1	1.831476	-0.53309	LYRM1	2.248807	-0.487
HMGN1	2.220304	-0.8304	ILK	1.546229	-0.59969	H2BC26	1.323532	-0.53247	EARS2	1.362175	-0.48698
NTHL1	1.485918	-0.822	ECHDC3	1.481126	-0.59765	NOA1	1.790154	-0.52562	EMC4	1.710993	-0.48542
RIOK3	2.699726	-0.80653	HMGN2	1.662443	-0.59316	ABL2	1.664495	-0.52415	VARS1	1.73688	-0.48072
HMGA1	1.590325	-0.79944	NUBP2	1.386203	-0.59203	MAP1B	1.644016	-0.52348	TMEM223	1.575831	-0.47961
H3-7	1.486642	-0.75815	UBR3	1.60578	-0.5917	AARS2	1.946703	-0.52342	PRKACA	1.891217	-0.47683
EHD4	2.801811	-0.72824	PURA	2.179581	-0.58643	MDN1	1.800724	-0.52218	AKAP12	2.704618	-0.47678
PEX1	2.40421	-0.72562	PCK2	2.293165	-0.58598	ISCA1	1.822942	-0.52195	IMMT	1.702555	-0.47564
H2AC11;H2AC12;H2AC14;H2AC18;H2AC20;H2AC7;H2AJ;H2AX;H2AZ1;H2AZ2	1.749445	-0.72459	BUD23	1.374158	-0.58309	HMGN5	1.948194	-0.52125	FAM117B	1.699676	-0.47475
SLC25A24	2.736773	-0.7222	NDUFAF7	3.508532	-0.5814	SLC25A13	1.823633	-0.51993	TOP1	1.40321	-0.47455
IDH3B	2.544224	-0.69277	ACSL1	1.99962	-0.57497	RPS27L	1.538697	-0.51965	UTP20	1.447163	-0.47384
CYFIP2	1.343947	-0.67681	QRSL1	2.154986	-0.56909	PKMYT1	1.864255	-0.51523	RPL7L1	1.370393	-0.47355
ACOT13	2.161877	-0.67151	CISD1	2.10377	-0.56655	PG	2.326167	-0.51247	FBXO30	1.321979	-0.47212
S100A16	1.869171	-0.66901	CCNB1	2.051448	-0.56447	NOB1	2.586606	-0.51195	TTC27	1.758612	-0.47034
WDTC1	2.444236	-0.65755	DPH1	2.418034	-0.56332	GIPC1	1.347446	-0.51013	ACTR10	1.513041	-0.46941
ATPAF2	1.4066	-0.65544	MAP1LC3B;MAP1LC3B2	1.842383	-0.55856	ACOT9	1.509932	-0.50981	AP3S2	1.441401	-0.46937
FBXO21	1.328011	-0.65469	COMTD1	1.597259	-0.55843	ALDH4A1	1.925056	-0.50836	YIF1A	1.501304	-0.46919
AAGAB	2.054645	-0.64572	FAH	1.416354	-0.55524	SCAF8	2.254356	-0.50461	UTP6	1.785588	-0.46888
TIMM17A	2.063151	-0.63971	SGTB	1.603877	-0.55192	C1QBP	1.982327	-0.50181	SLC25A12;SLC25A13	1.486866	-0.46813
EHHADH	1.441193	-0.63547	DDX49	1.386728	-0.5467	CCDC86	1.471848	-0.49911	TMEM41B	1.705986	-0.46727

Peptide	log pvalue	fold.change	Peptide	log pvalue	fold.change	Peptide	log pvalue	fold.change	Peptide	log pvalue	fold.change
MRM3	1.966318	-0.46707	PPP2R5C;PPP2R5D	1.566103	-0.42542	MAP2K4	2.120796	-0.39743	WDR46	1.412417	-0.37295
DCAF13	1.42655	-0.46527	OGFR	1.459437	-0.42542	CDKAL1	1.453559	-0.39693	MRPS6	1.345346	-0.3717
CLUH	2.043189	-0.46521	POLR3D	1.682337	-0.42352	LENG8	1.370217	-0.3939	CLCN7	1.803786	-0.37167
NEDD4L	1.882521	-0.46235	PROM1	2.20114	-0.42041	ATP6V0A1	1.730116	-0.39253	SUPT3H	1.336969	-0.37125
TOP3A	2.013417	-0.45693	TTI2	1.676856	-0.41958	MRPS10	1.745546	-0.39193	TMEM126B	1.404061	-0.37099
EPHX2	1.687243	-0.45686	HOMER1	1.630977	-0.41886	SCAMP2	1.634839	-0.3919	POLR3F	1.977206	-0.36817
HEATR1	1.345062	-0.45655	NDRG1	1.828021	-0.4169	ECSIT	1.46864	-0.39163	NDUFA9	1.77409	-0.36686
PNO1	2.520534	-0.45244	PPP2R5D	1.620722	-0.41671	ISCU	1.939136	-0.38953	HADHB	1.330989	-0.3668
FAR1	1.308811	-0.45052	PLS3	1.532558	-0.41657	POLR3C	2.000398	-0.38926	VRK1	1.418265	-0.36472
OSBPL11	1.481195	-0.45048	CDC34	1.551397	-0.41562	POLR1D	1.47543	-0.3889	HSDL2	1.624432	-0.36388
MRPL54	1.805091	-0.45041	IDH3A	1.949626	-0.41491	PUS1	1.448566	-0.38792	ARFIP2	1.552366	-0.36291
ATAT1	1.774332	-0.44932	TRMU	1.94986	-0.41323	TP53BP1	1.342092	-0.38598	COMMD4	1.550547	-0.36279
FASTKD2	1.411952	-0.44643	STUB1	2.482192	-0.41301	UTP14A	1.990646	-0.38534	PUM2	1.697838	-0.36218
REL	2.277501	-0.44342	ABCB10	1.30501	-0.41108	CTSA	1.810522	-0.38473	PTPN2	1.741363	-0.36201
MRPS15	1.367489	-0.44337	DPH2	2.211931	-0.4108	TLE3	1.777044	-0.38366	IGF2BP2	1.340321	-0.36188
DNM1	1.767707	-0.44316	TXNDC9	2.425844	-0.41041	GATB	1.49737	-0.38309	GSTK1	1.536176	-0.36131
MT-CO2	1.974325	-0.44259	UBE2G1	1.324322	-0.41037	NFS1	1.964377	-0.38227	ERGIC1	1.431797	-0.3606
FASTKD5	1.908354	-0.4419	TMX2	2.462298	-0.40838	CHD8+A195M1A173:A205A173:AA173:A338	1.972725	-0.38182	RTN4	1.421936	-0.36024
HLA-G	1.787197	-0.44174	SNX2	1.556402	-0.408	ACO2	1.611059	-0.37828	ZC3H14	1.570837	-0.36024
COMMD2	1.56651	-0.44125	ZC3HAV1	1.913235	-0.4056	TUFM	1.481191	-0.37766	SFXN1	1.350053	-0.35978
NUBP1	1.659544	-0.43603	ABT1	1.424109	-0.40329	ACADVL	2.092242	-0.37737	ERCC2	1.784881	-0.35959
CCDC88A	1.593963	-0.43538	HS1BP3	1.539491	-0.40279	NDUFS1	2.286646	-0.37585	NDUFS7	1.338436	-0.35905
PYGB	1.582888	-0.43309	RUFY1	1.483762	-0.40121	CLPX	1.381942	-0.37518	STARD7	1.546451	-0.35875
LSM14B	1.962391	-0.43004	DAF5	1.432185	-0.40067	CIAO2A	1.67279	-0.37444	TMEM70	1.371984	-0.35737
WDR18	1.860333	-0.4293	ACLY	1.489271	-0.39843	STEAP3	1.807655	-0.37435	PAXBP1	1.32162	-0.35716
ATP6V1C1	1.964644	-0.4279	ANKFY1	1.311911	-0.39777	TSR1	1.392016	-0.37321	IPO11	1.791076	-0.35707

Appendix 1.12. continued

Peptide	log pvalue	fold.change	Peptide	log pvalue	fold.change
DJB12	1.502931	-0.35463	UNC119B	1.451845	-0.32464
CYP51A1	1.308885	-0.35419	PDCL3	1.760834	-0.32174
ZBED1	1.599111	-0.3541	NDUFA2	1.772641	-0.31764
COBL	1.461908	-0.35358	MTG1	1.429744	-0.31747
NDUFV1	1.969868	-0.35308	MRPL37	1.574658	-0.31703
A30	1.370824	-0.35247	TRAP1	1.653671	-0.31666
NDUFAF1	1.363369	-0.34956	USP39	1.622462	-0.31627
MIPEP	1.662254	-0.34782	GPKOW	1.632905	-0.3161
KBTBD6	1.637115	-0.34729	OARD1	1.45308	-0.31526
LYRM4	1.721331	-0.34676	EIF3B	1.431327	-0.31511
HSP90AB1;HSP90B1	1.357979	-0.34632	NRDC	1.817728	-0.31393
NOL7	1.731505	-0.34612	CHMP3	2.259502	-0.31338
BYSL	2.525155	-0.34552	AP5M1	1.305096	-0.31268
FXN	1.412889	-0.34428	EIF3J	1.573808	-0.31194
DICER1	1.563795	-0.33937	ETF1	1.698047	-0.31071
MRPS2	1.31103	-0.33785	VTI1B	1.581703	-0.31004
MCCC2	1.59188	-0.33521	CLN5	1.801761	-0.30962
SRFBP1	1.517098	-0.33437	NDUFS8	1.419275	-0.30909
RAP2A;RAP2B;RAP2C	1.375657	-0.33397	GSTZ1	1.316342	-0.30907
PAF1	1.370315	-0.32969	SERPINF1	1.624774	-0.30635
CLPB	1.330352	-0.32962	AFDN	1.626136	-0.3063
FBXO22	1.657129	-0.32713	NDUFS2	1.358695	-0.30538
OSBPL9	1.74567	-0.32642	SLC27A2	1.352292	-0.30504
VAPB	2.349177	-0.32637	CBX1;CBX3	1.478065	-0.30266
ARFGAP1	2.097751	-0.32605	SDHB	1.908282	-0.30232
MRPS27	1.605819	-0.32476	WRAP73	1.634727	-0.30094
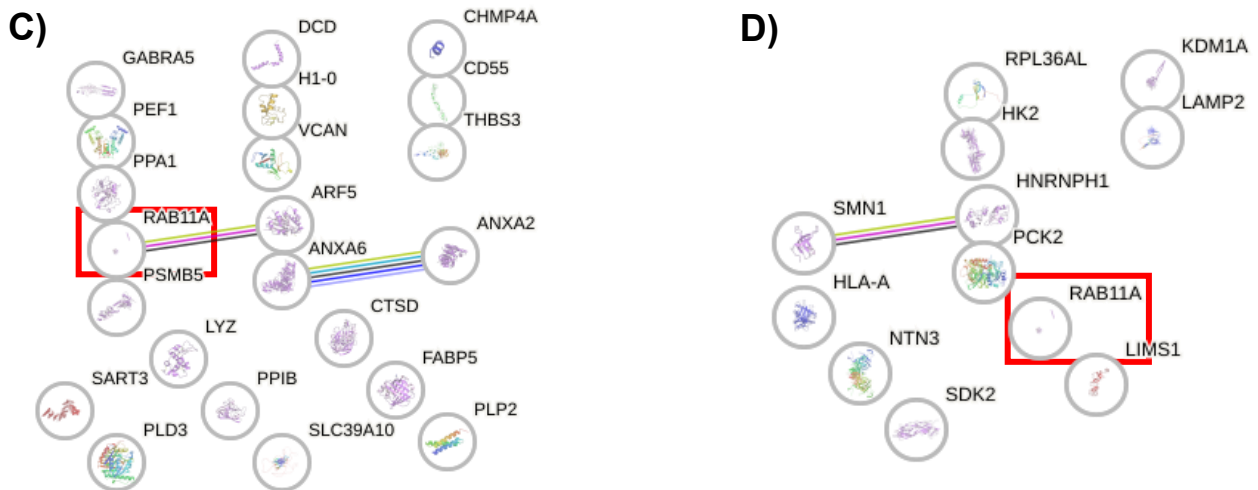
Appendix 1.13. STRING (Search Tool for the Retrieval of Interacting Genes/proteins) analysis of up- and downregulated proteins in cell lysates and extracellular vesicles derived from Rab11A knockout cells including Rab11A in the network *A) Upregulated proteins in cell lysates. B) Downregulated proteins in cell lysates. C) Upregulated proteins in extracellular vesicles. D) Downregulated proteins in extracellular vesicles. STRING pathway analysis of protein-protein interactions. Analysis was conducted with a high confidence score of 0.7. Line colour and number between proteins indicate the source used to determine the interaction (light blue – from curated databases, pink – experimentally determined, green – predicted gene neighbourhood, red – gene fusions, dark blue – gene co-occurrence, light green – textmining, black – co-expression, lilac – protein homology). Proteins are up or downregulated compared to expression in cell lysates or EVs derived from non-targeting control cell lines. Red box indicates position of Rab11A in the network.*

290
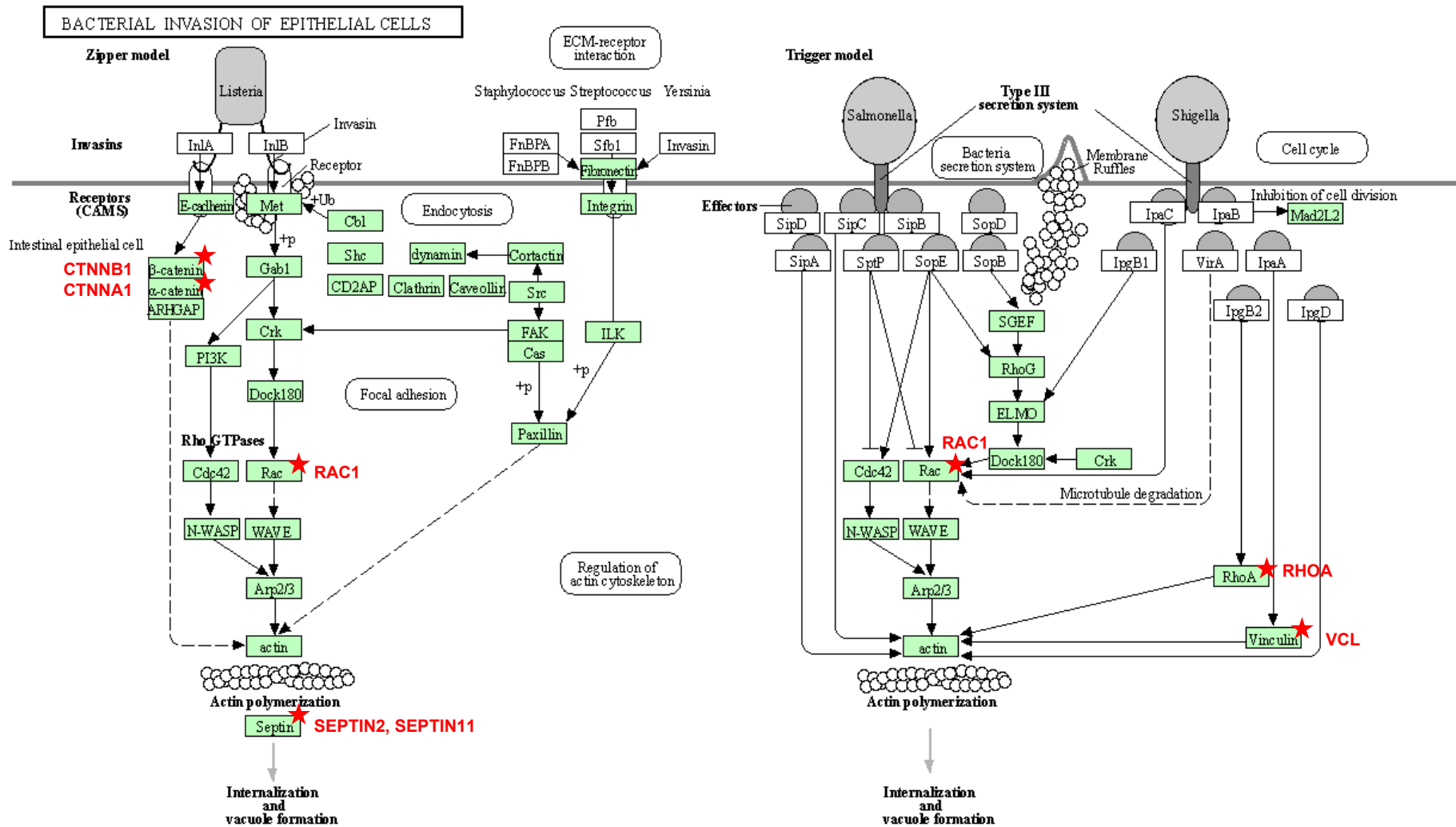
Appendix 1.14. Bacterial invasion of epithelial cells Kyoto Encyclopaedia of Genes and Genomes (KEGG) pathway with proteins upregulated in Rab11A knockout cells highlighted *Red stars indicate position of upregulated protein in the pathway. Red text indicates gene symbols from pathway analysis. Analysis conducted using the online bioinformatics tool DAVID (the Database for Annotation, Visualisation and Integration Discovery).*

Appendix 1.15. Proteins downregulated in metabolic pathways in Rab11A knockout cell lysates

Protein (Gene notation)	Metabolic pathway association	Protein (Gene notation)	Metabolic pathway association
ACADVL	Fatty acid degradation	IDH3B	Citrate (TCA) cycle
ACLY	Citrate (TCA) cycle	MCCC2	Valine, leucine and isoleucine degradation
ACO2	Citrate (TCA) cycle	MTHFD1L	Metabolism of cofactors and vitamins
ACSL1	Fatty acid biosynthesis and degradation	MT-CO2	Oxidative phosphorylation
AK6	Nucleotide metabolism	NDUFA2	Oxidative phosphorylation
ALDH4A1	Amino acid metabolism	NDUFA4	Oxidative phosphorylation
AMPD3	Nucleotide metabolism	NDUFA2	Oxidative phosphorylation
ATP6V0A1	Oxidative phosphorylation	NDUFA4	Oxidative phosphorylation
ATP6V1C1	Oxidative phosphorylation	NDUFA9	Oxidative phosphorylation
COX7C	Oxidative phosphorylation	NDUFS1	Oxidative phosphorylation
CYP51A1	Lipid metabolism	NDUFS2	Oxidative phosphorylation
EARS2	Aminoacyl-tRNA biosynthesis	NDUFS7	Oxidative phosphorylation
EHHADH	Fatty acid degradation and metabolism	NDUFS8	Oxidative phosphorylation
EPHX2	Lipid metabolism	NDUFV1	Oxidative phosphorylation
FAH	Amino acid metabolism	NFS1	Thiamine metabolism
GATB	Aminoacyl-tRNA biosynthesis	P4HA2	Arginine and proline metabolism
GSTK1	Glutathione metabolism	PCK2	Citrate (TCA) cycle
GSTZ1	Amino acid metabolism	PYGB	Carbohydrate metabolism
HADHB	Lipid metabolism	QRSL	Glycerolipid metabolism
IDH3A	Citrate (TCA) cycle	SDHB	Citrate (TCA) cycle
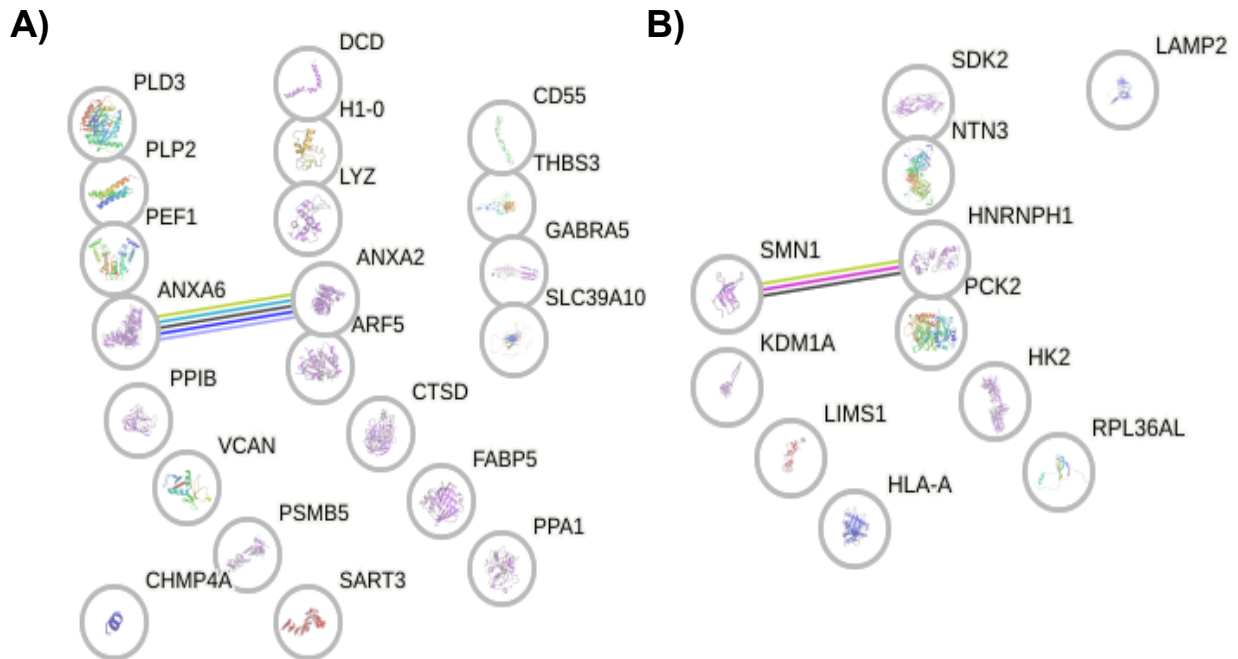
Appendix 1.16. STRING analysis of up- and downregulated proteins in extracellular vesicles derived from Rab11A knockout cells *A) Upregulated proteins. B) Downregulated proteins. STRING pathway analysis of protein-protein interactions. Analysis was conducted with a high confidence score of 0.7. Line colour and number between proteins indicate the source used to determine the interaction (light blue – from curated databases, pink – experimentally determined, green – predicted gene neighbourhood, red – gene fusions, dark blue – gene co-occurrence, light green – textmining, black – co-expression, lilac – protein homology). Proteins are up or downregulated compared to expression in EVs derived from non-targeting control cell*

Downregulated in EVs
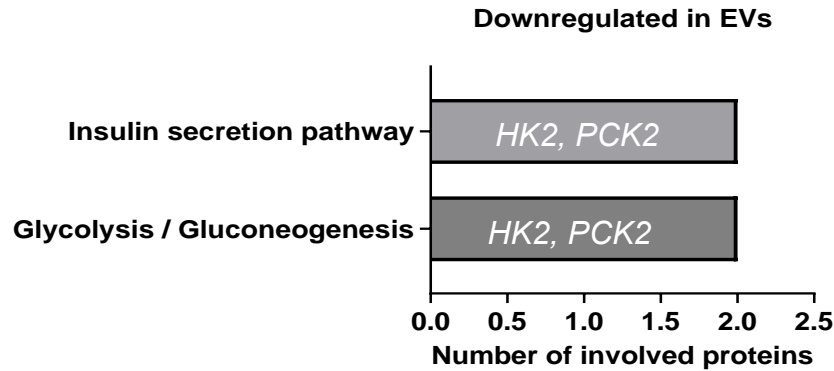
Appendix 1.17. KEGG pathway analysis of proteins downregulated in Rab11A knockout cell line extracellular vesicles. Analysis was conducted using the bioinformatics tool DAVID (the Database for Annotation, Visualisation and Integration Discovery). Pathways included had a statistical significance of p≤0.05. Pathways are ordered from most statistically significant (closest to the x-axis) to least statistically significant (closest to graph title). Identities of proteins within the pathways are shown in white text. Expression in Rab11A knockout EVs was compared to expression in non-targeting control cell line EVs.
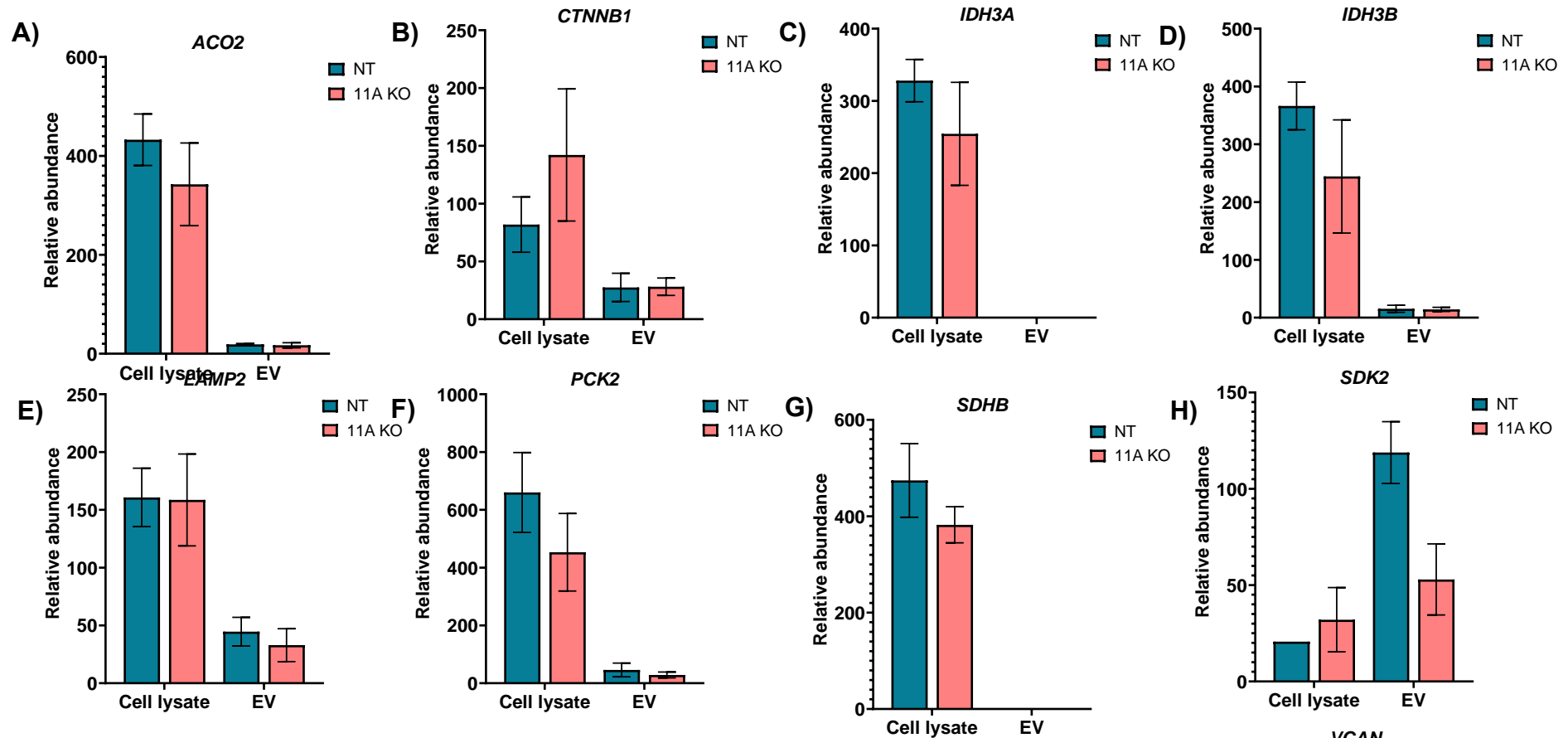
Appendix 1.18. Relative abundances of peptides highlighted in mass spectrometry analysis in cell lysate and extracellular vesicle samples *Relative abundances of the number of each peptide detected using SWATH-MS. A) ACO2, B) CTNNB1, C) IDH3A, D) IDH3B, E) LAMP2, F) PCK2, G) SDHB, H) SDK2, I) VCAN. Relative abundance in cell lysates was calculated by comparing the number of peptides detected to the amount of protein in the lysate sample. For extracellular vesicle (EV) samples this was calculated by comparing the number of peptides to the concentration of EVs in the sample. The statistical significance of abundance of the peptide in non-targeting (NT; blue) samples compared to Rab11A knockout (11A KO; pink) was calculated using Welch's t-test and GraphPad Prism. No statistical significance in expression was identified for any of the peptides. N = 9.*

295

Grants and awards

Grants:

May 2022 – Received £500 travel prize from the Researcher Academy to fund attending the International Society of Paediatric Neuro-oncology conference.

May 2023 – Received £11,540 from the UKRI BBSRC DTP to complete additional research for this thesis.

Awards:

April 2022 - First place third year presentation prize at BBSRC DTP Spring conference.

July 2022 – First place third year presentation prize at School of Life Sciences postgraduate conference.